“Synthesis and Evaluation of TEMPO Probes and Conjugates”

Dissertation

zur Erlangung des Doktorgrades der
Naturwissenschaften (Dr. rer. nat.)

der

Naturwissenschaftlichen Fakultät I
Biowissenschaften
der Martin-Luther-Universität
Halle-Wittenberg

vorgelegt von

Herrn M.Sc. Haider Na’mh Abdula Sultani
geb. am 25.08.1984 in Baghdad, Iraq
öffentlich verteidigt am 01.12.2020

Gutachter:
Prof. Dr. Bernhard Westermann
Prof. Dr. Peter Imming
Prof.Dr. Rodolfo Grifols Lavilla

The work presented in this dissertation has been conducted at the Leibniz-Institute of Plant Biochemistry (IPB) in cooperation with Martin-Luther Halle-Wittenberg University.

Supervisor and thesis editor: Prof. Dr. Bernhard Westermann, Prof. Dr. Peter Imming

"This dissertation is submitted according to the guidelines provided by the PhD-program of Martin-Luther University Halle-Wittenberg. The thesis includes three original research papers (one already published and two to be submitted for publication), which comprise the majority of the author's research work during the course of Ph.D."

Haider Na'mh Abdula Sultani

To my parents, sisters, and friends
For your love, support, and encouragement

The straw in a sea is driven by the current, the branch on a tree is driven by the wind, but only man is driven by his own will.

Mustafa Mahmoud.

Acknowledgments

I would like to acknowledge and express my gratitude to the following people for their valuable time and assistance, without whom the completion of this dissertation would not have been possible:

- Prof. Dr. Peter Imming, for serving as the first referee and his aid during this entire process.

- My advisor, Prof. Dr. Bernhard Westermann, for giving me the opportunity to work in his group, who has the attitude and the substance of a genius. During my Ph.D. time, he gave me his total support “in” and “out”-side the lab, I have learned a lot from his advice and fruitful scientific discussions that improved the quality of my thesis significantly, he continually and convincingly pushes this research to the limit. Without his guidance and persistent help, this research would not have been possible;

- Prof. Dr. Ludger A. Wessjohann for giving me the opportunity to conduct my work in the Department of Bioorganic Chemistry;

- Prof. Dr. Dariush Hinderberger and Dr. Haleh Hashemi Haeri for successful collaboration;

- Dr. Hidayat Hussain for all the help and quality advice provided and extensive proofreadings of this presented work;

- Dr. Jürgen Schmidt, Martina Lerbs and Dr. Andrej Frolov for extensive ESI-MS, HRMS measurements;

- Dr. Andrea Porzel Gudrun Hahn and for numerous NMR measurements;

- Dr. Katrin Franke and Dr. Norbert Arnold for a fruitful collaboration on various different projects during my Ph.D. work;

- My fellow lab-mates, friends, and co-workers for the stimulating discussions namely, Katharina, Annegret, Tristan, Hoai, Evelyn, Alfred, Nalin, Bruno, Renata, Rafael, Mehdi, Amina, Aaron, Manuel, Micjel, Christine, Martina, David and Thomas for their enthusiasm and nice work atmosphere.

- I would like to place a special acknowledgment to Dr. Goran Kaluđerović and Ibrahim Morgan for the anticancer assay and biological evaluation of the synthesized probes described in chapters 3 and 4.

- Dr. Roberta Drekener and Dr. Ligia Souza for all their help and support during my first years in Halle;

- Special thanks to my brother Ricardo for all the help and quality comments, during the time we spend in the lab, although it was quite short, we became brothers till today I really would like to express my deep appreciation to him for being my brother and for the honest friendship during all these years;

- To my sisters Zainab and Isra for their help;

- My family for believing in me and supporting me during all these years without their continues love and encouragement everything would have been much harder.

- To Christane Hülsbusch for all the love and support during my stay in Dortmund, I am truly blessed to have you in my life.

Haider Na'mh Abdula Sultani
Leibniz Institute of Plant Biochemistry (IPB)
Halle (Saale), September 2019

Table of contents

List of abbreviations

$[\alpha]_D^T$	specific optical rotation
τ_c	rotational correlation time
ε	molar absorptivity
ϕ	quantum yield
4CR	four-component reaction
A(^{14}N)	nitrogen 14 isotropic hyperfine splitting
Ac	acetyl
AnnV/PI	annexin V/propidium iodide
APS	ammonium persulfate
AsA	ascorbic acid
aa	amino acid
atm	atmosphere
B_0	constant, homogeneous magnetic field used to polarize spin
B (mT)	magnetic field in millitesla
Bcl-xL	B-cell lymphoma-extra large
Bn	benzyl
Boc	*tert*-butoxycarbonyl
BSA	bovine serum albumin
C°	degrees Celcius (centigrade)
Cbz	benzyloxycarbonyl
CSA	camphorsulfonic acid
CuAAC	copper-catalyzed azide-alkyne cycloaddition
CV	crystal violet
CW EPR	continuous-wave electron paramagnetic resonance spectroscopy
calcd.	calculated
c	concentration
DAPI	2-(4-amidinophenyl)-6-indolecarbamidine dihydrochloride
DBU	1,8-Diazabicyclo[5.4.0]undec-7-ene
DHR	dihydrorhodamine
DKPs	diketopiperazines
DMAP	4-Dimethylaminopyridine
DMEM	Dulbecco's modified Eagle medium
DMF	*N*,*N*-dimethylformamide
DMPO	5,5-dimethyl-pyrroline *N*-oxide
DMSO	Dimethyl sulfoxide
DNA	deoxyribonucleic acid
dd H_2O	double-distilled water
deg	degree
d	doublet in NMR
EDTA	ethylenediaminetetraacetic acid
EPR	electron paramagnetic resonance
ESI	electrospray ionization
ESR	electron spin resonance
EtOAc	ethyl acetate
e.g.	*exempli gratia* (for example)
equiv	equivalent
et al.	*et alia* (and others)
FACS	Fluorescence-activated cell sorting
FCS	Fetal Calf Serum
FITC	fluorescein isothiocyanate
Fmoc	9-fluorenylmethoxycarbonyl
GFP	green fluorescent protein
g	gram
HOMO	highest occupied molecular orbital
HPLC	high-performance liquid chromatography
HRMS	high-resolution mass spectrometry
HRP	horseradish peroxidase
HT-29	human colon cancer cell line
Hz	hertz
h	hour(s)
IC_{50}	median inhibitory concentration
IgG	rabbit anti-mouse IgG secondary antibody
IMCR	isocyanide multicomponent reaction
IPB	Leibniz institute for plant biochemistry
IPB	4-isocyanopermethylbutane-1,1,3-triol
ITC	isothermal titration calorimetry
i.e.	*id est* (that is)
I	nuclear spin
J	coupling constant (in NMR)
kHz	kilohertz
L	litter
LSM	laser scanning microscope
LUMO	lowest unoccupied molecular orbital
M	molar
MCPA	4-(4-chloro-o-tolyloxy)butyric acid
MCR	multicomponent reaction
Me	methyl
MeOH	methanol
MHz	megahertz
MSL	3-maleimido-proxyl
MS	mass spectrometry
MTSL	S-(1-oxyl-2,2,5,5-tetramethyl-2,5-dihydro-1H-pyrrol-3-yl)methyl methanesulfonothioate
MTT	3-(4,5-dimethylthiazol-2-yl)-2,5-diphenyltetrazolium bromide
min	minutes
m/z	mass-to-charge ratio
m	mili
m	multiplet (in NMR)
µ	micro
NIH3T3	normal fibroblast
NMP	nitroxide mediated polymerization
NMR	nuclear magnetic resonance
NO	nitroxide radical
NOBA	nitroxide boronic acid
Nu	nucleophile
n	nano

PBN	alpha-phenyl N-tertiary-butylnitrone
PBS	phosphate-buffered saline
PC3	human prostate cancer cell line
RPMI	Roswell Park Memorial Institute
PROXYL	2,2,5,5-tetramethyl-1-pyrrolidinyloxy
PS	phosphatidylserine
pO_2	partial pressure of oxygen
p-	*para*-
q	quartet (in NMR)
RFU	relative fluorescence units
ROS	reactive oxygen species
Rt	retention time
rt	room temperature
SDSL	site-directed spin labelling
SOMO	singly occupied molecular orbital
SPAAC	strain promoted azide-alkyne cycloaddition
S	electron spin
s	singlet (in NMR)
TEA	triethylamine
TEMED	tetramethylethylenediamine
TEMPO	2,2,6,6-Tetramethyl-1-piperidinyloxy
Texas-Red	sulforhodamine 101 acid chloride
TFA	trifluoroacetic acid
THF	tetrahydrofuran
TLC	thin-layer chromatography
TMIO	1,1,3,3-tetramethyl- isoindoline-2-oxyl
TRIS	tris(hydroxymethyl)aminomethane
t-	*tert*-(tertiary)
UDAC	Ugi-4CR/deprotection + activation/cyclization
UV	ultraviolet light
viz.	*videre licet* (namely)

Chapter 1

Nitroxide radicals: general introduction and its main application in pharmaceutical chemistry

Abstract

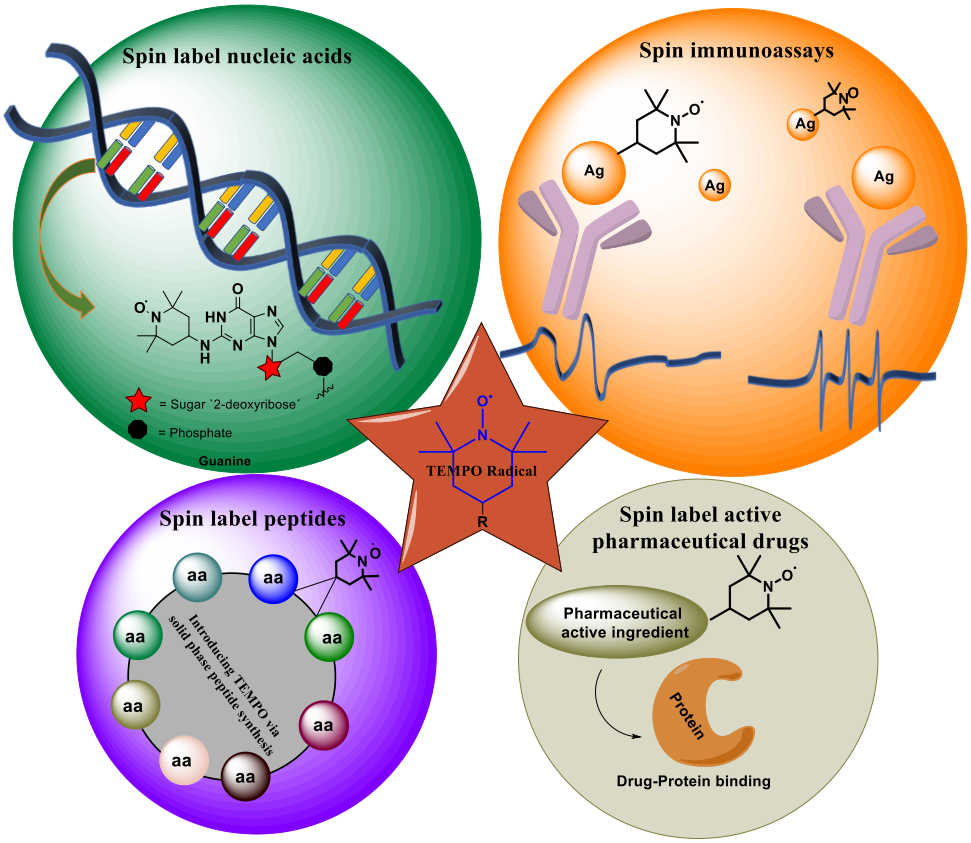

Nitroxide radicals such as (2,2,6,6-Tetramethylpiperidin-1-yl)oxyl commonly known as TEMPO radicals are an important class of reactive organic molecules. Their use and application in pharmaceutical and medicinal fields are in high demand with their incorporation into peptides and proteins becoming more popular. At the beginning of our studies, there was no report in the literature utilizing isocyanide based multicomponent reactions (IMCRs) as a synthetic tool to incorporate TEMPO radicals into either relevant macromolecular biological molecules such as proteins or smaller molecules such as peptides and other relevant natural products. Therefore, the aim of this chapter is to provide a comprehensive introduction to electron paramagnetic resonance (EPR) and an overview of TEMPO applications in the field of biological sciences. In addition, the end of this chapter describes different methods of introducing nitroxide radicals into divergent biological molecules.

1.1 Introduction

Since the discovery of electron paramagnetic resonance (EPR) by the Soviet physicist Zavoisky in the 1940s,[1] a growing interest by many researchers in products with unsaturated valences, known as free radicals, are observed. Indeed, many of the free radicals are of less importance since they are unstable molecules, highly reactive and short-lived which cannot be isolated and utilized further. The growing search for highly stable free radicals as a consequence was after all not surprising. Stable free radicals gained tremendous importance in chemistry as well as its important role to study living systems.[1,2] The discovery of long-lived free radicals not acting as reactive intermediates, as independent chemical compounds that can be synthesized and isolated in pure form at the bench, was an important development in the history of free radicals.[3] One of the most important classes of stable free radicals synthesized are the nitroxide radicals, which are characterized by the presence of an unpaired electron delocalized over the nitrogen and oxygen atoms (**Scheme 1. 1**).

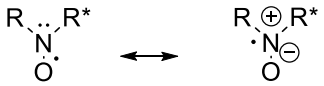

Scheme 1. 1 Delocalization stability of nitroxide radicals.

The spin population, which is mainly distributed on the nitrogen and oxygen atoms of the nitroxide radical, can be explained based on Hückel molecular orbital theory (**Figure 1. 1**). The overlap between the nitrogen and oxygen P_Z orbitals results in fully occupied π orbital and half occupied antibonding π* orbital. The energy of the $2P_Z$ orbital of nitrogen in contrast to the oxygen defines where the paramagnetic electron is being localized, i.e. the nitrogen versus oxygen antibonding π* orbital. The energy of the oxygen $2P_Z$ will decrease, relative to that of the nitrogen, if the polarity of the nitroxide environment increases (e.g. protic solvents). As a result, the antibonding π* orbital will increase the nitrogen character or, in other words, larger spin population on the nitrogen.[4]

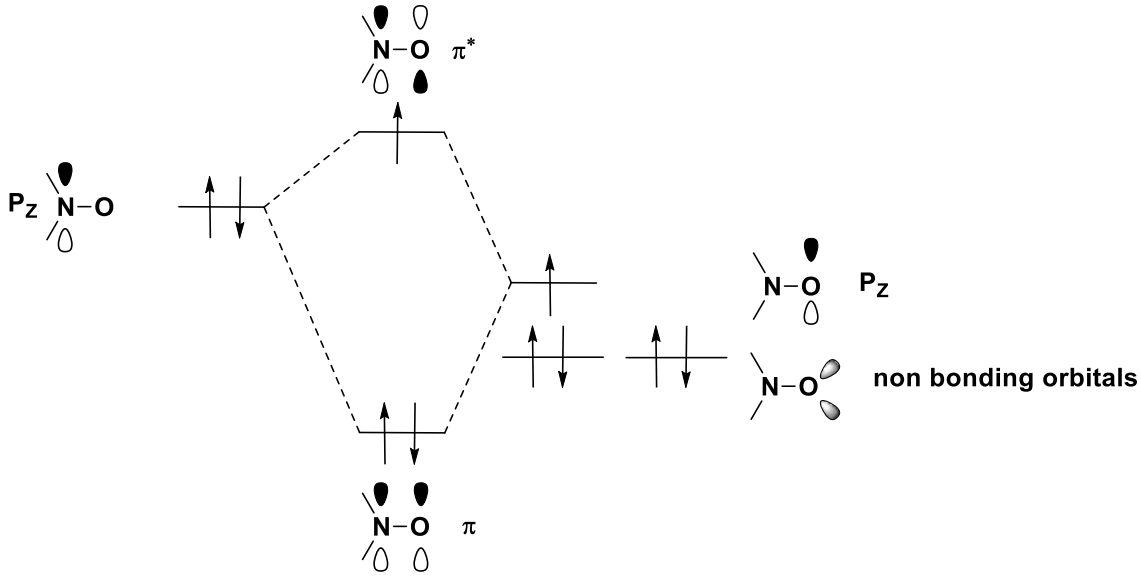

Figure 1. 1 Molecular orbitals of nitroxide radical.

The presence of this unpaired electron is being responsible for the inherent chemical properties of the nitroxide and also makes them paramagnetic.[5] The paramagnetic properties of this class of stable free radicals provide possibilities to detect them using electron paramagnetic (spin) resonance spectroscopy (EPR or ESR). In principle, the technique relies on the ability of the electron to change its spin state upon irradiation with microwave energy in a magnetic field.[6] EPR spectroscopy is a highly sensitive technique when compared to other spectroscopic methods such as nuclear magnetic resonance (NMR). Therefore, EPR spectroscopy has made innovative contributions in all areas ranging from medicinal chemistry applications, chemistry, biology, physics, and materials science.[7] This chapter focuses on nitroxide radicals, regarding its spectra, factors affecting its stability, some of the most important applications. In addition, this chapter will discuss the chemical methods used to synthesize the nitroxide group and the most common methods for introducing the nitroxide groups.

1.2 Nitroxide spectra

The EPR spectrum of the nitroxide radical can be described with an electron spin of S=1/2 which is coupled to a nuclear spin of ^{14}N which is I=1. The reason why the spin system is being described as such is due to the fact that 95% of the spin population is being shared on the nitrogen and oxygen atoms. In the absence of an external magnetic field, the paramagnetic electrons with S=1/2 are randomly spinning, and the two spin states are degenerated. In the presence of a strong external magnetic field $B_{0,}$ the two spin states will have different energies resulting in a splitting of the two energy levels due

to the fact that the single electron can either have its spin parallel or anti-parallel to the applied magnetic field. This splitting is known as the Electron Zeeman Effect as shown in **Figure 1. 2**.[4] In addition to the Zeeman Effect, the paramagnetic electron interacts also with the nitrogen nucleus with a nuclear spin of *I*=1 which causes further splitting. This interaction is known as the hyperfine interaction (EPR analogy to *J* coupling values in NMR spectroscopy) which is responsible for the three lines of a typical nitroxide radical (**Figure 1. 2**).[4]

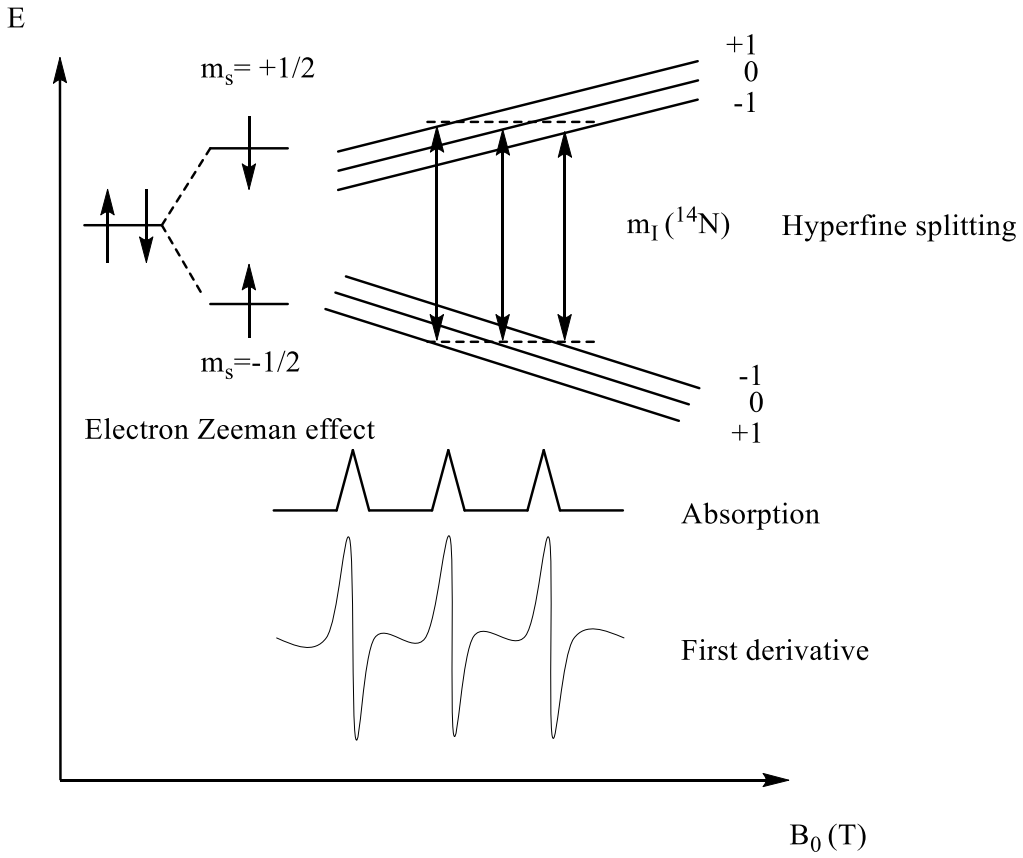

Figure 1. 2 Spectral characteristics of nitroxide radicals.

1.3 Redox character of nitroxides

To explain the redox behavior of nitroxides, one has to take into account its electron configuration (**Figure 1. 3**).

The single electron that is delocalized over both the nitrogen and oxygen atom can have dual behavior. Either it can gain an electron and be reduced to the hydroxylamine anion or it can lose an electron and be oxidized to the corresponding oxoammonium cation (**Figure 1. 3**).[4,8]

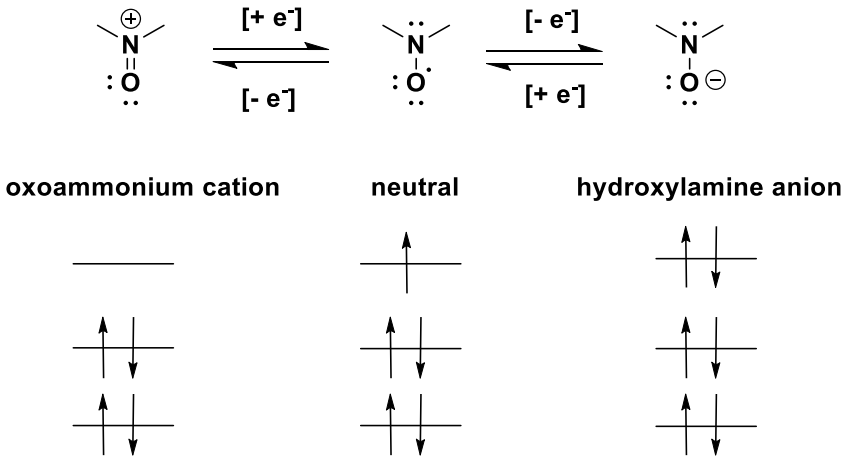

Figure 1. 3 Redox activity of nitroxide radicals.

Reduction of the nitroxide radical to the corresponding diamagnetic hydroxylamine anion is possible in the presence of weak reductants such as hydrazines or ascorbic acid *in vitro* (**Figure 1. 3**). One of the chemical drawback of nitroxides is their ability to be reduced to the diamagnetic hydroxylamine in the presence of reducing agents.[8] Fortunately, the radical species can be easily regenerated using mild oxidants, such as hexacyanoferrate(III) $[Fe(CN)_6]^{3-}$ and lead dioxide PbO_2. Simple exposure to air is also sufficient to generate the radical although this process may take more time depending mainly on the pH of the solution containing the hydroxylamine.[9] The reduction of nitroxide to the corresponding hydroxylamine is considered the major metabolic pathway *in vivo*. The real limitation is associated with its application *in vivo*, due to the loss of the nitroxide radical center without the possibility to regenerate it again.[10]

In contrast, the oxidation of stable nitroxide radicals, for instance, the bis-(*tert*-alkyl) nitroxide such as TEMPO, is quite troublesome and requires therefore strong oxidants, such as Br_2 or Lewis acid ($AlCl_3$). The oxidation will lead to the formation of the oxoammonium cation (**Figure 1. 3**).[10]

The resulting oxoammonium salt can then react further via two pathways: a) it can be reduced back to the nitroxide radical by a single electron transfer and b), it can undergo ring-opening of the piperidine core structure to an acyclic product (**Scheme 1. 2**).[11]

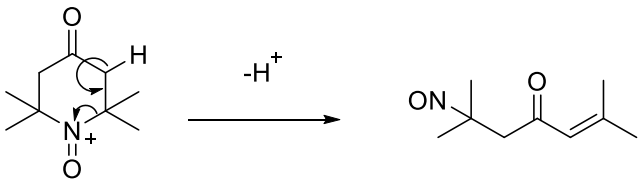

Scheme 1. 2 Ring-opening of oxoammonium cation.

1.4 Stability of nitroxide radicals

Stable nitroxides are chemical compounds that can be synthesized and isolated in pure form and stored for periods of up to several months without losing the paramagnetic center. The term used to describe this feature is called long-lived or persistent nitroxides.[12]

1.4.1 Factors affecting the stability of the nitroxide radicals

This outstanding stability of the nitroxide group in part arises from the three electron *N*-O bond (**Scheme 1. 1**). The high delocalization stability of the single electron over the N-O bond reaches values up to 32 kcal/mol, which render the radical center stable and prevents the dimerization of the well-known nitroxides, due to the fact that the formation of the dimerized product requires the loss of two stable nitroxide molecules to form a weaker peroxide bond, which is unlikely to occur according to thermodynamics (**Scheme 1. 3**).[10]

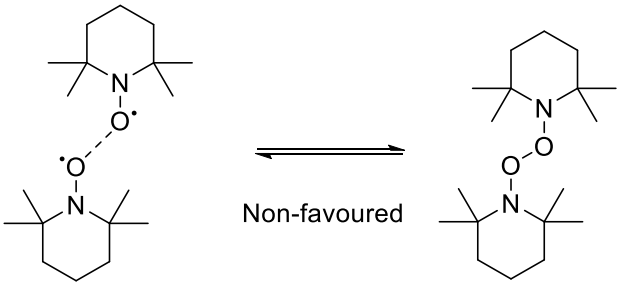

Scheme 1. 3 Theoretical dimerization of TEMPO radical.

The stability of the molecules containing nitroxide radicals depends in the first place on the surrounding of the radical center, which will determine the possible degradation reactions of the nitroxide, a phenomenon known as nitroxide disproportionation, as described in the following sections.[13] The presence of bulky substituents in the α-carbon of the nitroxide group prevents not only the possibility of disproportionation but also the tendency toward dimerization process, especially in the solid-state.[14]

1.4.2 Factors affecting the instabilities of the nitroxide radicals

The nature of the substitution at the nitroxide radical has a higher impact on its stability than the factors that aim to increase the thermodynamic stability. The nitroxide radical is stable by itself due to its electronic structure without additional effects, such as the neighboring group effect. Although certain types of neighboring groups may help on one hand to enhance the thermodynamic stability, on the other hand, it may lower the activation barrier for starting the degradation process, a phenomenon known as nitroxide disproportionation. The following section will discuss effects that lead to the loss of the radical center.[10]

1.4.2.1 The neighboring effect

A good example to fully understand the neighboring effect on the overall stability of nitroxide radical is the nitroxide **1** as shown in **Scheme 1. 4**.

For instance, having a benzene ring as a substituent adjacent to the nitroxide radical leads to electron density delocalization and lower the energy state, thereby increasing the thermodynamic stability. On the other hand, this electron delocalization on the benzene ring increases the chemical reactivity by introducing a new reaction center at the *para* position of the benzene ring which in the presence of another nitroxide radical **1** can dimerize. The dimer, eventually, undergoes rapid disproportion to produce the products **2** and **3**.[10]

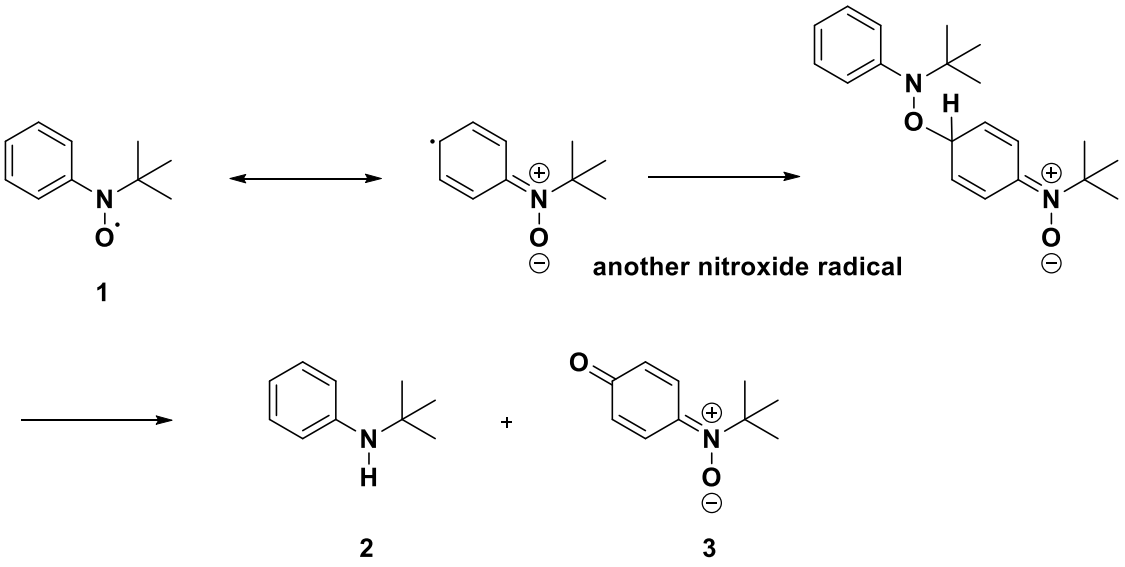

Scheme 1. 4 Degradation mechanism of phenyl substituted nitroxide.

A general rule can be formulated regarding the type of substitution in the α-position to the nitroxide radical: any nitroxide having carbon-carbon or carbon-heteroatom multiple bonds in the α-position displays in general weak stability. For instance, spin density delocalization to the carbon centers of acyl nitroxide **4** makes the stability of such nitroxide weak, due to the higher spin density on the nitroxide oxygen atom, therefore increasing its oxidation power (**Scheme 1. 5**).[15,16]

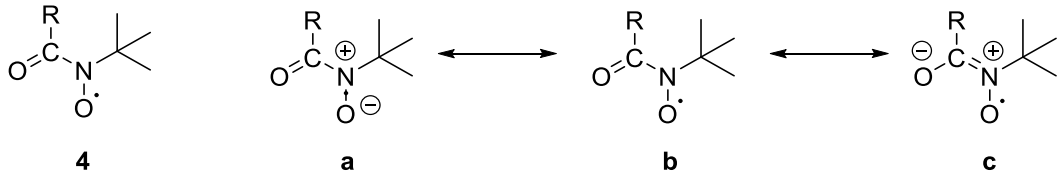

4 **a** **b** **c**

Scheme 1. 5 Disproportionation of acyl nitroxide**.**

Another example of a nitroxide containing carbon-carbon multiple bonds in the α-position to the nitroxide radical is compound **5**. As illustrated in **Scheme 1. 6** the spin density localization to the carbon β-carbon leads to the instability of such nitroxides.[15]

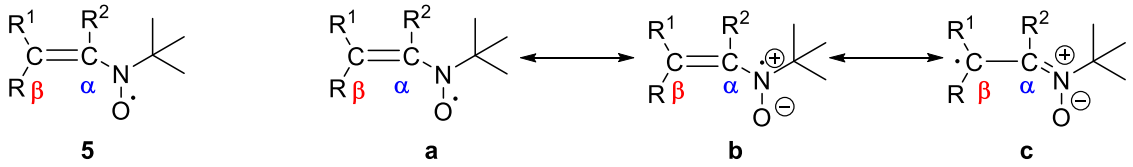

5 **a** **b** **c**

Scheme 1. 6 Weak stability of vinyl nitroxide.

1.4.2.2 The availability of α-hydrogen to the nitroxide radical

The stability of nitroxides connected at the α-position to two sp^3-hybridized carbons is highly dependent on the presence of hydrogen atoms on the hybridized carbon. The presence of even one hydrogen is sufficient to initiate the disproportionation process. The degradation of nitroxide **6** to produce nitrone **7** and hydroxylamine **8** is shown in **Scheme 1. 7**.[17]

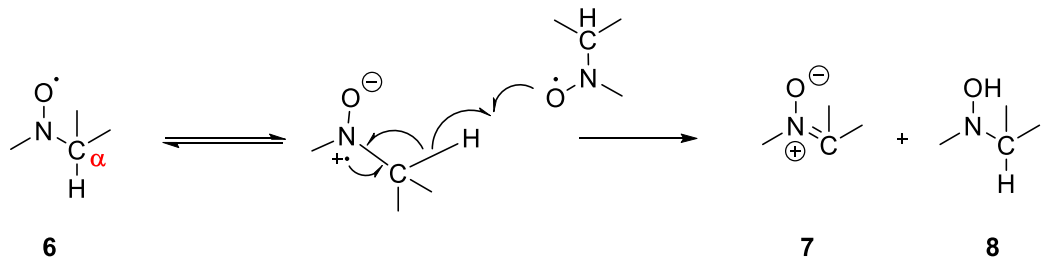

Scheme 1. 7 Disproportionation mechanism of nitroxides containing hydrogen atom bound to α-carbon.

Some nitroxides containing an α-hydrogen atom exist and are stable enough to be isolated, for instance, compound **9**. Another nitroxide radical for example is nitroxide radical **10** that can even exist in both crystal state and in solution. But as a general rule, dialkyl nitroxides that contain α-hydrogens are unstable and cannot be isolated (**Figure 1. 4**).[14,18]

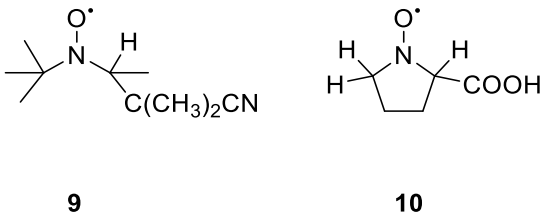

Figure 1. 4 Stable nitroxide radicals containing α-hydrogen.

As a consequence, numerous piperidine, pyrrolidine, pyrroline and isoindoline bis-(*tert*-alkyl) nitroxides lacking α-hydrogens and, thereby, unable to disproportionate to nitrones and hydroxylamines, have been synthesized. All these molecules show outstanding stabilities and highly persistent nitroxides TEMPO **11**, PROXYL **12**, MTSL **13** and TMIO **14** (**Figure 1. 5**) are representative examples of the most stable nitroxides used in laboratories today.[10,19,20]

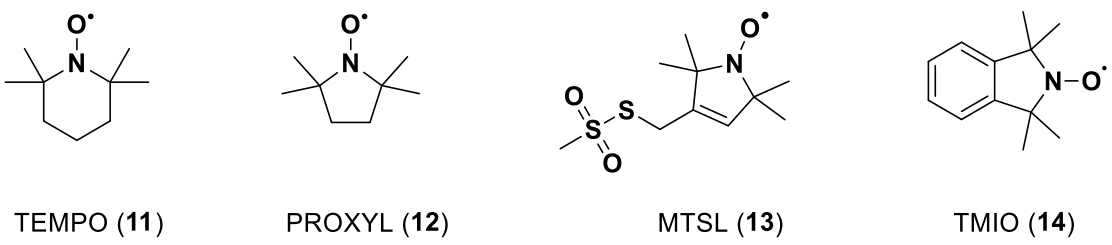

Figure 1. 5 Chemical structures of some stable nitroxides.

In summary, we can conclude that the main factor responsible for the overall stability of the nitroxide is the electron structure of the nitroxide group, which accounts for the thermodynamic stability of the radical center and thereby prevents any possible dimerization. Other factors are steric hindrance around the nitrogen atom of the nitroxide radical along with the absence of α-hydrogen atom in the α-carbon directly connected to the nitroxide radical which is a common feature of most bis-(*tert*-alkyl) nitroxides.[10]

1.4.2.3 The pH effect

The nitroxide radical displays weak basic properties, due to this fact the pH of the solution containing the nitroxide, plays an important role in the nitroxide radical stability. For instance, exposing TEMPO radical to strong acids such as HCl or TFA can disproportionate it to the oxoammonium salt cation and hydroxylamine species. This process can be reversible simply by treating TEMPO with basic buffer in an open flask for several hours to regenerate the NO radical (**Scheme 1. 8**).[21]

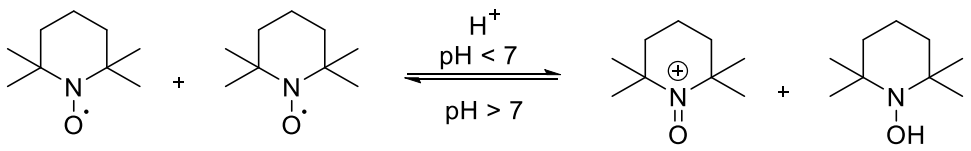

Scheme 1. 8 pH effects on the redox state of nitroxides.

1.5 Synthesis of nitroxide radicals

Many methods have been employed for the generation of nitroxide radicals. In this section, the main synthetic approaches to obtain the paramagnetic species are presented.

1.5.1 Oxidation of hydroxylamines

This method involves mild oxidants such as PbO_2, MnO_2, HNO_2 or H_2O_2 in the presence of Na_2WO_4. This mild oxidation reaction proceeds usually under mild conditions so that only the hydroxylamine group is being oxidized selectively while keeping the other functional groups unaffected. The first stable nitroxides to be produced by oxidation of hydroxylamines are Fremy's salt **15** and nitroxide **16** (**Figure 1. 6**) which were reported by Piloty and Schwerin in 1901.[22]

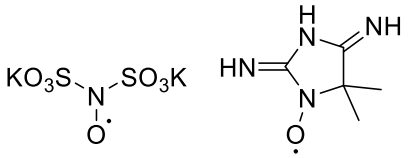

15 **16**

Figure 1. 6 Different nitroxide structures.

To understand the mechanism of the oxidation, hydroxylamine 1**7** was used to study the kinetics of the reaction as shown in **Scheme 1. 9**.

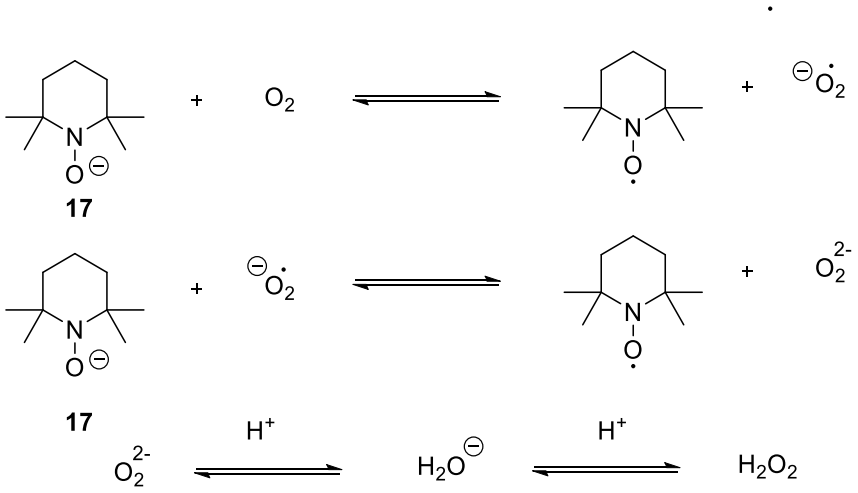

17

17

Scheme 1. 9 Proposed oxidation mechanism of hydroxylamine.

The kinetics of the reaction has been shown to be first-order between oxygen and the hydroxylamine anion. The ionization of the hydroxylamine turned out to be the rate-limiting step for the one-electron oxidation by the oxygen molecule.[23] Many bases were used for the deprotonation of the hydroxylamine. For instance, potassium *tert*-butoxide. The oxidation reaction can be accelerated in the presence of a copper salt. The copper ion in this process is the electron carrier from the hydroxylamine anion to the oxygen molecule.[22]

Generally, the oxidation of hydroxylamines to nitroxides is a mild process, but it may be not true for molecules where the hydroxylamine is part of large heterocycles. The oxidation process is also being affected by the electronic effect of functional groups in different position of the heterocycles.[24,25]

1.5.2 Oxidation of amines

Oxidation of amines is considered to be an important method for the synthesis of nitroxide radicals, although conditions are much more restricted compared to the more flexible conditions of hydroxylamine oxidation. The importance of this method toward the preparation of stable nitroxides is partly due to the fact that modern synthetic chemistry of stable nitroxides started its development strategies from piperidine derivatives, especially the triacetone amine, towards obtaining stable nitroxide radicals. In addition, the availability of tertiary substituted carbon amines is by far more than its corresponding hydroxylamine. As a result of these two reasons, oxidation of amines to nitroxide radicals were developed.[10]

Initial attempts for the synthesis of the first stable piperidine nitroxides were preformed using 2,2,6,6-tetramethylpiperidine as the amine component and sodium tungstate as the oxidant. This method was further developed and improved to the point that water or a methanol mixture of H_2O_2 with sodium tungstate is currently being used as an oxidant cocktail for obtaining stable nitroxide radicals.[10]

Although many nitroxides have been synthesized using this method, the protocol fails for secondary amines with low water solubility. Thus, an alternative oxidation procedure was required to be developed. One of the main alternative methods involved the use of peracids such as meta-Chloroperoxybenzoic acid (MCPA) being a major oxidant in methylene dichloride or chloroform as solvent.[26] The reaction mechanism for the oxidation of secondary amine with peracids is illustrated in **Scheme 1. 10**.[27]

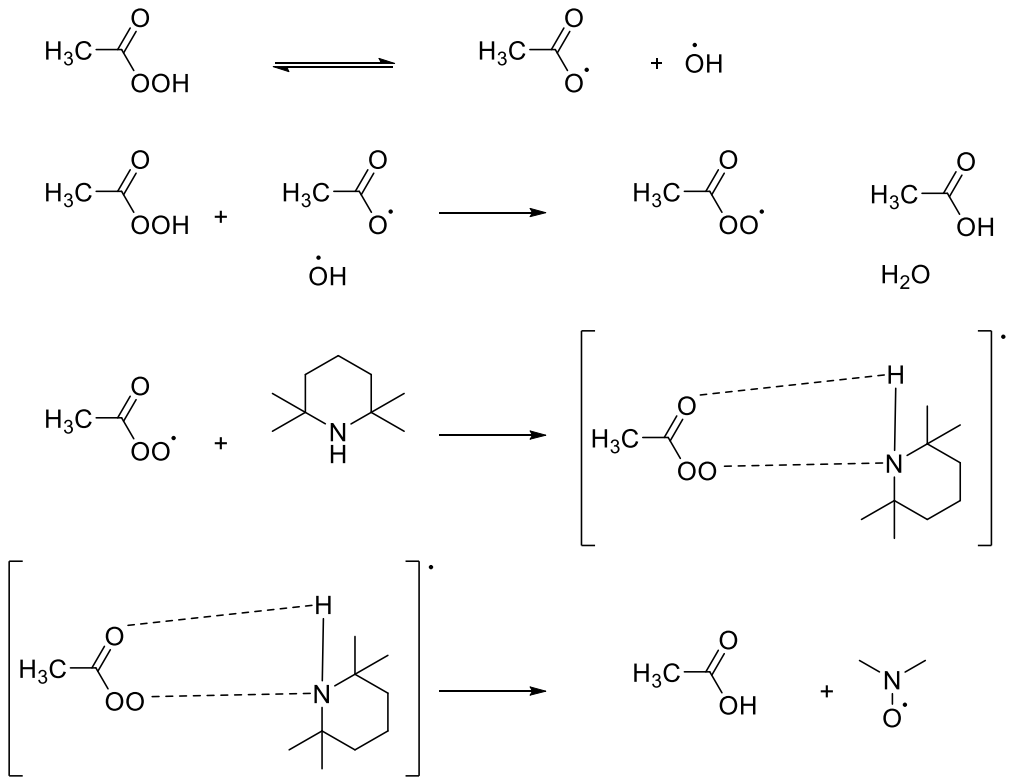

Scheme 1. 10 Proposed mechanism of nitroxide radical formation with peracids.

As shown in **Scheme 1. 10**, the reaction starts with the cleavage of the peracid to generate the peracid radical that in the presence of the secondary amine can form an unstable transition state, and finally decomposes to generate nitroxide radical species.

1.6 Applications of nitroxide radicals

This section will focus on the most important applications of nitroxide radicals.

1.6.1 Nitroxide radicals as spin traps and ROS detection

Spin trapping is a technique widely used in chemistry as well as in biology since the 1960s in which nitrone or nitroso compounds react with short-lived free radical intermediates, to form stable and identifiable nitroxide radicals that can easily be detected using EPR spectroscopy.[27] This section will focus on the use of spin traps to detect radicals in biological systems.[28]

There are mainly two approaches, in which the unstable transient radical can be trapped into more stable ones, which makes their detection using EPR possible.

The first approach depends mainly on the utilization of spin inactive probe which upon interacting with unstable short-lived radicals, they are converted into the spin active and EPR detectable nitroxide. The second approach relies on the utilization of an active spin probe which is EPR active. Upon interacting with unstable short-lived radicals, they are converted into spin inactive products which can be detected by mass spectroscopy (MS).

Conventionally, the most widely used spin trapping molecules are α-phenyl *N*-tertiary-butyl nitrone (PBN) **18** and 5,5-dimethyl-pyrroline *N*-oxide (DMPO) **19** (**Figure 1. 7**), are two examples representing the first approach. Although, these two nitrone derivatives react with short-lived radicals to produce a more stable nitroxide radical that can be detected using EPR spectroscopy. They rather rapidly decompose, due to the **α-hydrogen** next to the paramagnetic center, which can impair its detection using EPR spectroscopy (**Scheme 1. 11**). The lifetime of such spin active adducts are estimated to be within seconds to minutes.[29] In addition to the stability, the detection limit of such spin traps are in the micromolar range, which makes their use to detect free radicals in biological system troublesome.[30,31]

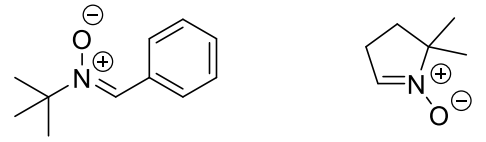

Figure 1. 7 Structures of some nitrone based spin trapping.

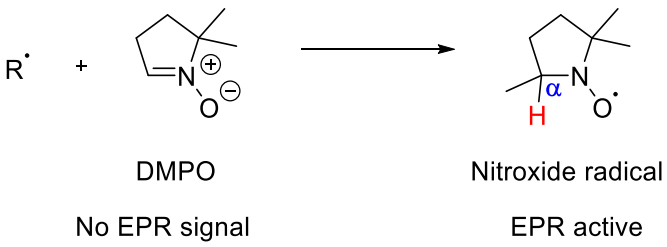

Scheme 1. 11 DMPO spin trapping mechanism of free radicals.

To overcome the problem of the instability of such spin traps, Canistro *et al.* proved that the diamagnetic hydroxylamine precursor of the TEMPO radical can trap reactive oxygen radicals, which converts the diamagnetic hydroxylamine to its corresponding paramagnetic stable radical (TEMPO). The stable radical can be then detected with EPR spectroscopy (**Scheme 1. 12**).[32] However this approach fails to solve the detection limit.

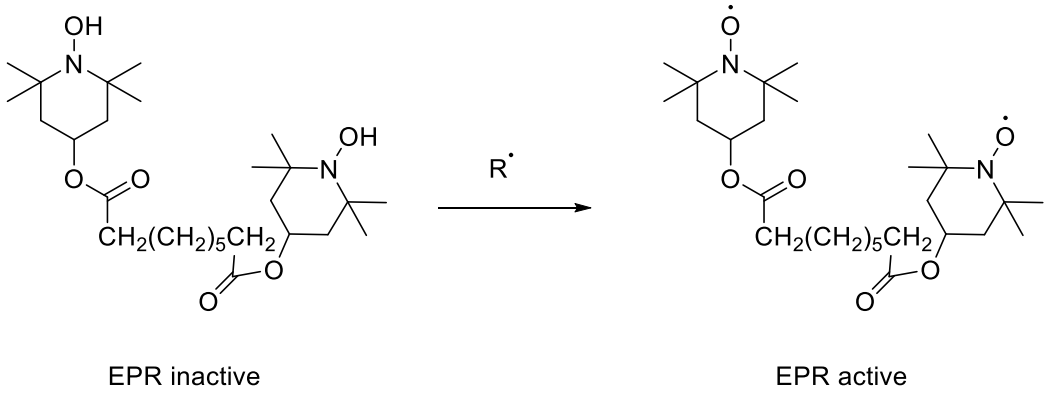

Scheme 1. 12 Spin trapping via the oxidation of hydroxylamine precursor to its corresponding nitroxide radical.

The second approach involves using nitroxide radicals such as TEMPO as a spin trap. TEMPO and other nitroxide radicals are capable of trapping many short-lived radicals.[33] Upon the interaction with short-lived radicals, the paramagnetic stable TEMPO nitroxide is converted to the diamagnetic adducts which can be detected using mass spectrometry (MS).[34]

Recently, a new short radical trap, probe **20** was synthesized that is able to interact with many short-lived radicals and in addition, it provides MS coupled to EPR spectroscopy for identification of different radicals with very high sensitivity (<nM adduct concentrations). This approach can be seen as the combination of the two approaches for trapping unstable radicals. The probe **20** was tested for radical detection. The advantages provided by this method is that a stable adduct can be detected by MS along with the stable nitroxide radical formation that can be detected by EPR spectroscopy (**Scheme 1. 13**).[35,36]

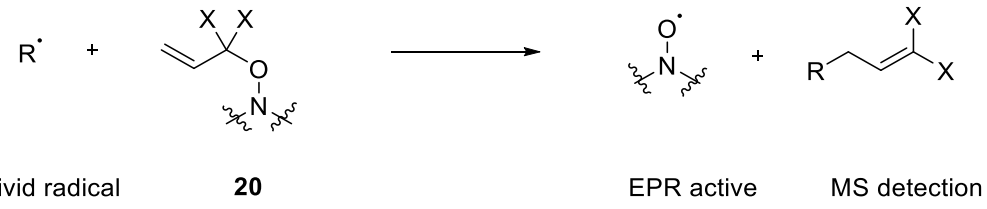

Scheme 1. 13 MS coupled EPR spin trapping for detecting and identifying free radicals.

1.6.2 Nitroxide radicals as fluorescence switching molecules

Nitroxide radicals are known to be efficient quenchers of the excited state of fluorescent molecules. The exact mechanism of this phenomenon can be illustrated in **Scheme 1. 14**.

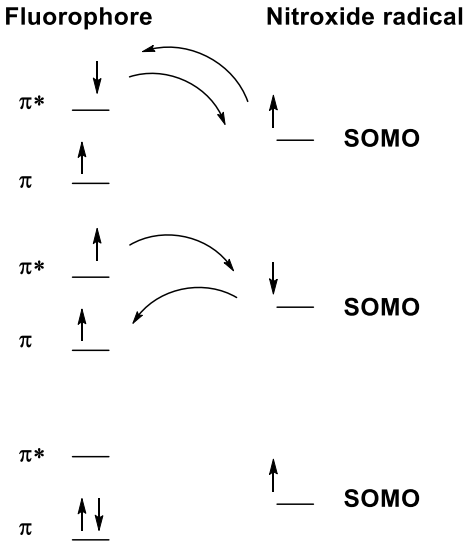

Scheme 1. 14 Mechanism of fluorescent quenching.

The mechanism of quenching can be explained using the electron configuration of the nitroxide radical and the excited state of the fluorophore. As illustrated in **Scheme 1. 14**, the electron on the nitroxide radical is close in energy to the excited state of the fluorophore which allows an electron exchange. This electron exchange between the radical electron and excited state of the fluorophore results in an intersystem crossing or internal conversion to the ground state. This phenomenon was discovered in 1998 by Blought and Simpson, subsequently, this technique has elicited great attention as pre-fluorescent probes.[37]

1.6.3 Nitroxide radicals mediated polymerization NMP

Nitroxide mediated polymerization, known as NMP, uses nitroxide radicals to trap or terminate the growing polymer radicals to form stable alkoxyamine species (**Scheme 1. 15**).[38,39]

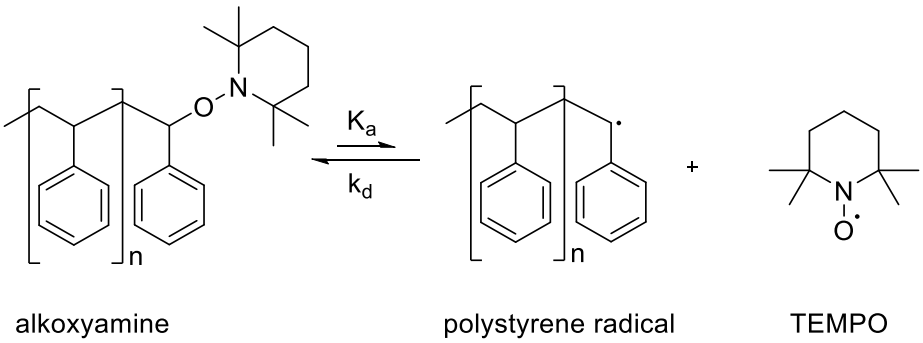

Scheme 1. 15 Nitroxide radical controlled polymerization.

At temperatures of 110-125 ^{o}C, the equilibrium coefficient as shown in **Scheme 1. 15** favors the formation of the non-reactive dormant alkoxyamine. This feature gives the nitroxide radical a great advantage in polymer synthesis, because the risk of termination caused by the addition of another monomer radical can be reduced, and thus the polymer growth is well controlled with narrow molecular weight distributions.[39]

1.6.4 Nitroxide radicals for measuring molecular oxygen "oximetry via EPR"

One of the most important applications in the medicinal field for nitroxide radicals is the ability of these radicals to quantify the amount of dissolved molecular oxygen. The TEMPO radical can interact with molecular oxygen which will lead to the line broadening of the nitroxide EPR spectra, and the degree of line broadening is proportional to O_2 (pO_2). This property is used to assess the availability of oxygen to the injured tissues especially for diabetic patients, whose ability to heal injuries is impaired due to lack of oxygen, which is essential for the healing process.[40]

Molecular oxygen is naturally occurring as triplet radical, but once it is dissolved it cannot be detected directly using EPR spectroscopy, due to its extremely short relaxation time. For that reason, the nitroxide spin label is added for the measurement of oxygen concentration. The changes in the EPR linewidth of the nitroxide spin label are caused by the interaction of the two paramagnetic species, the molecular oxygen, and the nitroxide spin label. The broadening of the EPR spectra allows the measurement of pO_2 or O_2 concentration.[41]

1.6.5 Nitroxide radicals in spin immunoassays

During the Vietnam War (1954-1975), the US army adopted one of the first widely used immunoassays for screening purposes to detect any drug abuse and specifically for morphine at that time. The immunoassay was based on the tumbling or rotation of the nitroxide radical when it is conjugated to the drug of interest and is required to test for either the absence or presence of an antibody for that specific drug. The immunoassay relies on the difference between the rotation of free versus immobilized drug in a solution. The hyperfine coupling which is produced as a consequence of the coupling between the unpaired electron and the nitrogen nucleus results in three lines at different resonance frequencies.

This hyperfine coupling is independent with respect to the orientation of the nitroxide in a magnetic field. Thus, the anisotropic hyperfine coupling can adopt many possible orientations in the solution having the spin-labelled drug immobilized by the existing antibody which eventually results in line broadening. However, fast and free rotation of the nitroxide drug conjugate will produce a sharp three-line spectrum (**Figure 1. 8**).[42]

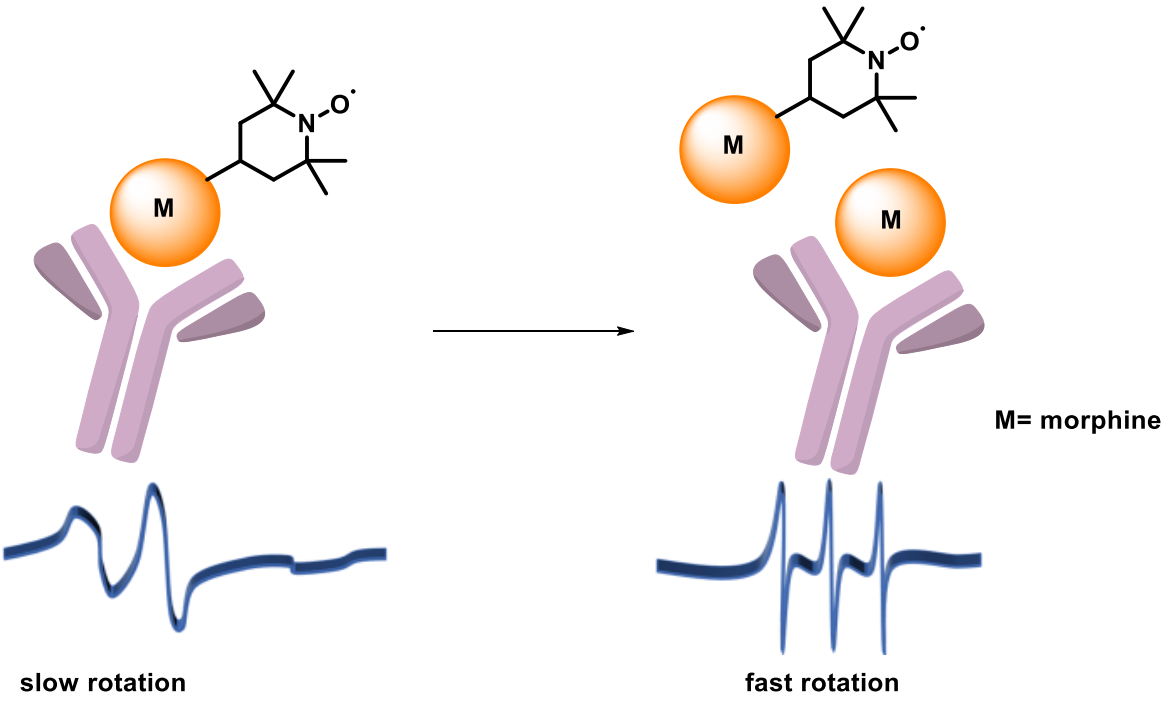

Figure 1. 8 Schematic representation for the principle of spin immunoassays.

As illustrated in **Figure 1. 8** in patients with no morphine drug abuse, the rate of tumbling is reduced quite significantly. When the nitroxide-labelled morphine binds to its anti-morphine antibodies, line broadening will occur.

On the other hand, in patients with morphine drug abuse, the binding of the nitroxide labelled morphine is inhibited due to the presence of free morphine, and the spectral lines become sharp. This was the base of spin immunoassays which was adopted by the US Army for screening its personal for morphine drug abuse during the Vietnam War.[42]

1.6.6 Pharmaceutical drug binding to proteins by nitroxide spin-labelling via EPR spectroscopy

The binding of active pharmaceutical drugs to target proteins, especially those that play vital roles as transporters such as human serum albumin, generated a great deal of attention in the field of drug-delivery systems.[43,44]

Protein drug binding can be studied by several techniques, such as NMR spectroscopy, isothermal titration calorimetry (ITC) and fluorescence spectroscopy. EPR spectroscopy can be also used as an alternative technique. Hinderberger *et al*. in 2016, investigated many active pharmaceutical drug bindings to albumin via EPR spectroscopy. Briefly, after spin-labelling of the active pharmaceutical drugs, EPR spectroscopy was used to discriminate between the amount of free rotating versus tightly bounded spin-labelled drugs to albumin. This was achieved by analyzing the rotation speed of the labelled drugs upon binding.[44]

1.6.7 Antitumor enhancing effect of nitroxide radicals

TEMPO radical derivatives have demonstrated anticancer activities. For instance, TEMPOL **21** inhibited the growth of C6 glioma cells both *in vivo* and *in vitro* experiments (**Figure 1. 9**). TEMPOL is known to target mitochondria and induce apoptosis through a radical dependent mechanism.[45]

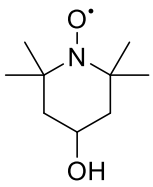

21

Figure 1. 9 TEMPOL radical used as antitumor against C6 glioma.

Suy *et al*. demonstrated that treating prostate tumor cells with TEMPOL nitroxide can also induce apoptosis through a caspase-dependent mechanism. In addition to that, the nitroxide can also arrest the cell cycle in the G2/M phase and decrease the number of growing cells in the S phase. The study resulted in an interesting conclusion that the TEMPO radical alone could be a potential novel small molecule as antineoplastic agent.[46]

Nitroxide radicals are also known to have a synergistic effect when attached to antineoplastic drugs.[47] Antitumor drugs such as chlorambucil **22** and doxorubicin **23** were conjugated or co-administered with the TEMPO radical. For example, the activity of the spin-labelled adducts **24** and **25**, were proven to be more active compared to chlorambucil **22** alone (**Figure 1. 10**). More interesting, the TEMPO radical, when given with Doxorubicin **23** for the treatment of colon cancer, can significantly minimize the side effects associated with doxorubicin. The mitochondrial reactive oxygen species play an important role in doxorubicin-induced platelet apoptosis. Therefore co-administration of TEMPO radicals with doxorubicin can be effective in minimizing the side effects associated with doxorubicin.[48]

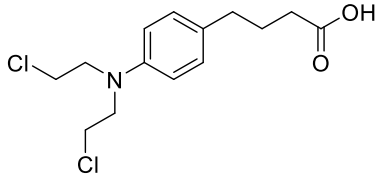

Chlorambucil (**22**)

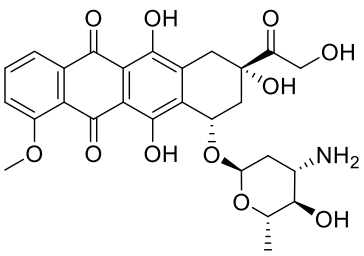

Doxorubicin (**23**)

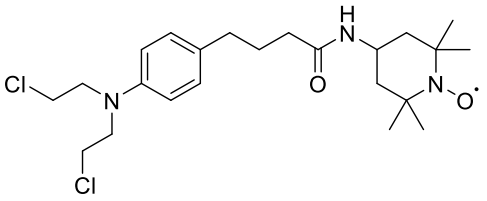

Chlorambucil TEMPO amide conjugate (**24**)

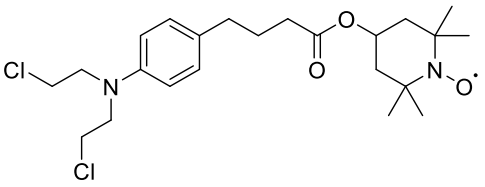

Chlorambucil TEMPO ester conjugate (**25**)

Figure 1. 10 TEMPO radical conjugation or co-administered to antineoplastic agents.

1.6.8 Nitroxide radicals as "site-directed spin labelling" (SDSL) of biologically active molecules

Site-directed spin labelling (SDSL) is a technique where a stable nitroxide radical is attached to specific sites of molecules of interest such as proteins, peptides or peptaibols, in combination with EPR. This section will give an overview of the applications of SDSL.

1.6.8.1 Site-directed spin labelling of proteins for secondary structure determination

The most common spin label used is 2,2,5,5-tetramethyl-1-oxyl-3-methyl methanethiosulfonate (MTSL) **13** (**Figure 1. 5**). This probe can be ligated to sulfhydryl side chains of cysteine amino acids.[49] One example of a protein studied by this method is T4 lysozyme (T4L), which is characterized by an α-helix as demonstrated by X-ray crystallography. Due to this distinct structure, T4L was used as a model for the SDSL protocol in order to determine the α-helicity using EPR spectroscopy. Briefly, a set of eight amino acid residues situated on the external helix were spin-labelled discretely and their accessibilities to broadening due to interaction with oxygen were plotted against the amino acid sequence (**Figure 1. 11**). A perfect behavior was observed when compared with spin wave function with periodicity of 3.6 which is characteristic of α-helicity.[49]

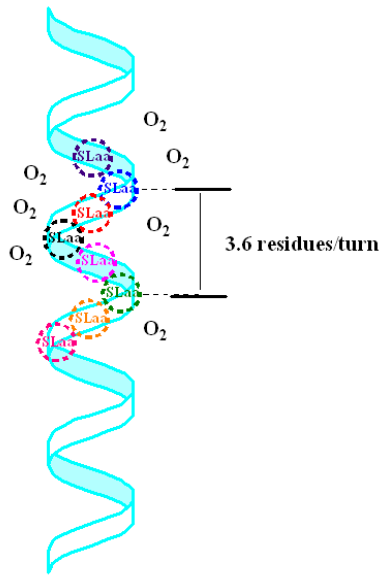

Figure 1. 11 A schematic representation of an α-helix.

1.6.8.2 Studying peptide-membrane interaction

Besides proteins, SDSL was also applied to peptides, especially to those peptides that partition between the membrane and the aqueous phase. Under equilibrium conditions where the distribution of the peptide between the membrane and the aqueous phase is reached, one can observe two sets of nitroxide signals that correspond to the signals from the two populations. This allows to conclude and determine the partition coefficient of the peptide without the need to perform any separation between the free and membrane-bounded peptide. One example is the membrane pore-forming antimicrobial peptide CM15. CM15 is a linear, synthetic hybrid antimicrobial peptide composed of the first seven residues of cecropin A and residues 2-9 of the bee venom peptide melittin (Ac-KWKLFKKIGAVLKVL-amide). An analogue was synthesized containing cysteine and replacing leucine at position 4. The spin-labelling step on the modified peptide analogue was done using MTSL spin label (**Figure 1. 12**).[50]

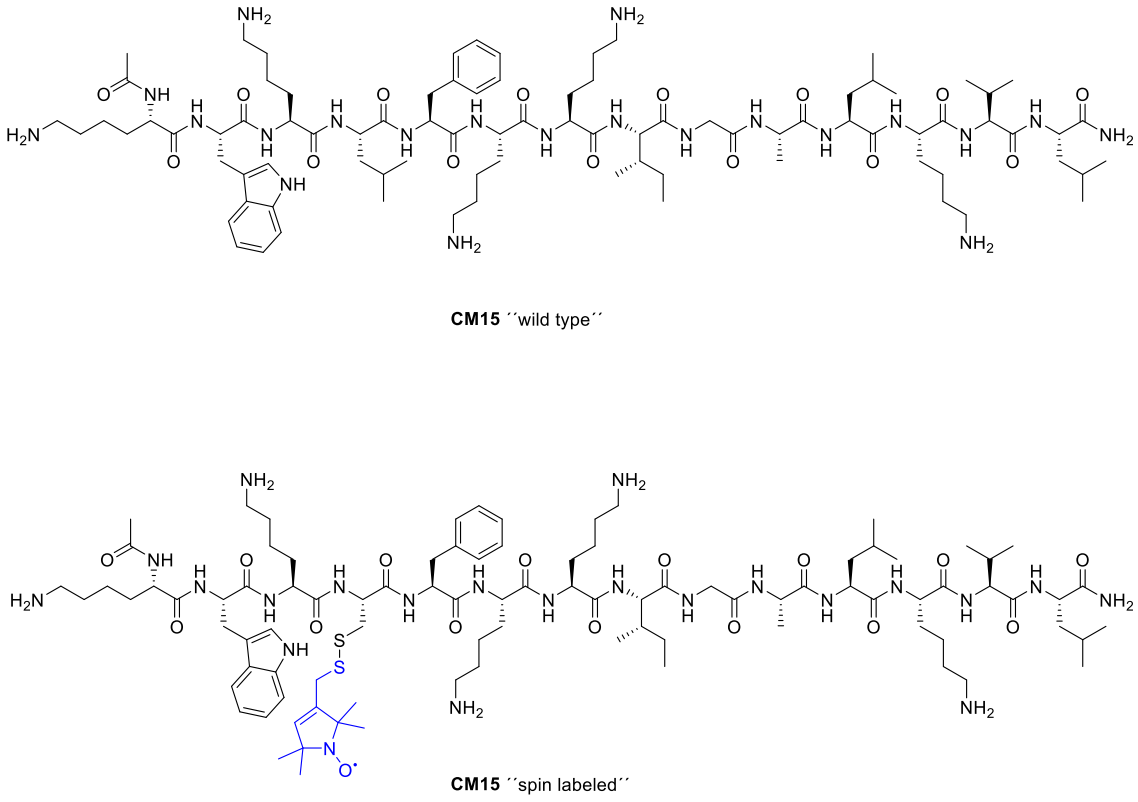

Figure 1. 12 Structure of spin-labelled of the antimicrobial peptide CM15.

The EPR spectrum was recorded for the spin-labelled CM15 peptide, in the presence and absence of liposomes. The fraction of the bound peptide was quantitatively determined by the reduction in signal amplitude as compared to the sample without liposomes.[50]

1.6.8.3 Site-directed spin labelling of peptaibols

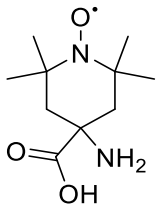

26

Figure 1. 13 Structure of TOAC nitroxide used for spin-labelling.

Peptaibols are naturally occurring helical peptides consisting of short sequences usually from seven up to twenty amino acids. Some of those amino acids are non-encoded such as α-aminoisobutyric acid and hydroxyproline. More interesting features include their N-terminus being acetylated and the C-terminus being reduced into alcohol.[51] Peptaibols display a variety of bioactivities such as antitumor, antibiotic and antiviral activities. Their amphipathic nature allows them to form voltage-dependent channels in cell membranes which leads to cell death due to the holes being created by these special peptides. The peptaibol membrane interactions make EPR spectroscopy with SDSL an ideal technique for studying such interactions.[52] 2,2,6,6-tetramethyl-piperidine-1-oxy-4-amino-4-carboxylic acid TOAC **26** (**Figure 1. 13**) are widely used in SDSL of peptaibols. Via solid-phase peptide synthesis, a peptaibol analogue is synthesized where the α-aminoisobutyric acid is being replaced with TOAC. Since both TOAC **26** and α-aminoisobutyric acid **27** (**Figure 1. 14**) are both strong α-helix inducers, TOAC is ideal for SDSL analyses of peptaibols.[53]

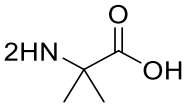

27

Figure 1. 14 Structure of the non-encoded amino acid α-aminoisobutyric acid.

1.7 Chemical methods for site-directed spin labelling introduction

As described before, SDSL is a method where nitroxide is introduced by forming a covalent bond to a specific site on a protein or peptide or in general, to a biomolecule that is of interest and intended to be studied using EPR spectroscopy. This section illustrates the most common reactions used for the introduction of nitroxide spin-labelling (**Figure 1. 15**).

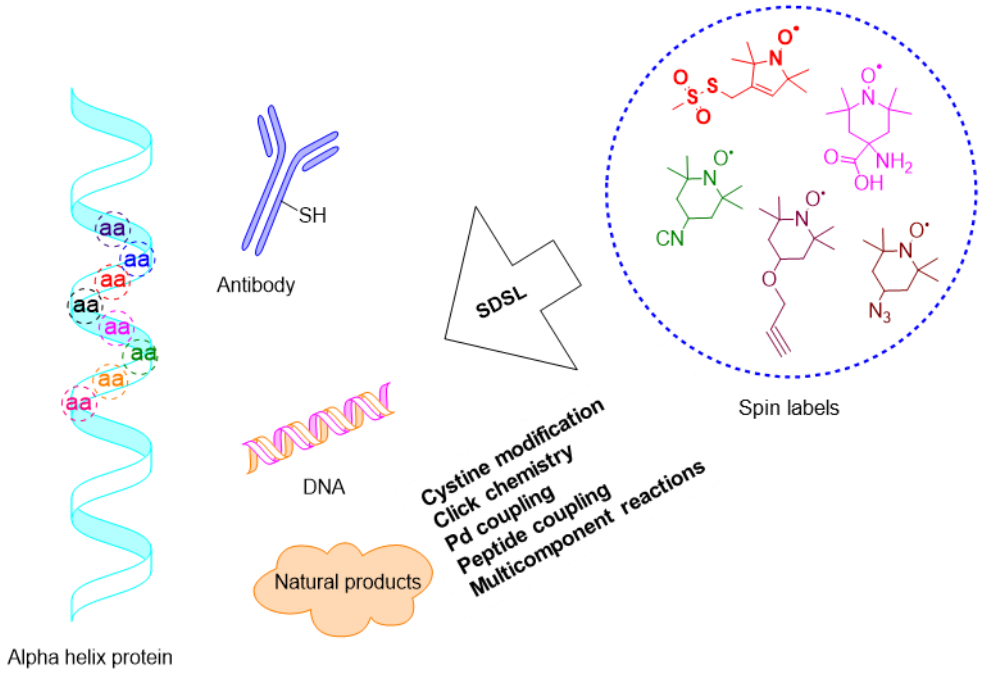

Figure 1. 15 Spin labels used for SDSL of biologically active molecules.

1.7.1 Site-directed spin labelling via cysteine residues side chains

The most common nitroxide spin label used is MTSL **13** (**Figure 1. 5**) and maleimide spin label 5-MSL **28** (**Scheme 1. 16**). This method requires the reactivity of the sulfhydryl group of the cysteine amino acid for spin label incorporation, any other native cysteines within the protein must be either replaced with another amino acid or proven to be unreactive to the spin-labelling step. Usually, the desired position for SDSL is prepared by introducing cysteine into the protein by site-directed mutagenesis, while other cysteine

residues can be replaced by serine or alanine. Many reports have been conducted, where a large number of proteins have been mutated to cysteine and spin-labelled without loss of function.[54]

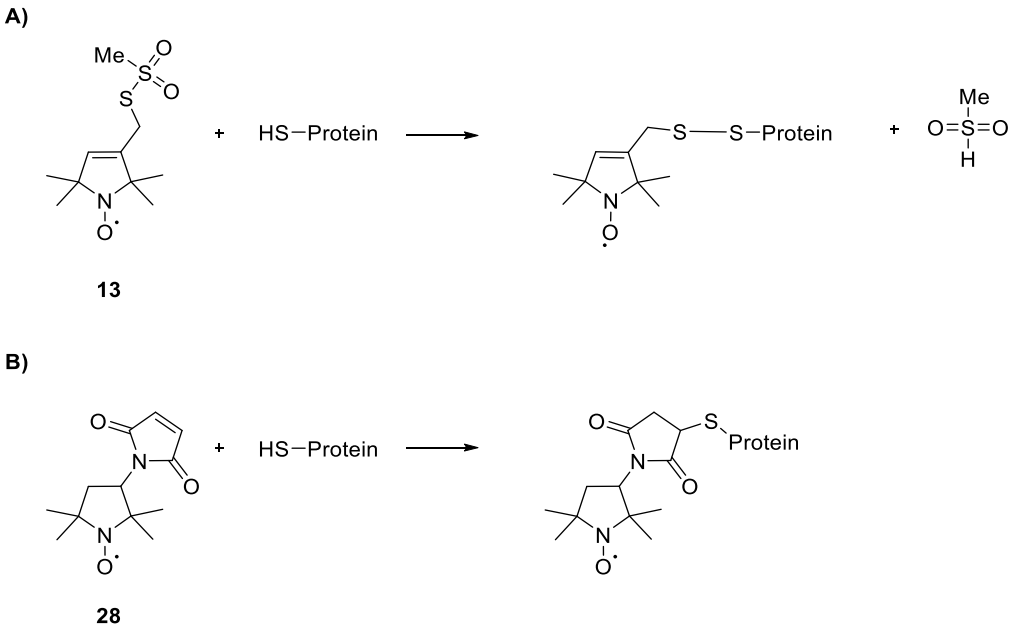

Scheme 1. 16 Spin-labelling of cysteine by A) MTSL and B) 5-MSL.

1.7.2 Site-directed spin labelling via non-sense suppressor methodology

This method requires the genetic incorporation of specific amino acids at the nonsense codon such as the amber codon,[55] Drescher *et al*. reported the incorporation of 4-iodo-L-phenylalanine into a protein. Spin-labelling was successfully accomplished with the boronic acid spin label **29** (NOBA) utilizing Suzuki-Miyaura coupling (**Scheme 1. 17**).[37]

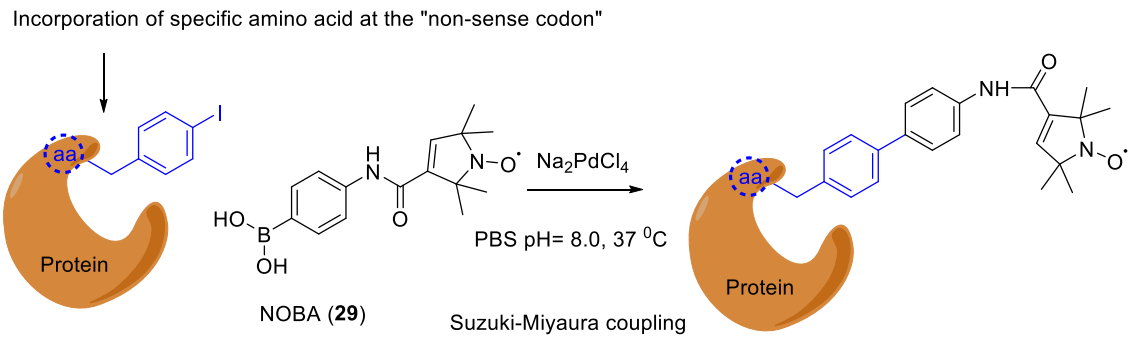

Scheme 1. 17 SDSL of proteins synthesized using nonsense suppressor methodology.

1.7.3 Site-directed spin labelling via solid-phase synthesis

TOAC **26** (**Figure 1. 13**) is incorporated into peptides or small proteins via peptide coupling using Fmoc solid-phase strategy (**Scheme 1. 18**). The incorporation of TOAC into model compounds such as the peptide hormone angiotensin II and some of its analogues were successfully accomplished.[56,57] One disadvantage of using TOAC is the disproportion reaction that occurs during peptide cleavage. However, ammonium hydroxide treatment at pH 10 for several hours was found to be successful to regenerate the nitroxide radical.[57]

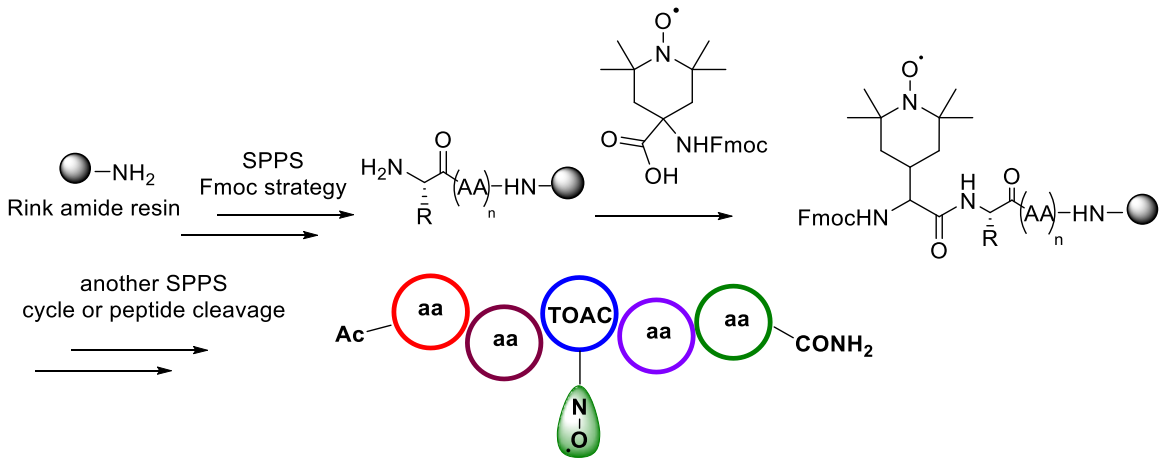

Scheme 1. 18 Peptide spin-labelling using TOAC via Fmoc solid-phase strategy.

1.7.4 Site-directed spin labelling via click chemistry

The click chemistry offers major advantages by providing fast and highly selective, biocompatible reaction between azide and alkyne groups. It can be carried out as a catalyzed azide-alkyne cycloaddition (CuAAC) or as strain promoted azide-alkyne cycloaddition (SPAAC), which is a copper-free click reaction. Both strategies were shown to be successful for SDSL of various biomolecules (**Scheme 1. 19**).[54]

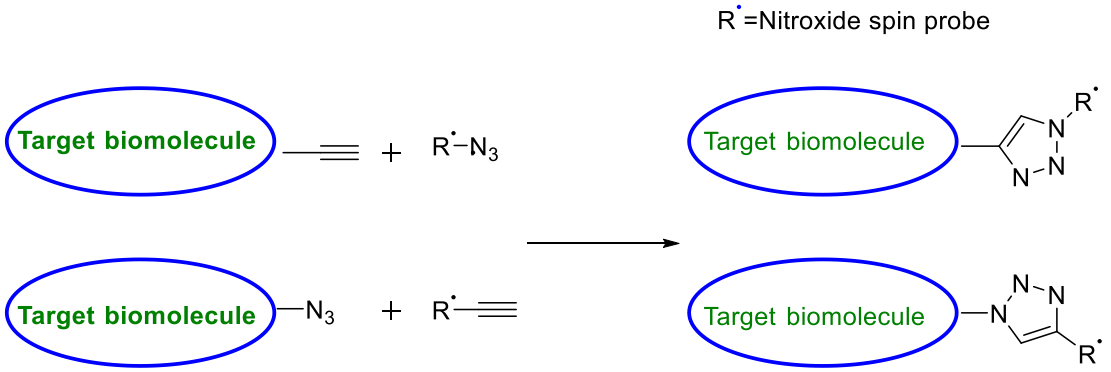

Scheme 1. 19 SDSL of various target biomolecules via click chemistry.

1.7.5 Ugi-multicomponent reaction as a new site-directed spin labelling strategy

Multicomponent reactions (MCRs), as the name implies, are chemical reactions where three or more components are brought together in one pot and in a single transformation. One obtains a peptide like core structure with the enormous advantage of obtaining highly diverse and complex molecules in a single step.[58]

The reaction itself is ideal to aim for highly diverse end products in one step. In this presented Ph.D. work, we have selected Ugi-reaction, or so-called isocyanide-based multicomponent reactions (IMCR), to be our synthetic method of choice since it has many advantages over other chemical methods such as; simple reaction setup, high yields, high atom economy and water as the only byproduct. These facts make the reaction environmentally friendly (**Scheme 1. 20**).[59]

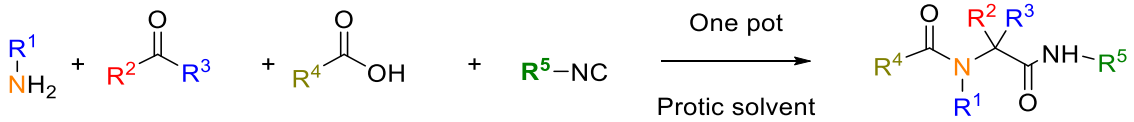

Scheme 1. 20 Ugi-multicomponent reaction.

The reaction as shown in **Scheme 1. 20** utilizes four different components viz., an amine, oxo-component which can be ketone or aldehyde followed by carboxylic acid moiety and an isocyanide. The reaction mechanism begins with the imine formation of the amine and the oxo-component. The formation of the imine is a prerequisite for obtaining the final product. After forming the imine, proton transfer from the acid component will lead to nitrogen protonation activating the imine for the next step.

The iminium cation along with the acid anion will react with the highly nucleophilic isocyanide forming an intermediate. In the end, the irreversible acyl transfer rearrangement (Mumm rearrangement) takes place to yield the final product (**Scheme 1. 21**).

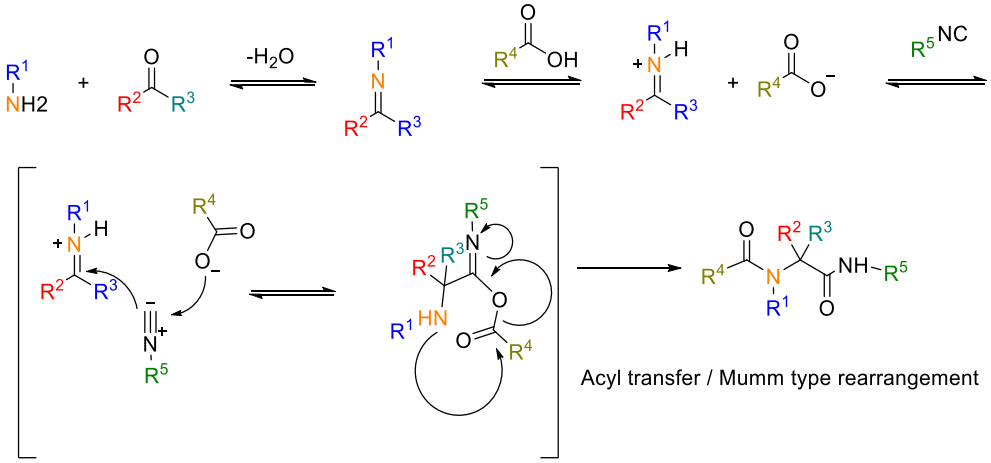

Scheme 1. 21 Ugi-multicomponent reaction mechanism.

Although a variety of methods have been already described for the SDSL of various biomolecules, at the beginning of the present study, the utilization of Ugi-reaction (Ugi-4CR) for SDSL of biologically active molecules has not been mentioned. The Ugi-approach allows for fast and efficient synthesis of diverse chemical spin-labelled probes for various applications. The introduction of a new chemical ligation method for SDSL was the driving force for investigating the applicability of isocyanide based Ugi-reaction for incorporating nitroxide radical for SDSL.

1.8 Aims of this Ph.D. work

The aim of this presented thesis is the introduction of Ugi-reaction as a new methodology for SDSL, and for generating new hybrid molecules, for achieving the following goals:

- Synthesis of spin-labelled cyclic peptides (diketopiperazines), and non-cyclic peptide-peptoids via Ugi-reaction.
- Synthesis of spin-labelled terpene adducts for achieving new antitumor drugs and the utilization of the convertible isocyanide for post-Ugi-modification for achieving further goals.
- Synthesis of prefluorescent nitroxide rhodamine adducts which allow for mitochondrial ROS detection.

1.9 References

(1) Salikhov, K. M.; Zavoiskaya, N. E. *Reson.* **2015**, 20, 963–968.
(2) Mayo, F. R. *J. Polym. Sci. B Polym. Lett. Ed.* **1974**, 12, 536–538.
(3) Blatter, H. M.; Lukaszewski, H. *Tetrahedron Lett.* **1968**, 9, 2701–2705.
(4) Goldfarb, D.; Stoll, S. *Modern EPR Spectroscopy;* John Wiley & Sons Incorporated, Newark, **2018**.
(5) Abragam, A. *The principles of nuclear magnetism,* Reprinted; Oxford Univ. Press, Oxford, **2007**.
(6) Elschner, B. *Ber. Bunsenges. Phys. Chem.* **1983**, 87, 1230.
(7) a) Drescher, M.; Jeschke, G.; Bordignon, E. *EPR spectroscopy*: Applications in chemistry and biology; Springer, Berlin, **2012**; b) Eichhoff, U.; Höfer, P. *Low Temp. Phys.* **2015**, 41, 62–66; c) Roessler, M. M.; Salvadori, E. *Chem. Soc. Rev*. **2018**, 47, 2534–2553;
(8) Kocherginsky, N.; Swartz, H. M.; Sentjurc, M. *Nitroxide spin labels*: Reactions in biology and chemistry; CRC Press, Boca Raton, Fla., **1995**.
(9) Johnson, D. H.; Rogers, M. A. T.; Trappe, G. *J. Chem. Soc.* **1956**, 1093.
(10) Volodarskij, L. B.; Reznikov, V. A.; Ovărenko, V. I. *Synthetic chemistry of stable nitroxides;* CRC Press, Boca Raton, Fla., **1994**.
(11) Breuer, E.; Nielsen, A.; Aurich, H. G.; Patai, S.; Rappoport, Z. *Nitrones, nitronates, and nitroxides;* Wiley, Chichester England, New York, **1989**.
(12) Thomas, D. D. *Redox Biol.* **2015**, 5, 225–233.
(13) Nilsen, A.; Braslau, R. *J. Polym. Sci. A Polym. Chem.* **2006**, 44, 697–717.
(14) Keana, J. F. W. *Chem. Rev.* **1978**, 78, 37–64.
(15) Aurich, H. G.; Hahn, K.; Stork, K. *Chem. Ber.* **1979**, 112, 2776–2785.
(16) Bologa, U.; Balaban, A. T.; Grecu, N.; Negoita, N.; Caproiu, M. T.; Walter, R. I. *J. Org. Chem.* **1987**, 52, 4176–4179.
(17) Ingold, K. U.; Adamic, K.; Bowman, D. F.; Gillan, T. *J. Am. Chem. Soc.* **1971**, 93, 902–908.
(18) Lin, J. S.; Tom, T. C.; Olcott, H. S. *J. Agric. Food Chem.* **1974**, 22, 526–528.
(19) Grigor'ev, I. A.; Volodarsky, L. B.; Starichenko, V. F.; Shchukin, G. I.; Kirilyuk, I. A. *Tetrahedron Lett.* **1985**, 26, 5085–5088.
(20) Glidewell, C.; Rankin, D. W. H.; Robiette, A. G.; Sheldrick, G. M.; Williamson, S. M. *J. Chem. Soc., A* **1971**, 478.
(21) Martin, L.; Vita, C.; Ivancich, A.; Formaggio, F.; Toniolo, C. *J. Pept. Res.* **2001**, 58, 424–432.
(22) Piloty, O.; Schwerin, B. G. *Ber. Dtsch. Chem. Ges.* **1901**, 34, 1870–1887.
(23) Keana, J. F. W.; Norton, R. S.; Morello, M.; van Engen, D.; Clardy, J. *J. Am. Chem. Soc.* **1978**, 100, 934–937.
(24) Zhukova, I. Y.; Kagan, E. S.; Smirnov, V. A. *Chem. Heterocycl. Compd.* **1992**, 28, 64–66.
(25) Volodarskij, L. B., Ed. *Imidazoline nitroxides;* CRC Press, Boca Raton, Fla., **1988**.
(26) Zakrzewski, J.; Jezierska, J.; Hupko, J. *Org. Lett.* **2004**, 6, 695–697.
(27) Griffiths, P. G.; Rizzardo, E.; Solomon, D. H. *Tetrahedron Lett.* **1982**, 23, 1309–1312.
(28) Rowlands, C. C.; Murphy, D. M. Chemical Applications of EPR. In *Encyclopedia of Spectroscopy and Spectrometry*; Elsevier, **1999**, pp 190–198.
(29) Buettner, G. R. *Free Radic. Res. Commun.* **1993**, 19, S79-87.
(30) Ranguelova, K.; Mason, R. P. *Magn. Reson.Chem.* **2011**, 49, 152–158.
(31) Fontmorin, J. M.; Burgos Castillo, R. C.; Tang, W. Z.; Sillanpää, M. *Water Res.* **2016**, 99, 24–32.
(32) Canistro, D.; Vivarelli, F.; Cirillo, S.; Babot Marquillas, C.; Buschini, A.; Lazzaretti, M.; Marchi, L.; Cardenia, V.; Rodriguez-Estrada, M. T.; Lodovici, M.; Cipriani, C.; Lorenzini, A.; Croco, E.; Marchionni, S.; Franchi, P.; Lucarini, M.; Longo, V.; Della

Croce, C. M.; Vornoli, A.; Colacci, A.; Vaccari, M.; Sapone, A.; Paolini, M. *Sci. Rep.* **2017**, 7, 2028.
(33) a) Busfield, W.K.; Heiland, K.; Jenkins, I. D. *Tetrahedron Lett.* **1994**, 35, 6541–6542; b) Busfield, W.K.; Heiland, K.; Jenkins, I. D. *Tetrahedron Lett.* **1995**, 36, 1109–1112;
(34) Wright, P. J.; English, A. M. *J. Am. Chem. Soc.* **2003**, 125, 8655–8665.
(35) Wang, X.; Zeng, H.; Zhao, L.; Lin, J.-M. *Talanta* **2006**, 70, 160–168.
(36) Conte, M.; Chechik, V. *Chem. Commun.* **2010**, 46, 3991–3993.
(37) Kugele, A.; Braun, T. S.; Widder, P.; Williams, L.; Schmidt, M. J.; Summerer, D.; Drescher, M. *Chem. Commun.* **2019**, 55, 1923–1926.
(38) W. Ma, J.; F. Cunningham, M.; B. McAuley, K.; Keoshkerian, B.; Georges, M. *Chem. Eng. Sci.* **2003**, 58, 1177–1190.
(39) Chauvin, F.; Dufils, P.-E.; Gigmes, D.; Guillaneuf, Y.; Marque, S. R. A.; Tordo, P.; Bertin, D. *Macromolecules* **2006**, 39, 5238–5250.
(40) Desmet, C. M.; Lafosse, A.; Vériter, S.; Porporato, P. E.; Sonveaux, P.; Dufrane, D.; Levêque, P.; Gallez, B. *Plos One* **2015**, 10, e0144914.
(41) Swartz, H. M.; Hou, H.; KHAN, N.; Jarvis, L. A.; Chen, E. Y.; Williams, B. B.; Kuppusamy, P. *Adv. Exp. Med. Biol.***2014**, 812, 73–79.
(42) Wild, D. G.; John, R. *The immunoassay handbook*: Theory and applications of ligand binding, ELISA and related techniques, 4th ed.; Elsevier, Amsterdam, **2013**.
(43) Zunszain, P. A.; Ghuman, J.; Komatsu, T.; Tsuchida, E.; Curry, S. *BMC structural biology* **2003**, 3, 6.
(44) Reichenwallner, J.; Hinderberger, D. *Biochim. Biophys. Acta* **2013**, 1830, 5382–5393.
(45) Suy, S.; Mitchell, J. B.; Samuni, A.; Mueller, S.; Kasid, U. *Cancer* **2005**, 103, 1302–1313.
(46) Zhao, H.; Meng, X.; Yuan, H.; Lan, M. *Chem. Pharm. Bull.* **2010**, 58, 332–335.
(47) Zhang, K.; Monteiro, M. J.; Jia, Z. *Polym. Chem.* **2016**, 7, 5589–5614.
(48) Wang, Z.; Wang, J.; Xie, R.; Liu, R.; Lu, Y. *Int. J. Mol. Sci.* **2015**, 16, 11087–11100.
(49) Hubbell, W. L.; Mchaourab, H. S.; Altenbach, C.; Lietzow, M. A. *Structure* **1996**, 4, 779–783.
(50) Chugh, J. K.; Wallace, B. A. *Biochm. Soc. Trans.* **2001**, 29, 565–570.
(51) Dalzini, A.; Bergamini, C.; Biondi, B.; Zotti, M. de; Panighel, G.; Fato, R.; Peggion, C.; Bortolus, M.; Maniero, A. L. *Sci. Rep.* **2016**, 6.
(52) Biondi, B.; Peggion, C.; Zotti, M. de; Pignaffo, C.; Dalzini, A.; Bortolus, M.; Oancea, S.; Hilma, G.; Bortolotti, A.; Stella, L.; Pedersen, J. Z.; Syryamina, V. N.; Tsvetkov, Y. D.; Dzuba, S. A.; Toniolo, C.; Formaggio, F. *Biopolymers* **2017**.
(53) Qin, P. Z.; Dieckmann, T. *Curr. Opin. Struct. Biol.* **2004**, 14, 350–359.
(54) Klare, J. P. Chemistry of Spin Labelling. In *Encyclopedia of Biophysics*; Roberts, G. C., Ed.; Springer Berlin: Berlin, **2013**, pp 287–293.
(55) Nakaie, C. R.; Goissis, G.; Schreier, S.; Paiva, A. C. *Braz. J. Med. Biol. Res.* **1981**, 14, 173–180.
(56) Nakaie, C. R.; Silva, E. G.; Cilli, E. M.; Marchetto, R.; Schreier, S.; Paiva, T. B.; Paiva, A. C. M. *Peptides* **2002**, 23, 65–70.
(57) Haugland, M. M.; El-Sagheer, A. H.; Porter, R. J.; Peña, J.; Brown, T.; Anderson, E. A.; Lovett, J. E. *J. Am. Chem. Soc.* **2016**, 138, 9069–9072.
(58) Dömling, A.; Ugi, I. *Angew. Chem. Int. Ed.* **2000**, 39, 3168–3210.
(59) Müller. *Multicomponent Reactions, Volume 1;* Georg Thieme Verlag, Stuttgart, **2014**.

Chapter 2

Spin-labelled diketopiperazines and peptide-peptoid chimera by Ugi-multi-component reactions

*Abstract**

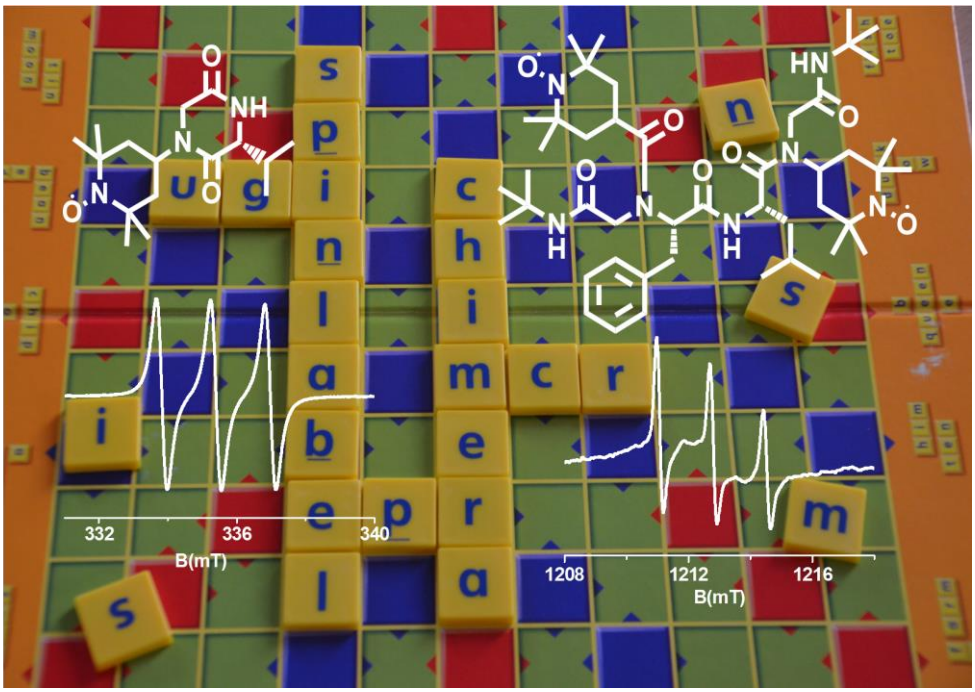

For the first time, spin-labelled biological active compounds for site-directed spin labelling (SDSL) have been obtained by isonitrile-based multi-component reactions (IMCRs). The typical IMCR Ugi-protocols offer a simple experimental setup that allows structural diversity by which spin-labelled diketopiperazines (DKPs) and peptide–peptoid chimera have been synthesized by this method. The reaction keeps the paramagnetic spin label intact and offers a simple and versatile route to a diverse range of new and chemically diverse spin labels.

* This Chapter was published: Sultani, Haider N.; Haeri, Haleh H.; Hinderberger, Dariush; Westermann, Bernhard. *Org. Biomol. Chem.*, **2016**, 14, 11336-11341.

** Own contribution: synthesis and characterization of diketopiperazines and the peptide peptoids compounds, measurements of EPR-spectra.

2.1 Introduction

The utilization of Electron Paramagnetic Resonance (EPR) spectroscopy is highly increasing as a well-established method and it is becoming a strong tool for the determination of structural features in biomolecules in particular as well as resolving interactions of membrane-peptide interactions.[1,2] EPR spectroscopy can also be used as an alternative method to isothermal titration calorimetry for elucidating drug proteins interactions, where it can give more detailed information parameters such as drug-protein binding, especially when the protein acts as drug carrier.[3]

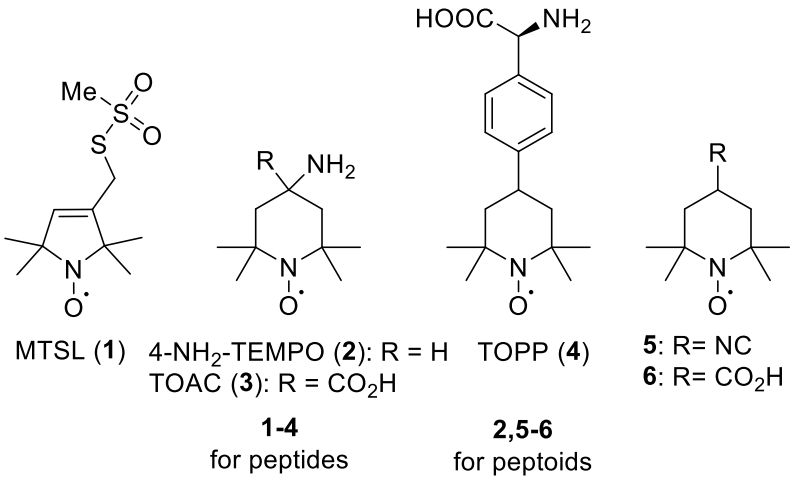

Figure 2. 1 Spin labels suitable for peptides and peptoids.

In EPR studies in the field of protein structural biology, the spin label bearing moiety is generally incorporated by covalent attachment to free cysteine amino acid side chains a technique known as site-directed spin labelling (SDSL). The suitability of the two popular spin probes; **1** (methane thiosulfonate spin label, MTSL) and **2** (4-amino TEMPO) which are shown in **Figure 2. 1**, has been widely demonstrated in the literature. In these applications, while being attached to the cysteine thiol group they have been proven to have a minimum or no impact on the secondary and tertiary structure of proteins.[4,5] The incorporation of genetically encoded non-canonical amino acids at the nonsense codon is considered the state of the art when it comes to the SDSL of proteins.[6] This allows later on for spin-labelling without the need of replacing or modifying any cysteine amino acids, especially in some proteins where the modification of cysteines may lead to structural perturbations and render the protein inactive. The 2,2,6,6-tetramethyl-*N*-oxyl-4-amino-4-carboxylic acid, (TOAC, **3**) spin label (**Figure 2. 1**) has brought great attention in the SDSL of peptides and peptaibols.[7]

The amino acid 4-(3,3,5,5-tetramethyl-2,6-dioxo-4-oxylpiperazin-1-yl)-L-phenylglycine, (TOPP, **4**) is also used as a spin label but to a lesser extent.[8,9] The utilization of spin labels **5** and **6** will come later in this chapter.

2,5-Diketopiperazines (2,5-DKP) are the simplest cyclic peptides and these small molecules are conformationally rigid. Moreover, they can participate as H-bond acceptors and donors. The availability of many sites for structural modification allows for the elaboration of new molecules with diverse activities. These properties enable them to bind with a strong affinity to a large diversity of receptors, exhibiting a wide range of biological activities. Many therapeutic agents contain DKPs were developed from lead to a clinical drug and their therapeutic activities were proven. Drugs such as Tadalafil (**7**) which acts as PDE5 inhibitor used to treat erectile dysfunction (ED). Retosiban (**8**), which is an oxytocin receptor antagonist, was developed by GSK for the treatment of preterm labor. Another drug developed by GSK is Epelsiban (**9**), which also acts as oxytocin receptor antagonist to be used in men to treat premature ejaculation. Another example of a 2,5-DKP being developed by GSK is Aplaviroc (**10**) which has been used to treat HIV infection. In October 2005, all studies of Aplaviroc were discontinued due to liver toxicity concerns (**Figure 2. 2**).[10]

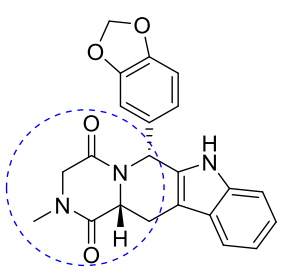

Tadalafil (**7**)

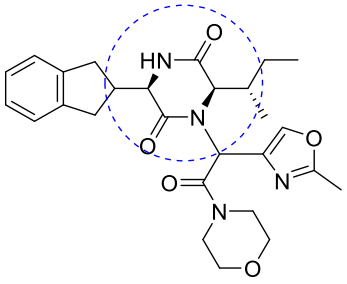

Retosiban (**8**)

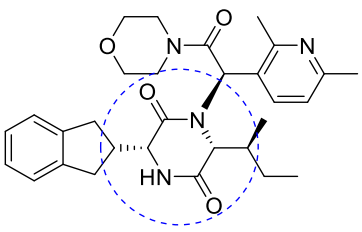

Epelsiban (**9**)

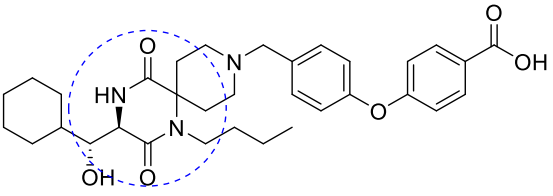

Aplaviroc (**10**)

Figure 2. 2 2,5-Diketopiperazines containing drugs.

2.2 Synthetic plan and EPR analysis of the synthesized spin-labelled products

Spin-labelling of small biologically active molecules bound to proteins or to DNA is carried out by introducing the spin label by different chemical methods. However, all these drug modifications provide single study solutions only, demanding an inevitable amount of experiments to access a variety of spin-labelled products.[3]

We show here, to the best of our knowledge, for the first time that spin-labelled products can be obtained via multicomponent reactions, namely the isonitrile-mediated Ugi-reaction. The Ugi-reaction can serve as an important synthetic tool for obtaining a broad library with reduced synthetic effort when compared to stepwise chemical synthesis.[11] By this, spin-labelled products such as diketopiperazines and peptide-peptoid chimera can be obtained. In addition, we have demonstrated that the conditions for the synthetic tool (Ugi-reaction) do not affect the integrity of the spin label.

The utilization of Ugi-reaction may seem discouraging in the sense of peptide modification as one has to choose which of the four components will be used as the spin label. The modification can be done using the carboxylic acid, the carbonyl, the isonitrile or lastly the amine component. In this study, we applied the utility of a multi-component reaction to introduce the spin label as an amine, carboxylic acid, and isonitrile component. The Ugi-products will be transferred to diketopiperazines (DKP) and peptide-peptoid chimera.[12,13] CW EPR spectroscopy analysis was performed for each synthetic step; we will discuss and analyze the spectra of chosen samples. Discussion will be done regarding their hyperfine coupling, solvent effect, and spectral line shape. For obtaining these values, the rigorous spectral simulation was conducted using a MATLAB-based EasySpin software package.[14]

2.2.1 Synthesis of spin-labelled diketopiperazines

For obtaining the spin-labelled Ugi-products **12a-d** and **13a-h** (see experimental part), no variations on the classical Ugi-reaction conditions were necessary (**Scheme 2. 1**).

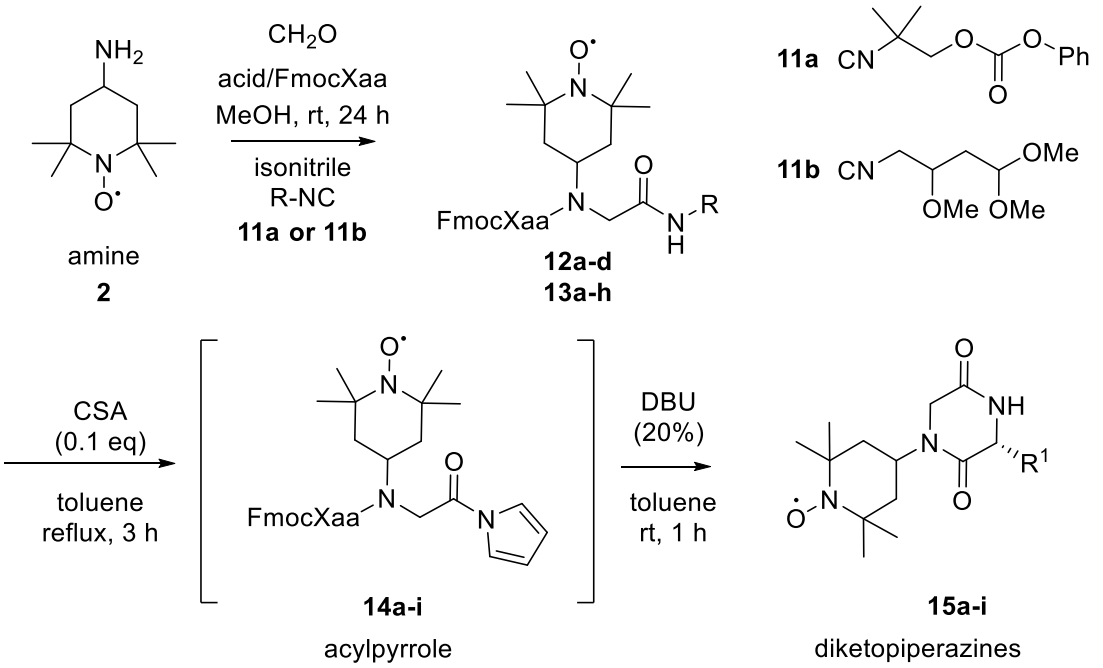

Scheme 2. 1 Synthesis of diketopiperazines **15** by Ugi-4CR/deprotection + activation/cyclization (UDAC) strategy.

For the Ugi-reaction as shown in **Scheme 2. 1**, two convertible isonitriles were used viz., **11a** which is known as Fukuyama's isonitrile[15] or **11b** which is called "IPB isonitrile", a convertible isonitrile that has been developed in our laboratory.[16,17] Both isonitriles allow further modification of the terminal amide bond. Initial attempts were made using **11a** as the convertible isonitrile, this is due to two reasons. Firstly, the basic conditions which are able to convert the isonitrile into *N*-acyloxazolidinones, upon which the amide bond is highly activated, and therefore it is susceptible to nucleophilic attack. Secondly, the intramolecular nucleophilic generation of the amine is formed upon the basic cleavage of the Fmoc-protecting group, which will lead to our desired diketopiperazines **15**. The basic conditions were favored to preserve the nitroxide radical and to prevent any potential disproportionation reactions. Nevertheless, the first approach to utilize **11a** for successful diketopiperazines synthesis could not be established.

For achieving the desired goal, we turned to a second approach using IPB **11b** as the convertible isonitrile. We used the established designed synthetic protocol which was developed earlier in our laboratory.[18]

The strategy relies on consecutive Ugi-4CR/deprotection + activation/cyclization, shortly known as (UDAC). As shown in **Scheme 2. 1** after the formation of Ugi-products **13a-h**, the activated acylpyrroles intermediates **14a-i** were formed after acidic treatment with 0.1 eq. camphor sulfonic acid (CSA) under reflux. To neutralize the reaction, a short workup was done, this was followed by DBU addition for the Fmoc cleavage. The generated nucleophile facilitates the spontaneous cyclization to the diketopiperazines **15a-i**, in overall good yields in the range of 50-70% (**Figure 2. 3**). Paraformaldehyde was used as oxo-component except in diketopiperazine **15i**, where isobutyric aldehyde was used instead of paraformaldehyde. In that case, the yields are comparable which shows the flexibility of using bulker aldehydes. The reaction afforded a diastereomeric mixture, as anticipated.

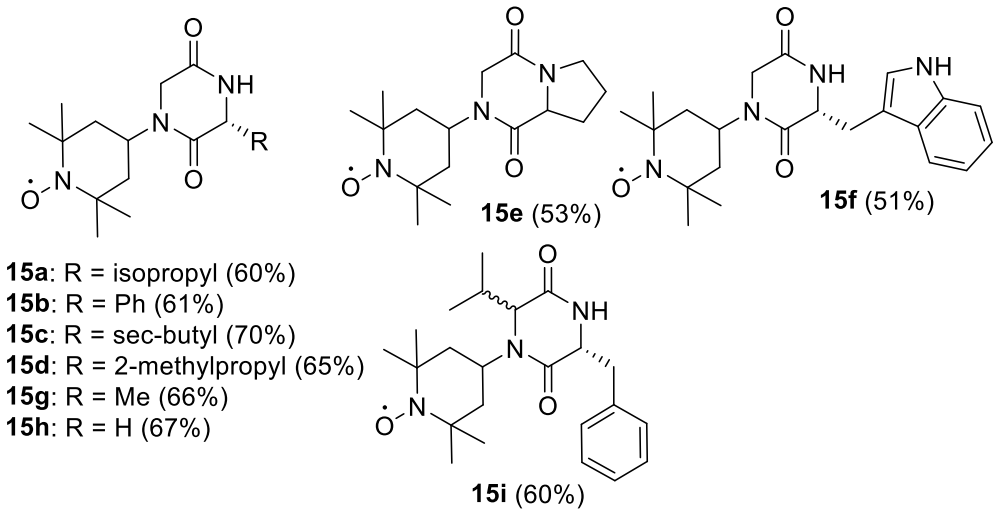

Figure 2. 3 The structures of diketopiperazines spin-labelled **15a-i**.

Besides the Ugi-products **13a-h**, we also synthesized other products using the classical Ugi-setup conditions and obtained peptoids **12a-d**. Peptoid **12a** was the linear precursor building block of the first approach (convertible isonitrile **11a**) while peptoid **12b** was the linear precursor building block of the second approach (convertible isonitrile **11b**). On the other hand peptoids, **12c** and **12d** have not been used for further reactions at this moment, but it can clearly deduce their role in Cu-catalyzed Azide-Alkyne cycloaddition (**Figure 2. 4**).[19]

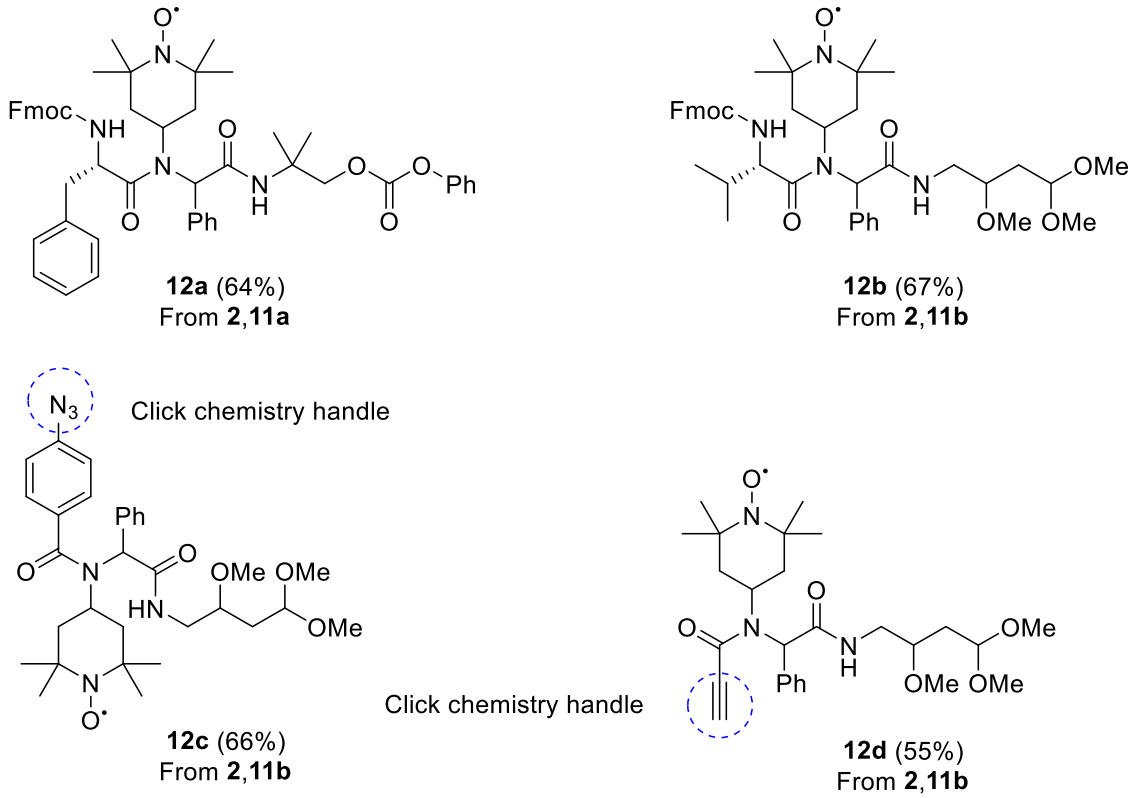

Figure 2. 4 The structures of spin-labelled Ugi-products **12a-d**.

2.2.2 EPR analysis of spin-labelled diketopiperazines

When we started analyzing the EPR spectra, we had doubts about whether the spin label could stay intact during the reaction course. Gratifyingly, we couldn't detect any sign of a disproportionation reaction. Even the slightly acidic condition combined with reflux for obtaining the acylpyrroles intermediates didn't affect or shape the intensity of the typical three lines pattern for nitroxide radical. The high persistence nitroxide radical allows the storage of the spin-labelled products for several weeks if not even months at 6 ^{o}C.

It is interesting to compare the spin-labelled Ugi-product **12b** and its corresponding DKP **15a** via EPR spectroscopy. Experimental spectra for each of the products along with their simulation are presented in **Figure 2. 5**.

The spectra of both analyzed compounds **12b** and **15a** show the typical three-line pattern of nitroxides due to hyperfine coupling between the oxygen radical and the nitrogen nucleus. Quantitative measurements were done to assess the chemical stability of the six-membered spin-labelled nitroxide radicals during synthesis and after treatment in acidic or basic conditions. The results were striking to us since these measurements show that no disproportionation/decay of the nitroxide radicals can be observed.

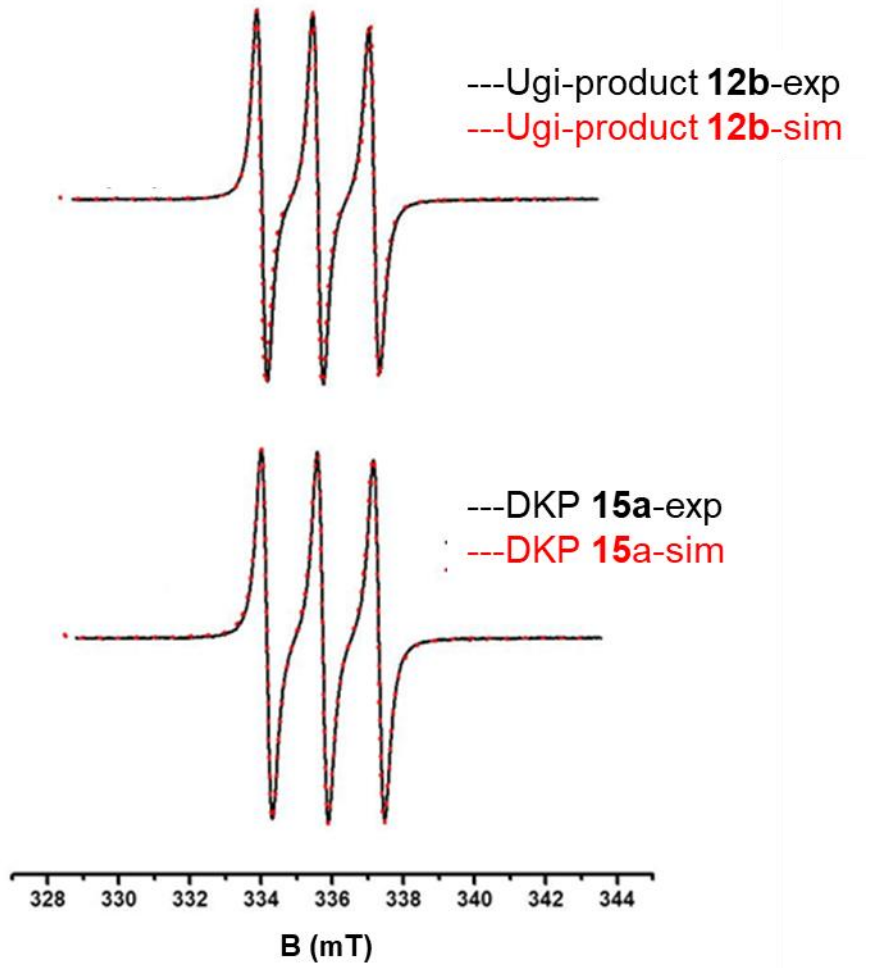

Figure 2. 5 Room temperature CW EPR spectra (black solid line) and their simulated spectra (red dotted line) of compounds **12b** and **15a**.

The analysis of the Ugi-intermediate **12b** showed that the peptoid has an isotropic hyperfine splitting, A(^{14}N) of 44.7 MHz. Similarly, for the final DKP **15a**, a similar value of 44.0 MHz has been found. We also analyzed these compounds in terms of their rotational correlation time (τ_c). As expected, we found different values for both the Ugi-intermediate **12b** and for the final DKP **15a**. As for the Ugi-intermediate **12b,** a value of 0.03 ns was obtained, which is in the range of fast-rotating nitroxide radical which is an expected value for spin label conjugated to medium size molecule. On the other hand, the obtained (τ_c) for the DKP **15a** was smaller when compared to the Ugi-product **12b**, this smaller value was expected due to the cleavage of the bulky Fmoc group, which leads to ten times faster rotation of the spin-labelled DKP. Finally, we found an isotropic g-value of 2.005 which is in the range of typical isotropic g-value for nitroxides.[20] The spectra of the remaining DKP spectra are shown in **Figure 2. 6**.

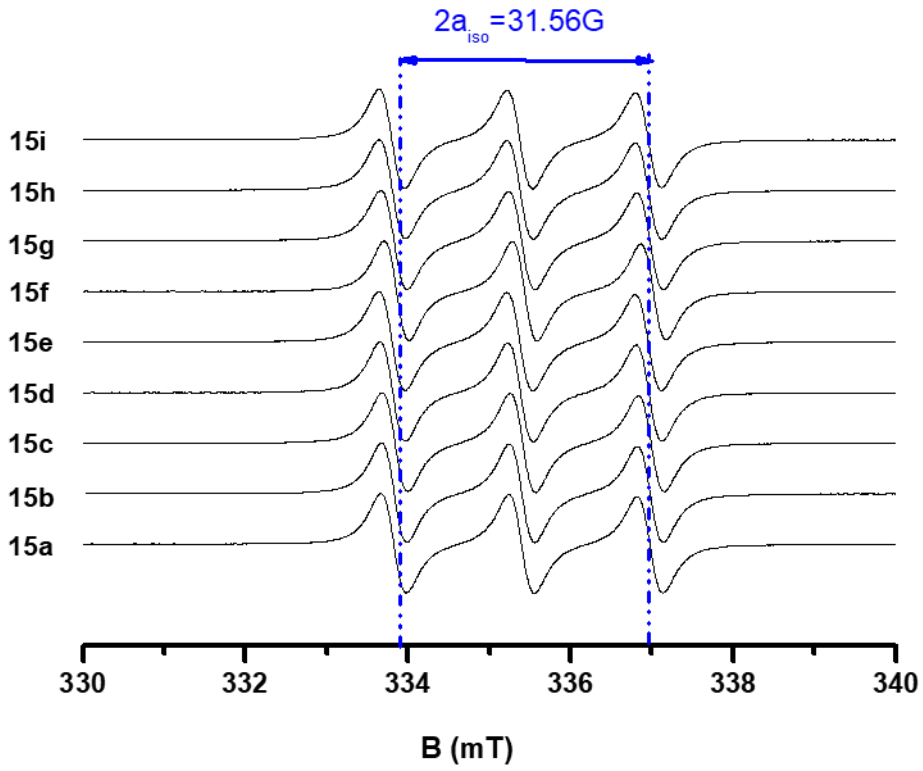

Figure 2. 6 Room temperature CW EPR spectra for DKPs **15a-i** in acetonitrile.

The sensitivity of EPR spectroscopy can be useful to detect slight modifications between the DKPs. For instance, when comparing the spectra of **15a** which was synthesized using valine as the acid component, and **15b** which was synthesized using phenylalanine as the acid component, both have a very close chemical structure. No difference was observed in the hyperfine coupling of the *N*-Oxide ($A(^{14}N)$) since it's not affected by the different substitution patterns. However, the size of the substitution will affect the rotation speed of **15a**. In fact, according to the simulation DKP **15a** rotate faster by a factor of 1.6 when compared to **15b**. Therefore, EPR spectroscopy can be used as a strong screening tool to detect any structural differences, which can be further studied and analyzed in detail using CW EPR spectroscopy (CW EPR spectra of DKP, **15b** are shown in attachments (**Table S1**). The solvent effect on the EPR spectra of the synthesized DKP was also analyzed for the potential application of our synthesized DKPs to be further tested in biological systems. The use of water as a solvent for the potential use of the spin-labelled DKP for biophysical or bioanalytical is mandatory. For that reason, we have chosen to study the DKP **15a** in the aqueous solvent and we observed the $A(^{14}N)$ value of 3.8 MHz, which is higher in the water when compared to acetonitrile.

This was not surprising at all since it is well established that the hyperfine splitting is very sensitive to the environmental polarity.[21,22] Another EPR feature affected by the solvent is the spectral line shapes and line shape contribution can be Lorentzian or Gaussian. We have observed a higher contribution from the Lorentzian line shape rather than Gaussian when using acetonitrile. On the other hand, we observed a higher contribution from Gaussian when water was used as a solvent. The solvent effect on the rotational dynamics can also be seen, as rotational dynamics in water is much slower than non-polar solvents. This effect can be inferred due to the formation of hydrogen bonds between the solvent molecules and the nitroxide radical, or other hydrogen bonding groups (amines, carbonyls) of the spin-labelled probes.

2.2.3 Synthesis of spin-labelled peptide-peptoid chimera

To expand the scope of Ugi-reaction spin-labelled products, peptide-peptoid chimera has also been synthesized.[23,24] Three different Ugi-amenable TEMPO derivatives were used to obtain the examples **16-19** presented in **Scheme 2. 2**. The spin labels **6**, **2** and **5** were introduced via the carboxylic acid, the amine, and the isonitrile moiety, respectively. **Scheme 2. 2** shows the synthesis of peptide-peptoid chimera **16-19**. Whereby, amino acids have been selected as the corresponding amine and carboxylic acid counterparts. Meanwhile, other functionalities have been protected using classical protecting groups viz., Cbz and Boc. The oxo-component was restricted to paraformaldehyde in order to avoid the formation of any stereoisomers. The examples presented in **Scheme 2. 2**, show the possibility of obtaining C- and N-terminal, as well as side chain, modified peptide-peptoid chimera, which clearly show the flexibility of using the nitroxide component as a spin label within the Ugi-reaction. A large library of desired compounds can be obtained in one step only.

As its clearly evidenced that the Ugi-reaction is successful in introducing the spin radical at any of the available components for constructing these peptide-peptoid chimera in a single step only. We also tested the potential of introducing two spin label nitroxide into the peptide core. For obtaining such double spin-labelled peptoid **20**, two subsequent Ugi-reactions were performed via a one-pot setup. As seen in **Scheme 2. 3** the acid component for the second cycle of Ugi-reaction needs to be prepared intermediary by saponification of the product obtained from the first Ugi-reaction cycle.

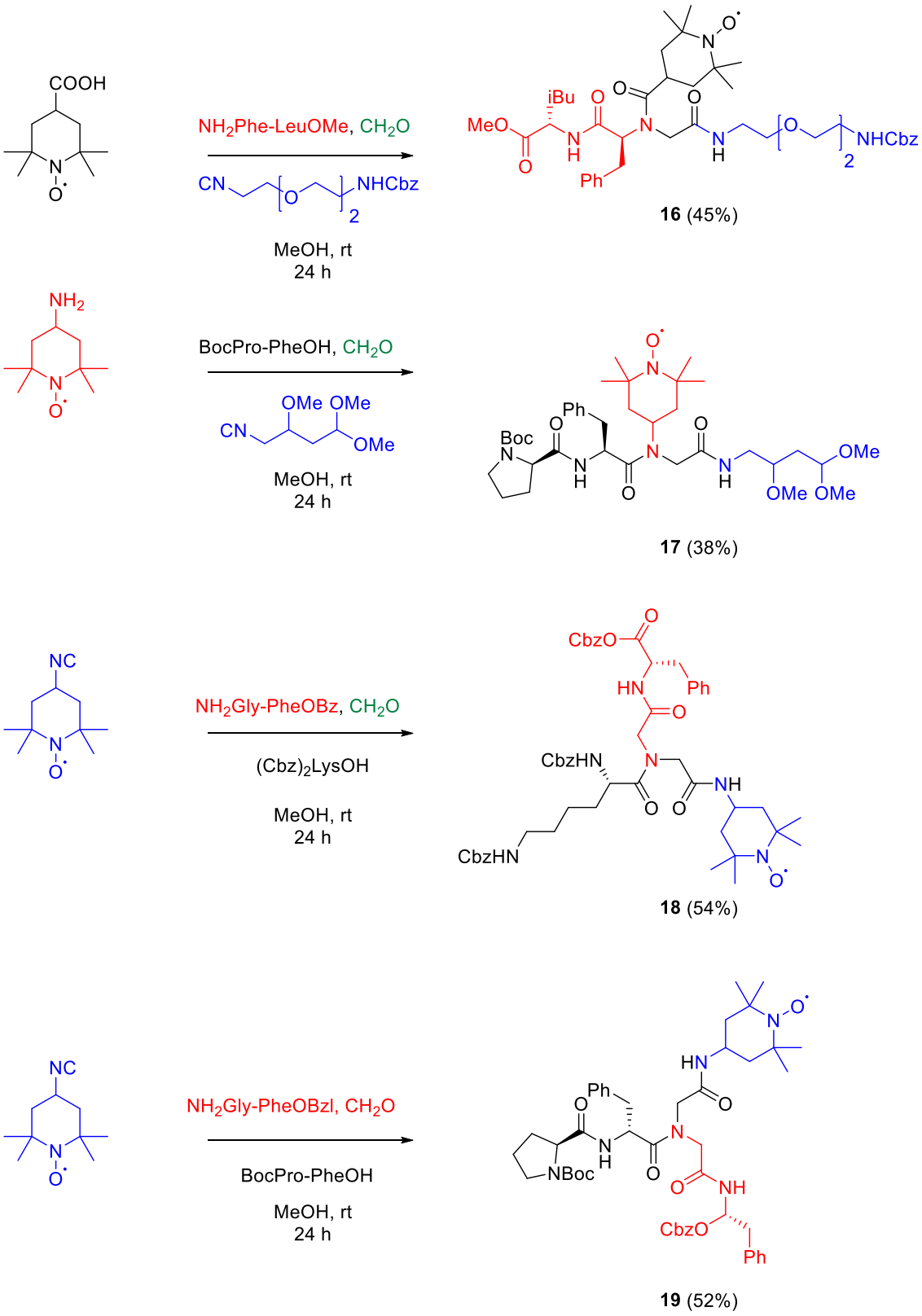

Scheme 2. 2 Synthesis of spin-labelled peptide-peptoid chimera **16-19**.

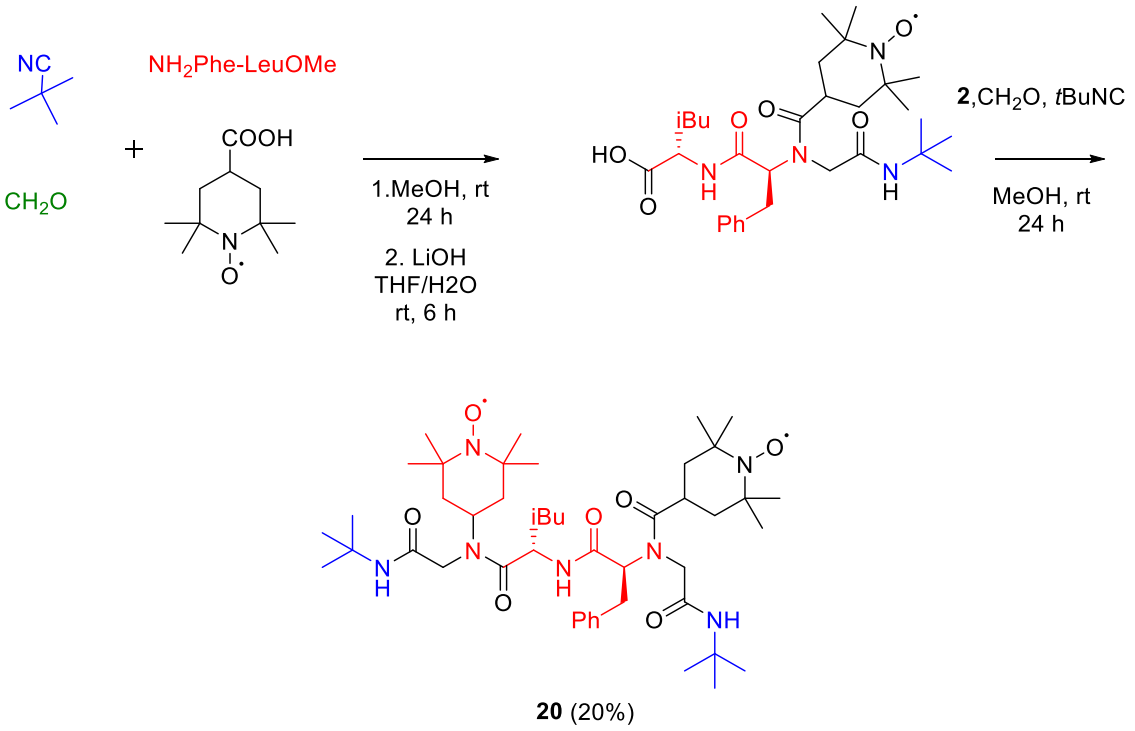

Scheme 2. 3 Synthesis of double spin-labelled **20** products.

2.2.4 EPR analysis of spin-labelled peptide-peptoid chimera

Figure 2. 7 shows the EPR spectra of the synthesized peptide-peptoid chimera **16-19**. The spectral properties which were obtained from the simulations are given in **Table 2. 1**.

Table 2. 1 Spectral properties of synthesized spin label peptides. Rotational correlation times are in nanoseconds (ns) and hyperfine splittings in MHz[a].

#Peptide	τ_c	A(^{14}N)	g_{iso}
16	0.18	47.50	2.005
17	0.26	47.60	2.005
18	0.14	45.60	2.005
19	0.046	47.50	2.005

[a]All peptides were recorded in water, except for **18**, which was measured in methanol.

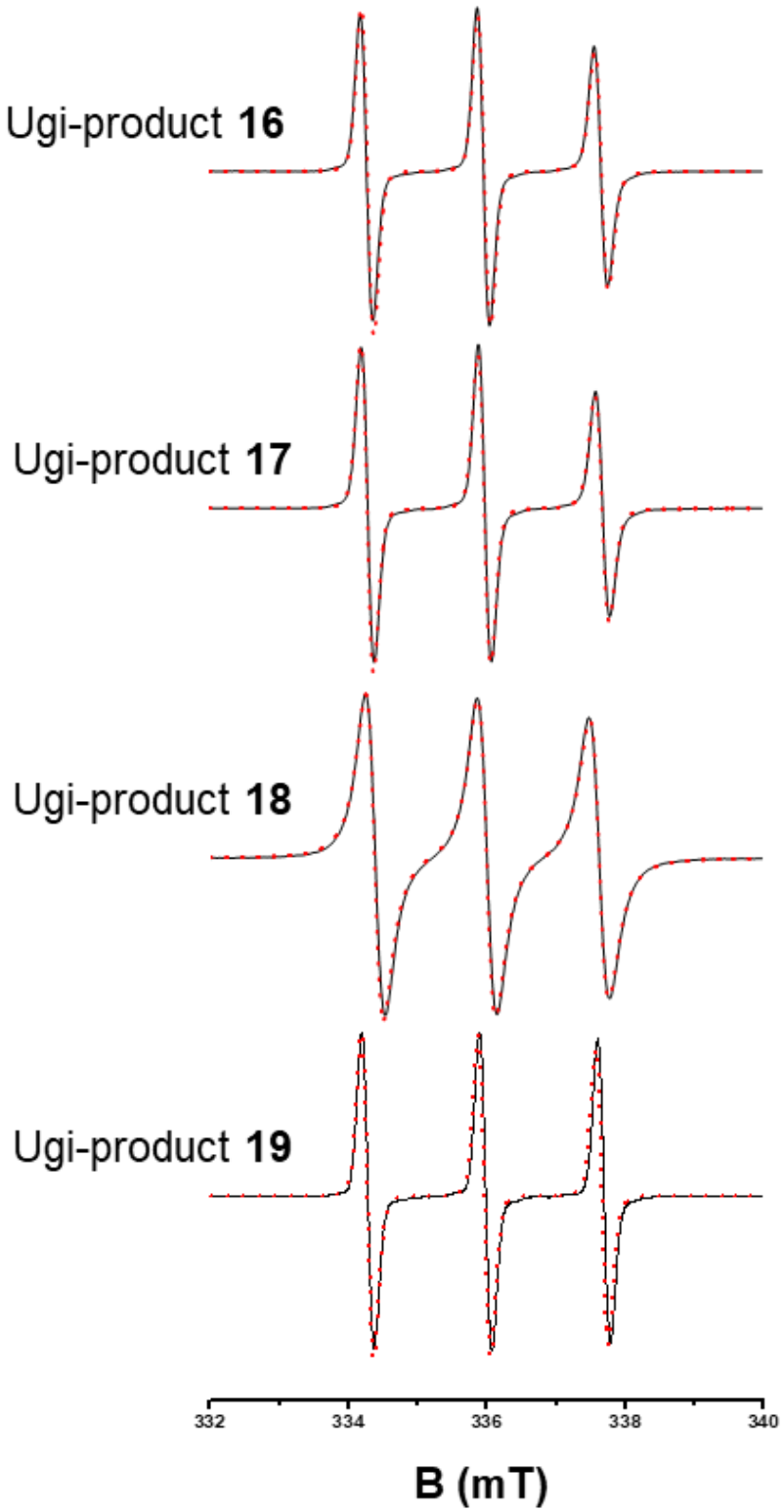

Figure 2. 7 Experimental (solid black line) and simulated (red dotted line) spectra of spin label Ugi-products **16-19**.

The degree of rotation in the synthesized peptides highly depends on the position where the spin labels were incorporated into the peptidic core. For instance, peptides **18** and **19** have their spin labels attached at the end of the chain. Due to that fact, they experience a higher degree of rotational freedom when compared to peptides **16** and **17**, where the spin label rotation is being hindered due to its incorporation in the middle of the peptidic core.[25] For that reason, peptides **18** and **19** rotate faster and have shorter correlation times when compared to two other peptides. It is worth to mention that peptide **19** has a higher rotational motion when compared to the rest of the tested molecules, which is due to its small molecular size compared to the rest of the tested molecules.

In addition, similar values of the simulated hyperfine splitting were found when compared to the values of the TEMPO derivatives from which the corresponding peptides were obtained. Looking carefully to the $A(^{14}N)$ and isotropic g-values of the synthesized peptides, one can indicate the presence of one or two hydrogen bonds attached to the nitroxide moiety.[21,22]

Peptide **18** was not well soluble in water and methanol was successfully able to dissolve the peptide and then the EPR spectrum was measured. Using methanol as a solvent leads to smaller $A(^{14}N)$ values and broader lines (the line broadening was due to an increased amount of dissolved molecular oxygen in methanol) for peptide **18**, when compared to the rest of the water, dissolved synthesized peptides. The only parameter which is not affected is the isotropic g-value which remains typical for nitroxides.

2.2.5 EPR analysis of the double spin-labelled peptide 20

Since peptide **20** was double spin-labelled, high resolved spectra with detailed information can be obtained at higher frequencies at higher magnetic fields. For that reason, we turned to a higher frequency of 34 GHz (Q-band, magnetic field B~1.1T), as well as to the measurements at X-band (9.4 GHz, B~0.35 T).

The Q-band spectrum of peptide **20** reveals a completely different rotational dynamic appearance when compared to the X-band spectrum at Q-band frequency (**Figure 2. 8**). The simulations also confirm that the spectrum is actually consisting of two components; a three-line spectrum of the two individual bi-radical nitroxides not interacting with each other, and a five-line spectra component, arising due to what is known as Heisenberg spin-exchange interaction.

In other words, when the two nitroxides are so close to each other due to the confirmation of the peptide in solution, they can collide with an exchange frequency.

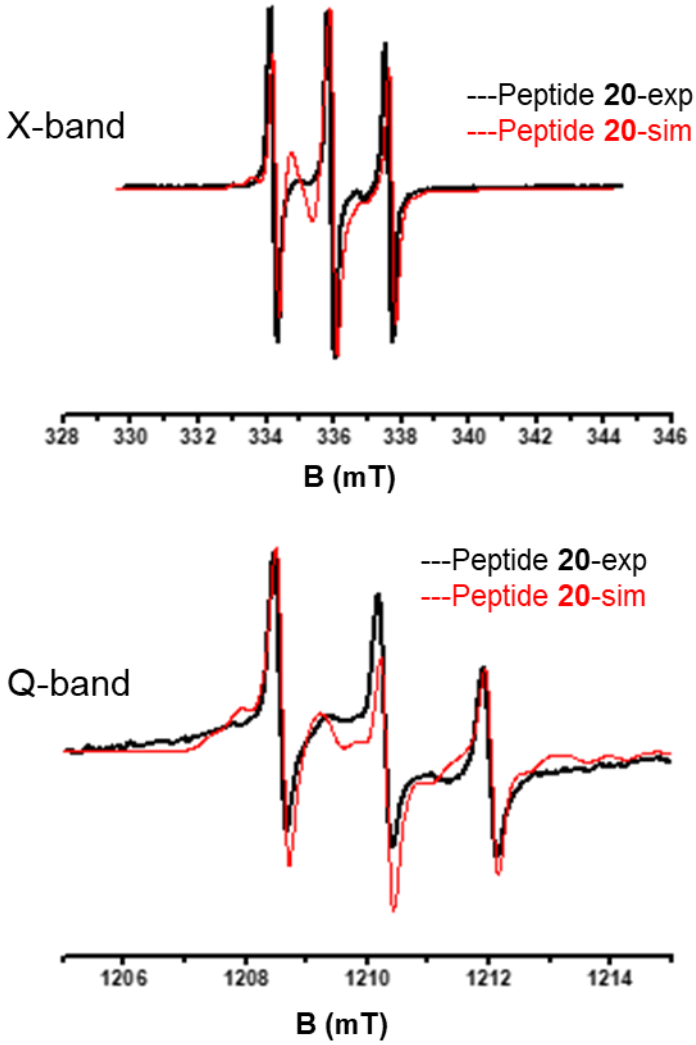

Figure 2. 8 EPR measurements of doubly spin-labelled peptide **20** in water. In a global simulation approach, the simulation parameters of the better resolved Q-band spectra were used for simulating the X-band spectrum.

As can be seen in **Figure 2. 8**, the five-line spectrum can be obviously observed when measuring at the Q-band. This contribution was found to be as much as 35% of the overall spectrum. The quantification of the isotropic part of the electron-electron spin-spin interaction can be measured at the exchange interaction frequency (Heisenberg spin exchange coupling constant J_{iso}), the value was 13.3 MHz which was found from the simulated spectrum at the Q-band.

2.3 Conclusions

To summarize, we have presented for the first time a synthetic route for obtaining a library of spin-labelled compounds via an isonitrole-mediated multicomponent reaction approach. To show the high flexibility of this approach different peptide, peptide-peptoid chimera and diketopiperazines with spin label radical attached in different positions have been synthesized. In addition, we proved that the spin label can be quite stable and did not deteriorate even upon refluxing the spin label in acidic conditions, which makes it compatible with post-Ugi-modifications. Quantitative EPR analysis was possible to be performed with all the synthesized products and we could even detect small changes in the different molecular structures. We believe that the Ugi-reaction will become an important and simple synthetic tool to provide biological interesting compounds for EPR analysis in the future. For example, it can be used for screening approaches of protein binding studies in the biomedical relevant cases.

2.4 Experimental part

General remarks

All commercially available reagents were used without further purification. Dichloromethane has been dried before use following conventional procedures. Convertible isocyanides 2-isocyano-2-methyl propyl phenyl carbonate **11a**, IPB **11b**, and PEG isocyanide was prepared following reported procedures.[15,16,26] HPLC grade methanol was used in all Ugi-reactions. Analytical thin-layer chromatography (TLC) was performed using silica gel 60 F254 aluminum sheets (Merck, Germany) and the visualization of the spots has been done under UV light (254 nm) or by developing with a solution of ninhydrin (0.2% in *n*-butanol with 1% acetic acid and heating). Flash column chromatography was performed using silica gel (0.040 – 0.063 mm). ^{1}H and ^{13}C NMR spectra were recorded in solutions on a 400 MHz Varian MERCURY-VX 400 at 22 °C at 400 MHz and 100 MHz, respectively. Chemical shifts (δ) are reported in ppm relative to TMS (^{1}H-NMR) and to the solvent signal (^{13}C NMR spectra). Note: due to the paramagnetism of nitroxide moiety, NMR cannot provide information useful for structural elucidation of nitroxides. The positive-ion high-resolution ESI mass spectra were obtained with an Orbitrap Elite mass spectrometer (Thermo Fisher Scientific, Germany) equipped with a HESI electrospray ion source (positive spray voltage 4 kV, capillary temperature 275 °C, source heater temperature 80 °C, FTMS resolution 60000). Nitrogen was used as sheath gas. The instrument was externally calibrated using the

Pierce LTQ Velos ESI positive ion calibration solution (product number 88323, Thermofisher Scientific, Rockford, IL, 61105 USA). The data were evaluated using the software Xcalibur 2.7 SP1. Instrumental details-EPR: X-Band (9.43 GHz) room temperature CW EPR measurements were performed on a Magnettech MiniScope MS400 benchtop spectrometer (Magnettech, Berlin, Germany). Spectra were recorded with a microwave power under the saturation limit (varied between 1-3 mW), 100 kHz modulation frequency, modulation amplitude of 0.1 mT and 4096 points. The lowest sample concentrations were 300 µM. The contribution of solvent to spectra was examined using water and acetonitrile. Since it is difficult to evaluate fully resolved hyperfine and g-tensors at X-band frequencies, only the isotropic values are reported. Q-band (33.9 GHz) room temperature CW EPR measurements were conducted on a Bruker EMX-plus spectrometer, using an ER5106QT resonator. A microwave power of 1 mW, 100 kHz modulation frequency, modulation amplitude of 0.1 mT and 2000 points were used during measurements.

Synthesis of 4-Amino-2,2,6,6-tetramethylpiperidine-*N*-oxyl (2)[27]

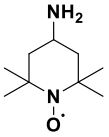

4-Acetamido-TEMPO (2.0 g, 9.40 mmol, available from TCI, Germany) was heated to reflux with KOH (6.32 g, 0.11 mmol) in MeOH (5 mL) and H_2O (18 mL) for 4 days. Subsequently, the product was extracted with Et_2O and the combined organic phases were dried over $MgSO_4$ and filtered. Removal of the solvents under reduced pressure to yield 4-Amino-TEMPO **2** (1.40 g, 8.17 mmol, 88%) as a red oil that forms crystals when stored at cold temperatures 2-5 °C. HRMS (ESI): m/z = calcd. for $C_9H_{19}N_2OH^+$ $[M+H]^+$172.1570; found 172.1566.

Synthesis of 2,2,6,6-Tetramethylpiperidin-*N*-oxyl-4-one[28]

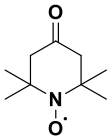

2,2,6,6-Tetramethyl-4-piperidone (2.0 g, 12.9 mmol) was dissolved in a mixture of MeOH/H_2O (3:2, 40 mL). $Na_2WO_4{\times}2H_2O$ (700 mg, 2.18 mmol) and H_2O_2 (8.80 mL, 77.4 mmol) were added and the reaction mixture was stirred for 5 days at rt. A catalytic amount of $Na_2WO_4{\times}2H_2O$ was added daily. The reaction completion was verified by TLC, upon which the reaction mixture was saturated with K_2CO_3 and extracted with Et_2O (3 × 20 mL). The combined organic layers were dried over $MgSO_4$, filtered and the solvent was removed under reduced pressure. The crude product was purified by silica gel column chromatography (EtOAc / *n*-hexane 3:2), to yield 4-Oxo-TEMPO (1.90 g, 11.2 mmol, 86%) as a red solid**.** The compound was used immediately for the next step.

Synthesis of 4-Cyano-2,2,6,6-tetramethyl-piperidine-*N*-oxyl[29]

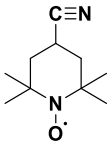

2,2,6,6-Tetramethylpiperidin-*N*-oxyl-4-one (1.0 g, 5.88 mmol) was dissolved in DME (50 mL) and tosyl methylisocyanide (1.20 g, 6.18 mmol, 1.05 eq) was added at 0 °C, after which a solution of *t*-BuOK (1.32 g, 11.8 mmol) in DME/*t*-butanol (1:1, 20 mL) was added to the reaction mixture. The reaction mixture was stirred for 45 min at 0 °C and for further 1h at rt. The reaction was stopped by the addition of H_2O (70 mL) and the product was extracted with Et_2O (3 × 50 mL). The combined organic layers were dried over $MgSO_4$, filtered and the solvent was removed under reduced pressure to yield 4-Cyano-TEMPO (1.0 g, 5.51 mmol, 94%) as a red solid and was used without further purification.

Synthesis of 4-Carboxy-2,2,6,6-tetramethyl-piperidine-*N*-oxyl (6)[29]

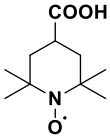

4-Cyano-2,2,6,6-tetramethyl-piperidine-*N*-oxyl (1.00 g, 5.51 mmol) was dissolved in MeOH (15 mL) and a mixture of $Ba(OH)_2 \times 8H_2O$ (6.50 g, 20.8 mmol) and NaOH (0.348 g, 8.70 mmol) in H_2O (50 mL) was added. The reaction mixture was refluxed for 24 h. After cooling to rt, the mixture was extracted with $CHCl_3$ (3 × 60 mL). The aqueous layer was acidified with HCl (aq. 10%) to pH 2 and extracted with $CHCl_3$ (3 × 60 mL). The combined organic layers were dried over $MgSO_4$, filtered and the solvent was removed under reduced pressure to yield 4-Carboxy-TEMPO (0.95 g, 4.74 mmol, 87%) as a red solid and was used without further purification. HRMS (ESI) m/z calcd. for $C_{10}H_{19}NO_3$ $[M + Na]^+$201.1359, found 201.1347.

Synthesis of 4-Formamido-2,2,6,6-tetramethylpiperidine-*N*-oxyl[30]

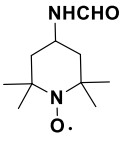

N-oxyl **2** (5.0 g, 25.1 mmol) was refluxed with an excess of ethyl formate (70 mL) overnight. The formation of the product was monitored by TLC (EtOAc / *n*-hexane 9:1), after which removal of the solvents under reduced pressure to yield 4-Formamido-TEMPO (4.0 g, 20.1 mmol, 80 %) as red oil and used without further purification.

Synthesis of 4-Isocyano-2,2,6,6-tetramethyl piperidine-*N*-oxyl (5)[30]

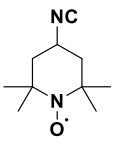

4-Formamido-2,2,6,6-tetramethylpiperidine-*N*-oxyl (1.99 g, 10.0 mmol), carbon tetrachloride (1.0 mL, 10.0 mmol), TEA (1.44 mL, 10.0 mmol) and triphenylphosphane (2.60 g, 10.0 mmol) are dissolved in $CHCl_3$ (12 mL) and

heated to 60 °C for 4 h. The reaction was allowed to cool to rt, then washed with sat. $NaHCO_3$-solution. The aqueous layer was extracted using chloroform and subsequently dried over $MgSO_4$ and filtered. Removal of the solvents under reduced pressure afforded the crude product which was purified by column chromatography (EtOAc / *n*-hexane 3:7) to yield 4-Isocyano-TEMPO **5** (0.80 g, 4.41 mmol, 44%) as red solid. HRMS (ESI): m/z = calcd. for $C_{10}H_{18}N_2OH^+$ $[M+2H]^+$183.1492, found 183.1488.

General procedure (1) for the Ugi-4CR

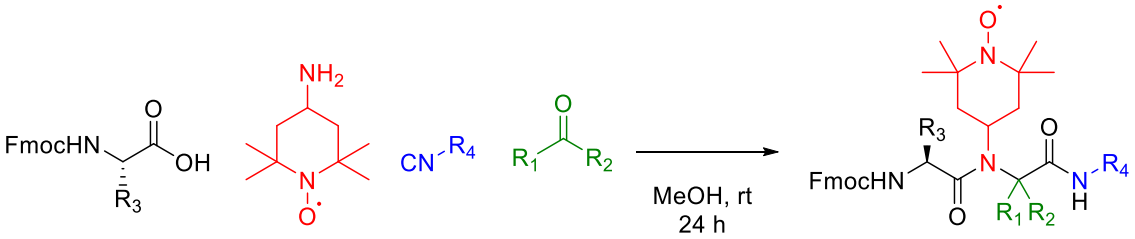

12a-d
13a-h

To a stirred solution of an *N*-oxyl amine **2** (1.0 mmol) in MeOH (2.5 mL) was added paraformaldehyde (1.0 mmol) and the mixture was stirred for 2 h. After this time the Fmoc-amino acid (1.0 mmol) and isonitrile (1.0 mmol) were added before stirring was continued for 18 h. The solvent was removed under reduced pressure and the crude material was purified by column chromatography to afford the desired products.

(9H-Fluoren-9-yl)methyl (S)-(1-((1-oxyl-2,2,6,6-tetramethylpiperidin-4-yl)(2-((2-methyl-1-((phenoxycarbonyl)oxy)propan-2-yl)amino)-2-oxoethyl)amino)-1-oxo-3-phenylpropan-2-yl)carbamate (12a)

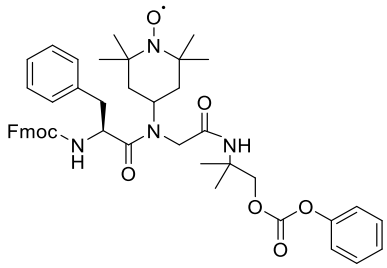

12a

Obtained using the general procedure **1**, 2-isocyano-2-methylpropyl phenyl carbonate **11a**, paraformaldehyde, Fmoc-*L*-phenylalanine and *N*-oxyl amine **2** were used, The crude material was purified by silica gel column chromatography (EtOAc / *n*-hexane 1:1) to yield peptoid **12a** (0.50 g, 0.63 mmol, 55%) as red solid. R_F 0.23 (EtOAc / *n*-hexane 1:1). HRMS (ESI) *m/z* calcd. for $C_{46}H_{53}N_4O_8$ $[M + H]^+$ 790.3936, found 790.3927.

(9H-Fluoren-9-yl)methyl ((2S)-1-((1-oxyl-2,2,6,6-tetramethylpiperidin-4-yl)(2-oxo-2-((2,4,4-trimethoxybutyl)amino)ethyl)amino)-3-methyl-1-oxobutan-2-yl)carbamate (12b)

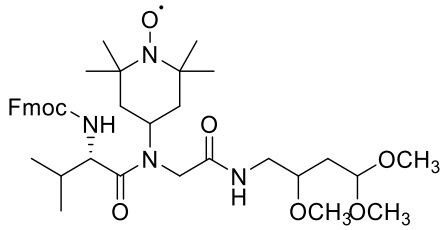

12b

Obtained using the general procedure **1**, IPB isonitrile **11b**, *N*-oxyl amine 2, Fmoc *L*-valine and *N*-oxyl amine **2** were used. The crude material was purified by silica gel column chromatography (EtOAc) to yield peptoid **12b** (0.47 g, 0.66 mmol, 67%) as red solid. R_F 0.4 (EtOAc). HRMS (ESI) *m/z* calcd. for $C_{38}H_{55}N_4O_8$ $[M]^+$ 695.4014, found 695.3995.

4-Azido-*N*-(1-oxyl-2,2,6,6-tetramethylpiperidinyl)-N-(2-oxo-2-((2,4,4-trimethoxybutyl) amino) ethyl)benzamide (12c)

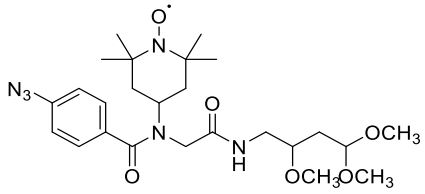

12c

Obtained using the general procedure **1**, IPB isonitrile **11b**, *N*-oxyl amine **2**, *p*-azido benzoic acid and paraformaldehyde were used. The crude material was purified by silica gel column chromatography (EtOAc / *n*-hexane 7:3) to yield peptoid **12c** (0.35 g, 0.67 mmol, 66%) as red solid. R_F 0.5 (EtOAc), HRMS (ESI) *m/z* calcd. for $C_{25}H_{39}N_6O_6Na$ $[M + Na]^+$542.2823, found 542.2809.

***N*-(2,2,6,6-Tetramethylpiperidin-4-yl)oxyl-*N*-(2-oxo-1-phenyl-2-((2,4,4-trimethoxybutyl) amino)ethyl)propiolamide (12d)**

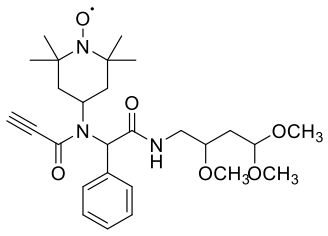

12d

Obtained using the general procedure **1**, IPB isonitrile **11b**, propiolic acid, benzaldehyde and *N*-oxyl amine **2** were used. The crude material was purified by silica gel column chromatography (EtOAc) to yield peptoid **12d** (0.28 g, 0.55 mmol, 55%) as red solid. R_F 0.46 (EtOAc), HRMS (ESI)

m/z calcd. for $C_{27}H_{40}N_3O_6Na$ $[M + Na]^+$ 525.2809, found 525.2796.

(9H-Fluoren-9-yl)methyl ((2S)-1-((1-oxyl-2,2,6,6-tetramethylpiperidin-4-yl)(2-oxo-2-((2,4,4-trimethoxybutyl)amino)ethyl)amino)-1-oxo-3-phenylpropan-2-yl)carbamate (13a)

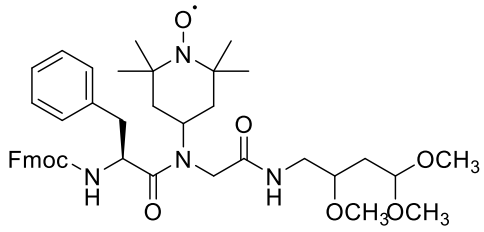

13a

Obtained using the general procedure **1**, IPB isonitrile **11b**, Fmoc-*L*-phenyl alanine, paraformaldehyde and *N*-oxyl amine **2** were used. The crude material was purified by silica gel column chromatography (EtOAc) to yield peptoid **13a** (0.34 g, 0.45 mmol, 46%) as red solid R_F 0.37 (EtOAc). HRMS (ESI) *m/z* calcd. for $C_{42}H_{56}N_4O_8$ $[M + H]^+$ 744.4093, found 744.4072.

(9H-Fluoren-9-yl)methyl ((2S,3S)-1-((1-oxyl-2,2,6,6-tetramethylpiperidin-4-yl)(2-oxo-2-((2,4,4-trimethoxybutyl)amino)ethyl)amino)-3-methyl-1-oxopentan-2-yl)carbamate (13b)

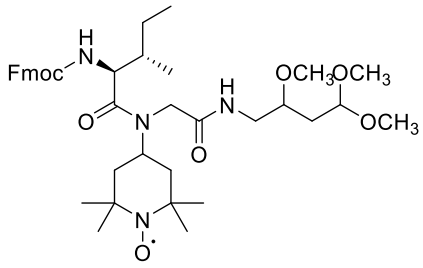

13b

Obtained using the general procedure **1**, IPB isonitrile **11b**, Fmoc-*L*-isoleucine, paraformaldehyde and *N*-oxyl amine **2** were used. The crude material was purified by silica gel column chromatography (EtOAc) to yield peptoid **13b** (0.35 g, 0.49 mmol, 50%) as red solid. R_F 0.45 (EtOAc). HRMS (ESI) *m/z* calcd. for $C_{39}H_{58}N_4O_8$ $[M + H]^+$ 710.4249, found 710.4222.

(9H-Fluoren-9-yl)methyl ((2S)-1-((1-oxyl-2,2,6,6-tetramethylpiperidin-4-yl)(2-oxo-2-((2,4,4-trimethoxybutyl)amino)ethyl)amino)-4-methyl-1-oxopentan-2-yl)carbamate (13c).

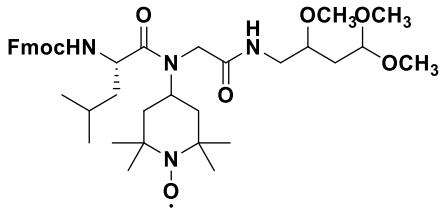

13c

Obtained using the general procedure **1**, IPB isonitrile **11b**, Fmoc-*L*-leucine, paraformaldehyde and *N*-oxyl amine **2** were used. The crude material was purified by silica gel column chromatography (EtOAc) to yield peptoid **13c** (0.43 g, 0.60 mmol, 61%) as red solid. R_F 0.50 (EtOAc). HRMS (ESI) *m/z* calcd. for $C_{39}H_{58}N_4O_8$ $[M + H]^+$ 710.4249, found 710.4221.

(9H-Fluoren-9-yl)methyl (2S)-2-((1-oxyl-2,2,6,6-tetramethylpiperidin-4-yl)(2-oxo-2-((2,4,4-trimethoxybutyl)amino)ethyl)carbamoyl)pyrrolidine-1-carboxylate (13d)

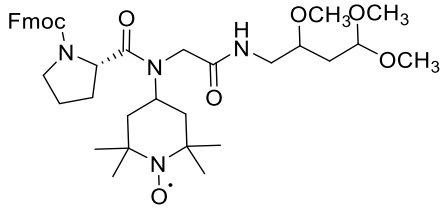

13d

Obtained using the general procedure **1**, IPB isonitrile **11b**, Fmoc-*L*-proline, paraformaldehyde and *N*-oxyl amine **2** were used. The crude material was purified by silica gel column chromatography (EtOAc) to yield peptoid **13d** (0.43 g, 0.62 mmol, 62%) as red solid. R_F 0.28 (EtOAc). HRMS (ESI) *m/z* calcd. for $C_{38}H_{54}N_4O_8$ $[M + H]^+$ 694.3936, found 694.3912.

(9H-Fluoren-9-yl)methyl ((2S)-1-((1-oxyl-2,2,6,6-tetramethylpiperidin-4-yl)(2-oxo-2-((2,4,4-trimethoxybutyl)amino)ethyl)amino)-3-(1H-indol-3-yl)-1-oxopropan-2-yl)carbamate (13e)

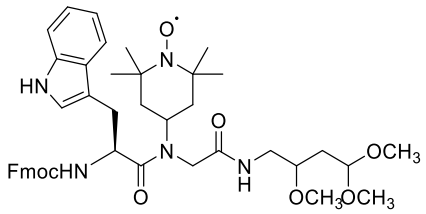

13e

Obtained using the general procedure **1**, IPB isonitrile **11b**, Fmoc-*L*- tryptophane, paraformaldehyde and *N*-oxyl amine **2** were used. The crude material was purified by silica gel column chromatography (EtOAc) to yield peptoid **13e** (0.25 g, 0.32 mmol, 32%) as red solid. R_F 0.35

(EtOAc). HRMS (ESI) *m/z* calcd. for $C_{44}H_{57}N_5O_8$ [M + H]$^+$ 783.4202, found 783.4194.

(9H-Fluoren-9-yl)methyl ((2S)-1-((1-oxyl-2,2,6,6-tetramethylpiperidin-4-yl)(2-oxo-2-((2,4,4-trimethoxybutyl)amino)ethyl)amino)-1-oxopropan-2-yl)carbamate (13f)

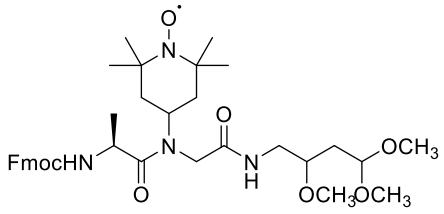

13f

Obtained using the general procedure **1**, IPB isonitrile **11b**, Fmoc-*L*-alanine, paraformaldehyde and *N*-oxyl amine **2** were used. The crude material was purified by silica gel column chromatography (EtOAc) to yield peptoid **13f** (0.37 g, 0.55 mmol, 55%) as red solid. R_F 0.32 (EtOAc). HRMS (ESI) *m/z* calcd. for $C_{36}H_{52}N_4O_8$ [M + H]$^+$668.3780, found 668.3760.

(9H-Fluoren-9-yl)methyl (2-((1-oxyl-2,2,6,6-tetramethylpiperidin-4-yl)(2-oxo-2-((2,4,4-trimethoxybutyl)amino)ethyl)amino)-2-oxoethyl)carbamate (13g)

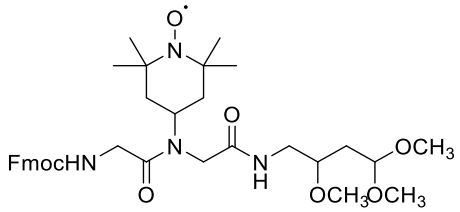

13g

Obtained using the general procedure **1**, IPB isonitrile **11b**, Fmoc- glycine, paraformaldehyde and *N*-oxyl amine **2** were used. The crude material was purified by silica gel column chromatography (EtOAc) to yield peptoid **13g** (0.39 g, 0.59 mmol, 60%) as red solid. R_F 0.45 (EtOAc). HRMS (ESI+) *m/z* calcd. for $C_{35}H_{50}N_4O_8$ [M + H]$^+$ 654.3623, found 654.3593.

(9H-Fluoren-9-yl)methyl ((2S)-1-((1-oxyl-2,2,6,6-tetramethylpiperidin-4-yl)(3-methyl-1-oxo-1-((2,4,4-trimethoxybutyl)amino)butan-2-yl)amino)-1-oxo-3-phenylpropan-2-yl) carbamate (13h)

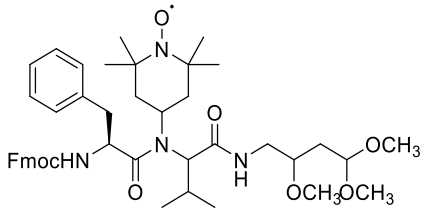

13h

Obtained using the general procedure **1**, IPB isonitrile **11b**, Fmoc-*L*-phenyl alanine, isobutyric aldehyde and *N*-oxyl amine **2** were used. The crude material was purified by silica gel column chromatography (EtOAc) to yield peptoid **13h** (0.39 g, 0.49 mmol, 59%) as red solid. R_F 0.48 (EtOAc). HRMS (ESI+) *m/z* calcd. for $C_{45}H_{62}N_4O_8$ $[M + H]^+$ 786.4562, found 786.4546.

General procedure (2) for the conversion of peptoids 12b, 13a-h to spin-labelled diketopiperazines 15a-i via *N*-acylpyrroles.

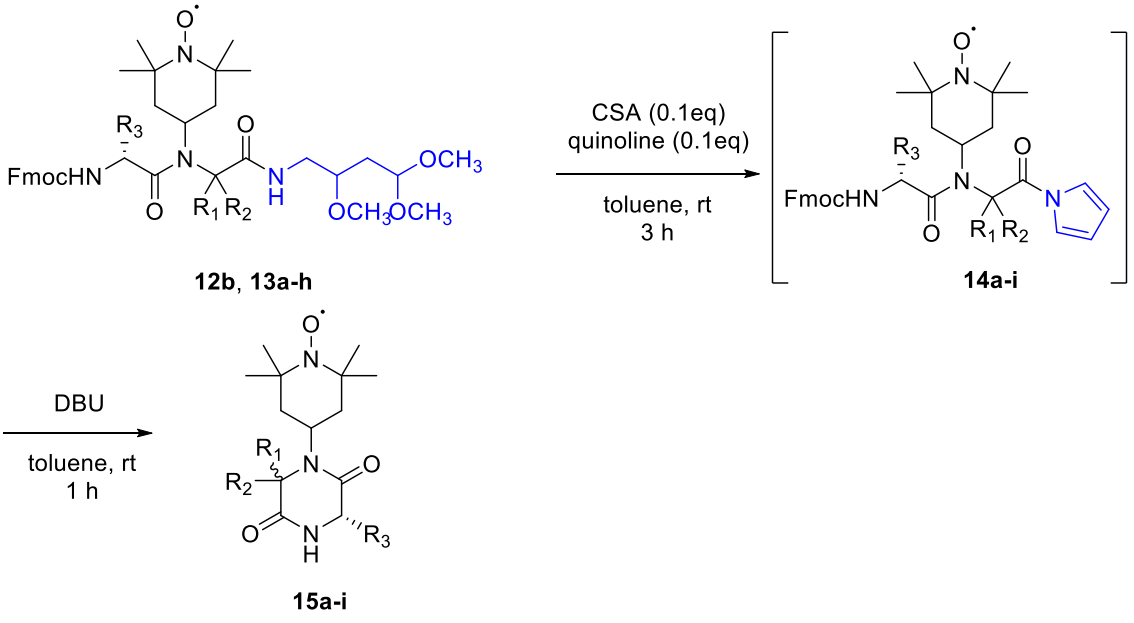

12b, **13a-h**

14a-i

15a-i

To a solution of linear Ugi-products **12b**, **13a-h** (0.5 mmol) in toluene (10 mL) was added 10-camphor sulfonic acid (10 mol%) and quinoline (10 mol%). The mixture was stirred for 1 min at rt and then refluxed for at least 30 min until TLC showed complete conversion. The mixture was cooled to rt, transferred to a separatory funnel and washed with 1M aqueous HCl (2 × 30 mL). The acidic aqueous phase was further extracted with ethyl acetate (1 × 20 mL). The organic layers were combined, washed with $NaHCO_3$ and brine (2 × 20 mL), dried over anhydrous Na_2SO_4, filtered and evaporated under reduced

pressure to obtain the *N*-acyl pyrrole derivative which was used in the next step without further purification.

The *N*-acylpyrroles **14a-i** (0.12 mmol) were dissolved in toluene (2 mL) and DBU (20 mol%) was added. The resulting reaction mixture was stirred at rt until completion of the reaction (determined by TLC). Subsequently, the reaction was concentrated under reduced pressure. The residual material was purified by silica gel column chromatography to give the desired product.

(S)-1-(1-Oxyl-2,2,6,6-tetramethylpiperidin-4-yl)-3-isopropylpiperazine-2,5-dione (15a)

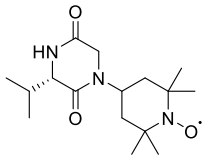

Obtained using the general procedure **2**, starting from **12b**, the crude material was purified by silica gel column chromatography (EtOAc / MeOH 95:5) to give diketopiperazine **15a** (28 mg, 0.09 mmol, 75%) as red solid. R_F 0.54 (EtOAc / MeOH 95:5). HRMS (ESI+) *m/z* calcd. for $C_{16}H_{29}N_3O_3$ [M + H]$^+$ 311.2203, found 311.2195, $[\alpha]_D^{20}$ = –5.2 deg (*c* 0.2 mmol, MeOH). IR (ATR) λ_{max} cm^{-1}: 3246, 2970, 2931, 1639, 1460–1347.

(**S)-3-Benzyl-1-(1-oxyl-2,2,6,6-tetramethylpiperidin-4-yl)piperazine-2,5-dione (15b)**

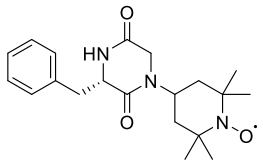

Obtained using the general procedure **2**, starting from **13a**, the crude material was purified by silica gel column chromatography (EtOAc / MeOH 95:5) to give diketopiperazine **15b** (27 mg, 0.07 mmol, 61%) as red solid. R_F 0.51 (EtOAc / MeOH 95:5). HRMS (ESI+) *m/z* calcd. for $C_{20}H_{29}N_3O_3$ [M + H]$^+$ 359.2203, found 359.2194, $[\alpha]_D^{20}$ = –14.0 deg (*c* 0.2 mmol, MeOH). IR (ATR) λ_{max} cm^{-1}: 3252, 2975, 2930, 1641, 1456–1334.

(S)-3-((S)-sec-Butyl)-1-(1oxyl-2,2,6,6-tetramethylpiperidin-4-yl)piperazine-2,5-dione (15c)

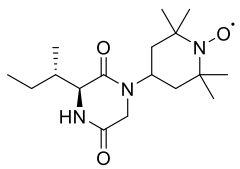

Obtained using the general procedure **2**, starting from **13b**, the crude material was purified by silica gel column chromatography (EtOAc / MeOH 95:5) to give diketopiperazine **15c** (27 mg, 0.08 mmol, 70%) as red solid. R_F 0.56 (EtOAc / MeOH 95:5). HRMS (ESI+) *m/z* calcd. for $C_{17}H_{31}N_3O_3$ [M + H]$^+$ 325.2360, found 325.2354. IR (ATR) λ_{max} cm^{-1} : 3248, 2970, 2931, 1638, 1455-1376.

(S)-1-(1-Oxyl-2,2,6,6-tetramethylpiperidin-4-yl)-3-isobutylpiperazine-2,5-dione (15d)

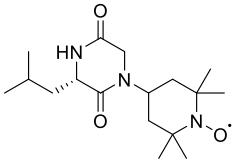

Obtained using the general procedure **2**, starting from **13c**, the crude material was purified by silica gel column chromatography (EtOAc / MeOH 95:5) to give diketopiperazine **15d** (25 mg, 0.07 mmol, 65%) as red solid. R_F 0.61 (EtOAc / MeOH 95:5). HRMS (ESI+) *m/z* calcd. for $C_{17}H_{31}N_3O_3$ [M + H]$^+$ 325.2360, found 325.2339, $[\alpha]_D^{20}$ = –8.0 deg (*c* 0.2 mmol, MeOH). IR (ATR) λ_{max} cm^{-1}: 3248, 2970, 2931, 1645, 1457–1345.

(S)-2-(1-Oxyl-2,2,6,6-tetramethylpiperidin-4-yl)hexahydropyrrolo[1,2-a]pyrazine-1,4-dione (15e)

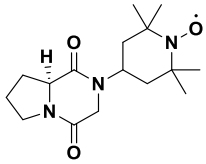

Obtained using the general procedure **2**, starting from **13d**, the crude material was purified by silica gel column chromatography (EtOAc / MeOH 95:5) to give diketopiperazine **15e** (20 mg, 0.06 mmol, 53%) as red solid. R_F 0.31 (EtOAc / MeOH 95:5). HRMS (ESI+) *m/z* calcd. for $C_{16}H_{27}N_3O_3$ [M + H]$^+$ 309.2047, found 309.2041, $[\alpha]_D^{20}$ = –71.9 deg (*c* 0.2 mmol, MeOH). IR (ATR) λ_{max} cm^{-1}: 2974, 2934, 1651, 1447–1364.

(S)-3-((1*H*-Indol-3-yl)methyl)-1-(1-oxyl-2,2,6,6-tetramethylpiperidin-4-yl)piperazine-2,5-dione (15f)

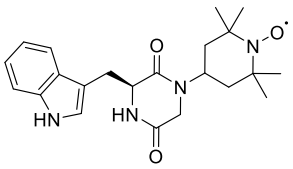

Obtained using the general procedure **2**, starting from **13e**, the crude material was purified by silica gel column chromatography (EtOAc / MeOH 95:5) to give diketopiperazine **15f** (24 mg, 0.06 mmol, 51%) as red solid. R_F 0.45 (EtOAc / MeOH 95:5). HRMS (ESI+) *m/z* calcd. for $C_{22}H_{30}N_4O_3$ [M + H]$^+$ 398.2312, found 398.2301, $[\alpha]_D^{20}$ =121.6 deg (*c* 0.2 mmol, MeOH). IR (ATR) λ_{max} cm^{-1}: 3403, 3242, 2974, 2920, 1648, 1458–1342.

(S)-1-(1-Oxyl-2,2,6,6-tetramethylpiperidin-4-yl)-3-methylpiperazine-2,5-dione (15g)

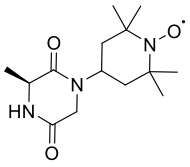

Obtained using the general procedure **2**, starting from **13f**, the crude material was purified by silica gel column chromatography (EtOAc / MeOH 95:5) to give diketopiperazine **15g** (23 mg, 0.08 mmol, 66%) as red solid. R_F 0.31 (EtOAc / MeOH 95:5). HRMS (ESI+) *m/z* calcd. for $C_{14}H_{25}N_3O_3$ $[M + H]^+$ 283.1890, found 283.1883, $[\alpha]_D^{20}$ = –11.8 deg (*c* 0.2 mmol, MeOH). IR (ATR) λ_{max} cm^{-1}: 3246, 2974, 2931, 1650, 1465–1374.

1-(1-Oxyl-2,2,6,6-tetramethylpiperidin-4-yl)piperazine-2,5-dione (15h)

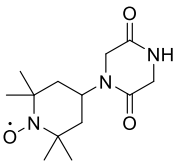

Obtained using the general procedure **2**, starting from **13g**, the crude material was purified by silica gel column chromatography (EtOAc / MeOH 95:5) to give diketopiperazine **15h** (16 mg, 0.06 mmol, 67%) as red solid. R_F 0.22 (EtOAc / MeOH 95:5). HRMS (ESI+) *m/z* calcd. for $C_{13}H_{23}N_3O_3$ $[M + H]^+$ 269.1734 found 269.1725. IR (ATR) λ_{max} cm^{-1}: 3292, 2997, 2937, 1648, 1460–1352.

(3S)-3-Benzyl-1-(1-oxyl-2,2,6,6-tetramethylpiperidin-4-yl)-6-isopropylpiperazine-2,5-dione (15i)

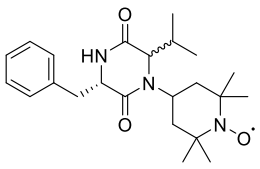

Obtained using the general procedure starting **2**, from **13h**, the crude material was purified by silica gel column chromatography (EtOAc / MeOH 95:5) to give diketopiperazine **15i** (29 mg, 0.07 mmol, 60%) as red solid. R_F 0.22 (EtOAc / MeOH 95:5). HRMS (ESI+) *m/z* calcd. for $C_{23}H_{35}N_3O_3$ $[M + H]^+$ 401.2673, found 401.2662**,** $[\alpha]_D^{20}$= –58.4 deg (*c* 0.2 mmol, MeOH). IR (ATR) λ_{max} cm^{-1}: 3241, 2972, 2932, 1639, 1466-1386.

Methyl ((S)-14-benzyl-13-(1-oxyl-2,2,6,6-tetramethylpiperidine-4-carbonyl)-3,11-dioxo-1-phenyl-2,7-dioxa-4,10,13-triazapentadecan-15-oyl)-L-leucinate (16)

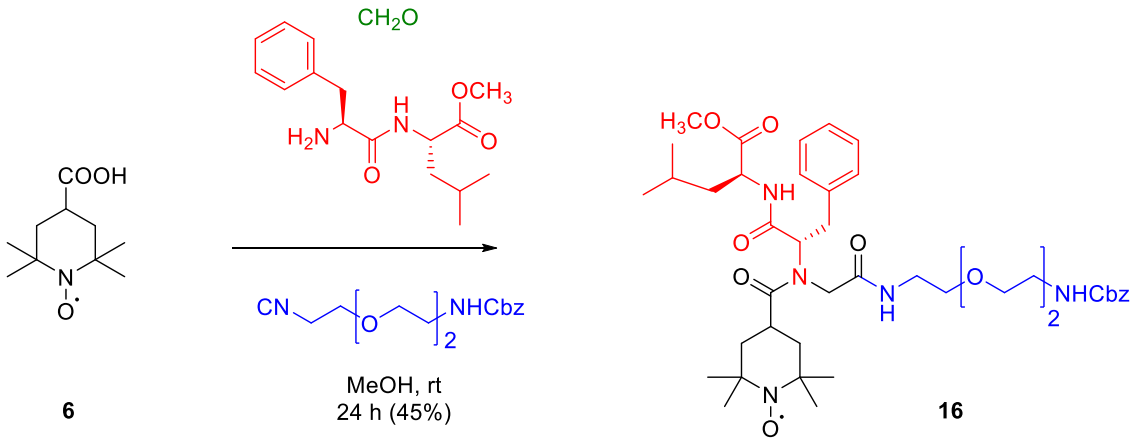

To a stirred solution of dipeptide H-L-Phe-L-Leu-OCH_3 (290 mg, 1.0 mmol) in MeOH (2.5 mL) was added paraformaldehyde (30 mg, 1.0 mmol) and the mixture was stirred at rt for 4 h. After this time TEMPO-derived carboxylic acid **6** (200 mg, 1.00 mmol) and PEG-isocyanide (290 mg, 1.0 mmol)[3] were added, before stirring was continued for 18 h. The solvent was removed under reduced pressure and the crude material was purified by silica gel column chromatography (EtOAc) to give peptoid **16** (365 mg, 0.45 mmol, 45%) as red solid. R_F 0.45 (EtOAc). HRMS (ESI) *m/z* calcd. for $C_{42}H_{63}N_5O_{10}$ $[M + H]^+$ 797.4569, found 797.4575. $[\alpha]_D^{20}$ = –72.7 deg (*c* 0.2 mmol, MeOH).

***tert*-Butyl (2S)-2-(((2S)-1-((1-oxyl-2,2,6,6-tetramethylpiperidin-4-yl)(2-oxo-2-((2,4,4-trimethoxybutyl)amino)ethyl)amino)-1-oxo-3-phenylpropan-2-yl)carbamoyl)pyrrolidine-1-carboxylate (17)**

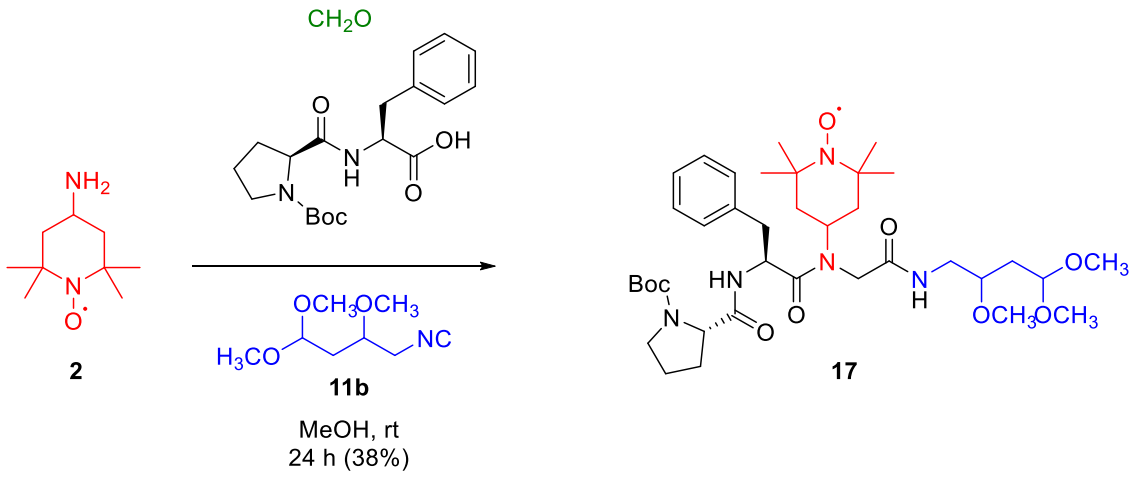

To a stirred solution of TEMPO-derived amine **2** (170 mg, 1.0 mmol) in MeOH (2.5 mL) was added paraformaldehyde (30 mg, 1.0 mmol) and the mixture was stirred for 4 h at rt. After this time Boc-L-Pro-L-Phe-OH (360 mg, 1.0 mmol) and IPB isocyanide **11b** (170 mg, 1.0 mmol) were added, before stirring was continued for 18 h. The solvent was removed under reduced pressure and the crude material was purified by silica gel column chromatography (EtOAc) to give peptoid **17** (270 mg, 0.37 mmol, 38%) as red solid. R_F 0.18 (EtOAc). HRMS (ESI) *m/z* calcd. for $C_{37}H_{61}N_5O_9$ $[M + H]^+$ 719.4464, found 719.4429. $[\alpha]_D^{20}$= –18.5815 deg (*c* 0.2 mmol, MeOH).

Benzyl *N*-(*N*2,*N*6-bis((benzyloxy)carbonyl)-L-lysyl)-*N*-(2-((1-oxyl-2,2,6,6-tetramethyl piperidine-4-yl)amino)-2-oxoethyl)glycylphenylalaninate (18)

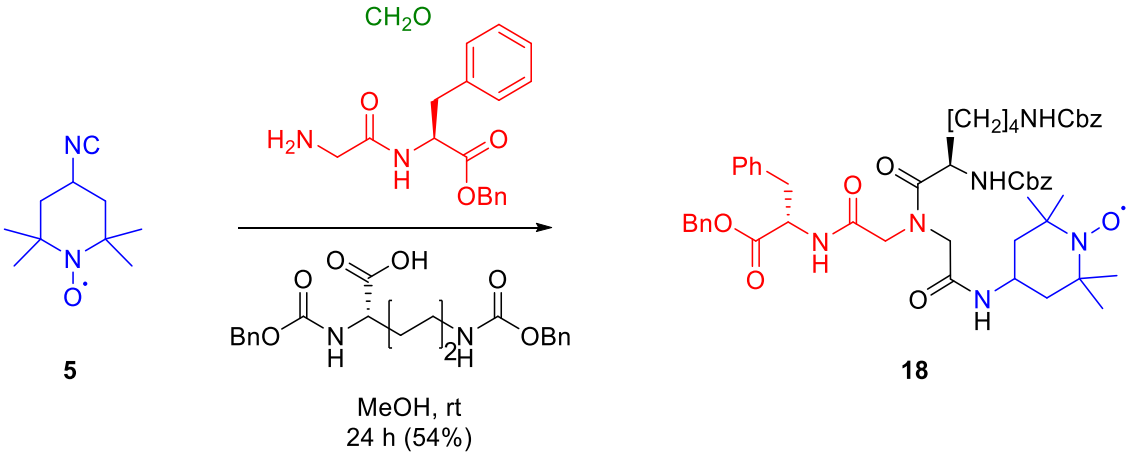

To a stirred solution of dipeptide H-Gly-L-Phe-OBn (310 mg, 1.0 mmol) in MeOH (2.5 mL) was added TEA (0.14 mL, 1.0 mmol) and paraformaldehyde (30 mg, 1.0 mmol). The mixture was stirred for 4 h at rt. After this time the amino acid Cbz-Lys(z)-OH (410 mg, 1.0 mmol) and TEMPO-derived isocyanide **5** (180 mg, 1.0 mmol) were added, before stirring was continued for 24 h. The solvent was removed under reduced pressure and the crude material was purified by silica gel column chromatography (EtOAc) to give peptoid **18** (494 mg, 0.53 mmol, 54%) as red solid. R_F 0.64 (EtOAc). HRMS (ESI) *m/z* calcd. for $C_{51}H_{64}N_6O_{10}$ $[M + H]^+$ 920.4678, found 920.4675, $[\alpha]_D^{20}$=7.88 deg (*c* 0.2 mmol, MeOH).

***tert*-Butyl (S)-2-(((S)-1-((2-(((S)-1-(benzyloxy)-1-oxo-3-phenylpropan-2-yl)amino)-2-oxoethyl)(2-((1-hydroxy-2,2,6,6-tetramethylpiperidin-4-yl)amino)-2-oxoethyl)amino)-1-oxo-3-phenylpropan-2-yl)carbamoyl)pyrrolidine-1-carboxylate (19)**

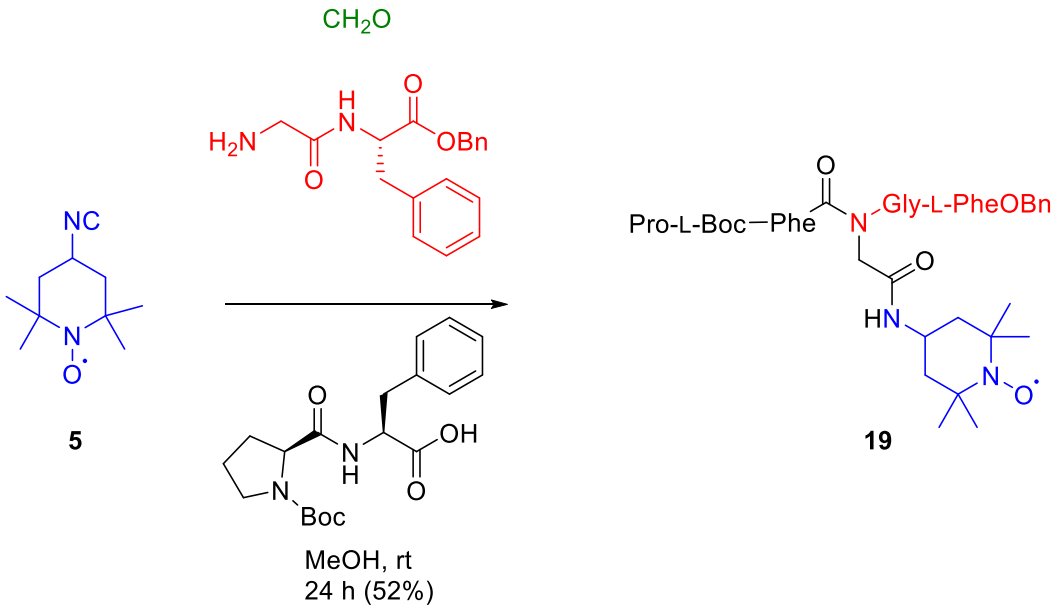

To a stirred solution of amine H-Gly-L-Phe-OBn (31 mg, 1.0 mmol) in MeOH (2.5 mL) was added TEA (0.14 mL, 1.0 mmol) and paraformaldehyde (30 mg, 1.0 mmol) and the mixture was stirred for 4 h. After this time the amino acid Boc-L-Pro-L-Phe-OH (360 mg, 1.0 mmol) and TEMPO-derived isocyanide **5** (180 mg, 1.0 mmol) were added, before stirring continued for 18 h at rt. The solvent was removed under reduced pressure and the crude material was purified by silica gel column chromatography (EtOAc / FA 0.3%) to give peptoid **19** (450 mg, 0.53 mmol, 52%) R_F 0.2 (EtOAc / FA 98:2). HRMS (ESI) *m/z* calcd. for $C_{48}H_{64}N_6O_9$ $[M + H]^+$ 868.4729, found 868.4728, $[\alpha]_D^{20}$= 24.5 deg (*c* 0.2 mmol, MeOH).

_N_-(2-(_tert_-butylamino)-2-oxoethyl)-_N_-((S)-1-(((S)-1-((2-(tert-butylamino)-2-oxoethyl)(1-oxyl -2,2,6,6-tetramethylpiperidin-4-yl)amino)-4-methyl-1-oxopentan-2-yl)amino)-1-oxo-3-phenylpropan-2-yl)-1-oxyl-2,2,6,6-tetramethylpiperidine-4-carboxamide (20)

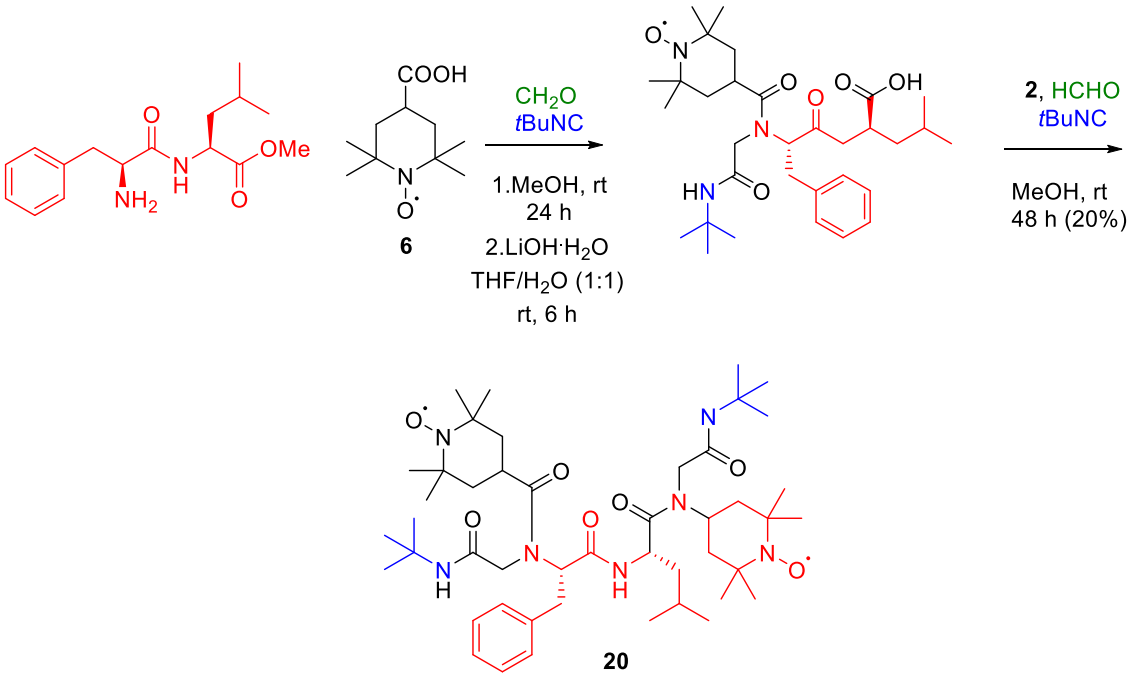

To a stirred solution of dipeptide H-L-Phe-L-Leu-OMe (290 mg, 1.0 mmol) in MeOH (2.5 mL) was added TEA (0.14 mL, 1.0 mmol) and paraformaldehyde (30 mg, 1.0 mmol) and stirred for 4 h at rt. After this time carboxy-derived TEMPO **6** (200 mg, 1.0 mmol) and *t*-butyl isocyanide (83 mg, 1.0 mmol) were added, before stirring was continued for 24 h. A solution of LiOH.H_2O (126 mg, 3.0 mmol) in THF:H_2O (1:1, 80 mL) was added in one portion at 0 °C. After stirring for 6 h, the mixture was transferred to a separatory funnel. The solution was acidified to pH 3 using a saturated $NaHSO_4$ solution and brine solution (20 mL) was added. The contents were extracted with ethyl acetate (3 × 40 mL). The organic layer was dried over Na_2SO_4 and the solvent was removed under reduced pressure after filtration to afford the first Ugi-intermediate which was subjected to the second Ugi-reaction using preformed imine from amino TEMPO **2** (170 mg, 1.0 mmol) and paraformaldehyde (30 mg, 1.0 mmol) followed by *tert*-butyl isocyanide (83 mg, 1.0 mmol) and the reaction is stirred for 48 h at rt. The solvent was removed under reduced pressure and the crude material was purified by silica gel column chromatography (EtOAc / *n*-hexane 8:2) to give peptoid **20** (170 mg, 0.20 mmol, 20%) as dark red solid. R_F 0.2 (EtOAc / FA 98:2). HRMS (ESI) m/z calcd. for $C_{46}H_{79}N_7O_7$ $[M + H]^+$ 840.5957, found 840.5948 $[\alpha]_D^{20}$= –24.0 deg (c 0.2 mmol, MeOH).

2.5 References

(1) a) Jeschke, G., *Annu. Rev. Phys. Chem.* **2012**, 63, 419–446; b) Reichenwallner, J.; Hinderberger, D. *Biochim. Biophys. Acta* **2013**, 1830, 5382–5393; c) Junk, M. J. N.; Spiess, H. W.; Hinderberger, D. *Biophys. J*. **2011**, 100, 2293–2301; d) Hubbell, W. L.; Mchaourab, H. S.; Altenbach, C.; Lietzow, M. A. *Structure* **1996**, 4, 779–783.

(2) Krstić, I.; Endeward, B.; Margraf, D.; Marko, A.; Prisner, T. F., *Top. Curr. Chem*. **2012**, 321, 159–198.

(3) Hauenschild, T.; Reichenwallner, J.; Enkelmann, V.; Hinderberger, D. *Chem. Eur. J*. **2016**, 22, 12825–12838.

(4) a) Fielding, A. J.; Concilio, M. G.; Heaven, G.; Hollas, M. A. *Molecules* **2014**, 19, 16998–17025; b) Hubbell, W. L.; López, C. J.; Altenbach, C.; Yang, Z. *Curr. Opin. Struct. Biol*. **2013**, 23, 725–733; c) Frantz, M.C.; Skoda, E. M.; Sacher, J. R.; Epperly, M. W.; Goff, J. P.; Greenberger, J. S.; Wipf, P. *Org. Biomol. Chem.* **2013**, 11, 4147–4153.

(5) Braun, P.; Nägele, B.; Wittmann, V.; Drescher, M. *Angew. Chem. Int. Ed.* **2011**, 50, 8428–8431.

(6) Kugele, A.; Braun, T. S.; Widder, P.; Williams, L.; Schmidt, M. J.; Summerer, D.; Drescher, M. *Chem. Commun.* **2019**, 55, 1923–1926.

(7) Milov, A. D.; Erilov, D. A.; Salnikov, E. S.; Tsvetkov, Y. D.; Formaggio, F.; Toniolo, C.; Raap, J. *Phys. Chem. Chem. Phys.* **2005**, 7, 1794–1799.

(8) Schreier, S.; Bozelli, J. C.; Marín, N.; Vieira, R. F. F.; Nakaie, C. R. *Biophys. Rev*. **2012**, 4, 45–66.

(9) Stoller, S.; Sicoli, G.; Baranova, T. Y.; Bennati, M.; Diederichsen, U. *Angew. Chem. Int. Ed.* **2011**, 50, 9743–9746.

(10) Borthwick, A. D. *Chem. Rev*. **2012**, 112, 3641–3716.

(11) Zakrzewski, J.; Jezierska, J.; Hupko, J. *Org. Lett*. **2004**, 6, 695–697.

(12) van Berkel, S. S.; Bögels, B. G. M.; Wijdeven, M. A.; Westermann, B.; Rutjes, F. P. J. T. *Eur. J. Org. Chem.* **2012**, 3543–3559.

(13) Brauch, S.; van Berkel, S. S.; Westermann, B. *Chem. Soc. Rev.* **2013**, 42, 4948–4962.

(14) Stoll, S.; Schweiger, A. *J. Magn. Reson.* **2006**, 178, 42–55.

(15) Rikimaru, K.; Yanagisawa, A.; Kan, T.; Fukuyama, T. *Synlett* **2004**, 41–44.

(16) Neves Filho, R. A.W.; Stark, S.; Morejon, M. C.; Westermann, B.; Wessjohann, L. A. *Tetrahedron Lett.* **2012**, 53, 5360–5363.

(17) Wessjohann, L. A.; Morejón, M. C.; Ojeda, G. M.; Rhoden, C. R. B.; Rivera, D. G. *J. Org. Chem.* **2016**, 81, 6535–6545.

(18) a) Rhoden, C. R. B.; Rivera, D. G.; Kreye, O.; Bauer, A. K.; Westermann, B.; Wessjohann, L. A. *J. Comb. Chem.* **2009**, 11, 1078–1082; b) Bohn Rhoden, C.; Westermann, B.; Wessjohann, L. *Synthesis* **2008**, 2077–2082.

(19) Meldal, M.; Tornøe, C. W. *Chem. Rev.* **2008**, 108, 2952–3015.

(20) a) Ondar, M.A., Grinberg, O. Ya., Dubinskii, A. A.; Lebedev, Ya. S. *Sov. J. Chem. Phys.* **1985**, 3, 781–792; b) Kawamura, T.; Matsunami, S.; Yonezawa, T. *Bull. Chem. Soc.* **1967**, 40, 1111–1115; c) Snipes, W.; Cupp, J.; Cohn, G.; Keith, A. *Biophys. J.* **1974**, 14, 20–32.

(21) a) Saracino, G. A. A.; Tedeschi, A.; D'Errico, G.; Improta, R.; Franco, L.; Ruzzi, M.; Corvaia, C.; Barone, V. *J. Phys. Chem. A* **2002**, 106, 10700–10706; b) Improta, R.; Barone, V. *Chem. Rev.* **2004**, 104, 1231–1254.

(22) a) Kurzbach, D.; Junk, M. J. N.; Hinderberger, D. *Macromol. Rapid Commun.* **2013**, 34, 119–134; b) Knauer, B. R.; Napier, J. J. *J. Am. Chem. Soc.* **1976**, 98, 4395–4400; c) Pavone, M.; Cimino, P.; Crescenzi, O.; Sillanpää, A.; Barone, V. *J. Phys. Chem. B* **2007**, 111, 8928–8939.
(23) Rivera, D. G.; León, F.; Concepción, O.; Morales, F. E.; Wessjohann, L. A. *Chem. Eur. J.* **2013**, 19, 6417–6428.
(24) Wessjohann, L. A.; Neves Filho, R. A. W.; Rivera, D. G. *In Isocyanide Chemistry,* ed., V. G. Nenajdenko, Wiley-VCH, Weinheim, Germany, **2012**, 233–262.
(25) Xia, Y.; Li, Y.; Burts, A. O.; Ottaviani, M. F.; Tirrell, D. A.; Johnson, J. A.; Turro, N. J.; Grubbs, R. H. *J. Am. Chem. Soc.* **2011**, 133, 19953–19959.
(26) Brauch, S.; Henze, M.; Osswald, B.; Naumann, K.; Wessjohann, L. A.; van Berkel, S. S.; Westermann, B. *Org. Biomol. Chem.* **2012**, 10, 958–965.
(27) Wagner, C. B.; Studer, A. *Eur. J. Org. Chem.* **2010**, 5782–5786.
(28) Couet, W. R.; Brasch, R. C.; Sosnovsky, C.; Lukszo, J.; Prakash, I.; Gnewech, C. T.; Tozer, T. N. *Tetrahedron* **1985**, 41, 1165–1172.
(29) Rauckman, E. J.; Rosen, G. M.; Abou-Donia, M. B. *J. Org. Chem.* **1976**, 41, 564–565.
(30) Zakrzewski, J.; Hupko, J. *Org. Prep. Proc. Int.* **2003**, 35, 387–390.

Chapter 3

Synthesis and anticancer evaluation of novel TEMPO-terpene adducts generated by Ugi-multi-component-reactions

*Abstract**

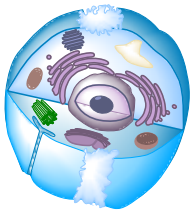

Cancer cell

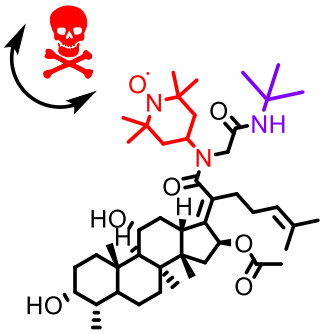

Spin-labelled Triterpenoic acid

Recently, spin-labelled biological active compounds were obtained utilizing the power of isonitrile based multicomponent reactions (IMCRs). To extend the scope and diversity of this strong synthetic tool we report here our results regarding the design, synthesis, and modification of triterpenoic acid derivatives viz.; betulinic-, fusidic- and cholic-acid by spin-labelling. Surprisingly the fusidic acid derivatives showed potent activity against the two investigated cancer cell lines viz.; prostate cancer (PC3) and colon cancer (HT-29). The spin-labelled fusidic acid derivative induces apoptosis by a caspase-dependent mechanism. Moreover, convertible amide modified spin-labelled fusidic acid was selected for post-Ugi-modification utilizing a wide range of reaction conditions which kept the paramagnetic center intact. This suggests that IMCRs can be considered as a strong tool towards the synthesis of novel anticancer agents combining natural products and spin labels.

**Own contribution: synthesis and characterization of spin-labelled products as well as the measurements of EPR-spectra.

3.1 Introduction

Reactive oxygen species (ROS) are free radicals, which can be defined as an atom or molecule, having one or more unpaired electrons and being capable of independent existence. The presence of unpaired electrons make it extremely unstable, therefore, ROS are highly reactive. In general, ROS can be of two types: free oxygen radicals and non-radical ROS. Superoxide and hydroxyl radicals are good examples of oxygen radicals while hydrogen peroxide and singlet oxygen are examples of non-radical ROS. Among ROS, superoxide, hydrogen peroxide and hydroxyl radicals are the most studied ROS in cancer. Moreover, increased ROS production is also involved in many pathological disorders such as atherosclerosis, cardiovascular diseases, hypertension, diabetes mellitus, neurodegenerative and immune-inflammatory diseases.[1] On the molecular level, ROS can induce oxidative stress that leads to altering the cell membrane structure (lipid peroxidation of polyunsaturated fatty acids), in DNA elevated ROS production can cause mutations which eventually leads to cancer.[2] Moreover, proteins are also affected by ROS, which can lead to alterations of its structure and thereby its function. On the microscopic level, mitochondria are considered the major source of ROS production, it has been estimated about 90% of the ROS is being generated in the mitochondria, eventually, mitochondria itself will sever from the high oxidative environment which will lead to mitochondrial dysfunction. The role of ROS in cancer is quite intriguing, on one hand, ROS can promote protumorigenic signaling, that facilitates cell growth and survival. To enhance this protumorigenic signaling, cancer cells increase their rate of ROS production by activating oncogenic mutations, increasing their metabolic activity and adapting to hypoxia. On the other hand, ROS can promote the antitumorigenic signaling which induces cancer cell death due to the buildup of ROS production. To prevent such an event and to restore a balanced redox, cancer cells increase their antioxidant capacity, in order to scavenge the excess ROS and to maintain it at a level that allows only for the activation of protumorigenic signaling pathways without promoting cell death.[3] This unique high ROS production in the cancer cells can be considered a golden opportunity, hence, strategies that are based on either, eliminating ROS or interfering with the redox state of the cell, maybe a potential strategy for cancer treatment.[4,5]

Many chemotherapeutic agents such as taxanes, Vinca alkaloids exert their cytotoxic activities by increasing ROS production, thus ROS production during cancer chemotherapy can interfere with the efficacy of the treatment[6]. Antioxidants, when they are co-administrated with the chemotherapeutic agents are proven to reduce some of the side effects caused by the chemotherapeutic agents. Recent studies exploring the

efficiency of antioxidants for cancer prevention have been published.[7] Among antioxidants, nitroxide radicals are stable persistent radicals that possess antioxidant properties. Nitroxides have been shown to protect the cell against a variety of agents that induce oxidative stress.[8] The antioxidant activity of nitroxide radicals can be explained by numerous chemical mechanisms including, superoxide dismutase mimic activity, oxidation of reduced metals that can catalyze the formation of hydroxyl radicals from hydrogen peroxide, catalase mimic activity [9], trapping of carbon-centered radicals, or to terminate chain reactions.[10]

In addition, conjugation of nitroxides with anticancer drugs was shown to enhance the activity of the existing agents toward the cancer cell[11], either by inducing apoptosis via caspase-dependent pathway[12] or eliminating the side effect of ROS generated by anticancer agents such as doxorubicin, thereby reducing its side effect.[13]

Betulinic acid **1**, and its natural analogues **2** and **3** (**Figure 3. 1**) are reported to act as cytotoxic natural products.[14] Many reports, were published regarding the modification of these triterpenes as a synthetic strategy for enhancing their existing biological activities.[15,16]

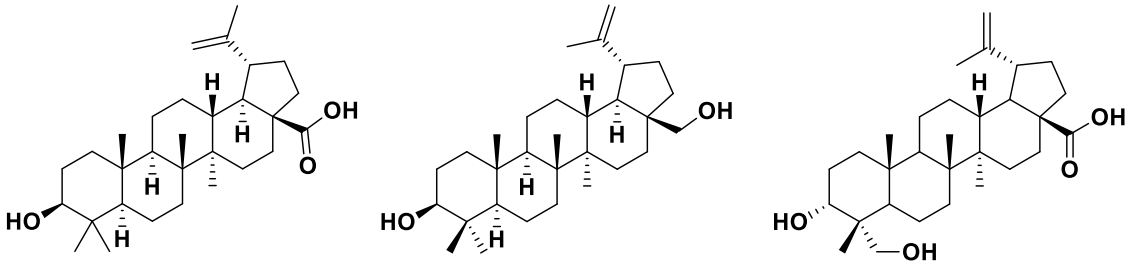

betulinic acid (**1**) betulin (**2**) 23-hydroxybetulinic acid (**3**)

Figure 3. 1 Structure of betulinic acid and its analogues.

Recently, spin-labelled amide derivatives of betulinic acid were synthesized, and their cytotoxic activity was evaluated on various cancer cell lines (e.g. CEM-13, U-937, MT-4).[17] In this chapter, we want to disclose our studies by utilizing multi-component reaction viz.; isonitrile based multicomponent reaction (IMCR) as our synthetic strategy, towards the syntheses of nitroxyl radical triterpenoid conjugates, with the aim of increasing its cytotoxic activities. Utilizing IMCR allows us for a very fast robust and strong synthetic strategy towards obtaining highly diversified products, which is the most significant feature for this reaction type. Betulinic acid (**1**) is used as the acid component in this study. Although IMCR modifications of betulinic acid have been described, none of the reported compounds contains nitroxyl radical.[18,19] In addition to betulinic acid (**1**), we have also described the conjugation of nitroxyl radical to fusidic- (**4**), and cholic acid (**5**)

(**Figure 3. 2**). These examples can verify and extend the scope of terpene TEMPO conjugates as potential cytotoxic compounds via ROS manipulation.

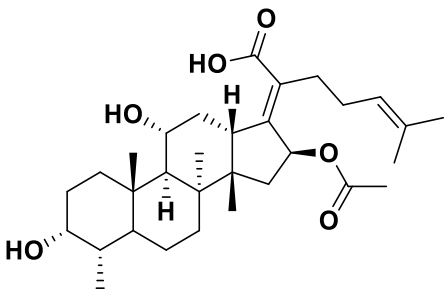

fusidic acid (**4**)

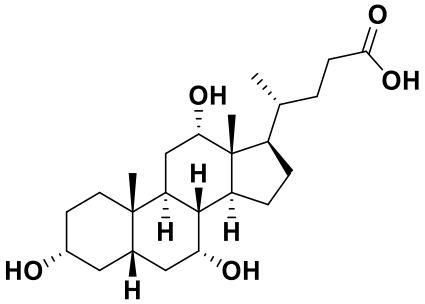

cholic acid (**5**)

Figure 3. 2 Fusidic acid and cholic acid structures.

3.2 Synthetic plan

In the previous chapter, we could demonstrate that U-4CR, which comprises the condensation of a carboxylic acid, oxo-component, amine, and isonitrile, as a new strategy for site-directed spin labelling (SDSL) of biologically active compounds.[20] The advantages of this methodology besides the high diversity are manifold, the reaction does not need any activation for the ligation of any of the partners, the reaction can be carried out at ambient conditions, and the sole by-product is water. Another advantageous feature of this approach is the formation of tertiary amides whose metabolic stability is increased compared to the most-present secondary amides.[21,22]

3.2.1 Synthesis of spin-labelled terpene derivatives

For obtaining the spin-labelled Ugi-adducts **7-13**, in this chapter again we turned our attention to utilize 4-amino-2,2,6,6-tetramethylpiperidine-1-oxyl (4-NH_2-TEMPO) as the spin label part (**Scheme 3. 1**). Previously we could prove that the spin label is not affected under the mild reaction conditions of the U-4CR, in addition we could also prove that post Ugi-modification is also possible without any disproportionation/decay of the radicals[20], which allows us to use this synthetic protocol for the synthesis of the spin-labelled natural product adducts. Formaldehyde was chosen as the carbonyl component to avoid the formation of diastereomers. On the other hand, we have selected betulinic, fusidic, and cholic acids (**1**, **4**, and **5**) as the carboxylic acid library. These natural carboxylic acids are slightly different regarding the chemical nature of carboxylic acid, ranging from tertiary (in betulinic acid **1**) to acrylic (in fusidic acid **4**) and finally secondary

in (cholic acid **5**). For the isonitrile, we have decided to use the commercially available *t*-butyl isonitrile and the IPB-isonitrile **6**, which was developed and synthesized and tested in our laboratory as convertible amide component for post-Ugi-derivatizations and decorations.[23,24]

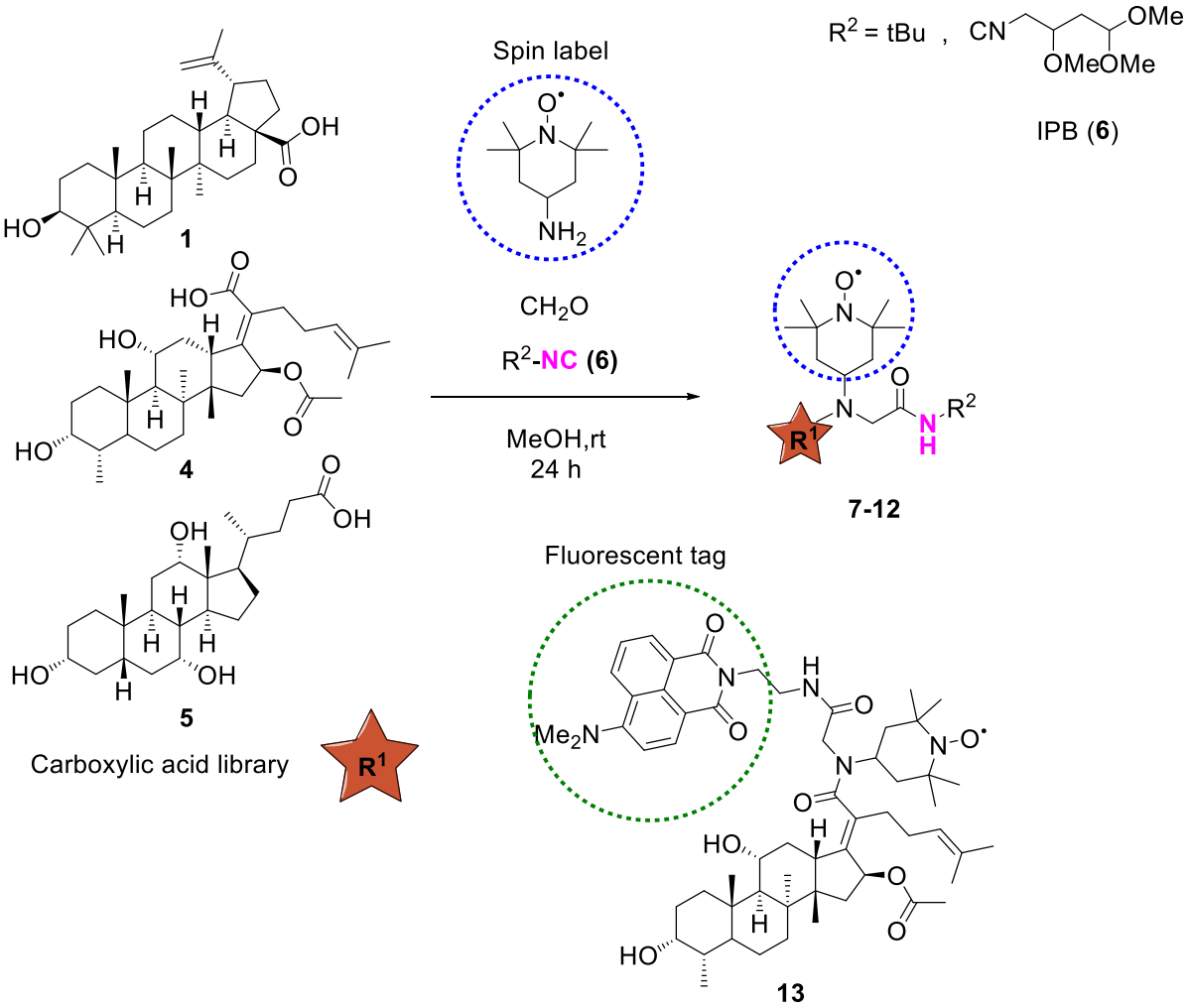

Scheme 3. 1 Synthesis of betulinic-, fusidic- and cholic-acid spin-labelled adducts **7-13**.

As shown in **Table 3. 1**, the yields for the spin-labelled adducts range from ~35-81%. These good yields clearly prove the versatility of the IMCR approach to achieve complex natural products in just one transformation. The nature of the carboxylic acid part had no big impact on product formation. The bird's-eye applicability of this approach can be seen in the formation of the dye-modified spin label adduct **13** in 33% yield, here an isonitrile modified dye was used as the isontirile component, which was designed by Yudin *et al*.[25] The spin label and the modified dye can be condensed in a single step without additional experimental efforts.

Table 3. 1 Yields of TEMPO terpene adducts.

Entry	Product	Acid/R^2	Yield [%]
1	**7**	**1**/*t*Bu	70
2	**8**	**1**/IPB	61
3	**9**	**4**/*t*Bu	57
4	**10**	**4**/IPB	69
5	**11**	**5**/*t*Bu	81
6	**12**	**5**/IPB	61
7	**13**	**4**/dye	35

3.2.2 Synthesis of post-Ugi-modified spin label adducts 15 and 17-19

The reactivity of the convertible isonitrile IPB **6** was utilized to expand the scope of the synthetic protocol and to show the diversity of products that can be obtained. We selected compounds **8** and **10**, which were synthesized using IPB **6** as the isonitrile counterpart. The resulting secondary amide can be transformed upon acidic treatment to acyl pyrroles, which are easily susceptible to nucleophilic attack. Furthermore, the conversion into acyl pyrroles was done by refluxing compounds **8** and **10** in the presence of camphor sulfonic acid (CSA) to yield the intermediates **14** and **16**, which upon treatment with KOH at room temperature converted into the carboxylates **15** and **18**, respectively (**Scheme 3. 2**).

However, in the case of the fusidic acid conjugate **16**, the basic conditions also cleaved the acetyl group, which is connected to C16 of ring D of the fusidic acid. Therefore, no selectivity could be obtained on the acetyl moiety in fusidic acid conjugate **16**. For achieving the controlled selectivity of the acyl pyrrole formation, we used another deprotection protocol. Treatment with DMAP in water/*t*-butanol as our deprotection cocktail yielded the carboxylate **17**. Post-Ugi-modification of the synthesized carboxylates could also be performed either to increase the activity/targeting of the synthesized compounds. One way for enhancing the activity and the selectivity of the Ugi-products toward the cancer cells is to conjugate the post-Ugi-modified spin label with a triphenylphosphine moiety. The triphenylphosphonium cation (TPP^+) is used to target parent compounds to the mitochondria matrix. Many reports showed that the mitochondria-targeted derivatives of betulinic acid (**1**) and betulin (**2**) (**Figure 3. 1**) showed stronger cytotoxicity than their parent drugs and good selectivity toward cancer cells over normal cells.[26]

For that reason, we envisioned to have a conjugate with a triphenylphosphine moiety. Again, the IMCR provided an excellent solution and, therefore, was chosen to be the synthetic protocol of choice. In a single step transformation, the reaction yielded the dual readout compound **19**, which conjugates the spin-labelled natural product **17**, not only to triphenylphosphine but also to the fluorescent dye (Yudin's dye) to track our conjugate using fluorescence microscopy (**Scheme 3. 2**). The yields of all post modified products are provided in **Table 3. 2**.

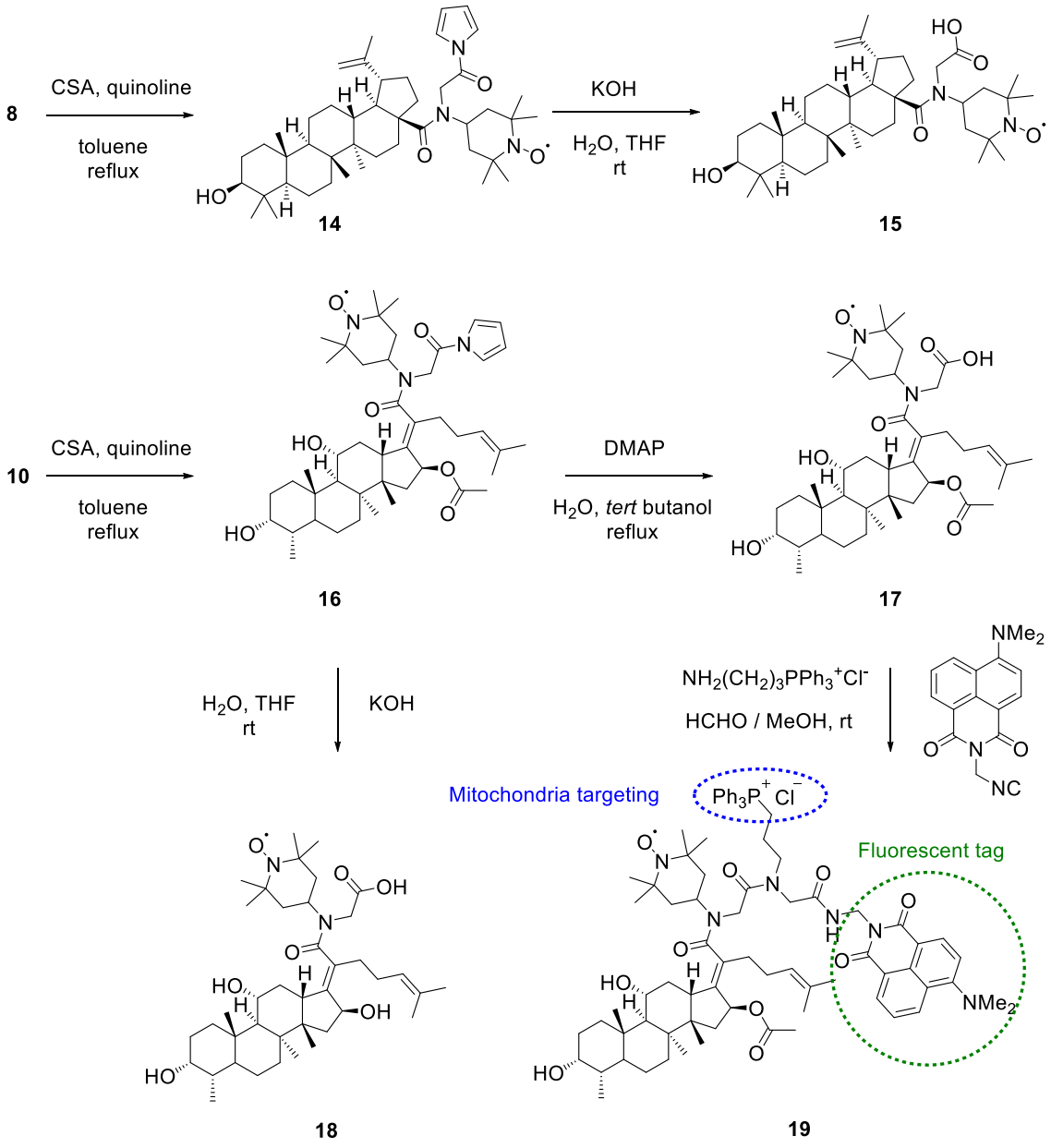

Scheme 3. 2 Post-Ugi-modification of compounds **8** and **10**.

Table 3. 2 Yields of post-Ugi-modified adducts.

Entry	Product	Yield [%]
1	**15**	70
2	**17**	66
3	**18**	58
4	**19**	34

All the synthesized products have been confirmed by HRMS, ^{1}H NMR, ^{13}C NMR, the purity of the all synthesized products were confirmed by recording the HPLC. EPR spectroscopy was recorded for some selected compounds. Recording the NMR-spectra requires the reduction of the spin label, otherwise, the spectra cannot be interpreted due to significant line broadening due to the interaction between the electron spin with the nucleus spin nearby. For this study, we have chosen phenylhydrazines **20** and hydrazobenzene **21** as reducing agents. In addition, any overlapping signals of the reducing agent and the signals from the corresponding hydroxylamines counterpart can be avoided (**Scheme 3. 3**).

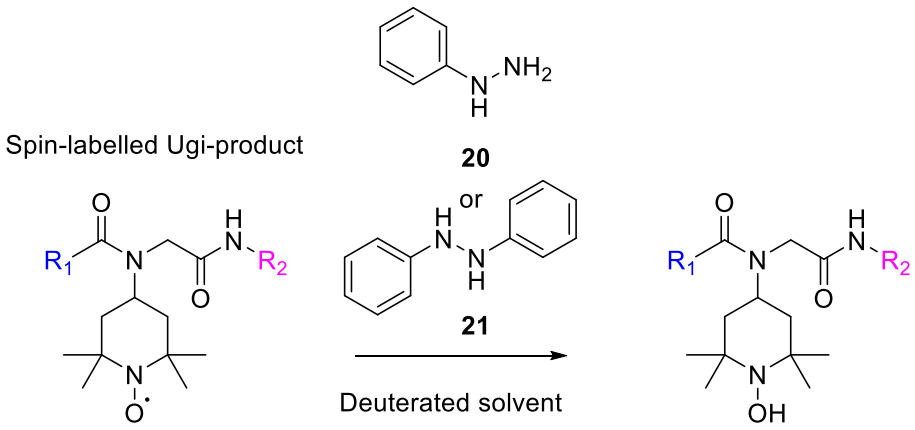

Scheme 3. 3 *In situ* "NMR" reduction of the synthesized spin-labelled products.

3.3 Biological evaluation of the spin-labelled adducts

In this section we selected the first set of the triterpenoic spin-labelled adducts **7-12** to be evaluated to have an overall view on their potential activity's against human cancer cell lines viz.; PC3 (prostate cancer) and HT-29 (colon cancer). The tested compounds were evaluated for their ability to reduce cell viability against PC3 and HT-29 cancer cell lines. IC_{50} values were calculated for the most active compounds to determine their cytotoxic potential. Afterward, flow cytometry analysis was performed for the most active compound to investigate its mode of action, followed by western blot analysis to study the effect of the most active compound on the expression levels of different proteins.

Moreover, the most active compound was tested for its ability to reduce the level of reactive oxygen species. Finally, fluorescence microscopy was performed to determine whether mitochondria targeting was successful with compound **13** and **19**.

3.3.1 Fast screening evaluation of spin-labelled adducts

At first, fast screening was performed for the synthesized compounds **7-12** against human cancer cell lines viz.; PC3 and HT-29 which represent prostate and colon cancer cell lines respectively, by applying two different concentrations of the compounds (0.1 and 10 µM). Their activities were compared to the activity of betulinic-, fusidic-, and cholic acid. The results were presented as a percentage compared to the viability of untreated cells which were determined using MTT and CV assays. The results are shown in **Figure 3. 3**. Compounds were considered active when showing activity at least at 10 µM concentration after 72 h.

As shown in **Figure 3. 3**, a significant reduction in the cell viability of PC3 and HT-29 cancer cell lines was only observed when treated with the spin-labelled betulinic-, fusidic acid derivatives **7**,**8** and **9**,**10** respectively. It can also be noticed, that the viability of PC3 and HT-29 was significantly decreased at 10 µM when treated with betulinic acid (**1**) alone, and no reduction in cell viability was seen with fusidic acid alone.

On the other hand, cholic acid (**5**) and its derivatives compounds **11** and **12**, showed no reduction in cell viability. The low anticancer activity of cholic acid and its derivatives can be attributed to the high lipophilic character log p ~ 2.02 and low water solubility, which makes it hard to cross the membranes effectively to be present in high concentrations in the cytosol of the cancer cells.[27] Cholic acid (**5**) is a naturally-occurring bile acid, its main function is to aid in the absorption of the dietary fats and liposoluble vitamins from the small intestine.[28]

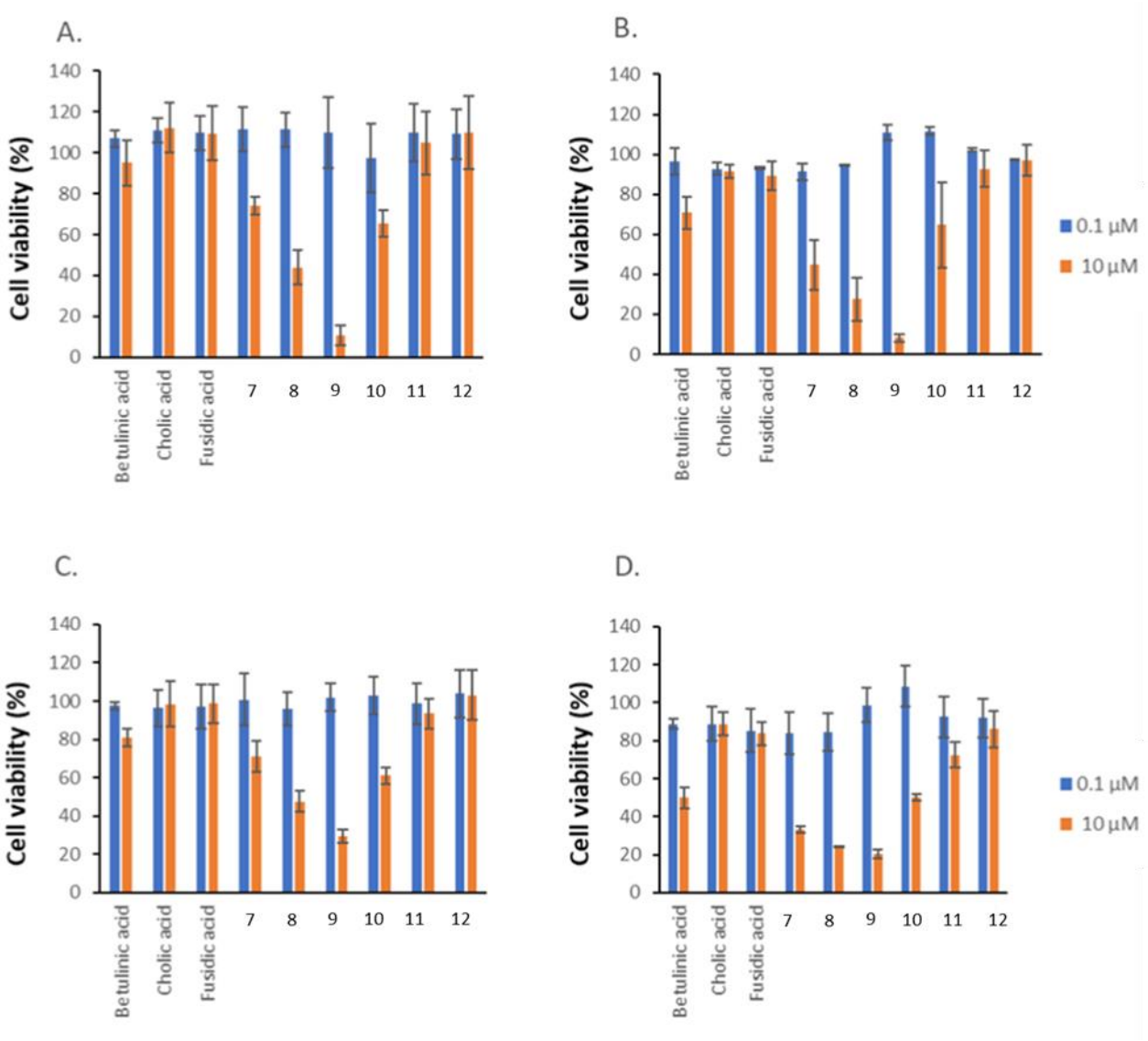

Figure 3. 3 Cell viability of HT-29 (A, B) and PC3 (C, D) cell lines treated by the investigated compounds for 48 h. Cell viability was determined using CV assay (A, C) and MTT assay (B, D).

No reports can be found in the literature regarding the anticancer activity of fusidic acid (**4**) or its derivatives. Indeed, in our hand fusidic acid (**4**) did not show anticancer activity in our control experiments. But unanticipated strong activity was observed by compounds **9** and **10** which contain fusidic acid in their core structure. The anticancer activity of betulinic acid (**1**) and its derivatives is widely known for this class of natural products. Their anticancer activity is due to its direct effect on mitochondria, which eventually triggers cell death.[30] Modifications of betulinic acid have a strong impact on its activity, which can be clearly seen in compounds **7** and **8** when compared to betulinic acid alone.

The next step was to calculate the IC_{50} values of the most active compounds **7-10**, to determine their cytotoxic potential, the results are shown in **Table 3. 3**.

Table 3. 3 IC_{50} values (µM) for the most active compounds against HT-29 and PC3 cell lines determined by MTT and CV assays.

Compound	PC3		HT-29		NIH3T3	
	CV	MTT	CV	MTT	CV	MTT
Betulinic acid	24.6±1.78	25.4±4.35	24.9±0.57	19.0±2.26	/	/
7	13.7±0.80	7.43±0.72	13.2±0.97	8.98±0.43	/	/
8	10.6±0.85	10.5±0.91	13.8±0.29	11.9±0.9	/	/
9	7.4±0.80	6.00±1.09	8.1±0.43	7.41±0.56	14±0.59	13.15±1.15
10	15.3±1.01	13.85±2.0	6.98±0.25	12.9±1.0	/	/

The IC_{50} values were calculated using the four-parameter logistic function and presented in mean. The assays were performed in biological replicates. As can be seen from **Table 3. 3**, compound **8**, which is spin-labelled betulinic acid conjugate exhibited cytotoxic activity towards PC3 (IC_{50}:10.59±0.85, CV; IC_{50}: 10.54±0.91, MTT) and HT-29 (IC_{50}: 13.82±0.29, CV; IC_{50}: 11.87±0.94, MTT). On the other hand compound **9** (**Figure 3. *4***), which is spin-labelled fusidic acid derivative was the most active compound against PC3 and HT-29 cancer cell lines towards PC3 (IC_{50}: 7.44±0.80, CV; IC_{50}: 6.00±1.09, MTT) and HT-29 (IC_{50}: 8.1±0.43, CV; IC_{50}: 7.41±0:56, MTT). Since no reports regarding the activity of fusidic acid (**5**) and its derivatives as anticancer, compound **9** (**Figure 3. 4**) which is a fusidic acid derivative, was chosen to be our model compound to study its mode of action.

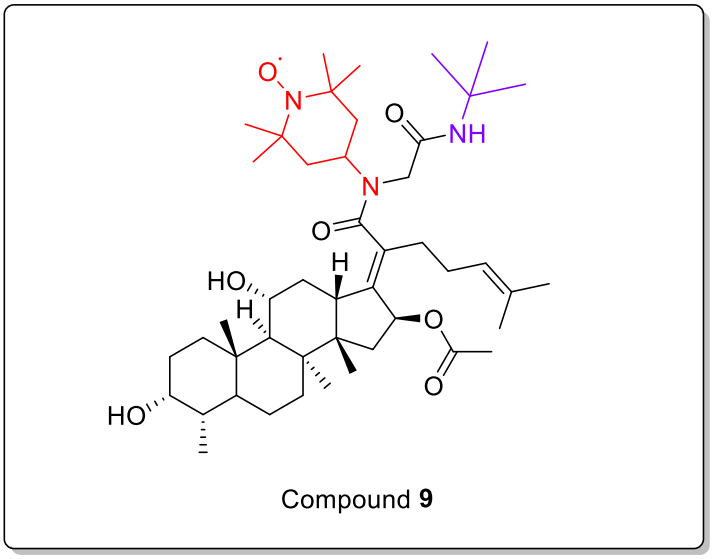

Figure 3. 4 The structure of the most active compound **9**.

3.3.2 Apoptosis analysis

AnnV/PI assay was performed, in order to determine the degree of apoptosis induced, when the PC3 cancer cell line is incubated with compound **9**. The assay utilizes the affinity of AnnV/PI double stain, in which AnnexinV stain binds to the phosphatidylserine which is expressed on the cell surface during early apoptotic events, while the propidium iodide stains the DNA matter occurred in the late apoptotic event. We tested two different concentrations (IC_{50}, 2 x IC_{50}) for 48 h and it was analyzed using flow cytometry. The results are shown in **Figure 3. 5**. When the PC3 cancer cells were treated with IC_{50} value, no apoptotic events were recorded when compared to the control. But it is clearly evident that when PC3 cancer cells were treated with compound **9** (2 x IC_{50}). An immense influence, on both early and late-stage apoptosis, was observed (68%, control 16%).

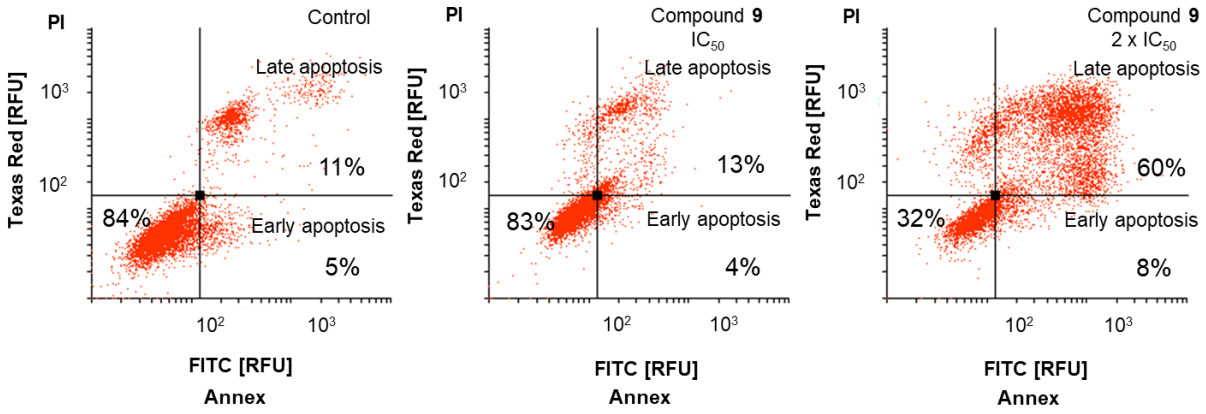

Figure 3. 5 Effect of compound **9** on apoptosis in PC3 cells uppon 48 h induction.

3.3.3 Cell division analysis

4´, 6-Diamidino-2-phenylindole (DAPI) is a fluorescent tag that binds firmly to adenine-thymine regions in DNA. DAPI assays provide single time point measurements that can reveal the distribution of cells in various cell cycles viz.; G1 vs S vs G2/M. As seen from **Figure 3. 6**, compound **9** induced a dose-dependent increase in tapping the cells in the sub-G1-phase which clearly evident that apoptosis is due to DNA fragmentation.[31]

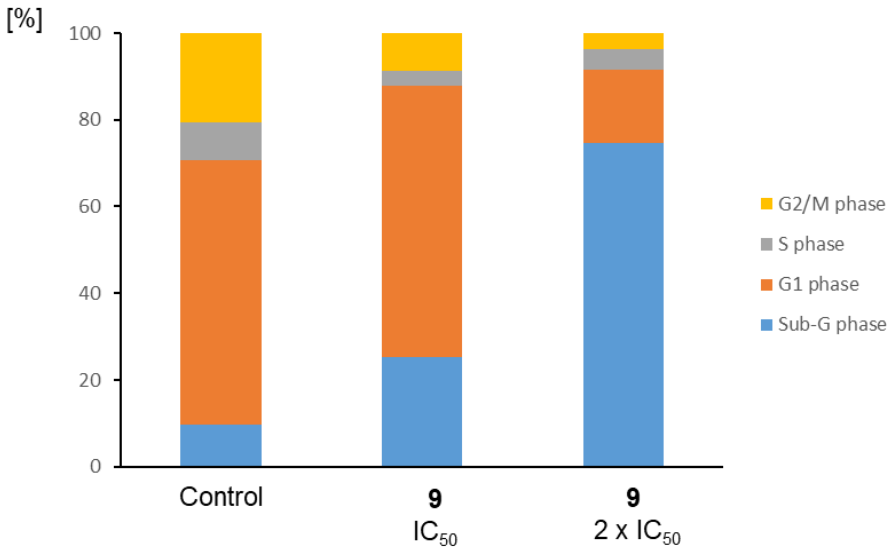

Figure 3. 6 Stacked column presentation of DAPI assay. Compound **9** was incubated with PC3 cells for 48 h.

3.3.4 Western blot analysis

Western blot analysis was conducted, not only to study the effect of compound **9** on the expression of different proteins in PC3 cancer cell line during apoptosis but also to support the data obtained from flow cytometry measurements.

Recently, Reyes *et al*. reported new natural triterpene Induce apoptosis in colon adenocarcinoma, via caspase 3 dependent mechanism.[32] In addition to that, nitroxides are known also in inducing apoptosis by caspase activation.[12] These reports encouraged us to investigate the effect of compound **9** on Caspase 3 as a potential pathway for apoptosis induction. The level of Bcl-xl, which is an anti-apoptotic protein, was also investigated in addition to the housekeeping proteins β-actin and α/β-tubulin (**Figure 3. 7**).

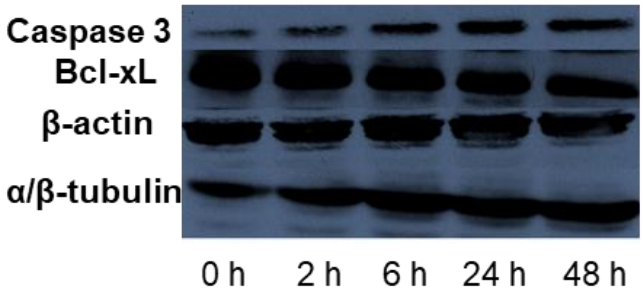

Figure 3. 7 Western blot analysis of compound **9** on different proteins.

The results are shown in **Figure 3. 7**. Compound **9** increased the expression level of caspase-3 significantly after 48 of incubation, which clearly indicates that compound **9**, induced apoptosis via activation of the caspase pathway event. The expression of the anti-apoptotic protein Bcl-XL which is a transmembrane molecule in the mitochondria was also measured. After 48 h of incubation, it is evident that the level of Bcl-XL decreases, as can be clearly seen in **Figure 3. 7**. Bcl-xL protein is located at the outer membrane of the mitochondria which acts as an anti-apoptotic by preventing the release of the mitochondrial contents such as cytochrome c. The disruption of the expression level of Bcl-xL leads to cytochrome c release into the cytosol. The release of cytochrome c in the cytosol will activate caspase-3, which finally activates caspase-dependent apoptotic pathway[33] The results shown in **Figure 3. 7** strongly support that, apoptosis mechanism of compound **9** is caspase-dependent mechanism. The level of β-actin expression was also evaluated. β-actin is a housekeeping protein that aids in cell motility, structure integrity. It is also known that β-actin expression is unaffected upon many cellular treatments which makes it a good choice as a loading control for western blot analysis.[34] After 48 h of incubation, no change in the expression level was observed. Finally, α/β-tubulins is another housekeeping protein that was also evaluated as control, the unexpected strong elevation of the expression level was obvious after 48h of incubation as shown in **Figure 3. 7**. A New study by Oropesa-Ávila *et al*. reported that during apoptosis microtubules expression level is being increased which acts as a physical barrier, thus preventing caspase to be spread into the cellular cortex. Moreover, microtubules increases phosphatidylserine (PS) externalization, which acts as a signaling molecule for macrophage for efficient clearance.[35]

3.3.5 Investigation of ROS level

The reduction of reactive oxygen species was monitored. Briefly, PC3 cells were stained with a 1 µM of dihydrorhodamine (DHR) solution for 10 min, cells were treated afterward with 7.4 µM and 17.8 µM, which represent IC_{50} and 2 × IC_{50} values of compound **9**. After 48 h, cells were trypsinized, washed with Phosphate-buffered saline (PBS) and the data were analyzed with flow cytometry. DHR fluorescence was detected using the FITC detection channel with excitation/emission wavelengths around (495 nm/519 nm). As shown in **Figure 3. 8**, compound **9** indeed reduced the level of the reactive oxygen species as anticipated.[36]

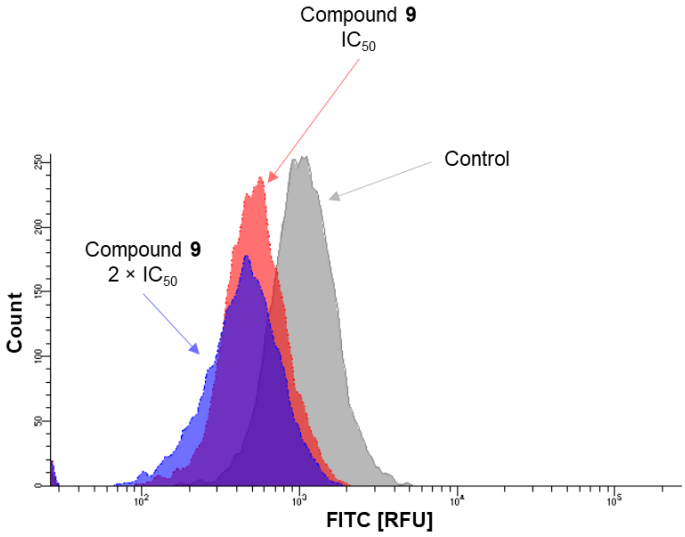

Figure 3. 8 Detection of ROS produced by PC3 cells treated with compound **9** for 48 h. DHR fluorescence was measured in the FITC channel.

3.3.6 Fluorescent imaging

Compound **13** which contains a fluorescent tag was used to determine whether fusidic acid triterpene derivative can actually target the mitochondria. Mitochondria is the major source of ROS generation and therefore, is more sensible for ROS manipulation. By achieving mitochondria targeting we can enhance both, the activity and the selectivity toward cancer cells. Unfortunately, after incubation of compound **13** with the PC3 cancer cell, no mitochondria targeting was observed (**Figure 3. 9**). Therefore, we turned to use the mitochondria targeting compound **19**. After 24 h of incubation of compound **19** with PC3 cancer cell line, a clear mitochondria targeting can be successfully achieved as shown in **Figure 3. 10**. The anticancer activity of compound **19** was also determined against PC3 and HT-29 cancer cell lines (**Table 3. 4**).

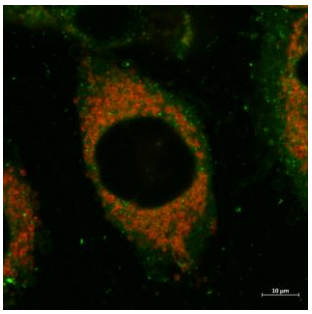

Figure 3. 9 Fluorescent imaging of compound **13** in the PC3 cancer cell line.

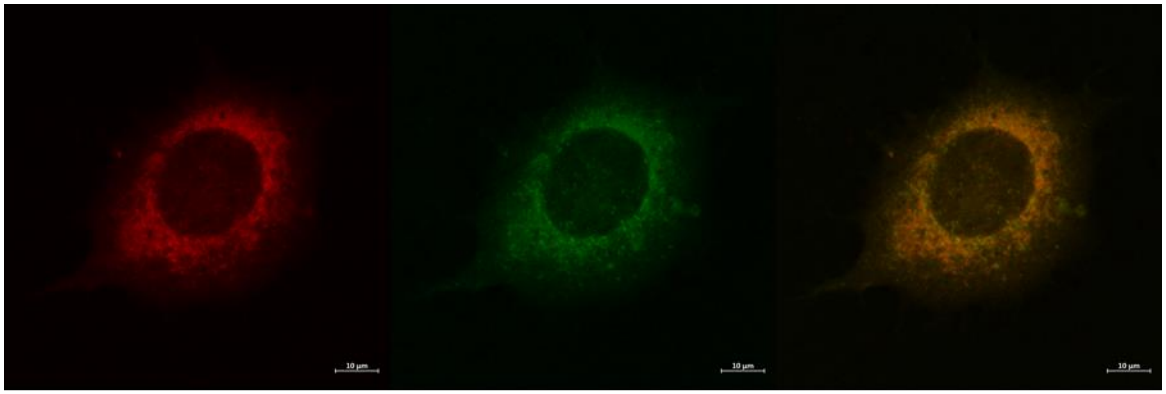

Figure 3. 10 Fluorescent imaging of compound **19** in the PC3 cancer cell line.

Table 3. 4 IC_{50} values (μM) for compound **19** against HT-29 and PC3 cell lines determined by MTT and CV assays.

Compound	PC3		HT-29	
	CV	MTT	CV	MTT
Betulinic acid	24.64±1.78	25.43±4.35	24.97±0.57	19.02±2.26
19	9.267±0.73	6.185±0.2	16.3±0.87	12.23±0.67

3.4 Conclusions

In conclusion, we have demonstrated that IMCRs can be used as synthetic protocol to design and synthesize different spin-labelled natural products analogues with wide variety and high specificity for the treatment of cancer. For the first time, we presented spin-labelled fusidic acid derivative compound **9** with anticancer activity against both PC3 and HT-29 cancer cell lines. It was proven that compound **9** induces apoptosis via the caspase-dependent mechanism. Moreover, compound **9** reduced the level of ROS load as predicted. Post-Ugi-modification was done for an attempt to target the mitochondria of the cancer cell. Indeed, MCR allowed us to introduce the triphenylphosphine moiety as the amine component and keeping the oxo-component as the formaldehyde and Yudin fluorescent tag as the isonitrile component, the post-MCR-modified product **19**, successfully targeted the mitochondria.

3.5 Experimental part

General remarks/chemistry

All commercially available reagents were purchased and used without further purification. Convertible isocyanides 2-isocyano-2-methylpropyl phenyl carbonate “IPB” was synthesized following reported procedures.[23] (3-Aminopropyl)triphenylphosphonium Bromide (TPP-NH_2) was synthesized following reported protocol.[37] HPLC grade methanol was used in all Ugi-reactions. Analytical thin-layer chromatography (TLC) was performed using silica gel 60 F254 aluminum sheets (Merck, Germany) and the visualization of the spots has been done under UV light (254 nm) or by developing with a solution of cerium sulphate. Flash column chromatography was performed using silica gel (0.040-0.063 mm). ^{1}H and ^{13}C NMR spectra were recorded in solutions on a 400 NMR Varian MERCURY-VX 400 at 22 °C at 400 MHz and 100 MHz, or on an Agilent (Varian) VNMRS 600 NMR spectrometer at 599.83 MHz and 150.83 MHz respectively. Chemical shifts (δ) are reported in ppm relative to TMS (^{1}H-NMR) and to the solvent signal (^{13}C NMR spectra). Note: due to the paramagnetism of nitroxide moiety, NMR cannot provide information useful for structural elucidation of nitroxides, therefore, reduction of the paramagnetic center was performed with phenylhydrazine or hydrazobenzene. The positive-ion high-resolution ESI mass spectra were obtained with an Orbitrap Elite mass spectrometer (Thermo Fisher Scientific, Germany) equipped with HESI electrospray ion source (positive spray voltage 4 kV, capillary temperature 275 °C, source heater temperature 80 °C, FTMS resolution 60000). Nitrogen was used as sheath gas. The instrument was externally calibrated using the Pierce LTQ Velos ESI positive ion calibration solution (product number 88323, Thermofisher Scientific, Rockford, IL, 61105 USA). The data were evaluated using the software Xcalibur 2.7 SP1. Analytical RP-HPLC analysis was performed with an Agilent 1100 system in a reverse-phase C18 column (4.6 × 150 mm, 5 µm) with a PDA detector. A linear gradient from 5% to 100% of solvent B in solvent A over 15-30 min at a flow rate of 0.8 mL min^{-1}. Detection was accomplished at 210 nm. Solvent A: 0.1% (v/v) formic acid (FA) in water. Solvent B: 0.1% (v/v) FA in acetonitrile. Instrumental details-EPR: X-Band (9.43 GHz) room temperature CW EPR measurements were performed on a Magnettech MiniScope MS400 benchtop spectrometer (Magnettech, Berlin, Germany). Spectra were recorded with a microwave power under the saturation limit (varied between 1-3 mW), 100 KHz modulation frequency, modulation amplitude of 0.1 mT and 4096 points. The lowest sample concentrations were 300 µM. Contribution of solvent to spectra was examined using water and acetonitrile. Since it is difficult to evaluate fully resolved hyperfine- and g-tensors at X-band frequencies, only the isotropic values are reported.

General remarks/biology

PBS, RPMI 1640 and Trypsin EDTA were from Capricorn Scientific, Germany. β-mercaptoethanol was from Bio-Rad, USA. Anti-rabbit IgG HRP- linked Antibody, α/β-Tubulin rabbit Ab, Caspase-3 rabbit Ab were purchased from Cell Signaling Technology, USA. While BCL-xL rabbit antibody was obtained from Abcam, UK. DMSO was bough from DuchefaBiochemie, Germany. ECL Prime Western Blotting System was supplied by GE Healthcare, USA. AnnV/PI, PAGE Ruler, EDTA Solution, Trypan blue, MitoTracker Deep Red and Halt Protease Inhibitor Cocktail were obtained from Thermofisher Scientific, USA. Ethanol, Na_2HPO_4, NaH_2PO_4, and BSA were bought from Merck, USA. Digitonin was from Riedel De HaenSeelze, Germany. Acetic acid, APS, FCS, Glycerol, Glycine, Methanol, NaOH, penicillin/streptomycin, Roti-quant “5x”, TEMED and TRIS were from Roth, Germany. Acrylamide/Bisacrylamide was bought from Serva, Germany. Finally Bromophenol blue, CV, DAPI, MTT, Triton X-100 and Tween-20 were from Sigma Aldrich, USA.

Cell lines and cultivation

PC3, HT-29, and NIH3T3 cell lines were supplied by Leibniz institute of plant biochemistry. PC3 and HT-29 were grown in RPMI 1640 medium while NIH3T3 was grown in DMEM medium. Both supplemented with 10% FCS, 1% glutamine and 1% penicillin/streptomycin at 37 °C and 5% CO_2. Cells were seeded at 5×10^3 cells/well in 96-well plates for viability determination and 1.5×10^5 cells/well in 6-well plates for flow cytometry and western blotting. NIH3T3 cell line was also supplied by the Leibniz institute.

MTT and CV assays

To determine the compounds with anticancer activities, the two cell lines were treated with 0.01 and 10 µM of the synthesized compounds **7-12**, for 48 h. The compounds which showed anticancer activity were further analyzed to determine their IC_{50}, in which, each compound was tested in 7 different concentrations (100, 50, 25, 12.5, 6.25, 3.125, 1.56 µM) for 48 h. For the CV assay, the cells were fixed by 4% paraformaldehyde for 15 min at RT and then the cells were stained with a 1% CV solution for 15 min. Afterward, the cells were washed with dd H_2O, dried overnight and the dye was dissolved using 33% acetic acid. For MTT assay, the cells were incubated with MTT (0.5 mg/mL) for 20 min. Then, the MTT solution was removed and the dye was dissolved using DMSO.

The dissolved dyes were measured using an automated microplate reader (Spectramax, Molecular Devices, USA) at 570 nm with a background wavelength of 670 nm. The results are presented as a percentage compared to control obtained from untreated cells.[38,39]

Cell cycle analysis

The PC3 cells were prepared in a 6-well and treated with IC_{50} and 2 × IC_{50} of compound **9** (7.44 and 14.88 µM) and incubated for 48 h at 37 °C and 5% CO_2. Afterward, the cells were fixed in 70% ethanol overnight at 2 °C and then stained with 1 µg/mL of DAPI in rt for 10 min. At last, the cells were analyzed by flow cytometry (FACSAria III, BD Biosciences, USA).[39]

Apoptosis analysis

The PC3 cells were prepared in a 6-well plate, treated with IC_{50} and 2 × IC_{50} of compound **9** and incubated for 48 h at 37 °C and 5% CO_2. After the incubation, cells were stained either by AnnV/PI (5 µl of AnnV, 2 µl of PI in 100 µl) PBS to determine apoptosis. The procedure was carried out according to the manufacturer's supplied instructions.[39]

Western blot analysis

PC3 cells were cultivated with an IC_{50} dose of **9** for 2 h, 6 h, 12 h, 24 h, and 48 h. The cell lysis was performed using protein lysis buffer (62.5 mM Tris–HCl (pH 6.8), 2% (w/v) SDS, 10% glycerol, and 50 mM dithiothreitol). The proteins were electrically separated using 12% SDS-polyacrylamide gels where a PageRuler prestained ladder was used as a protein molecular weight marker. The proteins were electrically transferred to nitrocellulose membranes by the western blot system (Owl HEP-1, Thermo Fischer Scientific, USA). The membranes were blocked by 5% (w/v) BSA in PBS with 0.1% Tween 20 for 1 h at rt. Afterward, Blots were incubated overnight at 4 °C with α/β- Tubulin rabbit Ab, Caspase-3 rabbit Ab, β-actin rabbit Ab and BCL-xL rabbit Ab. As a secondary antibody Anti-rabbit IgG, HRP- linked Antibody was used. Bands were visualized using an ECL Prime Western Blotting System.

Investigation of ROS production

For the detection of reactive oxygen and nitrogen species, PC3 cells were stained with 1 µM of DHR solution in 0.1% PBS for 10 min, afterward, the cells were treated with IC_{50} and 2 × IC_{50} of compound **9** for 48 h. Afterward, cells were trypsinized, washed with PBS and then analyzed with flow cytometry.[40]

Fluorescent microscopy

PC3 cells were seeded in a 6-well plate for 24 h at 37 °C and 5% CO_2. Afterward, cells were stained with 0.1 µM of MitoTracker Deep Red in a complete medium for 15 min (based on the manufacturer's protocol). The cells were washed twice with PBS. After washing, cells were treated with the IC_{50} of the tested compound for 24 h. The cells were washed twice PBS, 1 mL of medium was added. Finally, the cells were observed using GFP and Texas Red channels using LSM700 (Carl Zeiss, Germany) and EVOS FL AUTO (ThermoFisher, USA).

General procedure 1 for the Ugi-4CR

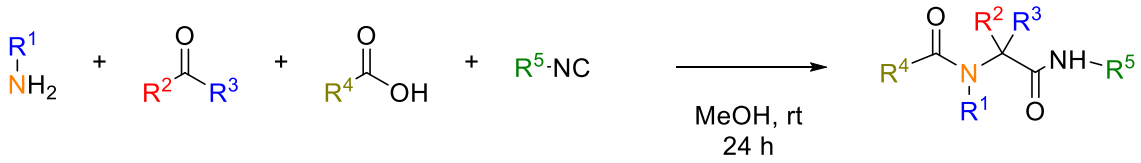

To a stirred solution of a TEMPO amine (0.1 mmol) in methanol (250 µL, 0.4 M) was added paraformaldehyde (0.1 mmol) and the mixture was stirred for 2 h. After this time the acid (0.1 mmol) and isonitrile (0.1 mmol) were added before stirring was continued for 18 h. The solvent was removed under reduced pressure and the crude material purified by column chromatography to afford the desired products.

(1R,3aS,5aR,5bR,7aR,9S,11aR,11bR,13aR,13bR)-N-(2-(tert-butylamino)-2-oxoethyl)-9-hydroxy-*N*-(1-oxyl-2,2,6,6-tetramethylpiperidin-4-yl)-5a,5b,8,8,11a-pentamethyl-1-(prop-1-en-2-yl) icosahydro-3aH-cyclopenta[a]chrysene-3a-carboxamide (7)

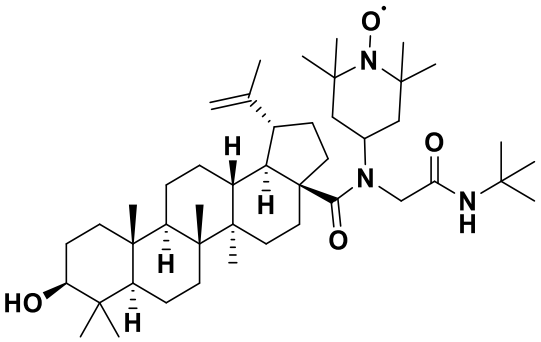

Obtained using the general method, *N*-oxyl amine and paraformaldehyde were used then, betulinic acid and *tert*-butyl isonitrile were later added. The crude reaction product was purified by silica gel column chromatography (EtOAc / *n*-hexane 8:2) to yield compound **7** (51 mg, 0.070 mmol, 70%) as red solid. R_F 0.77 (EtOAc / *n*-hexane 8:2). NMR of the corresponding hydroxylamine after phenylhydrazine reduction. ^{1}H (600 MHz, $CDCl_3$) δ 4.72 (s, 1H), 4.59 (s, 1H), 4.35 (d, J = 12.6 Hz, 1H), 3.65 (s, 2H), 3.16 (dd, J = 11.3, 4.8 Hz, 2H), 2.98 (m, 1H), 2.87 – 2.81 (m, 1H), 2.24 – 2.18 (m, 1H), 2.06-1.20 (m, 49H), 0.96 (s, 3H), 0.95 (s, 3H), 0.92 (s, 3H), 0.80 (s, 3H), 0.74 (s, 3H). ^{13}C NMR (151 MHz, $CDCl_3$): δ = 176.0 (*C*O), 109.5 (*C*H_2), 78.9 (*C*H), 55.5 (*C*), 54.9 (*C*), 53.0 (*C*), 50.9 (*C*H), 50.8 (*C*H_2), 49.3 (*C*H), 47.7 (*C*H), 45.8 (*C*H), 42.8 (*C*), 42.3 (*C*), 42.1 (*C*H_2), 40.8 (*C*H_2), 38.9 (*C*H_2), 38.8 (*C*H_2), 37.3 (*C*H_2), 36.9 (*C*), 36.1 (*C*), 34.3 (*C*), 32.2 (*C*), 32.0 (*C*H_2), 31.6 (*C*H_2), 29.9 (*C*H_2), 29.8 (*C*H_2), **28.7 (4 x CH_3 (TEMPO)),** 28.1 (*C*H_3 (*t*Bu)), 27.5 (*C*H_2), 25.7 (*C*H_2), 21.1 (*C*H_2), 20.1 (*C*H_2), 19.9 (*C*H_2), 19.6 (*C*H_2), 18.3 (*C*H_3), 16.2 (*C*H_3), 15.5 (*C*H_3), 14.8 (*C*H_3). *C*NCH2**).** HRMS (ESI) *m/z* calcd. for $C_{45}H_{76}N_3O_4$ $[M+H]^+$ 723.5836, found 723.5890.

(1R,3aS,5aR,5bR,7aR,9S,11aR,11bR,13aR,13bR)-9-hydroxy-*N*-(1-oxyl-2,2,6,6-tetramethylpiperidin-4-yl)-5a,5b,8,8,11a-pentamethyl-*N*-(2-oxo-2-((2,4,4-trimethoxybutyl)amino)ethyl)-1-(prop-1-en-2-yl)icosahydro-3aH-cyclopenta[a]chrysene-3a-carboxamide (8)

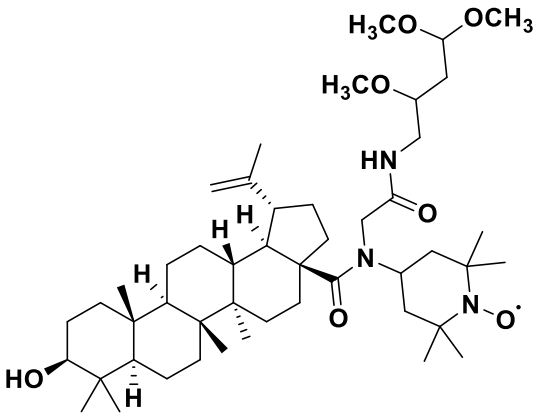

Obtained using the general method, *N*-oxyl amine and paraformaldehyde were used then, betulinic acid and IPB isonitrile were later added. The crude reaction product was purified by silica gel column chromatography (EtOAc / *n*-hexane 8:2) to yield compound **8** (50 mg, 0.061 mmol, 61%) as red solid. R_F 0.35 (EtOAc / n-hexane 8:2). NMR of the corresponding hydroxylamine after phenylhydrazine reduction. ^{1}H (600 MHz, $CDCl_3$) δ 4.72 (s, 1H), 4.59 (s, 1H), 4.54 – 4.49 (m, 1H). 4.38 (t, *J* = 12.5 Hz, 1H (ipb)), 3.66 (s, 2H), 3.36 – 3.30 (m, 12H). (IPB Ugi moiety), 3.16 (dd, *J* = 11.3, 4.8 Hz, 2H), 2.98 (m, 1H), 2.87 – 2.81 (m, 1H), 2.27 – 2.15 (m, 1H), 2.11 - 1.09 (m, 42H), 0.96 (s, 3H), 0.95 (s, 3H), 0.91 (s, Hz, 3H), 0.81 (s, *J* = 2.4 Hz, 3H), 0.75 (s, 3H). ^{13}C NMR (151 MHz, $CDCl_3$) δ 176.08 (*C*O), 109.50, 79.08, 57.04, 56.98, 56.49, 55.57, 55.47, 53.24, 53.07, 50.93, 45.82, 45.77, 42.59, 42.09, 41.51, 41.30, 40.86, 38.99, 38.85, 38.37, 37.34, 36.10, 35.20, 34.39, 32.21, 31.61, 31.52, 31.44, 31.01, 29.97, 29.82, **28.11(4 x CH3 (TEMPO))**, 27.53, 25.73, 21.21, 21.17, 20.32, 20.17, 19.71, 16.31, 16.08, 16.05, 15.48, 14.83. HRMS (ESI) *m/z* calcd. for $C_{48}H_{82}N_3O^{\bullet}_7$ $[M]^+$ 812.6153, found 812.6138.

(3R,4S,8S,9R,10S,11R,13S,14S,16S,E)-17-(1-((2-(tert-butylamino)-2-oxoethyl)(1-oxyl-2,2,6,6-tetramethylpiperidin-4-yl)amino)-6-methyl-1-oxohept-5-en-2-ylidene)-3,11-dihydroxy-4,8,10,14-tetramethylhexadecahydro-1H-cyclopenta[a]phenanthren-16-yl acetate (9)

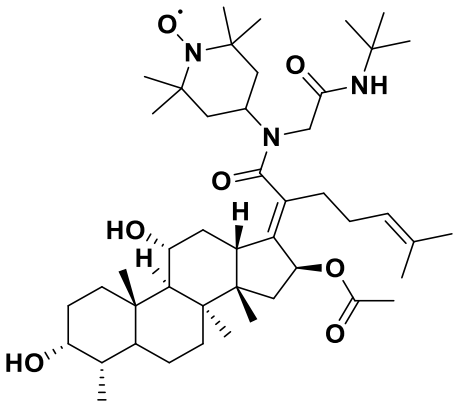

Obtained using the general method, *N*-oxyl amine and paraformaldehyde were used then, fusidic acid and *tert*-butyl isonitrile were later added. The crude reaction product was purified by silica gel column chromatography (DCM / MeOH 9:1) to yield compound **9** (51 mg, 0.057 mmol, 57%) as red solid. R_F 0.65 (DCM / MeOH 9:1). NMR of the corresponding hydroxylamine after phenylhydrazine reduction. ^{1}H (600 MHz, $CDCl_3$) δ 5.69 (d, *J* = 8.6 Hz, 1H), 5.07 (m, 1H), 4.33 – 4.22 (m, 3H), 3.71 (s, 2H), 3.26 (m, 1H), 3.05 – 3.02 (m, 1H), 2.80 – 2.75 (m, 2H), 2.32 – 2.28 (m, 1H), 2.22 – 2.02 (m, 5H), 1.89 (s, 3H), 1.86 – 1.82 (m, 2H), 1.76 – 1.71 (m, 4H), 1.68 (s, 3H), 1.61 (s, 3H), 1.60 – 1.53 (m, 4H), 1.34 (d, *J* = 7.0 Hz, 3H), 1.28 (s, 9H), 1.26 – 1.14 (m, 15H), 1.13 – 1.08 (m, 2H), 0.96 (s, 3H), 0.91 – 0.88 (m, 6H). ^{13}C NMR (151 MHz, $CDCl_3$) δ 173.21, 169.87, 169.06, 133.15, 132.45, 122.56, 74.81, 73.10, 71.29, 68.10, 50.95, 50.84, 49.76, 49.63, 49.42, 44.51, 41.63, 39.45, 39.26, 37.09, 36.22, 36.09, 35.22, 32.28, 32.28, 30.28, 30.24, 28.69, 28.57 **(4 x CH_3 (TEMPO))**, 28.52, 25.86, 22.97, 20.86, 20.51, 20.10, 18.05, 17.88, 16.03 HRMS (ESI) *m/z* calcd. for $C_{46}H_{77}N_3O_7$ $[M+H]^+$ 783.5744, found 783.5756.

(3R,4S,8S,9R,10S,11R,13S,14S,16S,E)-3,11-dihydroxy-17-(1-((1-oxyl-2,2,6,6-tetramethylpiperidin-4-yl)(2-oxo-2-((2,4,4-trimethoxybutyl)amino)ethyl)amino)-6-methyl-1-oxohept-5-en-2-ylidene)-4,8,10,14-tetramethylhexadecahydro-1H-cyclopenta[a]phenanthren-16-yl acetate (10)

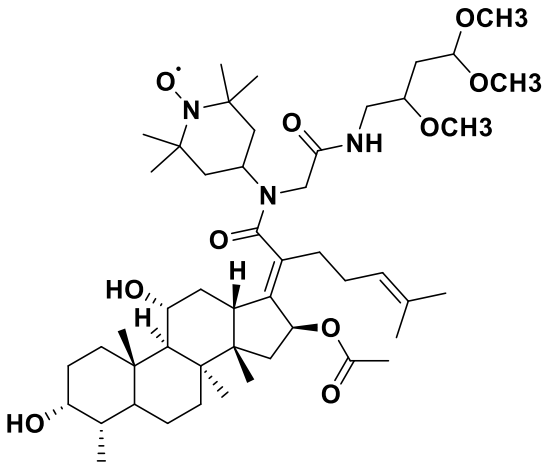

Obtained using the general method, *N*-oxyl amine and paraformaldehyde were used then, fusidic acid and IPB isonitrile were later added. The crude reaction product was purified by silica gel column chromatography (DCM / MeOH 9:1) to yield compound **10** (60 mg, 0.068 mmol, 69%) as red solid. R_F 0.72 (DCM / MeOH 9:1). NMR of the corresponding hydroxylamine after phenylhydrazine reduction. ^{1}H (600 MHz, $CDCl_3$) δ 5.69 (d, *J* = 8.4 Hz, 1H), 5.08 (m, 1H), 4.51 (m, 1H), 4.34 – 4.31 (m, 1H), 3.76 – 3.73 (m, 1H), 3.65 (s, 2H), 3.39 – 3.29 (m, 12H), 3.14 (m, 1H), 3.07 – 3.02 (m, 1H), 2.75 (m, 1H), 2.37 – 2.27 (m, 1H), 2.23 – 2.08 (m, 5H), 2.04 (s, 3H), 1.92 (s, 3H), 1.88 – 1.80 (m, 4H), 1.76 – 1.71 (m, 4H), 1.68 (s, 3H), 1.62 (s, 3H), 1.60 – 1.48 (m, 4H), 1.36 (s, 3H), 1.31 – 1.17 (m, 15H), 1.15 – 1.10 (m, 2H), 0.97 (s, 3H), 0.93 – 0.88 (m, 6H). ^{13}C NMR (151 MHz, $CDCl_3$) δ 173.21, 169.87, 169.06, 133.15, 132.45, 122.56, 74.81, 71.29, 68.10, 50.95, 49.63, 49.42, 44.51, 42.68, 39.45, 39.26, 37.09, 36.37, 36.22, 36.09, 35.22, 32.28, 30.28, 30.24, 30.07, 28.57 **(4 x *C*H$_3$ (TEMPO))**, 28.52, 27.81, 27.73, 25.86, 23.85, 22.97, 21.43, 21.21, 20.86, 20.51, 20.10, 18.19, 18.05, 17.88, 16.03.15.68 HRMS (ESI) *m/z* calcd. for $C_{49}H_{83}N_3O_{10}$ $[M+H]^+$ 873.6000, found 873.6062.

(R)-*N*-(2-(tert-butylamino)-2-oxoethyl)-*N*-(1-oxyl-2,2,6,6-tetramethylpiperidin-4-yl)-4-((3R,5S,7R,8R,9S,10S,12S,13R,14S,17R)-3,7,12-trihydroxy-10,13-dimethylhexadecahydro-1H-cyclopenta[a]phenanthren-17-yl)pentanamide (11)

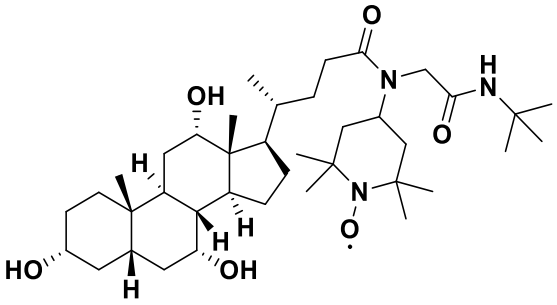

Obtained using the general method, *N*-oxyl amine and paraformaldehyde were used then, fusidic acid and *tert*-butyl isonitrile were later added. The crude reaction product was purified by silica gel column chromatography (DCM / MeOH 9:1) to yield compound **11** (55 mg, 0.081 mmol, 81%) as red solid. R_F 0.62 (DCM / MeOH 9:1). NMR of the corresponding hydroxylamine after phenylhydrazine reduction. ^{1}H NMR (600 MHz, $CDCl_3$) δ 4.14 – 4.08 (m, 1H), 4.06 – 3.98 (m, 2H), 3.97 – 3.91 (m, 1H), 3.85 – 3.75 (m, 1H), 2.51 – 2.42 (m, 1H), 2.36 – 2.28 (m, 1H), 2.27 – 2.13 (m, 4H), 1.94 – 1.80 (m, 5H), 1.79 – 1.60 (m, 7H), 1.61 – 1.46 (m, 7H), 1.37 – 1.15 (m, 25H), 1.13 – 1.00 (m, 3H), 0.97 (s, 3H), 0.87 (s, 3H), 0.67 (d, *J* = 7.5 Hz, 3H). ^{13}C NMR (151 MHz, $CDCl_3$) δ 173.21, 169.87, 169.06, 133.15, 132.45, 122.56, 74.81, 73.10, 71.29, 68.10, 50.95, 50.84, 49.76, 49.63, 49.42, 44.51, 41.63, 39.45, 39.26, 37.09, 36.22, 36.09, 35.22, 32.28, 32.28, 30.28, 30.24, 28.57, 28.52, 28.52, 25.86, 22.97, 20.86, 20.51, 20.10, 18.05, 17.88, 16.03. HRMS (ESI) *m/z* calcd. for $C_{39}H_{68}N_3O_6$ $[M+H]^+$ 675.5108, found 675.5164.

(4R)-*N*-(1-oxyl-2,2,6,6-tetramethylpiperidin-4-yl)-N-(2-oxo-2-((2,4,4-trimethoxybutyl)amino)ethyl)-4-((3R,5S,7R,8R,9S,10S,12S,13R,14S,17R)-3,7,12-trihydroxy-10,13-dimethylhexadecahydro-1H-cyclopenta[a]phenanthren-17-yl)pentanamide (12)

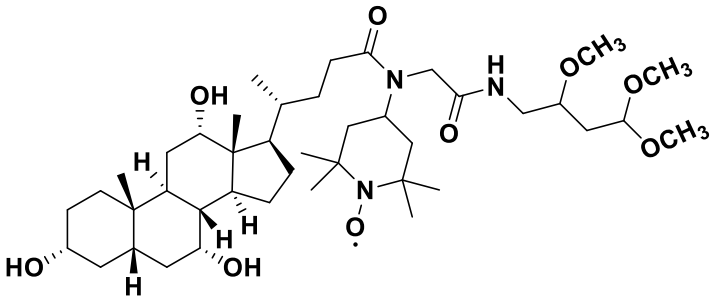

Obtained using the general method, *N*-oxyl amine and paraformaldehyde were used then, cholic acid and IPB isonitrile were later added. The crude reaction product was purified by silica gel column chromatography (DCM / MeOH 9:1) to yield compound **12** (47 mg, 0.061 mmol, 61%) as red solid. R_F 0.55 (DCM / MeOH 9:1). NMR of the corresponding hydroxylamine after phenylhydrazine reduction. ^{1}H NMR (600 MHz, $CDCl_3$) δ 4.55 – 4.48 (m, 1H), 4.12 – 4.00 (m, 1H), 3.95 – 3.81 (m, 2H), 3.45 (s, 3H), 3.37 – 3.28 (m, 12H), 3.28 – 3.22 (m, 1H), 2.48 (m, 2H), 2.36 – 2.11 (m, 5H), 1.98 – 1.80 (m, 6H), 1.80 – 1.69 (m, 5H), 1.69 – 1.39 (m, 7H), 1.40 – 1.16 (m, 15H), 1.15 – 1.00 (m, 4H), 0.96 (s, 3H), 0.88 (s, 3H), 0.68 (s, 3H). ^{13}C NMR (151 MHz, $CDCl_3$) δ 174.58, 170.07, 151.16, 101.75, 76.18, 72.86, 71.70, 68.28, 59.33, 59.28, 57.03, 53.33, 53.06, 52.96, 50.55, 46.99, 46.39, 45.61, 41.80, 41.38, 41.28, 35.57, 35.20, 35.09, 34.64, 32.16, 31.54, 30.85, 30.39, 28.20, 27.46, 26.51, 23.12, 22.42, 19.88, 17.44, 14.62, 12.48. HRMS (ESI) *m/z* calcd. for $C_{42}H_{74}N_3O_9^{\bullet}$ $[M]^+$ 764.5425, found 764.5410.

(3R,4S,8S,9R,10S,11R,13S,14S,16S,E)-17-(1-((2-((2-(6-(dimethylamino)-1,3-dioxo-1H-benzo[de]isoquinolin-2(3H)-yl)ethyl)amino)-2-oxoethyl)(1-oxyl-2,2,6,6-tetramethylpiperidin-4-yl)amino)-6-methyl-1-oxohept-5-en-2-ylidene)-3,11-dihydroxy-4,8,10,14-tetramethylhexadecahydro-1H-cyclopenta[a]phenanthren-16-yl acetate (13)

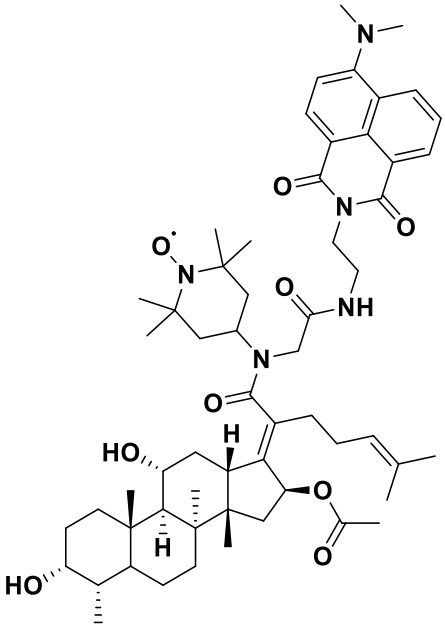

Obtained using the general method **1**, *N*-oxyl amine and paraformaldehyde were used then, fusidic acid and Yudin isonitrile were later added. The crude reaction product was purified by silica gel column chromatography (DCM / MeOH 9:1) to yield compound **13** (35 mg, 0.035 mmol, 35%) as yellow powder. R_F 0.1 (DCM / MeOH 9:1). NMR of the corresponding hydroxylamine after the additon of hydrazobenzene. ^{1}H NMR (400 MHz, DMSO-d_6) δ 8.49 (dd, *J* = 8.5, 2.1 Hz, 1H), 8.45 (d, *J* = 7.5 Hz, 1H), 8.34 (dd, *J* = 8.2, 1.9 Hz, 1H), 7.78 – 7.72 (m, 1H), 7.20 (d, *J* = 8.6 Hz, 1H), 5.65 (d, *J* = 8.5 Hz, 1H), 5.09 – 5.01 (m, 1H), 4.91 – 4.76 (m, 2H), 4.18 – 4.11 (m, 1H), 4.07 (d, *J* = 3.9 Hz, 1H), 3.99 (d, *J* = 3.9 Hz, 1H), 3.90 – 3.81 (m, 2H), 3.53 (s, 2H), 3.50 – 3.47 (m, 1H), 3.07 (s, 6H), 2.99 – 2.85 (m, 1H), 2.70 – 2.60 (m, 1H), 2.40 – 2.17 (m, 3H), 2.16 – 1.93 (m, 5H), 1.85 (d, *J* = 13.3 Hz, 2H), 1.62 (dd, *J* = 9.8, 5.2 Hz, 7H, (fusidic acid; 5H+TEMPO; 2H)), 1.57 – 1.50 (m, 6H), 1.49 – 1.28 (m, 6H), 1.25 (s, 3H), 1.08 – 0.95 (m, 17H, (fusidic;3H acid+TEMPO 14H)), 0.86 (s, 3H), 0.81 – 0.75 (m, 6H). ^{13}C NMR (101 MHz, DMSO-d_6) δ 171.61, 169.91, 169.10, 164.32, 163.64, 147.18, 133.72, 132.31, 131.95, 131.88, 130.94, 130.21, 125.46, 124.76, 123.96, 123.48, 114.04, 113.47, 74.34, 69.68, 66.23, 58.57, 58.38, 51.63, 49.42, 49.07, 48.98, 48.65, 44.84, 43.22, 39.05, 36.90, 36.81, 35.67, 35.55, 33.31, 33.05, 32.37, 32.25, 30.69, 29.93, 28.82, 28.49, 25.92, 23.94, 23.18, 20.67, 20.13, 18.01, 17.97, 16.74, 16.71. HRMS (ESI) *m/z* calcd. for $C_{58}H_{83}N_5O_9$ $[M]^+$ 993.6191, found 993.6145.

General procedure 2 for the conversion of Ugi-products 8 and 10 to corresponding spin-labelled *N*-acylpyrroles intermediates 14 and 16.

To a solution of linear Ugi-products **8, 10** (0.05 mmol) in toluene (10 mL) was added 10-camphor sulfonic acid (10 mol%) and quinoline (10 mol%). The mixture was stirred for 1 min at rt and then refluxed for at least 30 min until TLC showed complete conversion. The mixture was cooled to rt, transferred to a separatory funnel and washed with 1M aqueous HCl (2 × 30 mL). The acidic aqueous phase was further extracted with ethyl acetate (1 × 20 mL). The organic layers were combined, washed with $NaHCO_3$ and brine (2 × 20 mL), dried over anhydrous Na_2SO_4, filtered and evaporated under reduced pressure to obtain the *N*-acyl pyrrole derivative which was used in the next step without further purification.

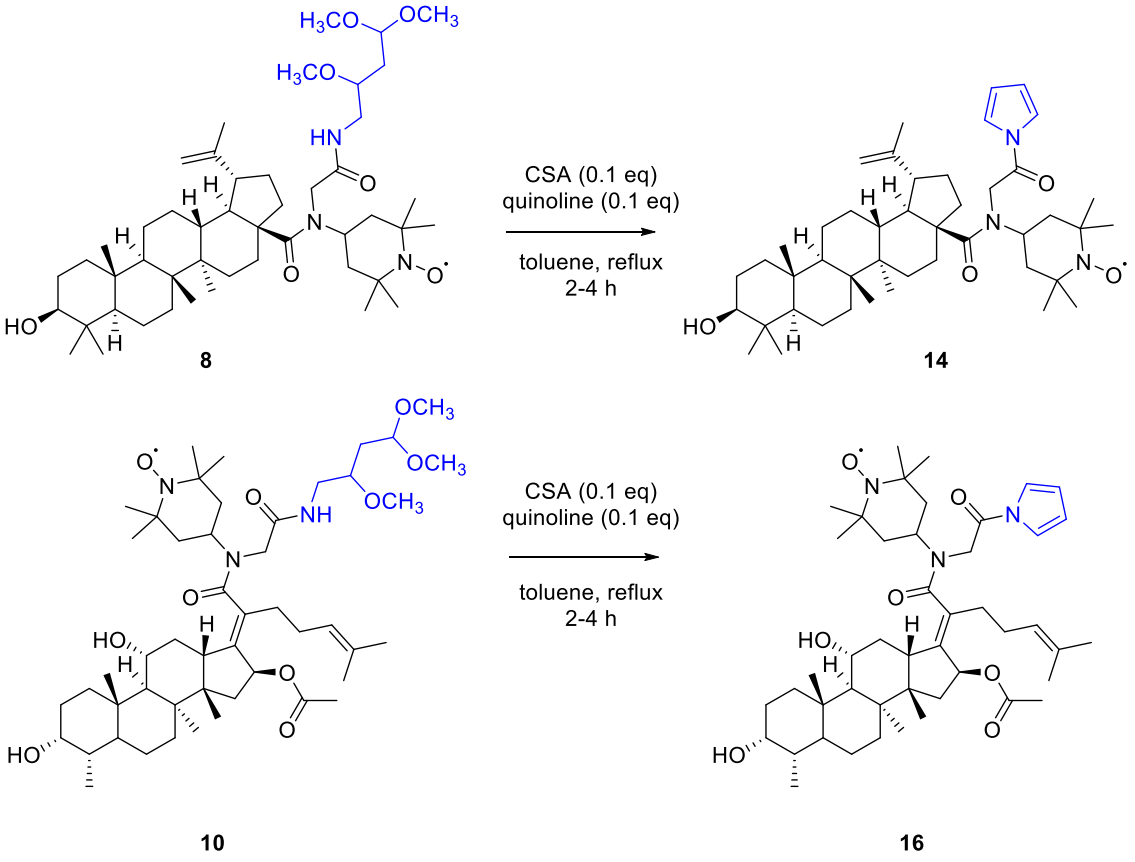

8 **14**

10 **16**

General procedure 3 for the conversion of the spin-labelled *N*-acylpyrroles intermediates 14 and 16 into their corresponding carboxylic acid derivatives compounds 15, 17 and 18.

Method 3.a:

To a solution of intermediates **14** and **16** (**0.025** mmol) in a mixture of THF (2 ml), methanol (2 ml) and water (2 ml), potassium hydroxide (**0.5** mmol) was added. This mixture was heated to 110 °C for 30 minutes in a microwave (90 W heating, 6 W keeping temperature). The reaction mixture was diluted with methanol (10 ml) and the pH value was set to pH = 2 by the addition of saturated aqueous $NaHSO_4$ solution. The aqueous phase was extracted with ethyl acetate (3 x 100 ml) and it was then dried over Na_2SO_4. After filtration and evaporation of the solvent, the crude residue was purified by column chromatography (DCM / MeOH 8:2). By this method compounds, **15** and **18** were obtained.

Method 3.b:

Method B was established to keep the Acetyl group intact on position **16** of the fusidic acid skeleton. *N*-acylpyrrole **16** (0.025 mmol) was dissolved in a mixture of *t*-BuOH (10 mL) and water (5 mL). Then, DMAP (0.015 mmol) was added and the reaction mixture was heated at reflux for 5 h, after which TLC (DCM / MeOH 8:2) indicated the saponification into the carboxylic acid **17**. The reaction mixture was concentrated to a volume of 10 mL in a rotary evaporator. Saturated $NaHCO_3$ solution (10 mL) and CH_2Cl_2 (20 mL) were added. After separation of the organic layer, the water layer was extracted with CH_2Cl_2 (2 × 30 mL). Then the water layer was acidified with $NaHSO_4$ (2 M) and extracted with ethyl acetate (3 × 20 mL). The combined organic solutions of the acidic extraction were dried over Na_2SO_4, filtered, and evaporated to give carboxylic acid derivative, which was further purified by column chromatography (DCM / MeOH 8:2).

_N_-(1-oxyl-2,2,6,6-tetramethylpiperidin-4-yl)-N-((1R,3aS,5aR,5bR,7aR,9S,11aR,11bR,13aR,13bR)-9-hydroxy-5a,5b,8,8,11a-pentamethyl-1-(prop-1-en-2-yl)icosahydro-1H-cyclopenta[a]chrysene-3a-carbonyl)glycine (15)

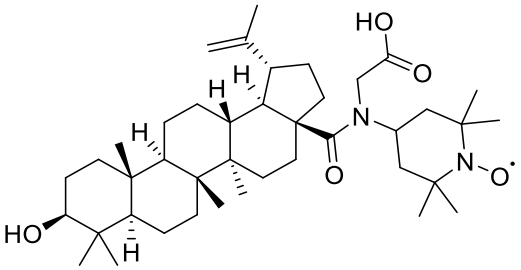

Obtained using the general method **3.a**, the crude reaction product was purified by silica gel column chromatography (DCM / MeOH 8:2) to yield compound **15** (11.8 mg, 0.014 mmol, 70%) as orange powder. R_F 0.12 (DCM / MeOH 8:2). NMR of the corresponding hydroxylamine after the additon of hydrazobenzene. ^{1}H NMR (400 MHz, DMSO-d_6) δ 11.92 (s, 1H), 4.64 (d, J = 2.7 Hz, 1H), 4.57 – 4.51 (m, 1H), 4.26 (d, J = 5.1 Hz, 1H), 3.80 – 3.62 (m, 1H), 3.52 (s, 2H), 2.97 (m, 2H), 2.80 (m, 1H), 2.68 (m, 1H), 2.36 – 2.31 (m, 1H), 1.96 (m, 2H), 1.78 (dd, J = 13.0, 9.0 Hz, 2H), 1.64 (s, 3H), 1.55 (t, J = 12.7 Hz, 5H), 1.51 – 1.38 (m, 6H), 1.38 – 1.21 (m, 8H), 1.08 (d, J = 3.1 Hz, 14H), 0.92 (s, 3H), 0.88 (s, 3H), 0.84 (s, 3H), 0.77 (s, 3H), 0.66 (s, 3H). ^{13}C NMR (101 MHz, DMSO-d_6) δ 173.71, 171.03, 151.04, 109.22, 76.75, 58.20, 54.97, 53.73, 52.04, 50.17, 48.12, 45.40, 43.82, 41.50, 38.48, 38.28, 38.23, 36.73, 35.18, 33.92, 32.46, 30.63, 29.07, 27.15, 27.12, 25.15, 20.65, 19.78, 19.63, 19.07, 17.93, 15.97, 15.85, 15.78, 14.31. HRMS (ESI) *m/z* calcd. for $C_{41}H_{66}N_2O_5$ $[M-H]^+$ 666.5050, found 666.4996.

_N_-((E)-2-((3R,4S,8S,9R,10S,11R,13S,14S,16S)-16-acetoxy-3,11-dihydroxy-4,8,10,14-tetramethylhexadecahydro-17H-cyclopenta[a]phenanthren-17-ylidene)-6-methylhept-5-enoyl)-N-(1-oxyl-2,2,6,6-tetramethylpiperidin-4-yl)glycine (17)

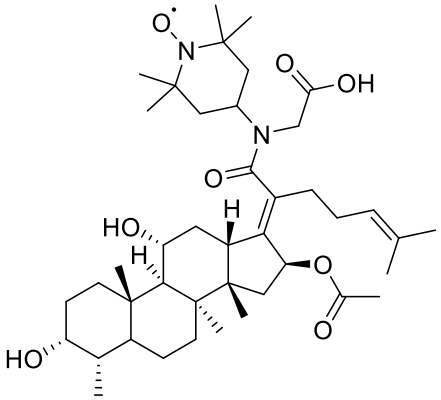

Obtained using the general method **3.b**, the crude reaction product was purified by silica gel column chromatography (DCM / MeOH 8:2) to yield compound **17** (12 mg, 0.016 mmol, 66%) as orange oil. R_F 0.15 (DCM / MeOH 8:2). NMR of the corresponding hydroxylamine after the addition of hydrazobenzene. ^{1}H NMR (400 MHz, DMSO-d_6) δ 8.89 (s, 1H), 5.44 (d, J = 8.5 Hz, 1H), 5.10 (t, J = 7.0 Hz, 1H), 4.18 – 4.13 (m, 1H), 3.98 (d, J = 3.7 Hz, 1H), 3.95 (d, 1H), 3.87 (m, 2H), 3.53 – 3.49 (m, 1H), 2.97 – 2.87 (m, 1H), 2.73 – 2.66 (m, 1H, TEMPO), 2.26 – 2.17 (m, 3H), 2.10 – 1.97 (m, 5H), 1.94 – 1.82 (m, 5H), 1.81 – 1.70 (m, 2H, TEMPO), 1.64 (s, 3H), 1.57 (s, 3H), 1.53 – 1.29 (m, 6H), 1.27 (s, 3H), 1.26 – 1.12 (m, 3H), 1.10 – 0.95 (m, 14H, TEMPO), 0.88 (s, 3H), 0.84 (s, 3H), 0.79 (d, J = 6.7 Hz, 3H). ^{13}C NMR (101 MHz, DMSO-d_6) δ 175.94, 171.54, 170.02, 154.96, 147.92, 133.53, 123.91, 74.27, 69.74, 66.27, 58.63, 58.47, 54.20, 49.43, 49.10, 48.97, 43.02, 39.25, 38.90, 36.94, 36.69, 36.09, 35.71, 31.77, 29.78, 27.52, 26.07, 23.86, 23.22, 21.37, 20.72, 20.18, 18.21, 18.15, 16.78, 14.43. HRMS (ESI) *m/z* calcd. for $C_{42}H_{66}N_2O_8$ $[M-H]^+$ 726.4897, found 726.4807.

_N_-(1-oxyl-2,2,6,6-tetramethylpiperidin-4-yl)-N-((E)-6-methyl-2-((3R,4S,8S,9R,10S,11R,13S,14S,16S)-3,11,16-trihydroxy-4,8,10,14-tetramethylhexadecahydro-17H-cyclopenta[a]phenanthren-17-ylidene)hept-5-enoyl)glycine (18)

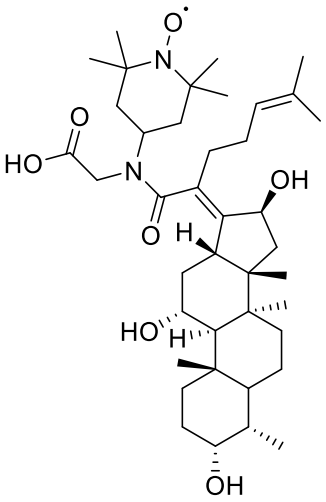

Obtained using the general method **3.a**, the crude reaction product was purified by silica gel column chromatography (DCM / MeOH 8:2) to yield compound **18** (10 mg, 0.014 mmol, 58%) as orange oil. R_F 0.1 (DCM / MeOH 8:2). NMR of the corresponding hydroxylamine after the additon of hydrazobenzene. ^{1}H NMR (400 MHz, DMSO-d_6) δ 10.22 (s, 1H), 5.46 (d, J = 8.6 Hz, 1H), 5.14 – 5.05 (m, 1H), 4.48 (d, J = 8.3 Hz, 1H), 4.17 – 4.07 (m, 1H), 4.00 (d, J = 3.6 Hz, 1H), 3.94 (d, J = 3.9 Hz, 1H), 3.51 (t, J = 3.2 Hz, 1H), 3.17 (dd, J = 15.1, 9.9 Hz, 1H), 2.99 – 2.75 (m, 1H), 2.71 – 2.55 (m, 1H), 2.40 – 1.93 (m, 8H), 1.93 – 1.66 (m, 4H), 1.63 (s, 3H), 1.55 (t, J = 2.2 Hz, 3H), 1.52 – 1.29 (m, 6H), 1.26 (s, 3H), 1.24 – 1.07 (m, 3H), 1.07 – 0.91 (m, 14H), 0.89 (d, J = 6.2 Hz, 6H), 0.79 (d, J = 6.7 Hz, 3H). ^{13}C NMR (101 MHz, DMSO-d_6) δ 174.42, 171.52, 147.95, 147.48, 135.99, 124.70, 69.98, 69.76, 66.50, 58.62, 58.55, 56.47, 49.67, 49.07, 48.89, 43.28, 41.71, 39.22, 36.97, 35.86, 35.67, 33.37, 33.13, 30.75, 29.57, 27.60, 25.89, 23.95, 23.06, 21.21, 19.01, 18.17, 16.77, 16.00. HRMS (ESI) *m/z* calcd. for $C_{40}H_{64}N_2O_7$ $[M-H]^+$ 684.4792, found 684.4732.

(3-(2-((E)-2-((3R,4S,8S,9R,10S,11R,13S,14S,16S)-16-acetoxy-3,11-dihydroxy-4,8,10,14-tetramethylhexadecahydro-17H-cyclopenta[a]phenanthren-17-ylidene)-*N*-(1-oxyl-2,2,6,6-tetramethylpiperidin-4-yl)-6-methylhept-5-enamido)-*N*-(2-((2-(6-(dimethylamino)-1,3-dioxo-1H-benzo[de]isoquinolin-2(3H)-yl)ethyl)amino)-2-oxoethyl)acetamido)propyl)triphenylphosphonium (19)

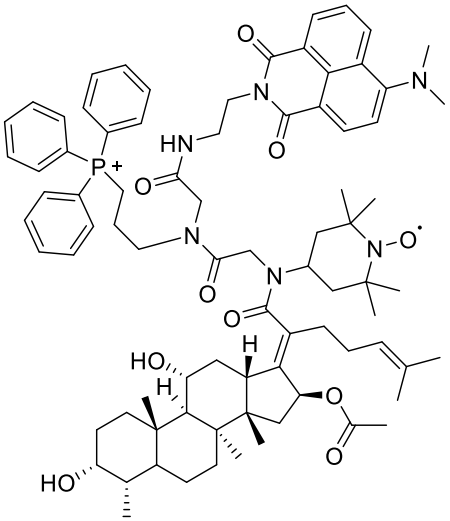

Obtained using the general method **1** in 0.013 mmol scale. (3-Aminopropyl) triphenylphosphonium and paraformaldehyde were used to form the imine. Then, the post-Ugi-modified fusidic acid **17** and Yudin isonitrile were added. The crude reaction product was purified by silica gel column chromatography (DCM / MeOH 8:2) to yield compound **19** (6 mg, 0.004 mmol, 34%) as yellow powder. R_F 0.12 (DCM / MeOH 8:2). NMR of the corresponding hydroxylamine after the additon of hydrazobenzene. ^{1}H NMR (400 MHz, DMSO-d_6) δ 8.57 (d, J = 8.8 Hz, 1H), 8.54 (d, J = 7.5 Hz, 1H), 8.51 (d, J = 8.3 Hz, 1H), 7.87 – 7.72 (m, 15H), 7.18 – 7.15 (m, 1H), 5.44 (q, J = 15.3, 12.0 Hz, 1H), 5.10 (d, J = 10.6 Hz, 1H), 4.62 (t, J = 7.3 Hz, 2H), 4.20 – 4.14 (m, 1H), 4.08 – 3.97 (m, 6H), 3.62 – 3.52 (m, 4H), 3.37 (d, J = 7.9 Hz, 2H), 3.16 (s, 4H), 3.10 (s, 6H), 2.95 – 2.88 (m, 1H), 2.69 – 2.62 (m, 1H), 2.46 – 2.11 (m, 8H), 2.11 – 1.92 (m, 7H), 1.50 (s, 3H), 1.47 – 1.32 (m, 6H), 1.30 (s, 3H), 1.24 (s, 3H), 1.15 – 0.95 (m, 17H), 0.89 (s, 3H), 0.85 (s, 3H), 0.80 (d, J = 6.7 Hz, 3H). ^{13}C NMR (101 MHz, DMSO-d_6) δ 171.12, 169.83, 169.46, 168.61, 163.83, 163.15, 156.51, 148.71, 135.13, 135.10, 133.60, 133.49, 132.17, 131.82, 131.51, 130.42, 130.29, 129.73, 128.76, 128.46, 124.98, 123.47, 122.99, 118.40, 117.82, 113.56, 112.99, 73.58, 69.19, 65.74, 58.08, 57.89, 54.62, 51.14, 48.94, 48.58, 48.16, 44.36, 43.54, 42.08, 38.59, 36.66, 36.42, 36.33, 36.26, 36.16, 35.84, 31.78, 30.21, 27.01, 25.55, 23.46, 23.33, 21.07, 20.80, 20.67, 20.08, 19.64, 18.37, 17.84, 17.71, 17.49, 16.25.HRMS (ESI) *m/z* calcd. for $C_{81}H_{105}N_6O_{10}P^+$ [M] $^+$ 1352.7624, found 1352.7621.

3.6 References

(1) Dröge, W. *Physiol. Rev*. **2002**, 82, 47–95.

(2) del Río, L. A.; Sandalio, L. M.; Palma, J. M.; Bueno, P.; Corpas, F. *J. Free Radical Bio. Med*. **1992**, 13, 557–580.

(3) Gorrini, C.; Harris, I. S.; Mak, T. W. *Nat. Rev. Drug Discov*. **2013**, 12, 931–947.

(4) a) Reczek, C. R.; Chandel, N. S. *Annu. Rev. Cancer Biol*. **2017**, 1, 79–98; b) Kumari, S.; Badana, A. K.; G, M. M.; G, S.; Malla, R. *Biomark. Insights* **2018**, 13.

(5) Liou, G.-Y.; Storz, P. *Free Radical Res.* **2010**, 44, 479–496.

(6) Conklin, K. A. *Integr. Cancer Ther*. **2004**, 3, 294–300.

(7) a) Zhang, X.; Gao, F. *Front. Pharmacol.* **2014**, 5, 3871; b) Firuzi, O.; Miri, R.; Tavakkoli, M.; Saso, L. *Curr. Med. Chem.* **2011**, 18, 3871–3888.

(8) Suy, S.; Mitchell, J. B.; Ehleiter, D.; Haimovitz-Friedman, A.; Kasid, U. *J. Biol. Chem.* **1998**, 273, 17871–17878.

(9) Krishna, M. C.; Russo, A.; Mitchell, J. B.; Goldstein, S.; Dafni, H.; Samuni, A. *J. Biol. Chem*. **1996**, 271, 26026–26031.

(10) a) Krasowska, A.; Piasecki, A.; Murzyn, A.; Sigler, K. *Folia Microbiol*. **2007**, 52, 45–51; b) Mitchell, J. B.; Samuni, A.; Krishna, M. C.; DeGraff, W. G.; Ahn, M. S.; Samuni, U.; Russo, A. *Biochemistry-Us* **1990**, 29, 2802–2807; c) Mitchell, J. B.; DeGraff, W.; Kaufman, D.; Krishna, M. C.; Samuni, A.; Finkelstein, E.; Ahn, M. S.; Hahn, S. M.; Gamson, J.; Russo, A. *Arch. Biochem. Biophys.* **1991**, 289, 62–70.

(11) Anderson, R. F.; Shinde, S. S.; Hay, M. P.; Denny, W. A. *J. Am. Chem. Soc.* **2006**, 128, 245–249.

(12) Suy, S.; Mitchell, J. B.; Samuni, A.; Mueller, S.; Kasid, U. *Cancer* **2005**, 103, 1302–1313.

(13) Wang, Z.; Wang, J.; Xie, R.; Liu, R.; Lu, Y. *Int. J. Mol. Sci.* **2015**, 16, 11087–11100.

(14) a) Fulda, S.; Kroemer, G. *Drug Discov. Today* **2009**, 14, 885–890; b) Kumar, P.; Bhadauria, A. S.; Singh, A. K.; Saha, S. *Life Sci*. **2018**, 209, 24–33.

(15) a) Sommerwerk, S.; Heller, L.; Kerzig, C.; Kramell, A. E.; Csuk, R. *Eur. J. Med. Chem*. **2017**, 127, 1–9; b) Wiemann, J.; Heller, L.; Perl, V.; Kluge, R.; Ströhl, D.; Csuk, R. *Eur. J. Med. Chem*. **2015**, 106, 194–210; c) Csuk, R.; Barthel, A.; Schwarz, S.; Kommera, H.; Paschke, R. *Bioorgan. Med. Chem.* **2010**, 18, 2549–2558.

(16) a) Wolfram, R. K.; Fischer, L.; Kluge, R.; Ströhl, D.; Al-Harrasi, A.; Csuk, R. *Eur. J. Med. Chem.* **2018**, 155, 869–879; b) Wolfram, R. K.; Heller, L.; Csuk, R. *Eur. J. Med. Chem*. **2018**, 152, 21–30.

(17) a) Antimonova, A.N.; Petrenko, N. I.; Schulz, E.E.; Polienko, Yu. F.; Shakirov, M. M .; Irtegova, I.G .; Pokrovsky, M.A.; Sherman, K. M .; Grigoriev, I.A .; Pokrovsky, A. G.; Tolstikov, G. A. *Bioorg. Khim*. **2013**, 39, 206–211; b) Popov, S. A.; Shpatov, A. V.; Grigor'ev, I. A. *Chem. Nat. Compd*. **2015**, 51, 87–90

(18) a) Govdi, A. I.; Sokolova, N. v.; Sorokina, I. v.; Baev, D. S.; Tolstikova, T. G.; Mamatyuk, V. I.; Fadeev, D. S.; Vasilevsky, S. F.; Nenajdenko, V. G. *Med. Chem. Commun.* **2015**, 6, 230–238; b) Govdi, A. I.; Vasilevsky, S. F.; Sokolova, N. v.; Sorokina, I. v.; Tolstikova, T. G.; Nenajdenko, V. G. *Mendeleev Commun.* **2013**, 23, 260–261.

(19) a) Wiemann, J.; Fischer Née Heller, L.; Kessler, J.; Ströhl, D.; Csuk, R. *Bioorg. Chem.* **2018**, 81, 567–576; b) Wiemann, J.; Heller, L.; Csuk, R. *Eur. J. Med. Chem.* **2018**, 150, 176–194.

(20) Sultani, H. N.; Haeri, H. H.; Hinderberger, D.; Westermann, B. *Org. Biomol. Chem.* **2016**, 14, 11336–11341.
(21) a) Chatterjee, J.; Rechenmacher, F.; Kessler, H. *Angew. Chem. Int. Edit*. **2013**, 52, 254–269; b) Chatterjee, J.; Gilon, C.; Hoffman, A.; Kessler, H. *Accounts Chem. Res*. **2008**, 41, 1331–1342.
(22) Barreto, A. d. F. S.; Vercillo, O. E.; Wessjohann, L. A.; Andrade, C. K. Z. Beilstein *J. Org. Chem*. **2014**, 10, 1017–1022.
(23) Neves Filho, R. A.W.; Stark, S.; Morejon, M. C.; Westermann, B.; Wessjohann, L. A. *Tetrahedron Lett.* **2012**, 53, 5360–5363.
(24) Kreye, O.; Westermann, B.; Wessjohann, L. *Synlett.* **2007**, 20, 3188-3192.
(25) Rotstein, B. H.; Mourtada, R.; Kelley, S. O.; Yudin, A. K. *Chemistry* **2011**, 17, 12257–12261.
(26) Ye, Y.; Zhang, T.; Yuan, H.; Li, D.; Lou, H.; Fan, P. *J. Med. Chem*. **2017**, 60, 6353–6363.
(27) Roda, A.; Minutello, A.; Angellotti, M. A.; Fini, A. *J. Lipid Res.* **1990**, 31, 1433–1443.
(28) Monte, M. J.; Marin, J. J. G.; Antelo, A.; Vazquez-Tato, J. *World J. Gastroentero*. **2009**, 15, 804–816.
(29) Sannasiddappa, T. H.; Lund, P. A.; Clarke, S. R. *Front. Microbiol*. **2017**, 8, 1581.
(30) Fulda, S. Int. *J. Mol. Sci*. **2008**, 9, 1096–1107.
(31) Pozarowski, P.; Darzynkiewicz, Z. *Analysis of Cell Cycle by Flow Cytometry. In: Schönthal A.H. (eds) Checkpoint Controls and Cancer. Methods in Molecular Biology* **2004**, 281, 301–311.
(32) Reyes, F. J.; Centelles, J. J.; Lupiáñez, J. A.; Cascante, M. *Febs. Lett*. **2006**, 580, 6302–6310.
(33) Gesing, A.; Masternak, M. M.; Wang, F.; Lewinski, A.; Karbownik-Lewinska, M.; Bartke, A. *Exp. Biol. M*. **2011**, 236, 156–168.
(34) Nie, X.; Li, C.; Hu, S.; Xue, F.; Kang, Y. J.; Zhang, W. *Biochem. Biophys. Rep*. **2017**, 12, 108–113.
(35) Oropesa-Ávila, M.; Fernández-Vega, A.; La Mata, M. de; Maraver, J. G.; Cordero, M. D.; Cotán, D.; Miguel, M. de; Calero, C. P.; Paz, M. V.; Pavón, A. D.; Sánchez, M. A.; Zaderenko, A. P.; Ybot-González, P.; Sánchez-Alcázar, *J. A. Cell Death Dis*. **2013**, 4, e527.
(36) a) Ide, T.; Tsutsui, H.; Kinugawa, S.; Suematsu, N.; Hayashidani, S.; Ichikawa, K.; Utsumi, H.; Machida, Y.; Egashira, K.; Takeshita, A. *Circ. Res*. **2000**, 86, 152–157; b) Yu, H.; Cao, L.; Li, F.; Wu, Q.; Li, Q.; Wang, S.; Guo, Y. *Rsc. Adv*. **2015**, 5, 63655–63661.
(37) Xu, J.; Zeng, F.; Wu, H.; Wu, S. *J. Mater. Chem. B*. **2015**, 3, 4904–4912.
(38) Sladowski, D.; Steer, S. J.; Clothier, R. H.; Balls, M. *J. Immunol. Methods*.**1993**, 157, 203–207.
(39) Kaluđerović, G. N.; Krajnović, T.; Momcilovic, M.; Stosic-Grujicic, S.; Mijatović, S.; Maksimović-Ivanić, D.; Hey-Hawkins, E. *J. Inorg. Biochem*. **2015**, 153, 315–321.
(40) a) Krajnović, T.; Kaluđerović, G. N.; Wessjohann, L. A.; Mijatović, S.; Maksimović-Ivanić, D. *Pharmacol. Res*. **2016**, 105, 62–73; b) Maksimovic-Ivanic, D.; Mijatovic, S.; Harhaji, L.; Miljkovic, D.; Dabideen, D.; Fan Cheng, K.; Mangano, K.; Malaponte, G.; Al-Abed, Y.; Libra, M.; Garotta, G.; Nicoletti, F.; Stosic-Grujicic, S. *Mol. Cancer Ther*. **2008**, 7, 510–520.

Chapter 4

Smart (Competent) ROS probes targeting mitochondria: Cationic fluorophores and redox sensing moieties combined by Ugi-multi-component-reactions

*Abstract**

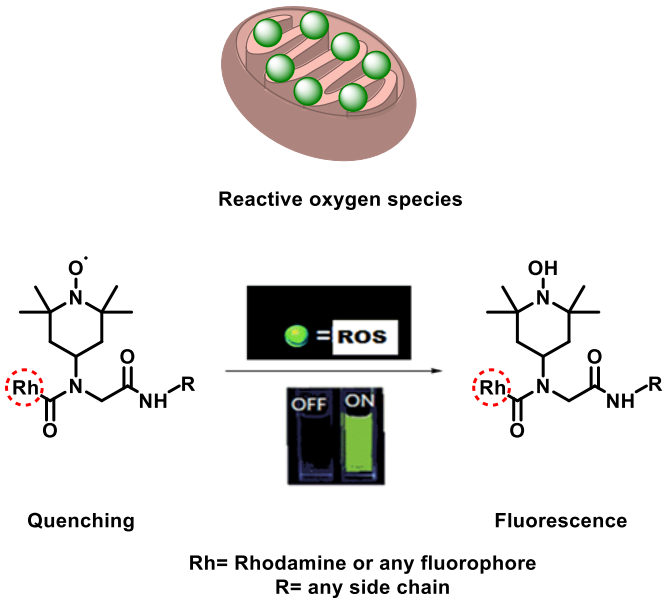

Recently, a new series of prefluorescent rhodamine nitroxide conjugates were synthesized utilizing the well-known isonitrile based multicomponent reactions (IMCRs). The synthesized probes were able to target the mitochondria of PC3- and NIH3T3-cells which represent cancer and normal cell line. The high selectivity of these probes was tested for evaluating different levels of ROS species and, thereby, different levels of fluorescence can be measured which corresponds to the amount of ROS produced in living organisms. The multicomponent reaction provides easy reaction setup and diversity, a library of products can be obtained simply by changing one or more of the Ugi-components, which offer distinct advantages over other previously reported methods for constructing probes capable of ROS detection.

* Own contribution: synthesis and characterization of the probes as well as the measurements of EPR-spectra.

4.1 Introduction

The monitoring of biological processes within cells is an ongoing process, though modern analytical tools have been constantly developed which provide for fast, reliable and reproducible results to pressing questions and needs in the context of disease-related problems. Among the cellular processes which disclose a clear indication of the nature and the status thereof is the formation of reactive oxygen species (ROS). ROS includes hydroxyl radical and superoxide anion which represents oxygen radicals although non-radical ROS also exists such as hydrogen peroxide and ozone. Approximately 1% of the oxygen taken up in our bodies by inhaling is being converted to ROS.[1] Excess generation of ROS causes cellular damage, which results in oxidative stress and ultimately cell death. As a result of excess ROS production, DNA damage may occur which ultimately results in gene mutation. In addition, many diseases are also associated with excess ROS production, diseases such as neurodegenerative disease (Alzheimer) include excess ROS interaction with biomacromolecules, several studies correlate the role of superoxide anion, hydroxyl radical, hydrogen peroxide and nitric oxide with neurodegeneration in Alzheimer (AD).[2] Other studies proved that vascular superoxide production is a major contributor to hypertension.[3] Myocardial damage induced by ischemia/reperfusion (IR) is also ROS mediated.[4] One of the mechanisms underlying the loss of cardioprotection involves abnormal redox status and the generation of highly reactive oxygen species.[4] Excessive ROS production is induced by hyperglycemia in diabetic patients and glycemic control in those patients effectively reduces the amount of ROS produced.[5] Indeed, ROS production in cancer cells is the major manifestation which is due to its high metabolic activity when compared to the normal cells.[6]Therefore, understanding the reasons and the conditions causing these distortions is a mandate to develop promising measures. The localization of these processes to specific cellular regions is also indispensable. As the electron transport chain is located in the mitochondrial membrane, it is most likely that this organelle is a major source of ROS, indeed, 90% of the ROS production takes place in the mitochondria which are formed during oxidative phosphorylation, amino acid, and fatty acid metabolism and hormone biosynthesis.[7] Due to their high degree of inherent redox processes which starts with the flow of electrons from the electron transport chain to oxidize molecular oxygen to the radical oxygen species, mitochondria are a well-studied cell compartment. Due to the increasing demand to detect and to quantify ROS in mitochondrial and to gain insight into the physiological and pathological processes, new/advanced probes for elucidating and monitoring the ROS state are required.

Accordingly, the designed probes must fulfill several requirements such as high sensitivity, accuracy, reproducibility, and the most important requirement is the ability of the synthesized probe to effectively target the mitochondria. EPR spectroscopy has been used for ROS detection especially hydroxyl radicals, but using EPR spectroscopy alone is not sufficient for real-time imaging of OH radicals in individual cells to detect ROS due to their low sensitivity (detection limit is in µM range) and its low spatial resolution and the radical probe must be chemically modified in order to target the mitochondria. One way to overcome these limitations is to couple fluorescent spectroscopy to EPR in order to increase both sensitivity and the spatial resolution for ROS detection. Moreover, mitochondria targeting can be achieved by careful selection of the fluorophore. For instance, cationic fluorophores such as rhodamine are known to be localized in the mitochondria, due to their lipophilic nature and charge delocalization which facilitates the penetration of such dyes through the cell membrane. After internalization, the dye accumulates in the mitochondrion interior matrix, which is negatively charged.[8] Therefore, a perfect match can be seen when combining both EPR and fluorescence spectroscopy which allows for an improved determination of ROS within the specific mitochondrial environment. The most common EPR probes used for ROS detection are nitroxides radicals. One of the most recent applications of nitroxide radicals is their conjugation to fluorophores and to utilize these conjugates as pre-fluorescent dual-functional (spin and fluorescence) sensors molecules.[9,10] Nitroxides are known to act as pre-fluorescent probes throw their ability to quench excited state of fluorescent tags.[11,12] However, upon interaction with reactive oxygen species the nitroxide radical is being reduced to its corresponding hydroxylamine resulting in a fluorescent analyte that offers the possibility to monitor the mitochondrial ROS.

4.2 Synthetic plan

For the synthetic approach to probes offering these potentials, we envisioned the Ugi-multicomponent reaction to be the method of choice, in only one step a product with four different components can be assembled. The functional groups which need to react to the peptide framework are an aldehyde, an amine, a carboxylic acid, and an isonitrile. In our design, we want to use the fluorescent tag thereof as the carboxylic acid and the TEMPO radical as the amine counterpart. In earlier studies, we could prove that the utilization of rhodamine in Ugi-reactions leads to peptoids which cannot be transformed to the leuko form upon change of pH (**Scheme 4. 1.a**).[13]

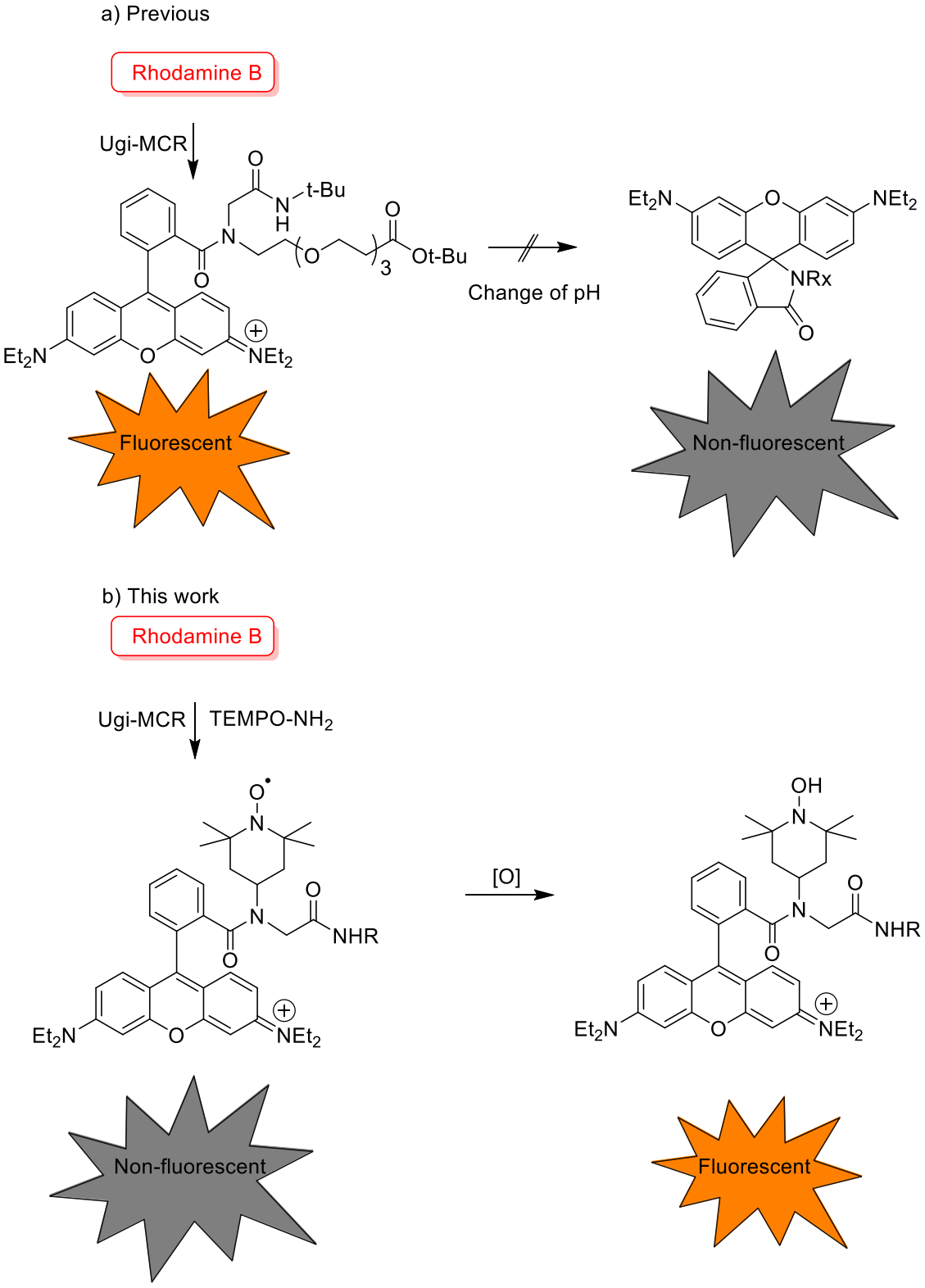

Scheme 4. 1 Comparison between previous and current work.

In our studies to target mitochondria, the rhodamine fluorophore was selected, because it has been proven that such lipophilic cationic dyes can localize into that particular organelle, therefore acting as the fluorophore as well as the targeting group.[14]

Moreover, Rhodamines gained high attraction due to its desirable photophysical properties, such as; high quantum yield (ϕ) and high molar absorptivity (ε), but due to its excellent photostability, rhodamines are widely used in biological studies.[15] Rhodamines are also known to possess high chemical stability, several reports showing their stability toward pH, metal ions, anions, thiols, and most important feature is their stability towards reactive oxygen species.[16,17,18] In close proximity to the dye, we envisioned to install a TEMPO-moiety for maximum quenching efficiency since the quenching of the fluorophore is highly dependent on how close the nitric oxide radical to the fluorescent tag.[19] The Ugi-reaction offers the possibility to use TEMPO-NH_2, the adduct is thus non-fluorescent due to the quenching by the radical. However, upon oxidation, this probe will turn into a fluorescent analyte offering to monitor the ROS upon change of intensity of the Ugi-adduct. In addition, the incorporation of the TEMPO-radical also offers the possibility to use this sensor as a double readout probe, the second readout being EPR-spectroscopy.

4.2.1 Synthesis of spin-labelled ROS probes

The Ugi-reaction is a well-established one-pot synthetic protocol to achieve diversity in only one synthetic operation. The scope is rather broad, and a variety of functional groups can be used without the need of protection strategies. In earlier studies we could demonstrate the conditions of the Ugi-reaction do not interfere with the TEMPO-radical, keeping the radical character intact throughout the synthesis. For this study, we envisioned to use the TEMPO radical as the amine component. As shown in **Scheme 4. 2** the acid component was different rhodamines fluorophores namely, rhodamine B (**1**), rhodamine 101 (**2**), rhodamine 110 (**3**) and rhodamine 19 (**4**). As the carbonyl compound, we used formaldehyde to avoid any formation of stereoisomers. Finally, as the isonitrile, we used various derivatives that allow further functionalization, which can be seen in **6** (transformation into acylpyrrole) and **4** (ester cleavage). Different rhodamines behave similarly in the Ugi-reaction as demonstrated in the synthesis of **11** and **12** (**Figure 4. 1**). With these materials in hand, further evaluation of the suitability of these probes could be done. All the analysis described in the following chapters was done on **5** and will be discussed thoroughly.

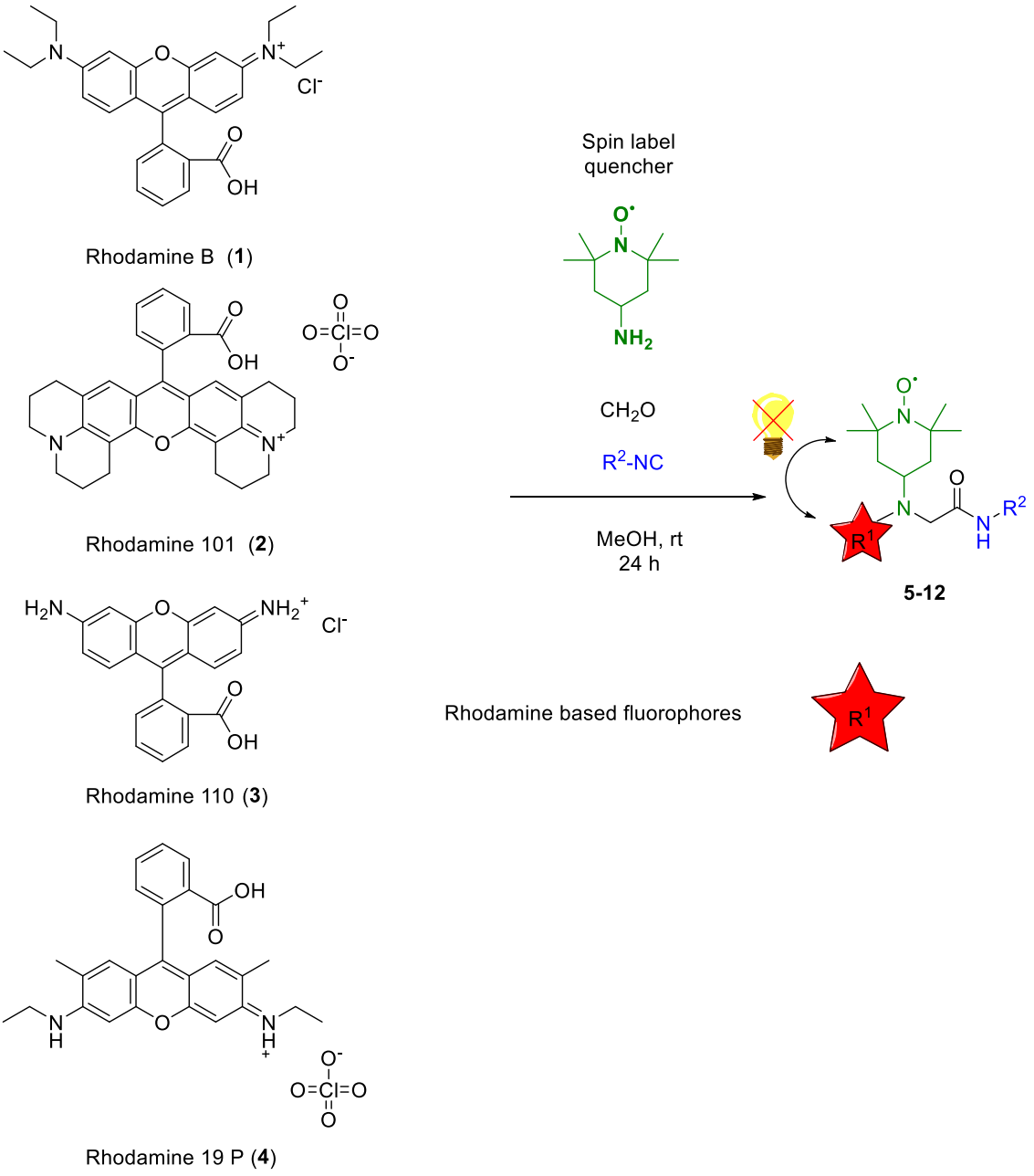

Scheme 4. 2 Synthesis of spin-labelled probes **5-12**.

The yields for the synthesis of spin-labelled probes **5-12** range from ~50-70%. These good yields clearly prove the versatility of the MCR approach to achieve a broad range of rhodamine radical sensors in just one transformation. The nature of the carboxylic acid part had no big impact on product formation. Instead, different rhodamine tags can be used in order to cover different emission wavelengths as can be seen with spin-labelled probe **11**, which emit in the green wavelength region (**Figure 4. 1**).

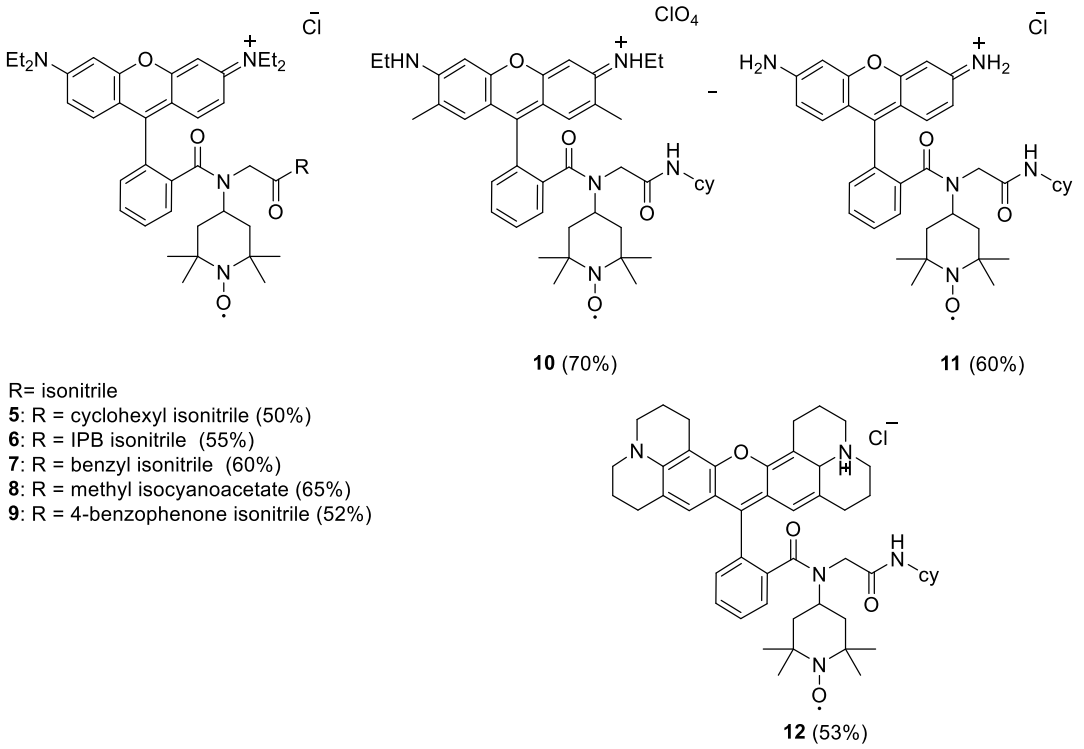

Figure 4. 1 Structures of Rhodamine spin-labelled probes **5-12**.

All the synthesized products have been confirmed by HRMS, the purity of all synthesized products was confirmed by recording the HPLC. EPR spectroscopy was recorded for all synthesized probes. For recording ^{1}H NMR, ^{13}C NMR we chose ascorbic acid (AsA) for the reduction of the spin label, otherwise, the spectra cannot be interpreted due to significant line broadening due to the interaction between the electron spin with the nucleus spin nearby.

4.3 NMR of spin-labelled probe 5

In order to record the NMR spectra of the spin-labelled probe **5**, the nitroxide moiety must be reduced to its corresponding hydroxylamine. The reduction of the spin-labelled probe **5** was performed *in situ* utilizing the reducing agent ASA. The reaction was monitored via NMR for 66 min (**Figure 4. 2**).

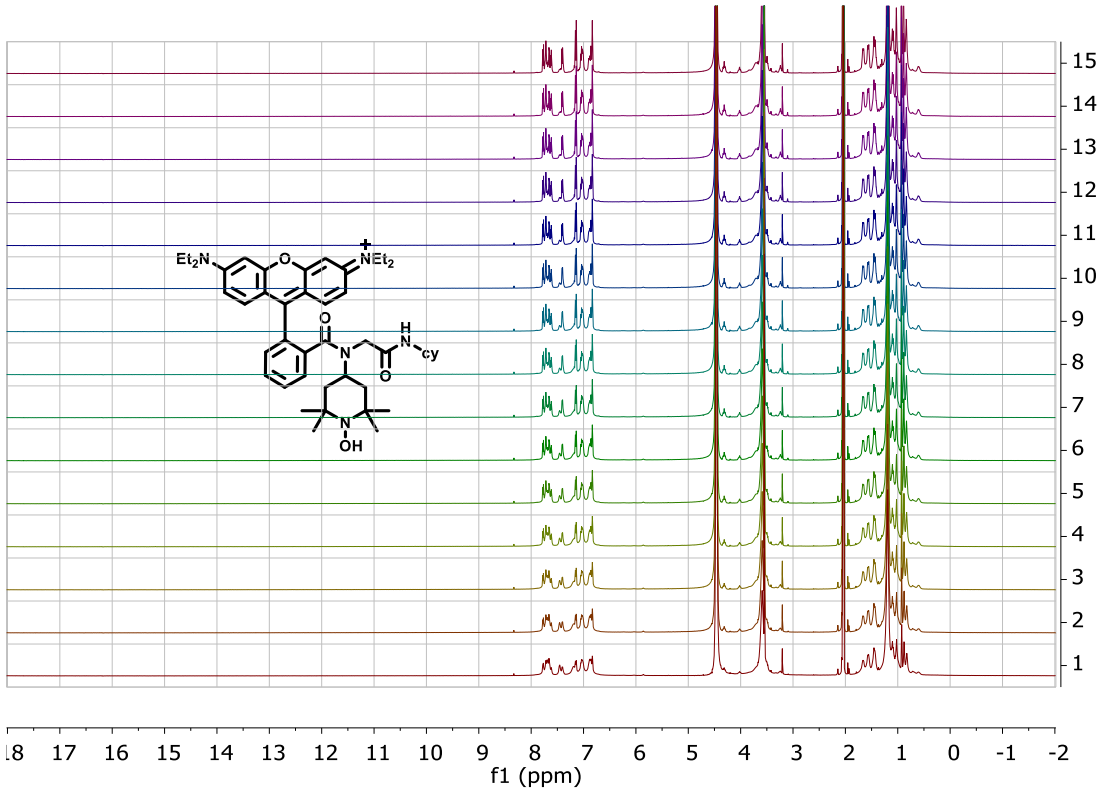

Figure 4. 2 *In situ* NMR spectra of the spin-labelled probe **5** after reduction with AsA.

4.4 UV/EPR spectroscopic properties of the spin-labelled probe 5

In this section, we selected spin-labelled probe **5** to test whether it can be reduced to the corresponding hydroxylamine and thereby, the rhodamine dye can gain back its fluorescence. For this purpose, we have selected AsA as our reducing agent in different concentrations (**Scheme 4. 3**). The spectral characteristics of our synthesized spin-labelled probe **5** was tested in the absence and presence of AsA (**Figure 4. 3**). Both EPR and fluorescence spectroscopy were used to follow the reaction. The results show a dose-dependent response relationship between AsA and our spin-labelled probe **5**. Before AsA was added almost no fluorescence was recorded for spin-labelled probe **5** (50 µM in methanol) as seen in the orange line in **Figure 4. 3**. But as we started to increase the molar ratio of AsA from 6.25 µM, 12.5 µM, 25 µM, and finally 50 µM while keeping the concentration of 50 µM of spin label probe **5** the fluorescent intensity increases as shown in **Figure 4. 3**. Moreover, the EPR spectrum was also recorded before adding AsA for spin-labelled probe **5** and as shown in **Figure 4. 4** for the EPR measurements different concentrations were used from the ones used for the fluorescent spectroscopy.

The EPR spectrum of the spin-labelled probe **5** was recorded at 150 µM in methanol, typical three lines for the spin-labelled probe **5** can be clearly seen due to the TEMPO radical. After adding AsA in molar ratio starting from 150 µM, 75 µM, 37.5 µM, 18.75 µM and finally 9.37 µM the intensity of the typical three lines spectrum of spin-labelled probe **5** decreases until almost no EPR signal can be detected (**Figure 4. 4**). The spectral properties of the synthesized probes **5**-**12** are shown in **Table 4. 1**.

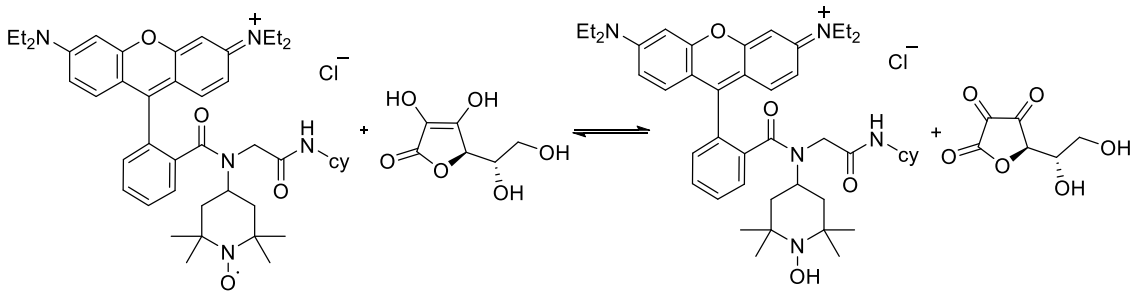

Scheme 4. 3 Reduction of the spin-labelled probe **5** with AsA.

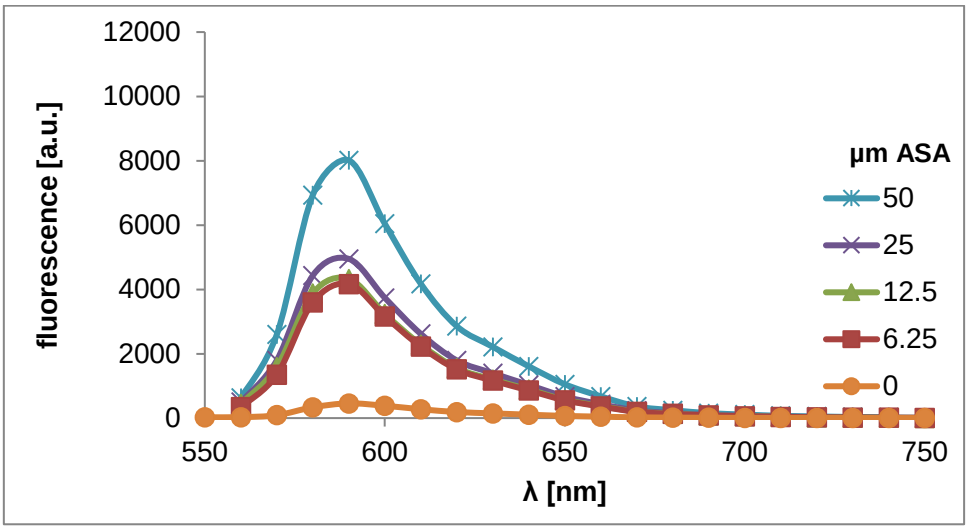

Figure 4. 3 Fluorescence response of the spin-labelled probe **5** to AsA.

Table 4. 1 Spectral properties of the spin-labelled synthesized probes (**5-12**) in methanol.

Probe	Λ_{abs} [nm]	Λ_{em} [nm]	ε/M cm^{-1}
5	560	590	38.400
6	560	590	29.900
7	560	590	31.600
8	560	590	35.300
9	560	590	36.000
10	520	540	29.500
11	510	540	34.000
12	570	600	34.800

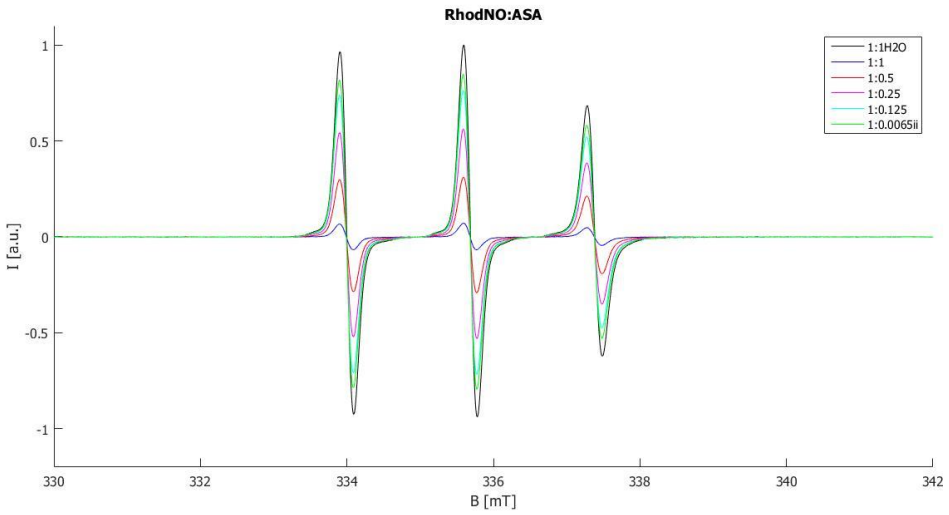

Figure 4. 4 EPR response of the spin-labelled probe **5** to AsA.

4.5 Biological safety of the synthesized spin-labelled probes (5-8)

Before proceeding to test the ability of the spin-labelled probe **5** to detect the ROS in a cancer cell line, the safety of the synthesized probes must be confirmed first. Both, NIH3T3 cells which represent mouse normal fibroblasts, as well as PC3 cancer cells which represent human prostate cancer, were used as models.

Both (MTT and CV assays) were performed at 0.1, 1 and 10 µM. The tested spin-labelled probes **5-8** did not significantly affect the normal cell growth at 0.1 and 1 µM, neither mitochondrial function compared to untreated cells. Thus, under the used concentrations the synthesized probes were found non-toxic against the selected tumor and normal cells (**Figure 4. 5**).

The spin-labelled probes **5-8**, showed high safety and were tolerated by both PC3 prostate tumor and the normal fibroblast NIH3T3 (**Figure 4. 5**). The results encouraged us to continue with the follow-up studies as described before. We envisioned to use the spin-labelled probe **5** as our model probe, although the spin-labelled probe **6** and **7** performed very well, to prove the theory of our study, we need only to choose one representative probe.

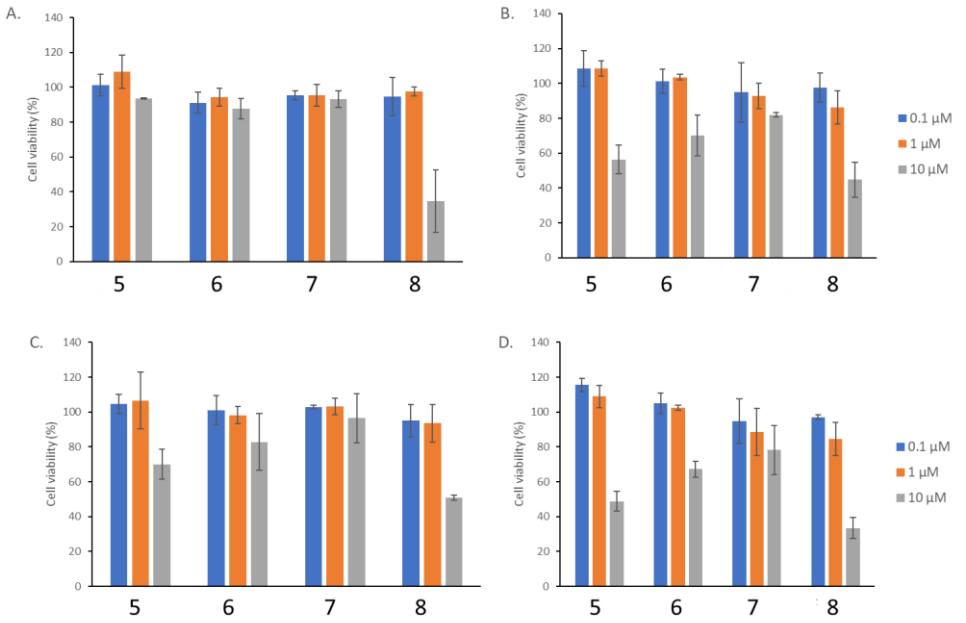

Figure 4. 5 Cell viability determined after 48 h of treatment with probes (**5**-**8**) of (A) NIH3T3 and (B) PC3 cells evaluated with MTT assay, (C) NIH3T3 and (D) PC3 cells evaluated with CV assay.

4.6 ROS detection of the spin-labelled probe 5 via Flow cytometry analysis

To evaluate the ROS detection potential of TEMPO-containing probes, cells were treated with spin-labelled probe **5** and flow cytometry analysis was performed (**Figure 4. 6**). Briefly, PC3 and NIH3T3 were stained with dihydrorhodamine (DHR) dye, then co-treated with the spin-labelled probe **5** to investigate and compare the ROS production in the normal as well as in the tumor cells. DHR dye is an uncharged and non- fluorescent ROS indicator, upon interaction with ROS, the dye is oxidized to cationic rhodamine, which localizes in the mitochondria and exhibits green fluorescence (**Scheme 4. 4**).

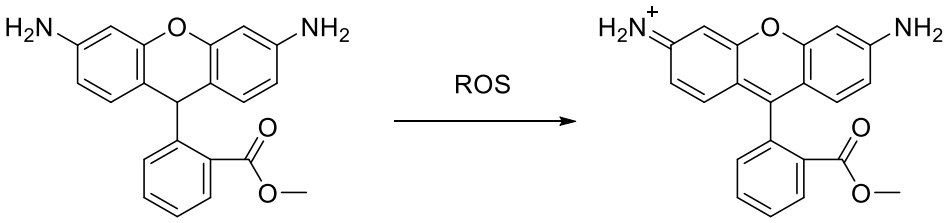

Scheme 4. 4 Oxidative conversion of DHR to its corresponding oxidized fluorescent product upon interaction with ROS.

Two different detection channels with different excitation/emission wavelengths were used to record the fluorescence of both DHR and the spin-labelled probe **5**. FITC detection channel was used for DHR with excitation/emission wavelengths around (495 nm/519 nm) and Texas red detection channel with excitation/emission wavelengths around (561 nm/619 nm)[20] was used for the spin-labelled probe **5**. As positive control cells co-treated with rhodamine and DHR are used for comparison. In theory, when cells are treated with rhodamine alone, high fluorescent is expected to be seen for both, PC3 and NIH3T3 cell lines. From DHR detection it can be clearly seen that the ROS production is more prominent in the tumor PC3 than in normal NIH3T3 cells (**Figure 4. 6**).

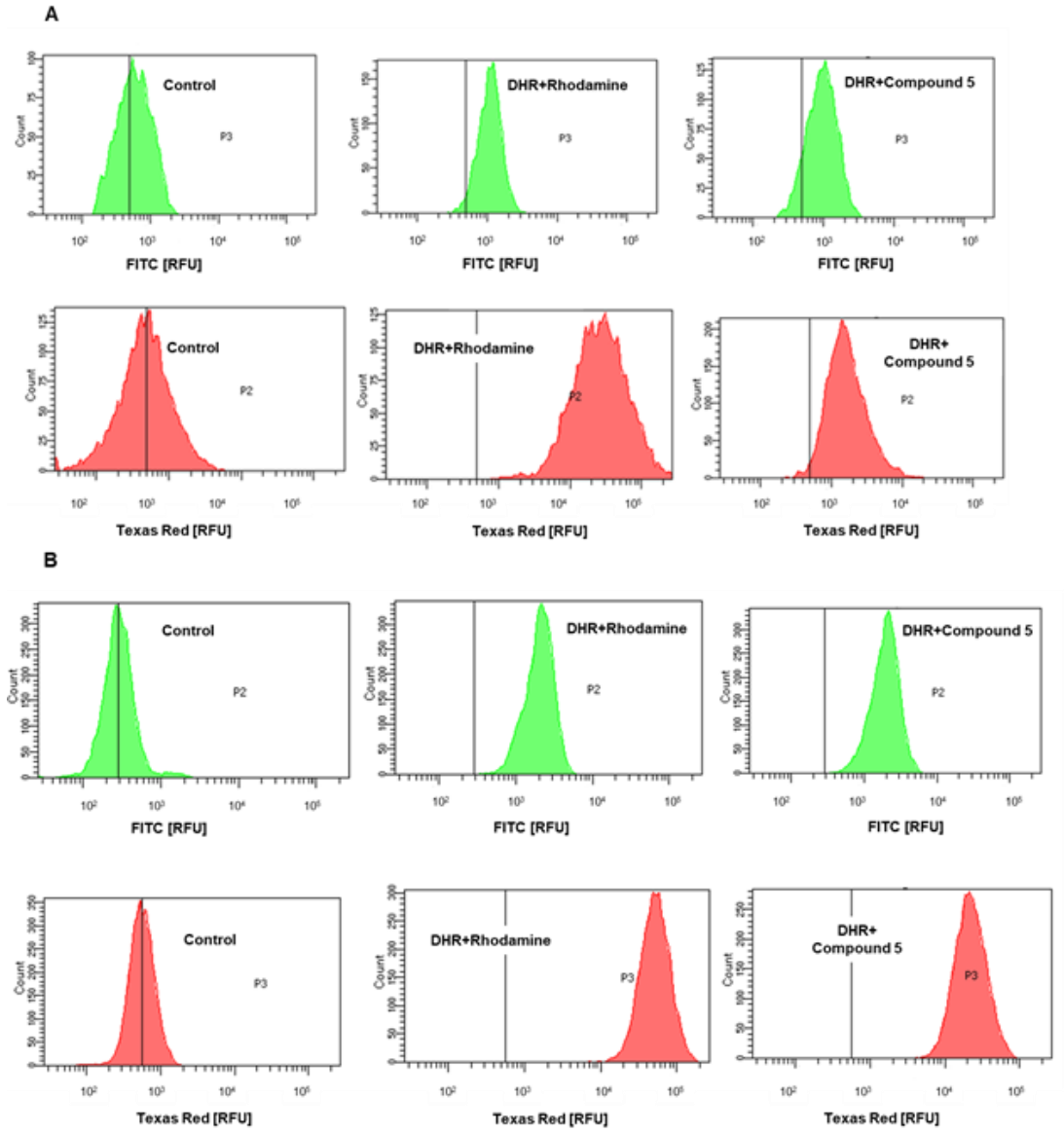

Figure 4. 6 Flow cytometry analysis of (A) NIH3T3 and (B) PC3 cells double-stained with DHR (10 min) and spin-labelled probe **5** (45 min). DHR fluorescence was measured in the FITC channel, while rhodamine and spin-labelled probe 5 was measured in the Texas Red channel.

As expected, namely, the difference in the fluorescence shift corresponds to the level of ROS species production. When the cells were double-stained with rhodamine and DHR, no correlation between ROS levels and fluorescence shift is observed in normal and tumor cells were found as anticipated. In contrast, the cells co-treated with DHR and spin-labelled probe **5** exhibited to a high extent correlation between ROS levels and fluorescence shift. The fluorescence intensity is a concentration-dependent which is due to the fact that the nitroxide radical is being reduced to its corresponding hydroxylamine upon interaction with ROS thereby losing its ability to quench the fluorescence of rhodamine (**Figure 4. 6**).

4.7 Mitochondria targeting of spin-labelled probe 5

Localization of the novel spin-labelled probe **5** in the cells was determined using fluorescence microscopy (**Figure 4. 7**.**B**). The tumor PC3 as well as normal NIH3T3 cells were treated with MitoTracker Green™ and subsequently with rhodamine, as control, and the spin-labelled probe **5**, respectively. The images obtained by fluorescent microscopy showed that rhodamine localizes in the mitochondria (**Figure 4. 7.A**) and (**Figure 4. 8.A**).[21] As shown in flow cytometry experiments, independently from the ROS levels the intensity of rhodamine fluorescence is similar in NIH3T3 and PC3 cells. NIH3T3 cells stained with the spin-labelled probe **5** did not show fluorescence (**Figure 4. 8.B**). On the other hand, PC3 cells treated with spin-labelled probe **5** exhibited high fluorescent intensity (**Figure 4. 7.B**). This difference in the fluorescence intensity, in agreement with flow cytometry data, is due to the higher production of ROS by PC3 than NIH3T3 cells. The distribution panel of the spin-labelled probe **5** is exactly the same as MitoTracker Green™, a commercial stain that localizes exclusively the mitochondria. In short, rhodamine treated cells showed no difference in the intensity of the fluorescence between both cell lines while the spin-labelled probe **5** treated cells showed the presence of fluorescence in the case of PC3 cells since TEMPO-group is sensitive to ROS much more present in tumor than in the normal cells. Significantly, the innovative TEMPO-probe can be successfully applied for the detection of ROS levels as well as localization of mitochondria in living cells *in vitro*.

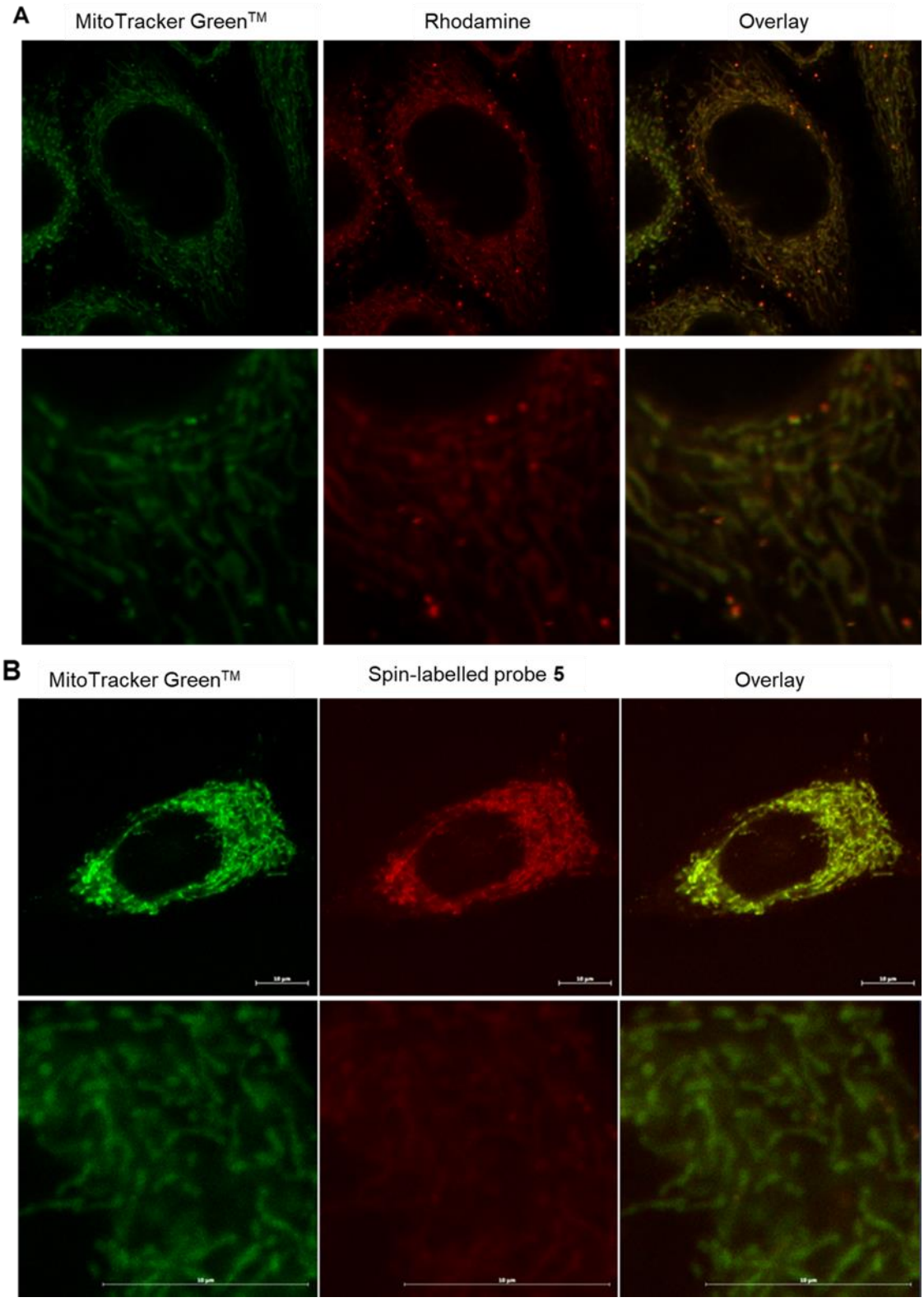

Figure 4. 7 Fluorescence microphotographs: PC3 cells stained with MitoTracker Green™ (FITC channel) and rhodamine (A; Texas Red channel) or spin-labelled probe **5** (B; Texas Red channel).

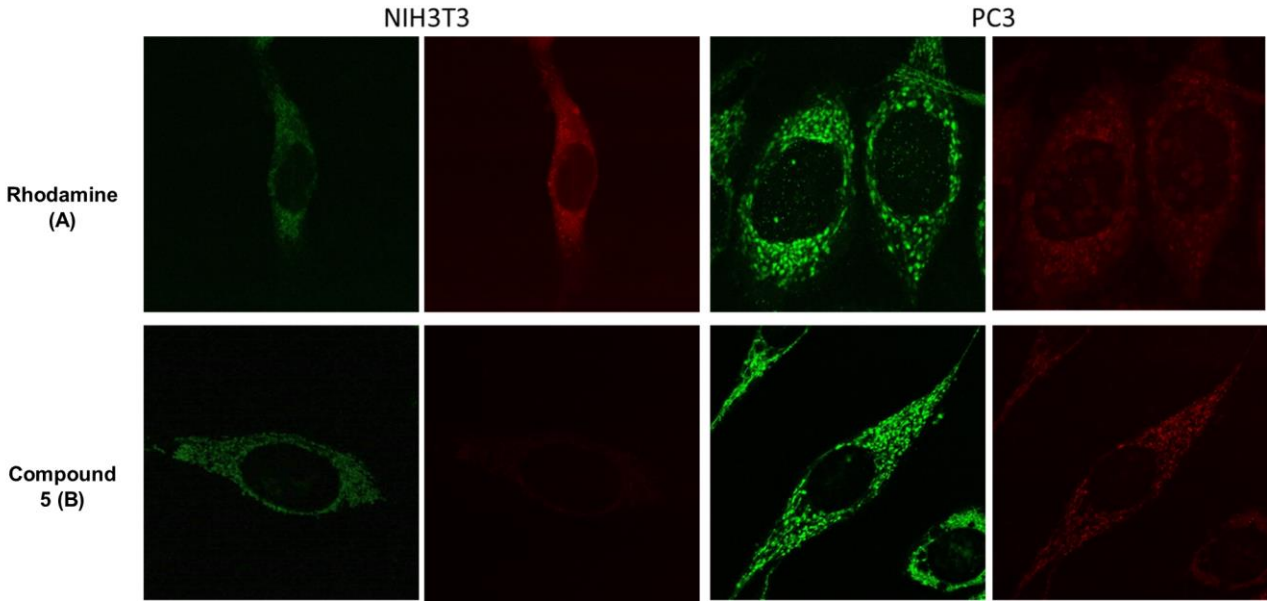

Figure 4. 8 Fluorescence microphotographs: comparison of NIH3T3 and PC3 cells stained with MitoTracker Green™ (FITC channel) and rhodamine (Texas Red channel) or spin-labelled probe **5** (Texas Red channel).

4.8 Spin-labelling for protein or antibody conjugation

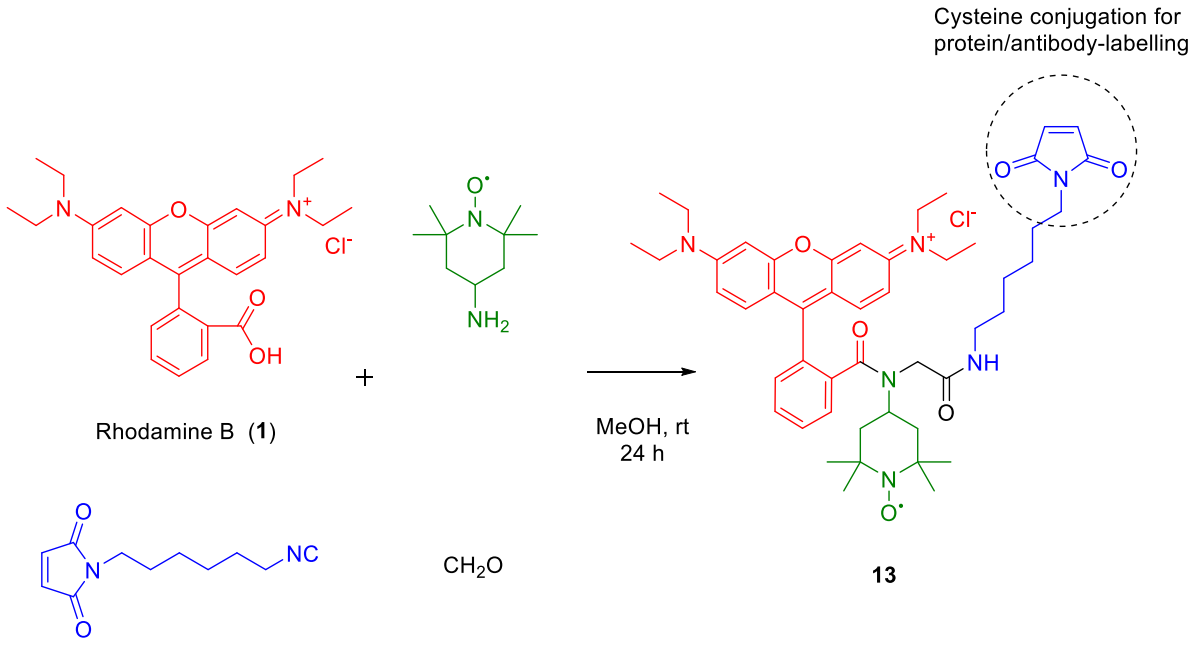

Scheme 4. 5 Synthesis of spin-labelled probe **13**.

Site-directed spin labelling (SDSL) of proteins or antibodies is extensively described in the literature[22] Indeed, one of the most important methods of SDSL of proteins is through the cysteine amino acid.[23]

For achieving cysteine spin-labelling, many methods are reported in the literature[24,25] but indeed, one of the well-known and most reported method for cysteine spin-labelling is via maleimide moiety.[26]

For that reason, we envisioned to utilize maleimide as the isonitrile counterpart to synthesized probe **13**. The probe was tested to label cysteine amino acids in an antibody. Furthermore, probe **13** was successfully conjugated which suggests the possibility to utilize this methodology for protein/antibody conjugation, which opens the opportunity for further applications (**Scheme 4. 5**).

4.9 Conclusions

In conclusion, it's clearly evident that Ugi-multicomponent reaction can be used as a synthetic protocol to develop new rhodamine nitroxide probes for ROS detection. The spin-labelled probe **5** performed exceptionally to detect ROS species. Moreover, the novel probes localize in the mitochondria. The results were confirmed by both flow cytometry and fluorescent imaging. The spin-labelled probe **5** exhibited high selectivity towards the ROS and a high fluorescence shift can be seen in the PC3 cancer cell line with almost no fluorescence for the NIH3T3 cell line. Furthermore, the multicomponent reaction can also be used to develop rhodamine nitroxide with a maleimide as a reactive handle for post-Ugi-modification via reaction with the cysteine amino acids for protein or antibody conjugation. We envisioned that MCR will be used to excess specific probes to detect specific cancer types.

4.10 Experimental part

General remarks/chemistry

All commercially available reagents were purchased and used without further purification. Convertible isocyanides 2-isocyano-2-methyl propyl phenyl carbonate, IPB, was synthesized following reported procedures.[27] HPLC grade methanol was used in all Ugi-reactions. Analytical thin-layer chromatography (TLC) was performed using silica gel 60 F254 aluminum sheets (Merck, Germany) and the visualization of the spots has been done under UV light (254 nm) or by developing with a solution of cerium sulphate. Flash column chromatography was performed using silica gel (0.040-0.063 mm). ^{1}H and ^{13}C NMR spectra were recorded in solutions on a 400 MHz Varian MERCURY-VX 400 at 22 °C at 400 MHz and 100 MHz, respectively.

Chemical shifts (δ) are reported in ppm relative to TMS (^{1}H-NMR) and to the solvent signal (^{13}C NMR spectra). Note: due to the paramagnetism of nitroxide moiety, NMR cannot provide information useful for structural elucidation of nitroxides, therefore, reduction of the paramagnetic center was performed with AsA. The positive-ion high-resolution ESI mass spectra were obtained with an Orbitrap Elite mass spectrometer (Thermo Fisher Scientific, Germany) equipped with HESI electrospray ion source (positive spray voltage 4 kV, capillary temperature 275 °C, source heater temperature 80 °C, FTMS resolution 60000). Nitrogen was used as sheath gas. The instrument was externally calibrated using the Pierce LTQ Velos ESI positive ion calibration solution (product number 88323, Thermofisher Scientific, Rockford, IL, 61105 USA). The data were evaluated using the software Xcalibur 2.7 SP1. Analytical RP-HPLC analysis was performed with an Agilent 1100 system in a reverse-phase C18 column (4.6 × 150 mm, 5 µm) with a PDA detector. A linear gradient from 5% to 100% of solvent B in solvent A over 15 min at a flow rate of 0.8 mL min^{-1}. Detection was accomplished at 210 nm. Solvent A: 0.1% (v/v) formic acid (FA) in water. Solvent B: 0.1% (v/v) FA in acetonitrile. Instrumental details EPR: X-Band (9.43 GHz) room temperature CW EPR measurements were performed on a Magnettech MiniScope MS400 benchtop spectrometer (Magnettech, Berlin, Germany). Spectra were recorded with a microwave power under the saturation limit (varied between 1-3 mW), 100 kHz modulation frequency, modulation amplitude of 0.1 mT and 4096 points. The lowest sample concentrations were 300 µM. Contribution of solvent to spectra was examined using water and acetonitrile. Since it is difficult to evaluate fully resolved hyperfine- and g-tensors at X-band frequencies, only the isotropic values are reported.

General remarks/biology

PC3 and PBS, RPMI 1640 and Trypsin EDTA were from Capricorn Scientific, FCS, acetic acid, penicillin/streptomycin, paraformaldehyde was from Roth, Germany. DMSO was bought from Duchefa Biochemie, Germany. DHR was obtained from BD Horizon, USA. MitoTracker Green FM was from Invitrogen. Finally, CV and MTT were from Sigma Aldrich, USA.

Cell lines and cultivation

Two different cell lines were used in all biological experiments, fibroblast NIH3T3 cells obtained from mice representing normal cells and prostate PC3 cancer cells of a human. Both cell lines were purchased from the German Collection of Microorganisms and Cell

Cultures (Leibniz-DSMZ, Germany). The cell lines were grown in 10 mL of complete medium (10% FCS and 1% penicillin/streptomycin in RPMI 1640) in T75 flasks.

The cells were observed every day. When the cell confluency reached 90%, the passage was performed. For cell passage, cells were washed with PBS, detached with 1 mL of 0.05% trypsin-EDTA and 7×10^5 cells were transferred to a new flask containing 10 mL of complete medium. For 96-well plate, 5000 cells were seeded per well. While for the 6-well plates, 1×10^5 cells were seeded per well. Stock solutions (20 mM) were prepared in DMSO shortly before cell viability determination.

Cell viability

The spin-labelled probes **5-8** were tested against two different cell lines in 96-well plate; NIH3T3 and PC3 for 48 h in three different concentrations: 0.1 µM, 1 µM, and 10 µM. After incubation, the cell viability was determined with MTT and CV assay. For MTT assay, the cells were incubated in MTT working solution (0.5 mg of MTT in 1 mL complete medium) for at least 20 min. Afterward, the MTT solution was discarded and the formed formazan bodies were dissolved using 50 µL of DMSO. The absorbance was measured at 570 nm and the background at 670 nm. The viability is represented as a percentage compared to untreated cells.[28] For CV assay, the cells were fixed for 20 min with 4% paraformaldehyde followed by drying at RT for 20 min. Afterward, 50 µL of CV working solution (100 mg of CV in 100 mL of PBS) was used to stain the cells for 20 min. The staining solution was discharged, cells were washed with dd H_2O and the cells were dried overnight. After overnight drying, the stain was dissolved in 50 µL of 33% acetic acid and the absorbance was measured as illustrated in MTT assay.[28]

Flow cytometry

The cells were double-stained by both DHR and the tested probes. For staining by DHR [29], the cells were treated with 1 mL of DHR working solution (1 µM DHR, 0.1% FCS in 1 mL of PBS) and incubated at 37 °C and 5% CO_2 for 10 min. Afterward, the staining process was deactivated by medium and the cells were seeded in a 6-well plate. Cells stained by DHR were detected by the FITC channel (exc/emi: 488/530). For staining with the tested probes, the cells were stained with a working solution (1 µM of the tested probe in 1 mL of RPMI 1640) for 45 min. Afterward, the cells were washed with PBS, detached using 0.05% trypsin-EDTA. The detachment process was stopped by fresh medium and then the cells were resuspended in PBS for the flow cytometry analysis. The tested spin-labelled probes were detected by the PE-Texas Red channel (exc/emi: 561/610).[29]

Fluorescence microscopy

The PC3 or NIH3T3 cells were double-stained with MitoTracker Green FM™, a commercially available stain that targets the mitochondria[30,31], and the tested probes. For MitoTracker Green FM™ staining, the process was carried out exactly as illustrated by the product manual. The cells afterward were stained with 1 µM of the tested probes for 45 min and washed PBS and finally observed by fluorescent microscopy. Both cell lines were also stained in the same manner with double stain however using MitoTracker Green FM™ and rhodamine as described above.

General procedure for the Ugi-4CR

To a stirred solution of a TEMPO amine (0.1 mmol) in MeOH (250 µL, 0.4 M) was added paraformaldehyde (0.1 mmol) and the mixture was stirred for 2 h. After this time the acid (0.1 mmol) and isonitrile (0.1 mmol) were added before stirring was continued for 18 h. The solvent was removed under reduced pressure and the crude material purified by column chromatography to afford the desired products.

***N*-(9-(2-((2-(cyclohexylamino)-2-oxoethyl) (1-oxyl-2,2,6,6-tetramethylpiperidin-4-yl) carbamoyl) phenyl)-6-(diethylamino)-3H-xanthen-3-ylidene)-*N*-ethylethanaminium (5)**

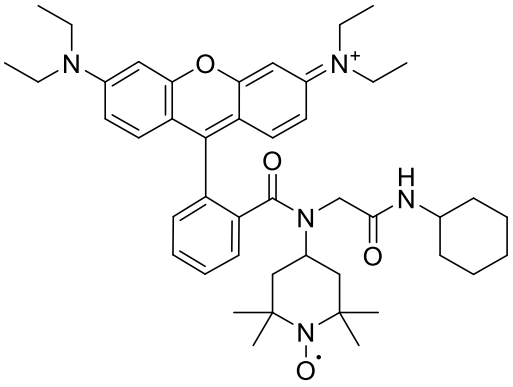

Obtained using the general procedure, cyclohexyl isonitrile, *N*-oxyl amine, rhodamine b and paraformaldehyde were used. The crude material was purified by silica gel column chromatography (CH_2Cl_2 / MeOH 9:1) to give probe **5** (37 mg, 0.05 mmol, 50%) as deep violet powder. R_F 0.2 (CH_2Cl_2 / MeOH 9:1). NMR of the corresponding hydroxylamine after reduction with AsA. ^{1}H NMR (600 MHz, (CD_3COCD_3) δ 7.77 – 7.61 (m, 3H), 7.47 – 7.39 (m, 2H), 7.17 (d, *J* = 9.5 Hz, 2H), 7.08 (d, *J* = 9.5 Hz, 1H), 7.05 – 6.99 (m, 1H), 6.90 (m, 1H), 3.59 (m, 8H), 3.43 (m, 1H), 1.70 – 1.27 (m, 12H), 1.25 – 1.06 (m, 26H).^{13}C NMR (151 MHz, CD_3COCD_3) δ 171.16, 170.12, 168.82, 168.55, 158.03, 156.08, 155.47,

155.07, 136.03, 134.21, 130.76, 130.73, 130.62, 130.57, 127.88, 126.99, 114.60, 114.35, 96.39, 57.37, 54.99, 50.17, 46.15, 39.12, 32.25, 25.39, 24.86, 24.21, 12.37.). HRMS (ESI) *m/z* calcd. for $C_{45}H_{61}N_5O_4^{\bullet+}$ $[M]^+$ 735.4718, found 735.4725.

_N_-(6-(diethylamino)-9-(2-((1-oxyl-2,2,6,6-tetramethylpiperidin-4-yl)(2-oxo-2-((2,4,4-trimethoxybutyl)amino)ethyl)carbamoyl)phenyl)-3H-xanthen-3-ylidene)-_N_-ethylethanaminium (6)

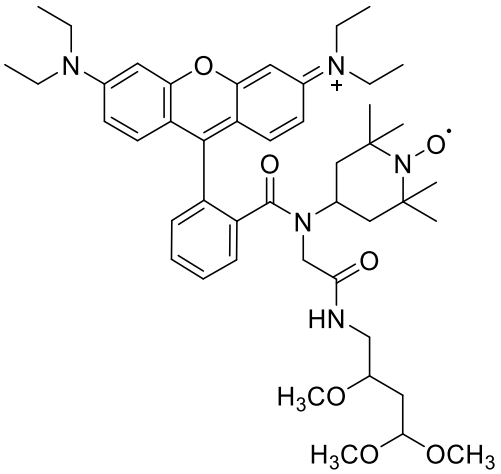

Obtained using the general procedure, ipb isonitrile, *N*-oxyl amine, rhodamine b, and paraformaldehyde were used. The crude material was purified by silica gel column chromatography (CH_2Cl_2 / MeOH 9:1) to give probe **6** (44 mg, 0.06 mmol, 55%) as a deep violet powder. R_F 0.12 (CH_2Cl_2 / MeOH 9:1). HRMS (ESI) *m/z* calcd. for $C_{46}H_{65}N_5O_7^{\bullet+}$ $[M]^+$ 799.4879, found 799.4862.

_N_-(9-(2-((2-(benzylamino)-2-oxoethyl)(1-hydroxy-2,2,6,6-tetramethylpiperidin-4-yl)carbamoyl)phenyl)-6-(diethylamino)-3H-xanthen-3-ylidene)-_N_-ethylethanaminium chloride (7)

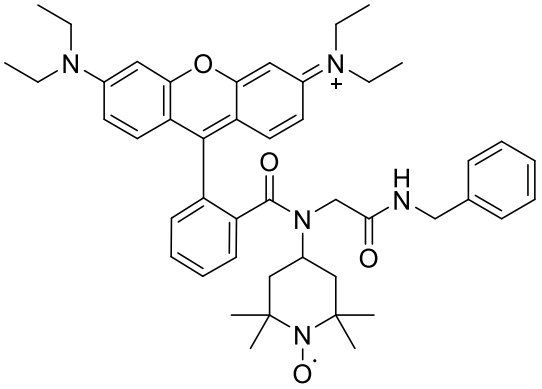

Obtained using the general procedure, benzyl isonitrile, *N*-oxyl amine, rhodamine b, and paraformaldehyde were used. The crude material was purified by silica gel column chromatography (CH_2Cl_2 / MeOH 9:1) to give probe **7** (45 mg, 0.06 mmol, 60%) as a deep violet powder. R_F 0.15 (CH_2Cl_2 / MeOH 9:1). HRMS (ESI) *m/z* calcd. for $C_{46}H_{57}N_5O_4^{\bullet+}$ $[M]^+$ 743.4405, found 743.4391.

_N_-(6-(diethylamino)-9-(2-((1-hydroxy-2,2,6,6-tetramethylpiperidin-4-yl)(2-((2-methoxy-2-oxoethyl)amino)-2-oxoethyl)carbamoyl)phenyl)-3H-xanthen-3-ylidene)-_N_-ethylethanaminium chloride (8)

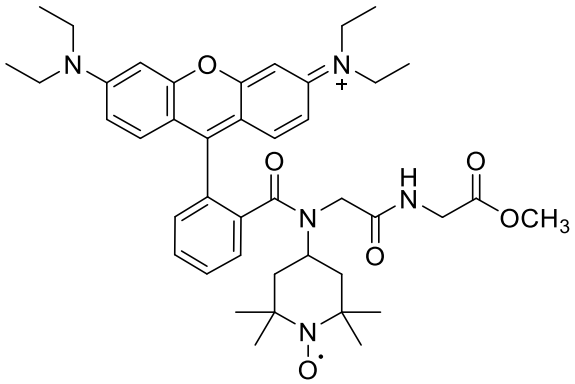

Obtained using the general procedure, methyl isocyanoacetate, *N*-oxyl amine, rhodamine b and paraformaldehyde were used. The crude was material purified by silica gel column chromatography (CH_2Cl_2 / MeOH 9:1) to give probe **8** (51 mg, 0.07 mmol, 70%) as a deep violet powder. R_F 0.13 (CH_2Cl_2 / MeOH 9:1). HRMS (ESI) *m/z* calcd. for $C_{42}H_{55}N_5O_6^{\bullet+}$ $[M]^+$ 725.4147, found 725.4139.

_N_-(9-(2-((2-((4-benzoylphenyl)amino)-2-oxoethyl)(1-hydroxy-2,2,6,6-tetramethyl piperidin-4-yl)carbamoyl)phenyl)-6-(diethylamino)-3H-xanthen-3-ylidene)-_N_-ethyl ethanaminium chloride (9)

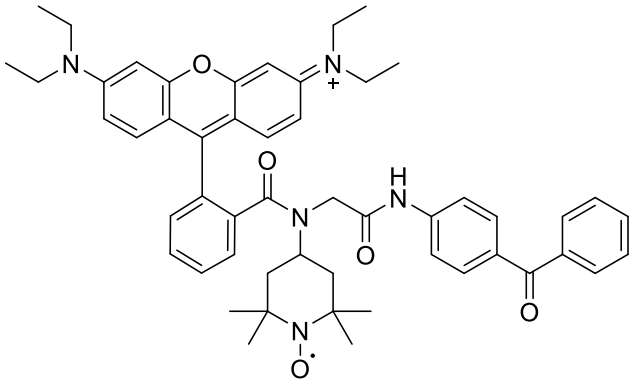

Obtained using the general procedure, 4-benzophenone isonitrile, *N*-oxyl amine, rhodamine b and paraformaldehyde were used. The crude material was purified by silica gel column chromatography (CH_2Cl_2 / MeOH 9:1) to give probe **9** (43 mg, 0.05 mmol, 52%) as a deep violet powder. R_F 0.16 (CH_2Cl_2 / MeOH 9:1). HRMS (ESI) *m/z* calcd. for $C_{52}H_{59}N_5O_5^{\bullet+}$ $[M]^+$ 833.4511, found 833.4518.

(Z)-_N_-(9-(2-((2-(cyclohexylamino)-2-oxoethyl)(1-oxyl-2,2,6,6-tetramethylpiperidin-4-yl)carbamoyl)phenyl)-6-(ethylamino)-2,7-dimethyl-3H-xanthen-3-ylidene)ethanaminium perchlorate (10)

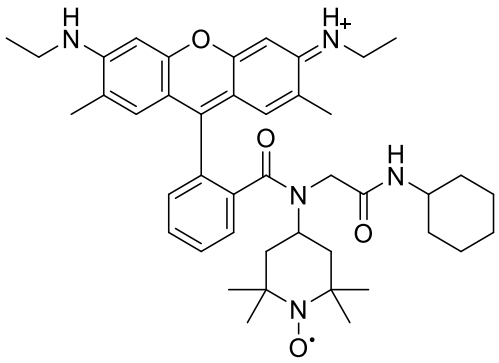

Obtained using the general procedure, cyclohexyl isonitrile, *N*-oxyl amine, rhodamine 19 P and paraformaldehyde were used. The crude material was purified by silica gel column chromatography (CH_2Cl_2 / MeOH 9:1) to give probe **10** (50 mg, 0.07 mmol, 70%) as a deep violet powder. R_F 0.12 (CH_2Cl_2 / MeOH 9:1). HRMS (ESI) *m/z* calcd. for $C_{43}H_{57}N_5O_4^{\bullet+}$ $[M]^+$ 707.4405, found 707.4398.

9-(2-((2-(cyclohexylamino)-2-oxoethyl)(1-oxyl-2,2,6,6-tetramethylpiperidin-4-yl)carbamoyl)phenyl)-3-imino-3H-xanthen-6-aminium chloride (11)

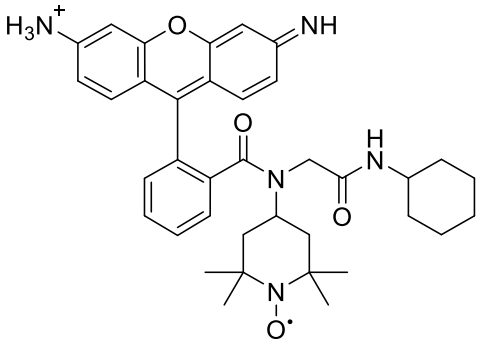

Obtained using the general procedure, cyclohexyl isonitrile, *N*-oxyl amine, rhodamine 110 and paraformaldehyde were used. The crude material was purified by silica gel column chromatography (CH_2Cl_2 / MeOH 9:1) to give probe **11** (37 mg, 0.06 mmol, 60%) as a deep violet powder. R_F 0.1 (CH_2Cl_2 / MeOH 9:1). HRMS (ESI) *m/z* calcd. for $C_{37}H_{45}N_5O_4^{\bullet+}$ $[M+H]^+$ 623.3466, found 623.3453.

***N*-(cyclohexyl)-*N*2-(1-oxyl-2,2,6,6-tetramethylpiperidin-4-yl)-*N*2 -{[2-(2,3,6,7,12,13,16,17-octahydro-1H,5H,11H,15H pyrido [3,2,1-ij] quinolizino [1´,9´:6,7,8] chromeno[2,3-f]quinolin-4-ium-9-yl)phenyl]carbonyl}glycinamide chloride (12)**

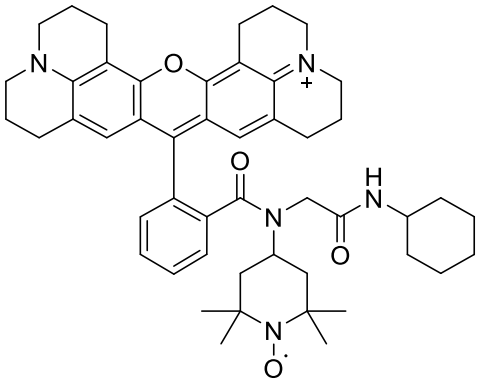

Obtained using the general procedure, cyclohexyl isonitrile, *N*-oxyl amine, rhodamine 101 and paraformaldehyde were used. The crude material was purified by silica gel column chromatography (CH_2Cl_2 / MeOH 9:1) to give probe **12** (41 mg, 0.05 mmol, 53%) as a deep violet powder. R_F 0.12 (CH_2Cl_2 / MeOH 9:1). HRMS (ESI) *m/z* calcd. for $C_{49}H_{61}N_5O_4^{\bullet+}$ $[M+H]^+$ 783.4718, found 783.4712.

_N_-(6-(diethylamino)-9-(2-((2-((6-(2,5-dioxo-2,5-dihydro-1H-pyrrol-1-yl)hexyl)amino)-2-oxoethyl)(1-oxyl-2,2,6,6-tetramethylpiperidin-4-yl)carbamoyl)phenyl)-3H-xanthen-3-ylidene)-_N_-ethylethanaminium (13)

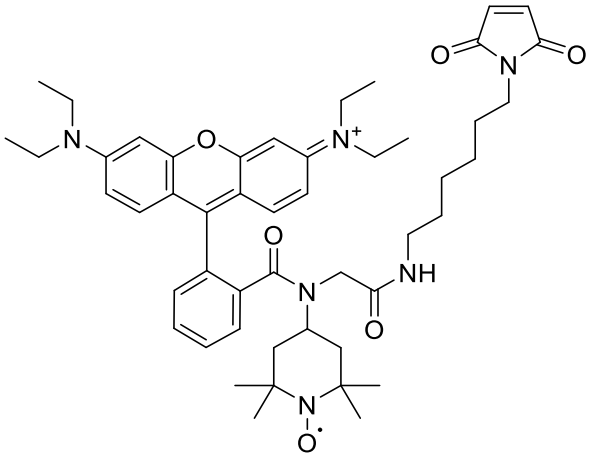

Obtained using the general procedure, maleimide isonitrile, *N*-oxyl amine, rhodamine b and paraformaldehyde were used. The crude material was purified by silica gel column chromatography (CH_2Cl_2 / MeOH 9:1) to give probe **13** (21 mg, 0.05 mmol, 50%) as a deep violet powder. R_F 0.14 (CH_2Cl_2 / MeOH 9:1). HRMS (ESI) *m/z* calcd. for $C_{49}H_{64}N_6O_6^{\bullet+}$ $[M+H]^+$ 832.4882, found 832.4870.

Spectral properties of the synthesized Probes

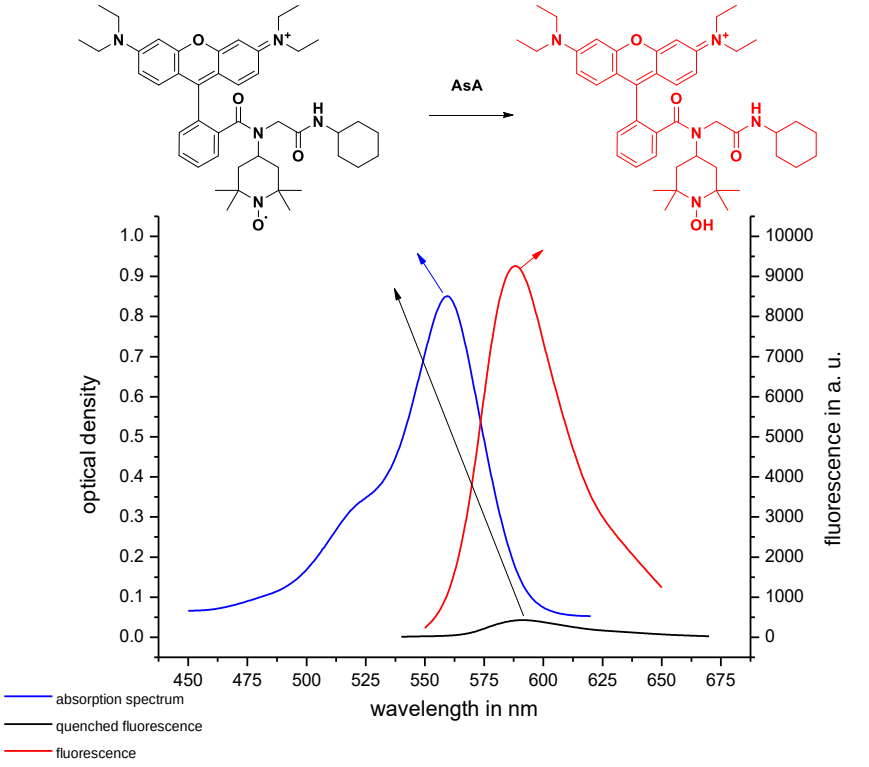

Spectrum of spin-labelled probe **5**.

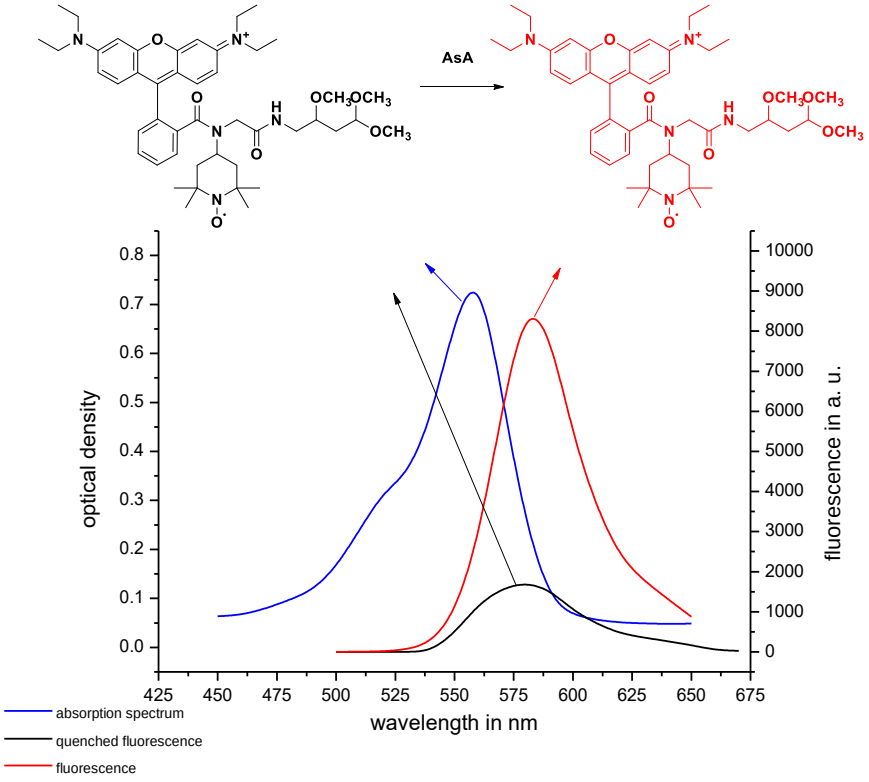

Spectrum of spin-labelled probe **6**.

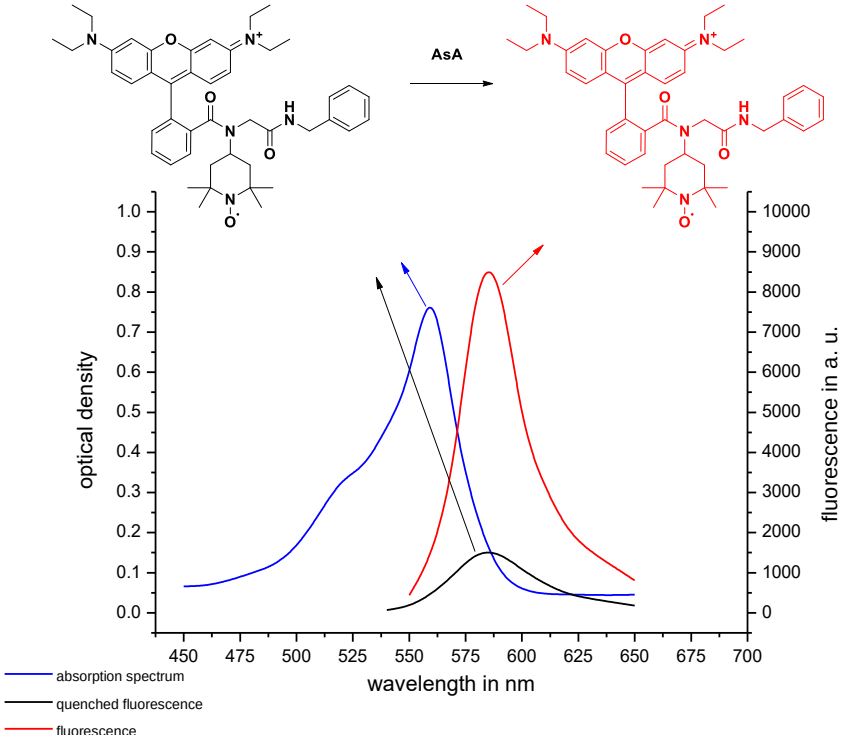

Spectrum of spin-labelled probe **7**.

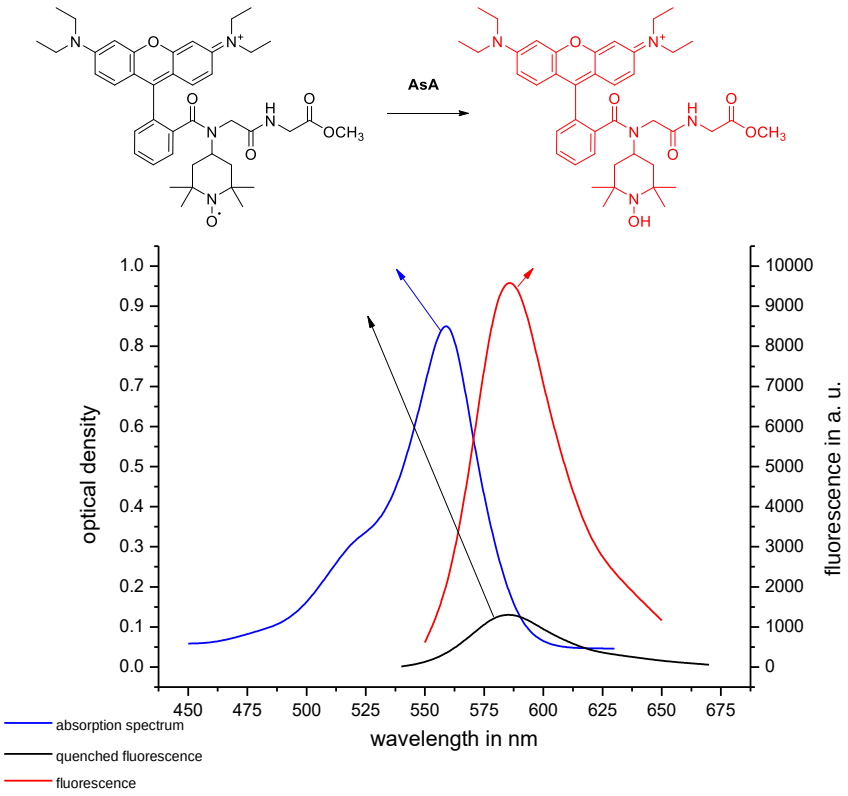

Spectrum of spin-labelled probe **8**.

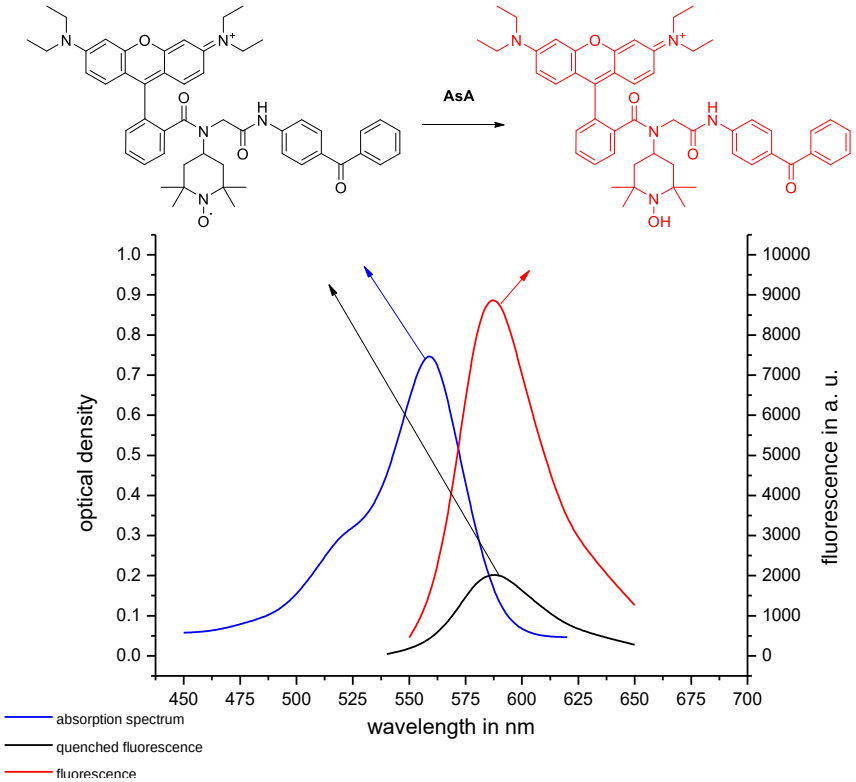

Spectrum of spin-labelled probe **9**.

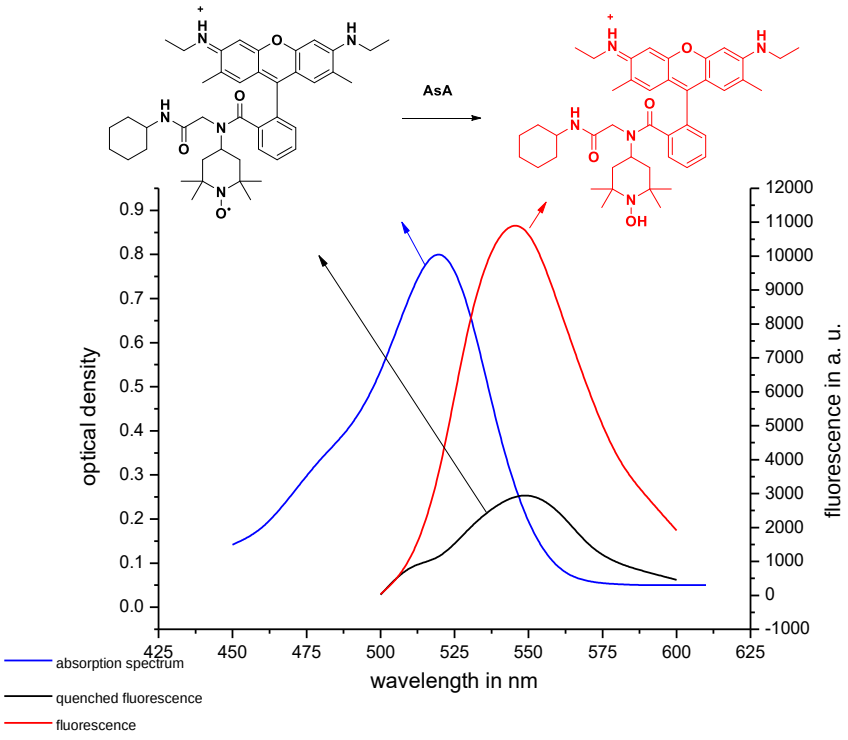

Spectrum of spin-labelled probe **10**.

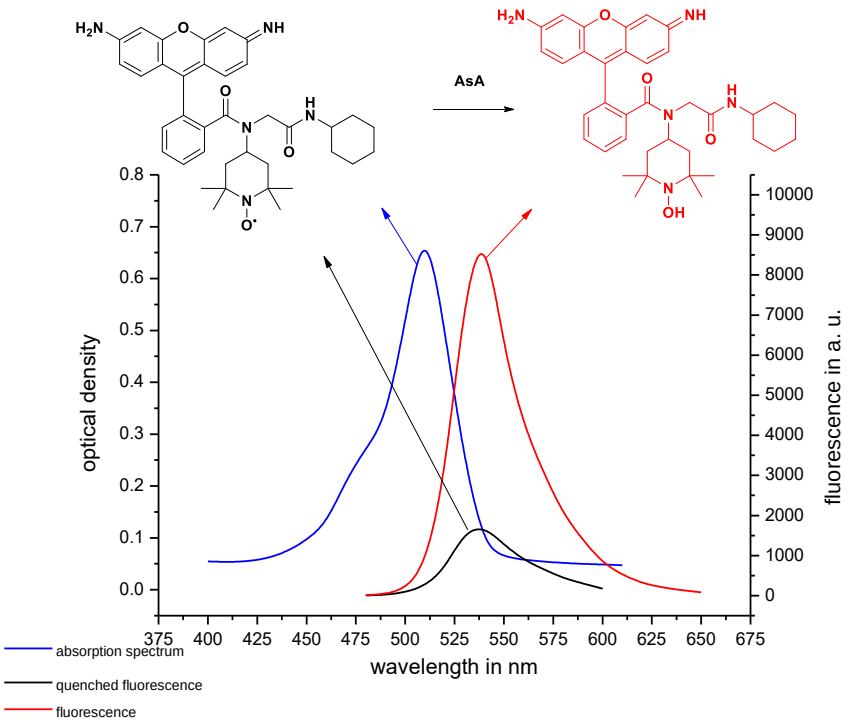

Spectrum of spin-labelled probe **11**.

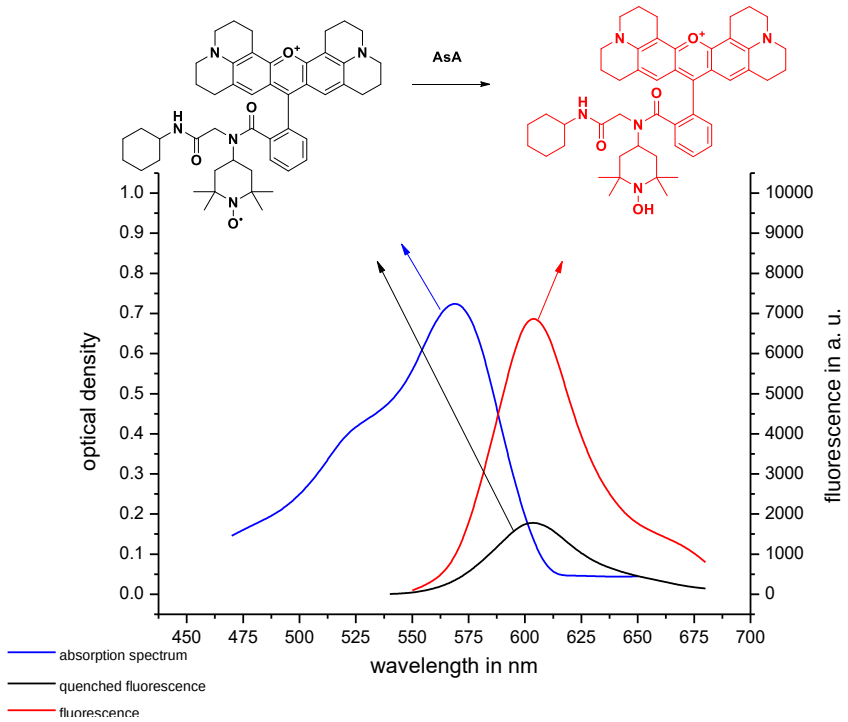

Spectrum of spin-labelled probe **12**.

4.11 References

(1) Ban, S.; Nakagawa, H.; Suzuki, T.; Miyata, N. *Bioorg. Med. Chem*. *Lett*. **2007**, 17, 1451–1454.

(2) Chen, X.; Guo, C.; Kong, *J. Neural Regene. Res*. **2012**, 7, 376–385.

(3) Dikalova, A. E.; Kirilyuk, I. A.; Dikalov, S. I. *Redox Biol*. **2015**, 4, 355–362.

(4) Escobales, N.; Nuñez, R. E.; Jang, S.; Parodi-Rullan, R.; Ayala-Peña, S.; Sacher, J. R.; Skoda, E. M.; Wipf, P.; Frontera, W.; Javadov, S. *J. Mol. Cell Cardiol.* **2014**, 77, 136–146.

(5) Volpe, C. M. O.; Villar-Delfino, P. H.; Dos Anjos, P. M. F.; Nogueira-Machado, *J. Cell Death Dis*. **2018**, 9, 119.

(6) Kumari, S.; Badana, A. K.; G, M. M.; G, S.; Malla, R. *Biomark. Insights* **2018**, 13.

(7) Balaban, R. S.; Nemoto, S.; Finkel, T. *Cell* **2005**, 120, 483–495.

(8) Zielonka, J.; Joseph, J.; Sikora, A.; Hardy, M.; Ouari, O.; Vasquez-Vivar, J.; Cheng, G.; Lopez, M.; Kalyanaraman, B. *Chem. Rev.* **2017**, 117, 10043–10120.

(9) a) Verderosa, A. D.; Dhouib, R.; Fairfull-Smith, K. E.; Totsika, M. *Antibiotics* **2019**, 8; b) Hideg, K.; Kálai, T.; Sár, C. P. *J. Heterocyclic Chem.* **2005**, 42, 437–450.

(10) Jia, M.; Tang, Y.; Lam, Y.-F.; Green, S. A.; Blough, N. V. *Anal. Chem*. **2009**, 81, 8033–8040.

(11) a) Weiss, D. S. *J. Photochem*. **1976**, 6, 301–304; b) Chattopadhyay, S. K.; Das, P. K.; Hug, G. L. *J. Am. Chem. Soc*. **1983**, 105, 6205–6210.

(12) a) Gijzeman, O. L. J.; Kaufman, F.; Porter, G. *J. Chem. Soc*., *Faraday Trans*. 2 **1973**, 69, 727; b) Green, M. M.; Andreola, C.; Munoz, B.; Reidy, M. P.; Zero, K. *J. Am. Chem. Soc*. **1988**, 110, 4063–4065:

(13) Brauch, S.; Henze, M.; Osswald, B.; Naumann, K.; Wessjohann, L. A.; van Berkel, S. S.; Westermann, B. *Org. Biomol. Chem*. **2012**, 10, 958–965.

(14) Best, Q. A.; Johnson, A. E.; Prasai, B.; Rouillere, A.; McCarley, R. L. *Acs Chem. Biol*. **2016**, 11, 231–240

(15) Beija, M.; Afonso, C. A. M.; Martinho, J. M. G. *Chem. Soc. Rev*. **2009**, 38, 2410–2433

(16) Kenmoku, S.; Urano, Y.; Kojima, H.; Nagano, T. *J. Am. Chem. Soc.* **2007**, 129, 7313–7318.

(17) Xiang, Y.; Tong, A. *Org. Lett*. **2006,** 8, 1549–1552.

(18) Tang, B.; Yin, L.; Wang, X.; Chen, Z.; Tong, L.; Xu, K. *Chem. Commun*. **2009**, 5293–5295.

(19) Aliaga, C.; Fuentealba, P.; Rezende, M. C.; Cárdenas, C. *Chem. Phys. Lett.* **2014**, 593, 89–92.

(20) Taldone, T.; Gomes-DaGama, E. M.; Zong, H.; Sen, S.; Alpaugh, M. L.; Zatorska, D.; Alonso-Sabadell, R.; Guzman, M. L.; Chiosis, G. *Bioorg. Med. Chem. Lett.* **2011**, 21, 5347–5352.

(21) Johnson, L. V.; Walsh, M. L.; Chen, L. B. P. *Natl. Acad. Sci*. **1980**, 77, 990–994.

(22) Kugele, A.; Braun, T. S.; Widder, P.; Williams, L.; Schmidt, M. J.; Summerer, D.; Drescher, M. *Chem.Comm.* **2019**, 55, 1923–1926.

(23) Roser, P.; Schmidt, M. J.; Drescher, M.; Summerer, D. *Org. Biomol. Chem.* **2016**, 14, 5468–5476.

(24) Kim, Y.; Ho, S. O.; Gassman, N. R.; Korlann, Y.; Landorf, E. V.; Collart, F. R.; Weiss, S. *Bioconjugate Chem.* **2008**, 19, 786–791.

(25) Puljung, M. C.; Zagotta, W. N. *Current protocols in protein science* **2012**, Chapter 14,14.14.
(26) Nanda, J. S.; Lorsch, J. R. *Method. Enzymol*. **2014**, 536, 79–86.
(27) Neves Filho, R. A.W.; Stark, S.; Morejon, M. C.; Westermann, B.; Wessjohann, L. A. *Tetrahedron Lett.* **2012**, 53, 5360–5363.
(28) Krajnović, T.; Maksimović-Ivanić, D.; Mijatović, S.; Drača, D.; Wolf, K.; Edeler, D.; Wessjohann, L. A.; Kaluđerović, G. N. *Nanomaterials-Basel* **2018**, 8.
(29) Dikalov, S. I.; Harrison, D. G. *Antioxid. Redox Sign*. **2014**, 20, 372–382.
(30) Presley, A. D.; Fuller, K. M.; Arriaga, E. A. J. *Chromatogr. B* **2003**, 793, 141–150.
(31) Samudio, I.; Konopleva, M.; Hail, N.; Shi, Y.-X.; McQueen, T.; Hsu, T.; Evans, R.; Honda, T.; Gribble, G. W.; Sporn, M.; Gilbert, H. F.; Safe, S.; Andreeff, M. *J. Biol Chem.* **2005**, 280, 36273–36282.

Summary and Outlook

Site-directed spin labelling (SDSL) along with electron paramagnetic resonance (EPR) spectroscopy arise as a well-established method that recently gained high popularity as an experimental technique, with diverse applications in biological and chemical sciences. Technical advances in the EPR field, as well as the development in the labelling strategies, are the driving force behind the increase in utilizing EPR instrumentation. Prior to the study the molecule of interest such as (proteins, peptides, active pharmaceutical ingredient) utilizing EPR, one is required to introduce a paramagnetic probe at a well-defined position, a method known as SDSL. The most common nitroxide used in the spin-labelling of proteins are the MTSL and the 5-MSL spin labels, both require the accessibility of cysteine amino acid (**Scheme 1**), in this case, the native cysteine can be used for the labelling step or when needed the cysteine can be introduced into protein by site-directed mutagenesis. Another method of SDSL is the incorporation of special amino acids at the nonsense codon such as the amber codon a recent technique known as “SDSL via non-sense suppressor methodology” (**Scheme 2**). TOAC is another spin label that is widely used in spin-labelling of peptides. It can be added directly into the peptide core via a normal peptide coupling procedure (**Scheme 3**). Till today, no reports were done of utilizing multicomponent reactions (MCRs), in which the incorporation of the spin label can be accomplished in a single step, providing an efficient and step-economical route of spin-labelling (**Scheme 4**). Therefore, the aim of this research project is to develop a new method for SDSL strategy based on IMCRs towards obtaining spin-labelled products with numerous biological applications as anti-cancer compounds and reactive oxygen species sensor.

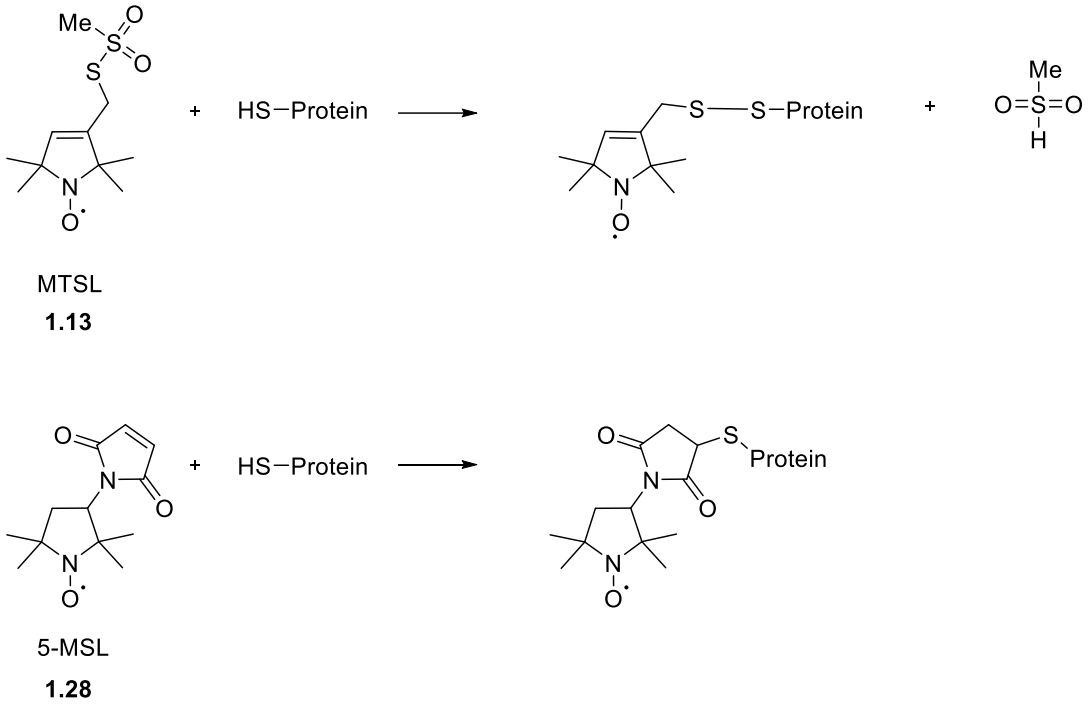

Scheme 1 Spin-labelling of cysteine by A) MTSL and B) 5-MSL.

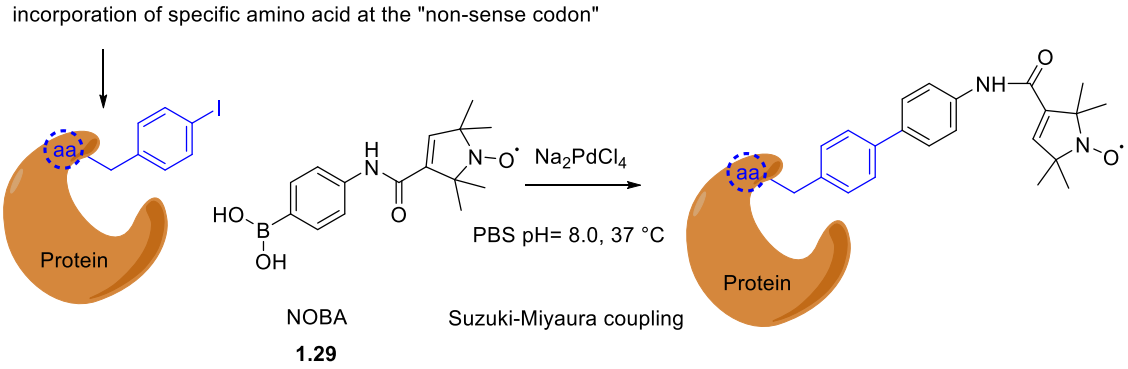

Scheme 2 SDSL of proteins synthesized using nonsense suppressor methodology.

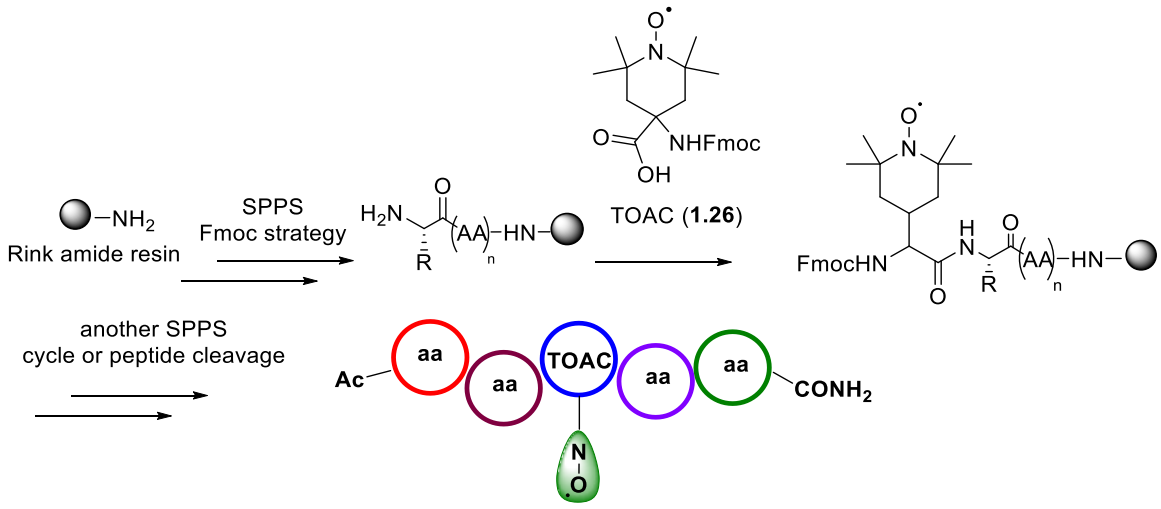

Scheme 3 Peptide spin-labelling using TOAC via Fmoc solid-phase strategy.

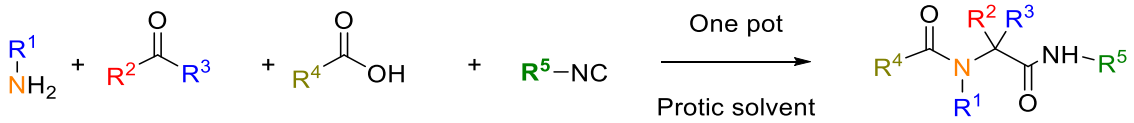

Spin label can be introduced as the amin, acid or isonitrile component

Scheme 4 Ugi-multicomponent-reaction.

Chapter **1** presents a general introduction to nitroxide as spin labels regarding its spectral features, factors affecting its stability and an overview of some of its most important applications in the field of biological and pharmaceutical science. It also presents an overview of the most common methods reported for introducing the spin label.

In Chapter **2**, we presented for the first time the utilization of an isonitrole-mediated multicomponent reaction (IMCR) approach toward obtaining a library of spin-labelled compounds. We also demonstrated high flexibility of this approach by synthesizing different peptide, peptide-peptoid chimera and diketopiperazines with spin label radical attached in different positions. In addition, we proved that the condition of IMCR didn't affect the stability of the spin label even upon refluxing the spin label in acidic conditions, which makes it compatible with post-Ugi-modifications (**Scheme 5**). Quantitative EPR spectroscopic analysis was performed with all the synthesized products and we could even detect small changes in the different molecular structures (**Scheme 6** and **Scheme 7**).

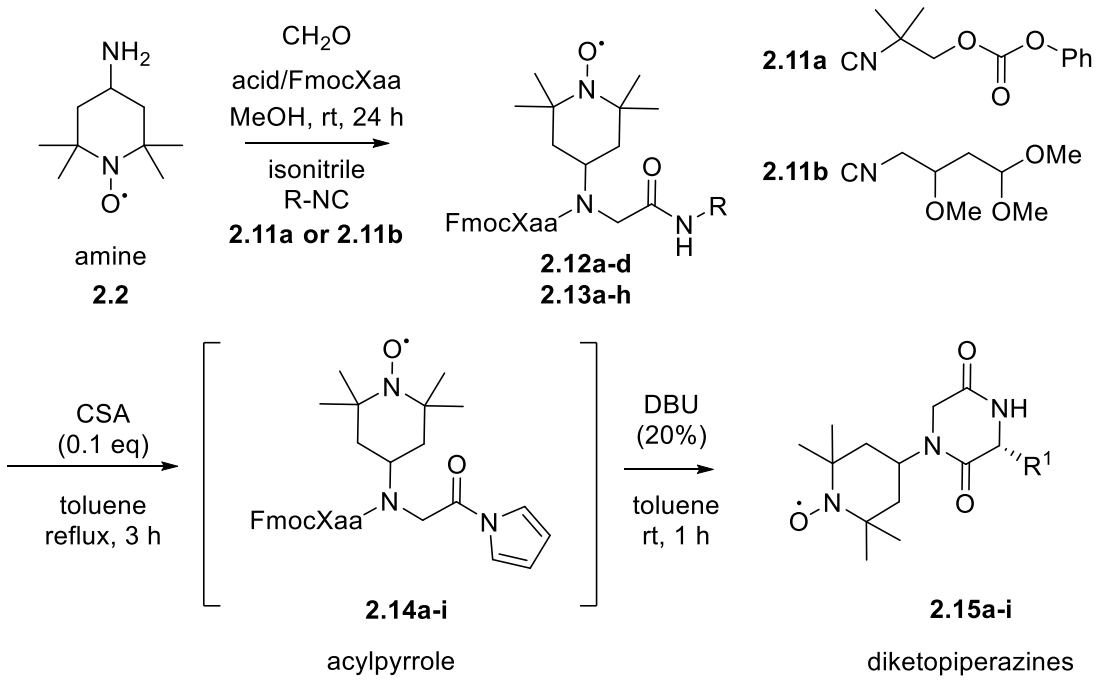

Scheme 5 Synthesis of diketopiperazines, by Ugi-4CR/deprotection + activation/cyclization (UDAC) strategy.

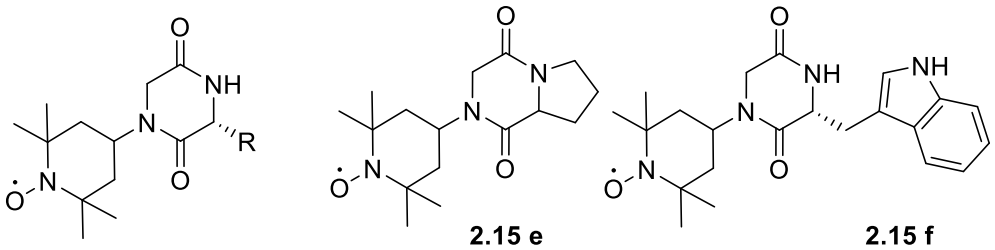

2.15 e **2.15 f**

2.15 a, R = isopropyl
2.15 b, R = Ph
2.15 c, R = sec-butyl
2.15 d, R = 2-methylpropyl
2.15 g, R = Me
2.15 h, R = H

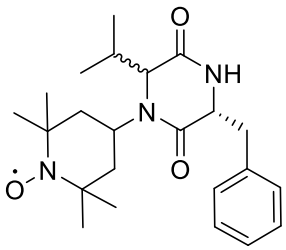

2.15 i

Scheme 6 Structures of diketopiperazines spin-labelled **2.15 (a-i)**.

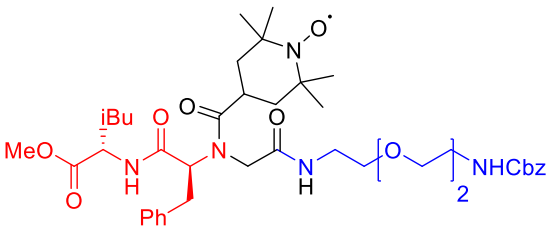

2.16

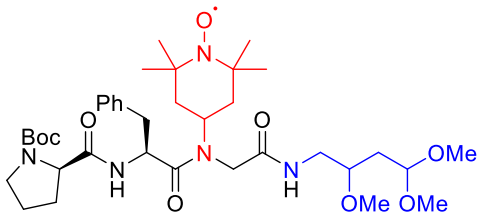

2.17

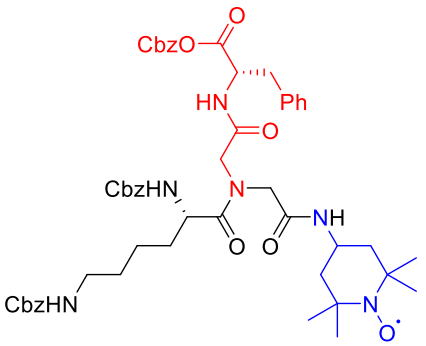

2.18

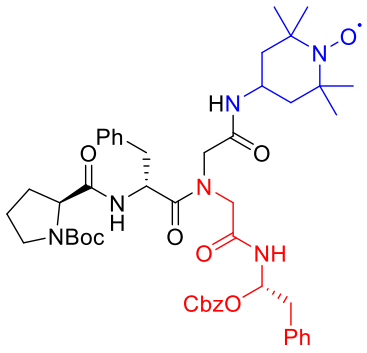

2.19

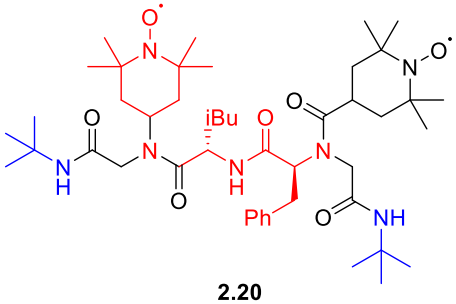

2.20

Scheme 7 Structures of spin-labelled peptide-peptoid chimera **2.16**-**2.20**.

The focus of Chapter **3** was on the development of a new spin-labelled natural product via an isonitrole-mediated multicomponent reaction (IMCR) approach. The natural products used for this chapter were betulinic, cholic and fusidic acids (**3.1**,**3,4**,**3.5**). The spin-labelled compounds **3.7**-**3.12** (**Scheme 8**) were evaluated against both PC3 and HT-29 cancer cell lines (**Figure 1**). Surprisingly the fusidic acid spin-labelled product **3.9** and **3.10** showed interesting activity against the aforementioned cancer cell lines (**Scheme 9**). Post-Ugi-modification was done on compound **3.17** in order to target the mitochondria of the cancer cell (**Scheme 10**). The mitochondria targeting was proven by fluorescent imaging compound **3.19** (**Figure 2**). This work was the first application of the IMCR reaction in the synthesis of spin-labelled natural products for the treatment of cancer.

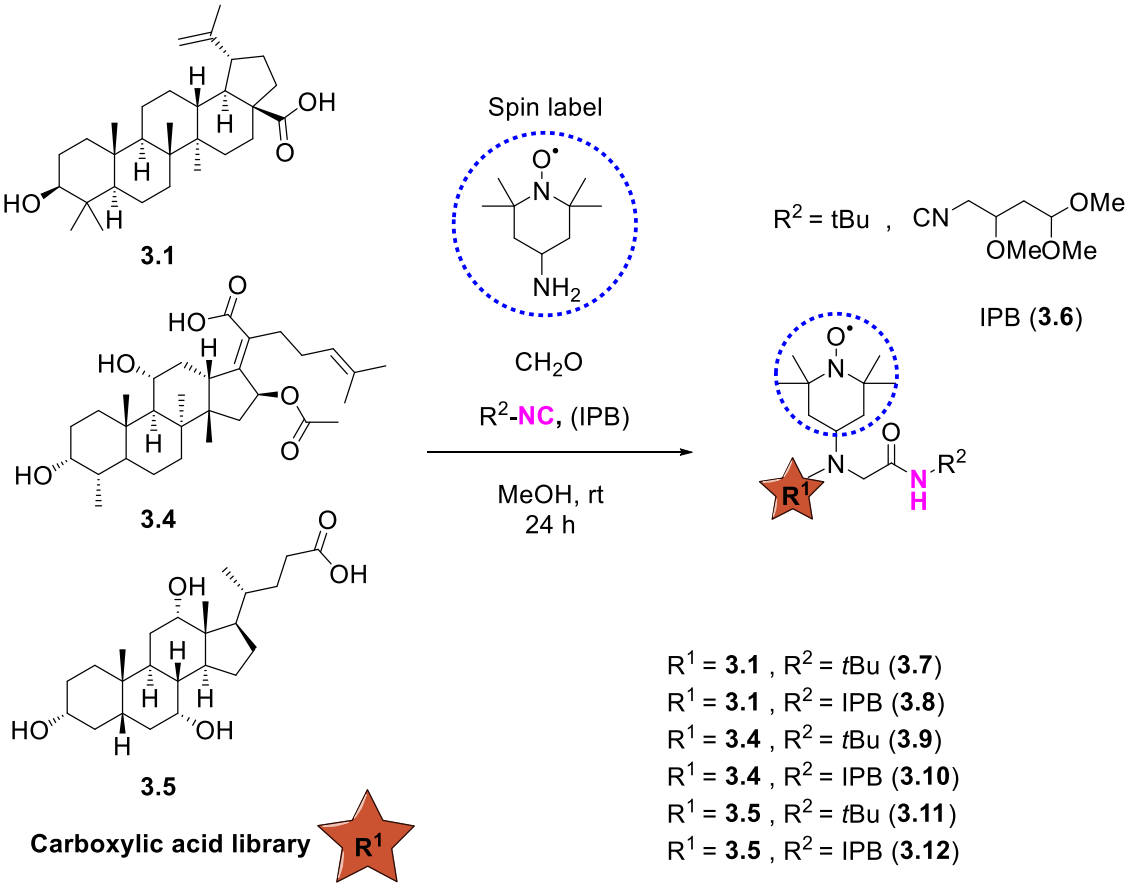

Scheme 8 Synthesis of betulinic-, fusidic- and cholic-acid spin-labelled adducts.

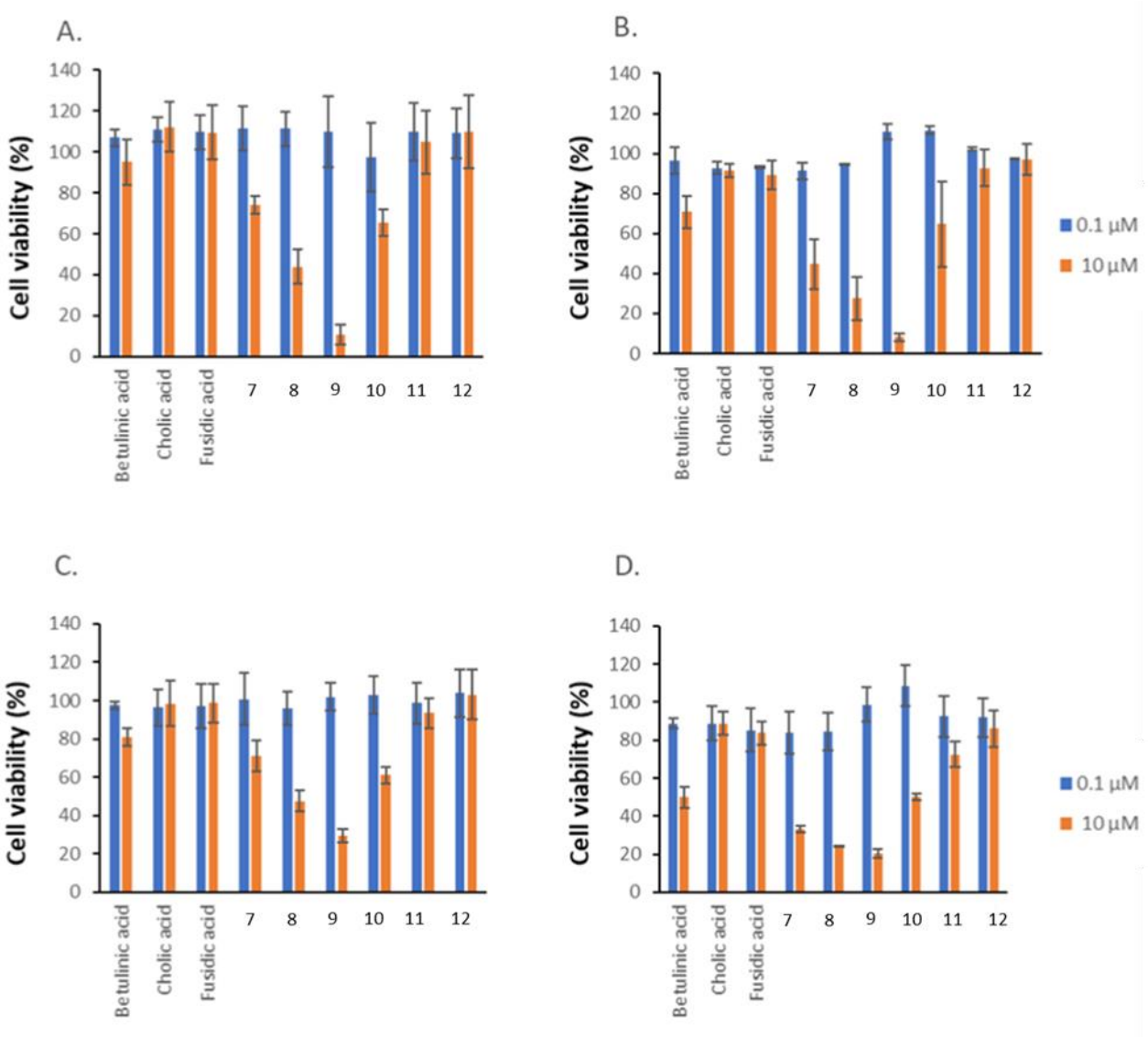

Figure 1 Cell viability of HT-29 (A, B) and PC3 (C, D) cell lines treated by the investigated compounds for 48 h. Cell viability was determined using CV assay (A, C) and MTT assay (B, D).

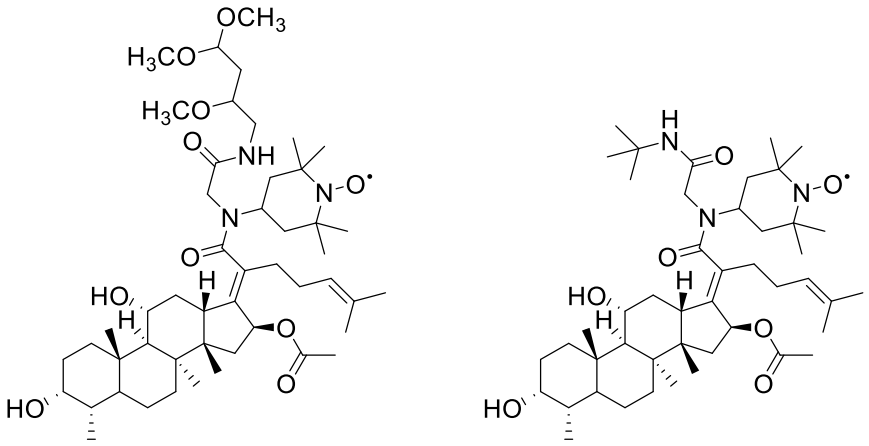

3.10 **3.9**

Scheme 9 Compounds **3.9** and **3.10**.

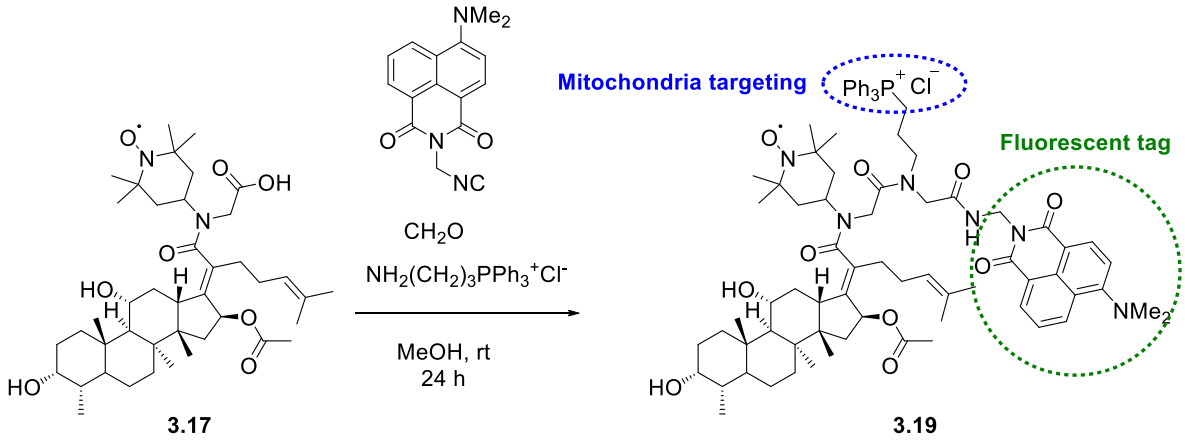

Scheme 10 Post-Ugi-modification of the compound **3.17**.

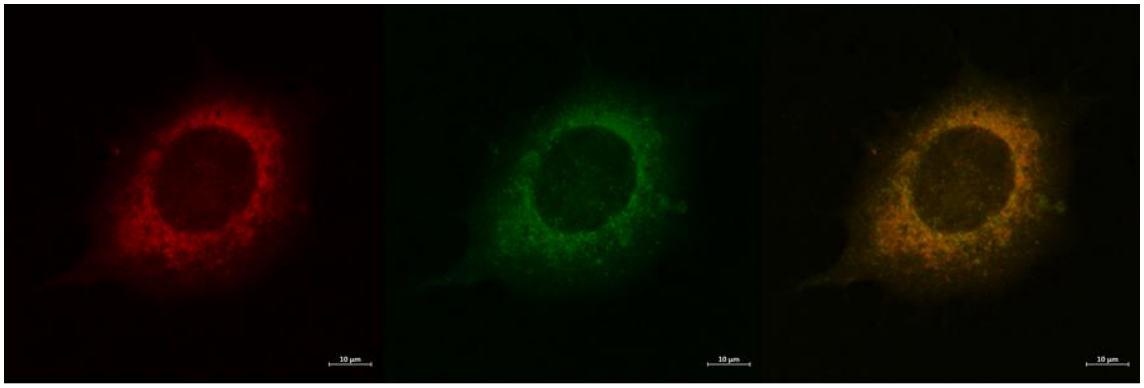

MitoTracker Deep Red | Compound **3.19** | Overlay

Figure 2 Fluorescent imaging of compound **3.19**.

Chapter **4** describes the development of a new rhodamine nitroxide probes for ROS detection. The approach makes use of isonitrole-mediated multicomponent reaction to functionalize a commercially available, widely used mitochondria targeting fluorescent tag “rhodamine” to synthesize new rhodamine nitroxide probes (**Scheme 11**). The nitroxide radical in this study was to act as profluorescent probes, upon interaction with ROS species the nitroxide radical is being reduced to its corresponding hydroxylamine rendering the probe into a fluorescent analyte which offers then the possibility to monitor the ROS. All the synthesized products were tested against ROS detection *in vivo* against the PC3 cancer cell lines. Probe **4.5** was shown to be high selectivity against cancer cell line PC3 and almost no selectivity for the normal fibroblast NIH3T3 cell line (**Figure 3**).

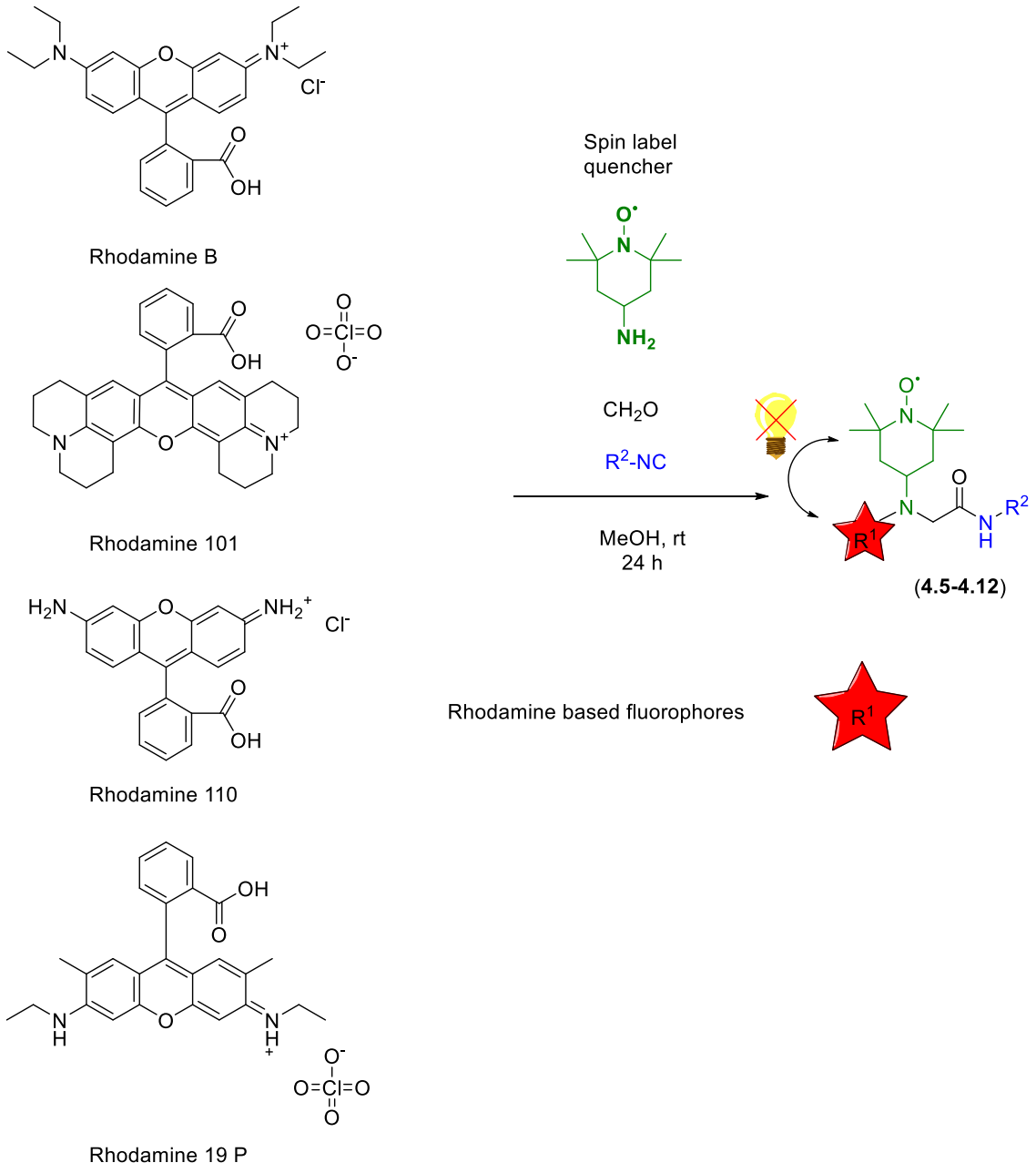

Scheme 11 Synthesis of spin-labelled probes **4.5-4.12**.

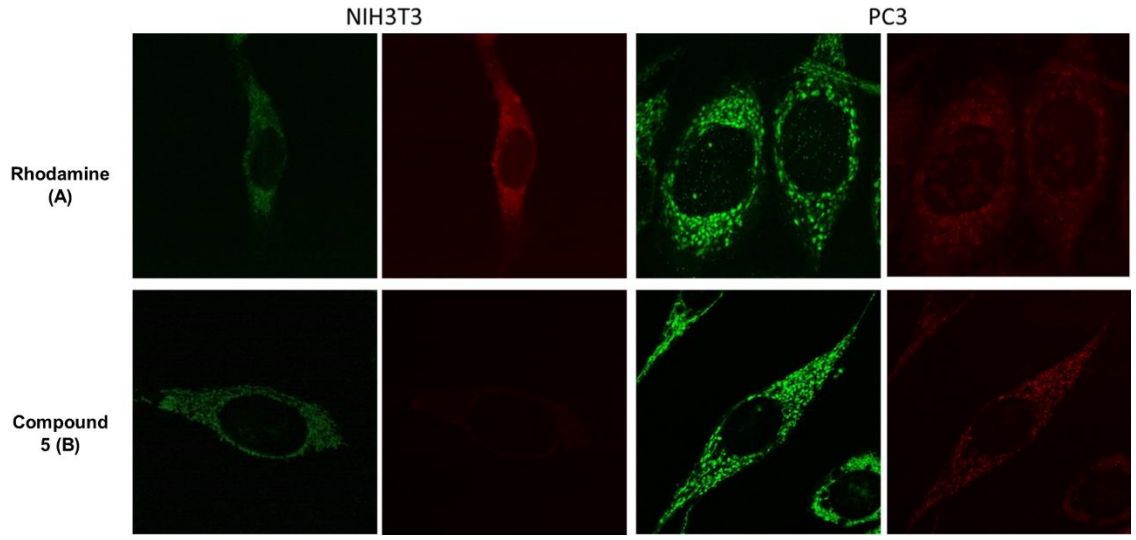

Figure 3 Fluorescence microphotographs: comparison of NIH3T3 and PC3 cells stained with MitoTracker Green™ (FITC channel) and rhodamine (Texas Red channel) or probe **4.5** (Texas Red channel).

These results provide further evidence of the potential of IMCRs as powerful synthetic tools toward detecting ROS in cancer cells.

Zusammenfassung und Ausblick

Die ortsspezifische Spinmarkierung (site-directed spin labeling, SDSL) ist zusammen mit der Elektronenspinresonanz (electron paramagnetic resonance, EPR) eine Methode, die in jüngster Zeit als experimentelle Technik in Biologie und Chemie eine breite Anwendung findet. Technische Weiterentwicklungen im EPR-Bereich und neuartige Labelingstrategien machen die Verwendung von EPR zunehmend attraktiver. Um Proteine, Peptide und pharmazeutische Wirkstoffe mittels EPR untersuchen zu können, ist die Einführung einer paramagnetischen Sonde an einer genau definierten Position im Molekül die Grundvoraussetzung. Daher wird diese Methode als "ortsspezifische Spinmarkierung" (SDSL) bezeichnet. Die häufigsten Nitroxide, die bei der Spinmarkierung von Proteinen verwendet werden, sind MTSL (**1.5**)- und 5-MSL (**1.16**)-Spinmarkierungen, die beide an das Vorhandensein von Cystein gekoppelt sind (**Schema 1**). Dabei kann entweder nativ vorhandenes Cystein für den Markierungsschritt verwendet werden oder Cystein, das durch eine gerichtete Mutagenese in das Zielprotein eingeführt wurde. Eine zweite Methode der ortsspezifischen Spinmarkierung ist der Einbau spezieller Aminosäuren wie. 4-Iod-L-Phenylalanine am Nonsense-Codon (z. B. Amber-Codon). Diese neue Technik ist als "ortsspezifische Spinmarkierung mittels Non-Sense-Supressor Methode" bekannt geworden (**Schema 2**). Eine weitere Spinmarkierung für Peptide ist 2,2,6,6-Tetramethyl-Piperidine-1-oxy-4-amino-4-carboxylat TOAC (**1.13**), das über ein einfaches Peptidkupplungsverfahren direkt in den Peptidkern eingeführt wird (**Schema 3**). Bisher sind keine Berichte über Mehrkomponentenreaktionen (Multicomponent Reactions, MCRs) bekannt geworden, bei denen der Einbau der Spinmarkierung in einem einzigen Schritt erfolgen kann. Damit wird eine effiziente Route für die Spinmarkierung bereitgestellt (**Schema 4**).

Ziel der vorliegenden Arbeit ist es daher, eine neue Methode für die SDSL-Strategie auf der Grundlage von Isonitril-Multikomponentenreaktionen (IMCR) zu entwickeln, um spinmarkierte Produkte mit biologischen Potential etwa als Antikrebsmittel oder als Sensor für reaktive Sauerstoffspezies zu erhalten.

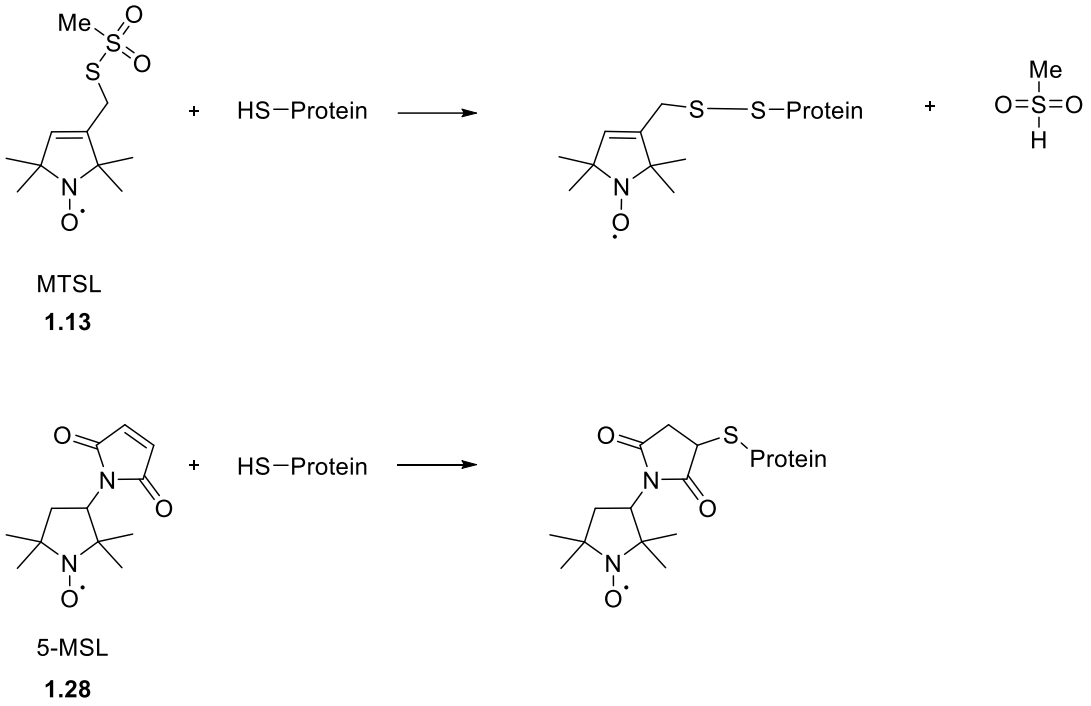

Schema 1 Spinmarkierung an Cysteinen durch A) MTSL und B) 5-MSL.

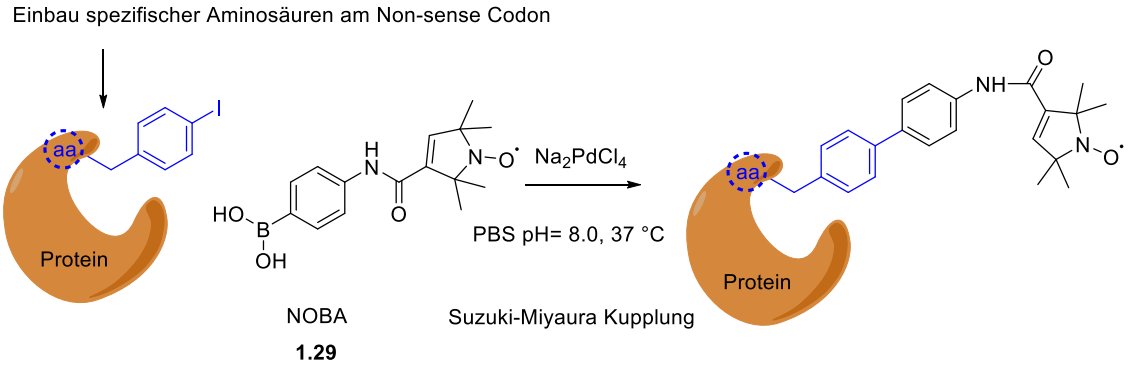

Schema 2 Ortsspezifische Spinmarkierung von Proteinen mittels der Non-sense Supressor Methodik.

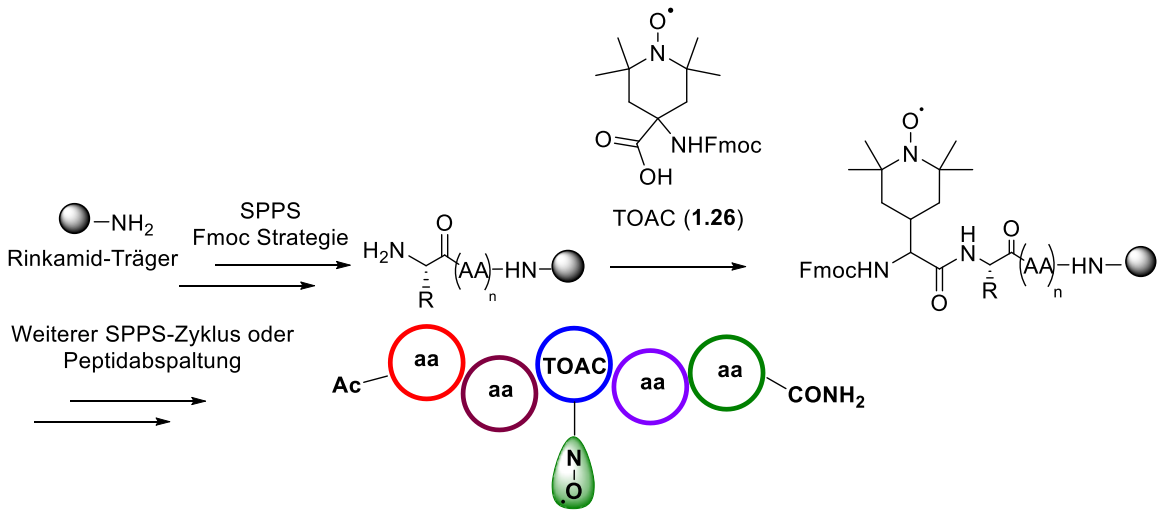

Schema 3 TOAC Spinmarkierung via Fmoc-Strategie der Festphasen-Peptidsynthese.

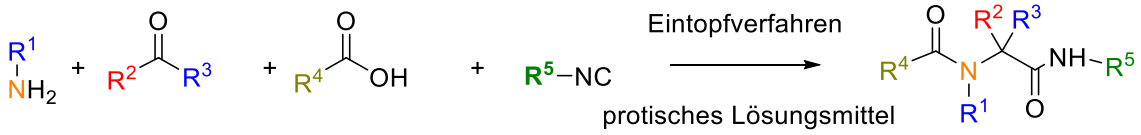

Spinlabel kann als Amin, Carbonsäure oder Isonitril eingeführt werden

Schema 4 Ugi-Multikomponentenreaktion.

Kapitel **1** der vorliegenden Arbeit beschreibt zunächst die Rolle von Nitroxiden als Spinmarkierungsreagenzien, ihre spektralen Eigenschaften und Faktoren, die ihre Stabilität beeinflussen. Zudem wird ein Überblick für wichtige Anwendungen in der biologischen und pharmazeutischen Forschung gegeben. Außerdem werden die gängigsten Methoden zur Einführung des Spinlabels beschrieben.

In Kapitel **2** wird die Isonitrol-vermittelten Mehrkomponentenreaktion (IMCR) zur Erzeugung einer Bibliothek von spinmarkierten Verbindungen vorgestellt. Es konnte gezeigt werden, dass die hohe Flexibilität dieses Ansatzes es erlaubt, verschiedene Peptide, Peptid-Peptoid-Chimäre und Diketopiperazine mit Spin-Label-Radikalen, die an verschiedenen Positionen gebunden sind, chemisch darzustellen. Darüberhinaus konnte bewiesen werden, dass die Stabilität der Spinmarkierung unter sauren Bedingungen nicht beeinflusst wird, wodurch auch Post-Ugi-Modifikationen möglich sind (**Schema 5**). Alle synthetisierten Proben wurden quantitativ EPR-spektroskopisch analysiert, dabei konnten kleinste Änderungen der Molekülstrukturen erkannt werden (**Schema 6** und **Schema 7**).

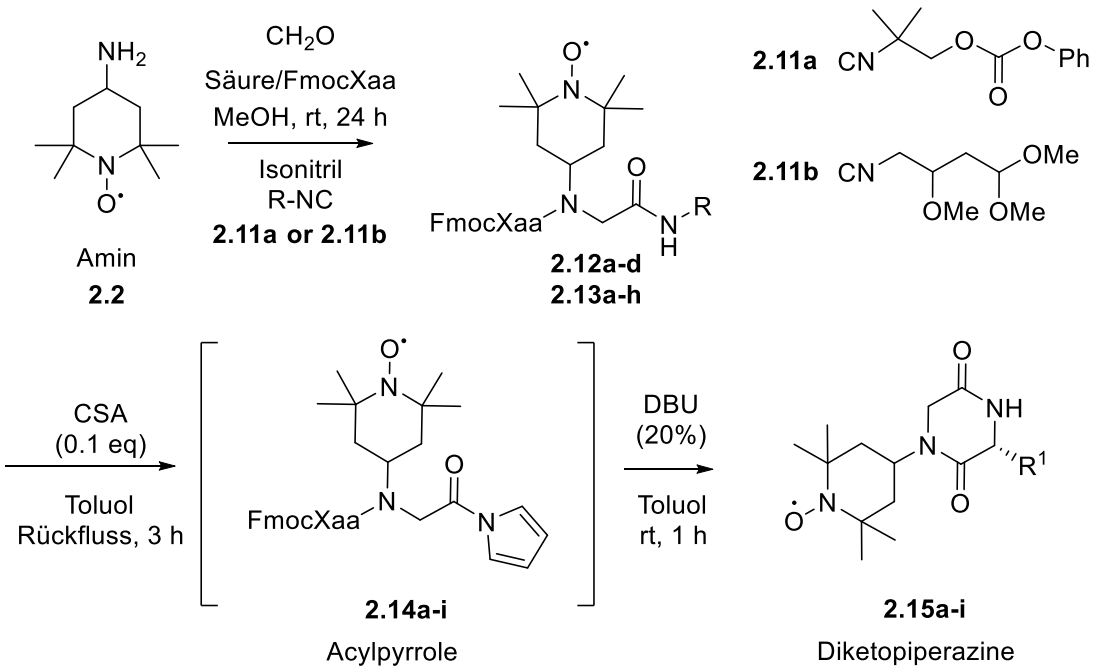

Schema 5 Diketopiperazine mittels Ugi-4CR/Entschützung + Aktivierung/Zyklisierungsstrategie (UDAC).

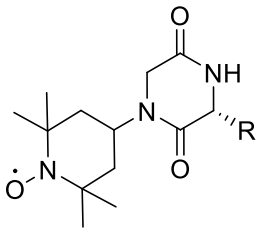

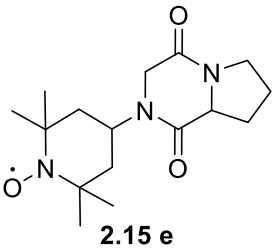

2.15 e

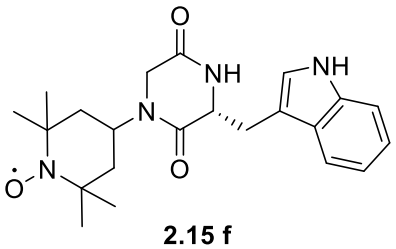

2.15 f

2.15 a, R = isopropyl
2.15 b, R = Ph
2.15 c, R = sec-butyl
2.15 d, R = 2-methylpropyl
2.15 g, R = Me
2.15 h, R = H

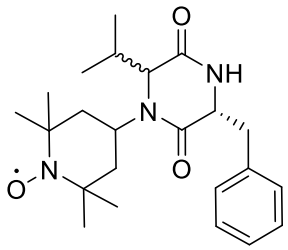

2.15 i

Schema 6 Strukturen der spinmarkierten Diketopiperazine **2.15 (a-i)**.

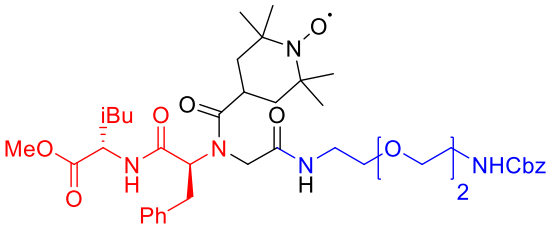

2.16

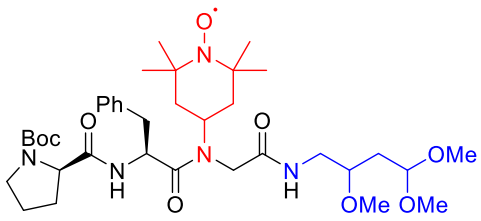

2.17

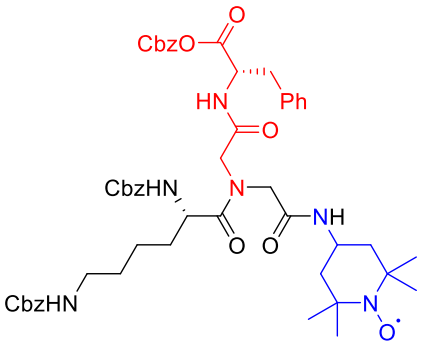

2.18

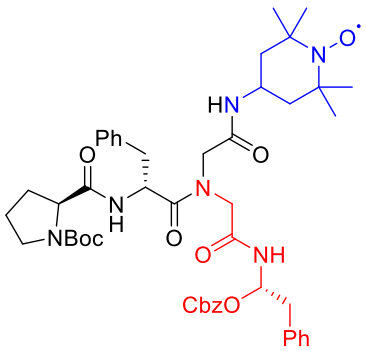

2.19

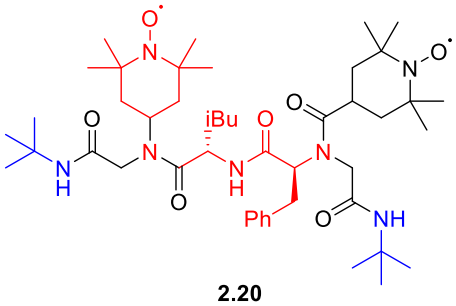

2.20

Schema 7 Strukturen spinmarkierter Peptid-Peptoidchimäre **2.16-2.20**.

Kapitel **3** befasst sich mit der chemisch-synthetischen Herstellung spinmarkierter Naturstoffderivate ausgehend von einer Isonitril-vermittelten Mehrkomponentenreaktion (IMCR). Als Ausgangsstoffe dienten die Naturstoffe Betulin-, Fusidin- und Cholsäure **3.1**,**3.4**,**3.5**. Die spinmarkierten Verbindungen (**3.7**-**3.12**) (**Schema 8**) wurden sowohl gegen PC3- als auch gegen HT-29-Krebszelllinien getestet (**Abbildung 1**). Überraschenderweise zeigte die Fusidinsäure-spinmarkierten Produkte **3.9** und **3.10** eine bemerkenswerte Aktivität gegenüber den genannten Krebszelllinien (**Schema 9**). Die post-Ugi-Modifikation wurde an Verbindung **3.17** durchgeführt (**Schema 10**). Mit der synthetisierten fluoreszierenden Verbindung **3.19** wurde das s.g. Mitochondrientargeting durchgeführt (**Abbildung 2**).

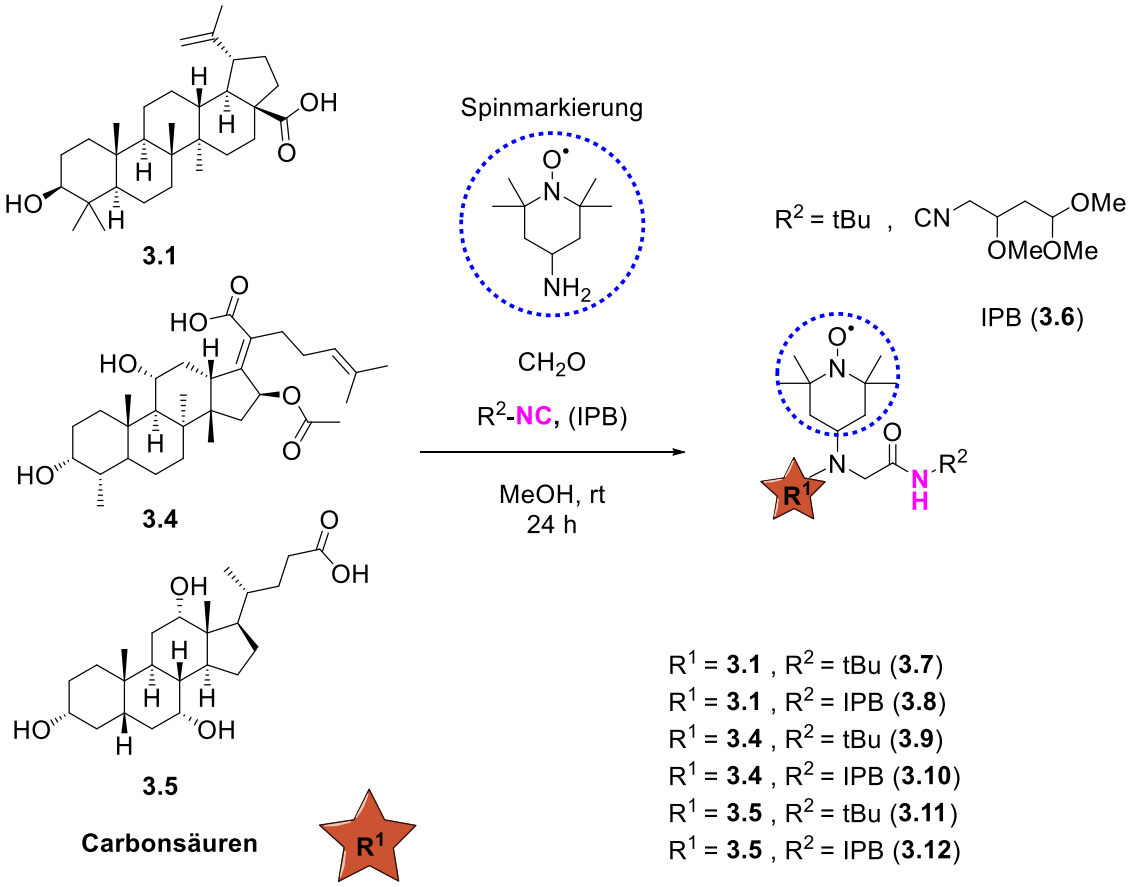

Schema 8 Synthese von Betulin-, Fusidin- und Cholsäure mit Spinlabeln.

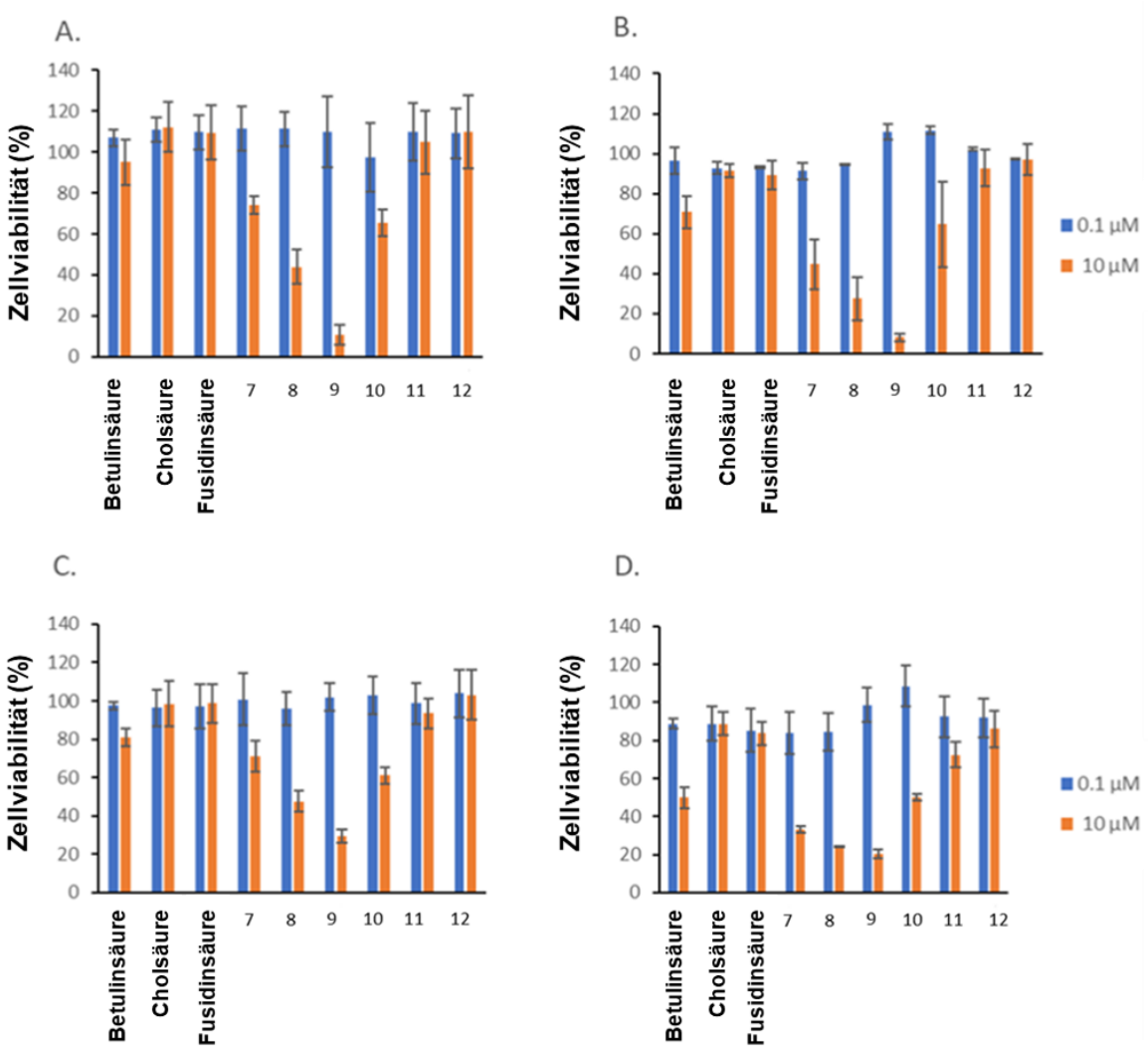

Abbildung 1 Zellviabilität der Zelllinien HT-29 (A, B) und PC3 (C, D) nach Behandlung mit den untersuchten Verbindungen für 48 h. Die Zellviabilität wurde mit CV- (für A, C) und MTT-Tests (für B, D) bestimmt.

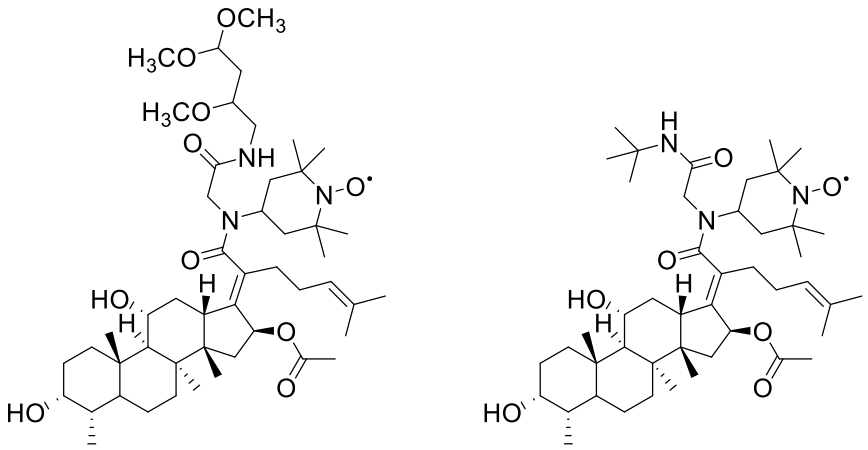

3.10 **3.9**

Schema 9 Derivate **3.9** and **3.10**.

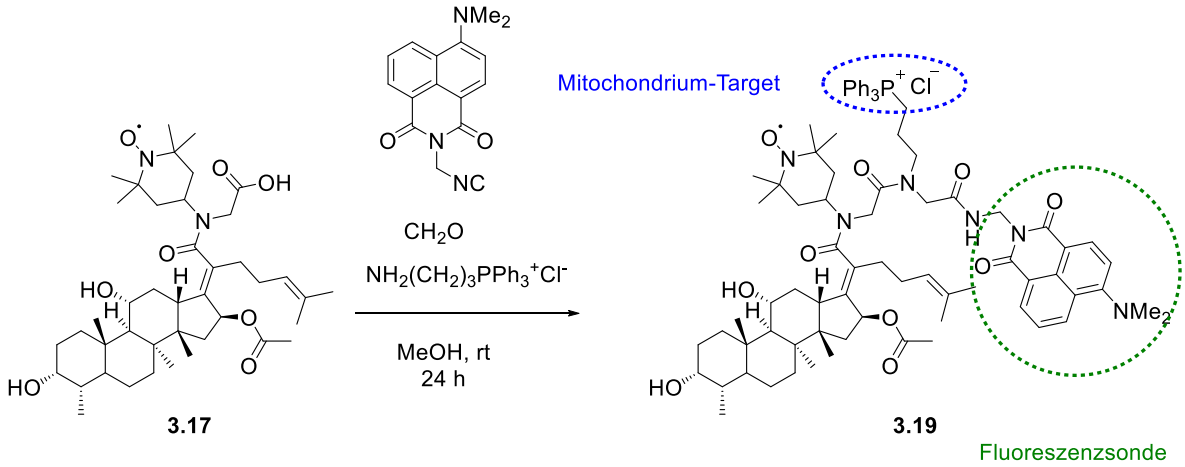

Schema 10 Post-Ugi-Modifikation von **3.17**.

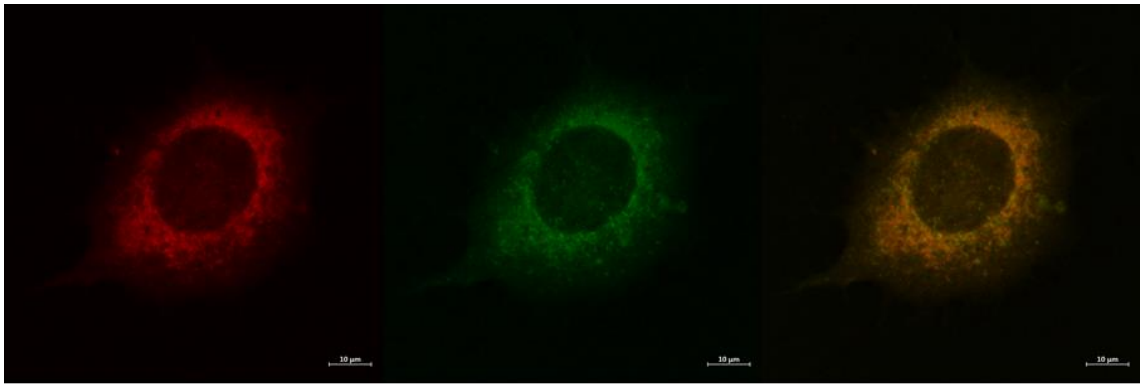

MitoTracker Deep Red | Verbindung **3.19** | Überlagerung

Abbildung 2 Fluoreszenzaufnahmen von **3.19**.

In Kapitel **4** wird die Entwicklung einer neuartigen Rhodamin-Nitroxid-Sonde zum Nachweis von reaktiven Sauerstoffspezies (ROS) in Mitochondrien beschrieben. Der Ansatz nutzt eine Isonitril-vermittelte Mehrkomponentenreaktion (IMCR) zur Funktionalisierung des kommerziell erhältlichen Rhodamins, einer weit verbreiteten Mitochondrien-Fluoreszenzsonde (**Schema 11**). Das vorgeschlagene Nitroxidradikal wirkt als profluoreszierende Sonde; bei Wechselwirkung mit reaktiven Sauerstoffspezies wird das Nitroxidradikal zum entsprechenden Hydroxylamin reduziert, was zu einem stark fluoreszierenden Analyten führt. Damit können reaktive Sauerstoffspezies effektiv detektiert werden. Alle synthetisch hergestellten Sonden wurden *in vivo* für die Detektion von ROS in PC3-Krebszelllinien getestet. Es konnte gezeigt werden, dass Sonde (**4.5**) eine hohe Selektivität gegenüber PC3 und nahezu keine Selektivität gegenüber der normalen Fibroblasten-NIH3T3-Zelllinie aufweist (**Abbildung 3**).

Diese Ergebnisse zeigen das große Potenzial von IMCRs als leistungsstarke Synthesewerkzeuge für Sonden, die zum Nachweis von ROS in Krebszellen eingesetzt werden können.

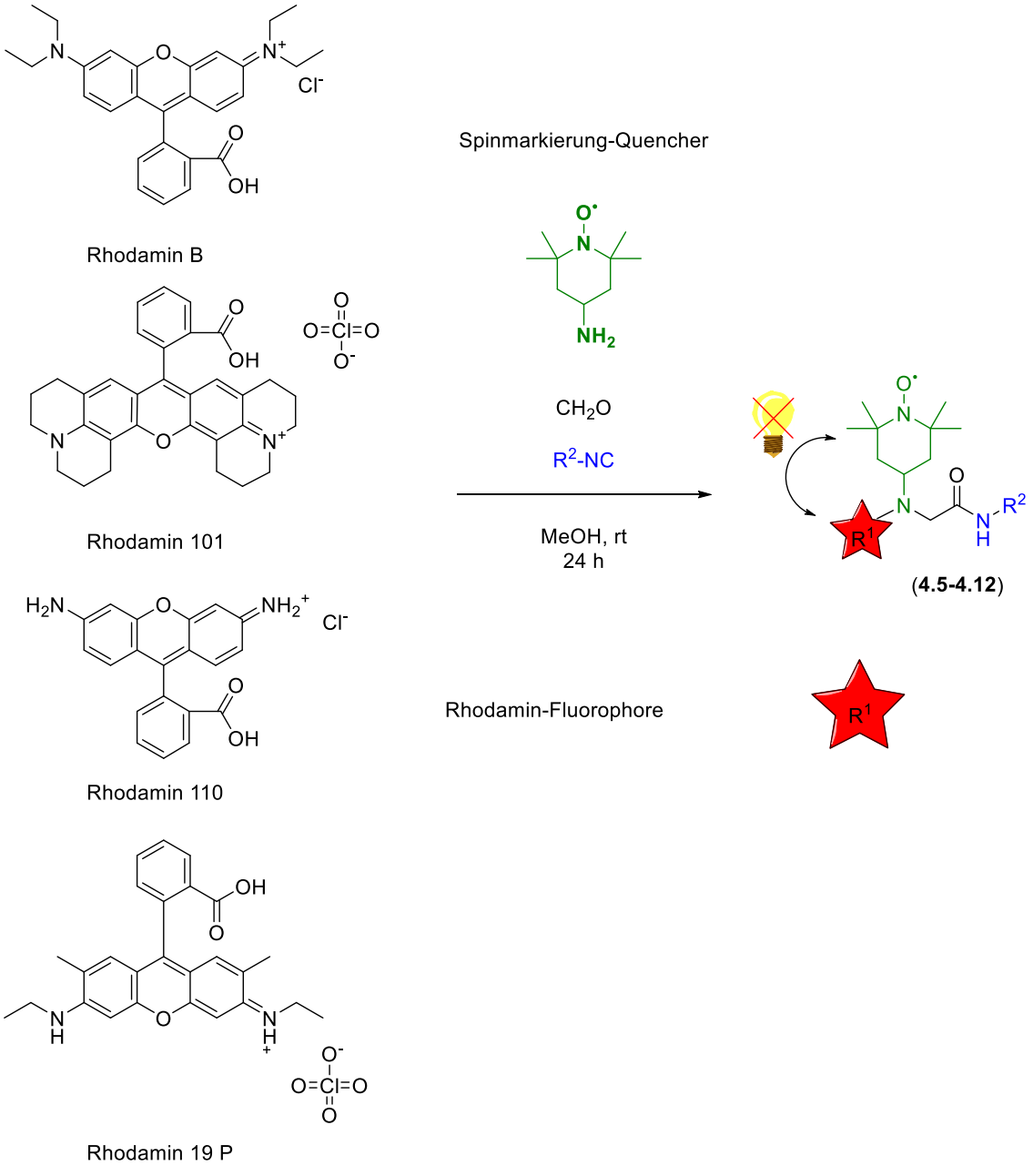

Schema 11 Synthese von Fluoreszenzsonden **4.5**-**4.12**.

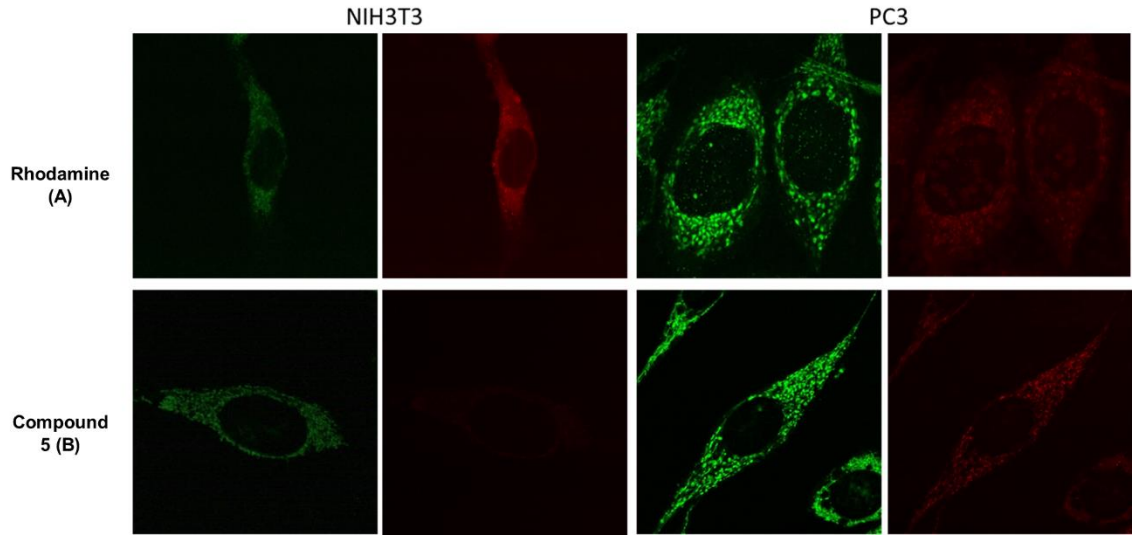

Abbildung 3 Mikroskopische Fluoreszenzaufnahmen: Vergleich von NIH3T3 und PC3-Zellen, die mit MitoTracker Green (FITC-Kanal), Rhodamin (Texas-Rot-Kanal) und Sonde **4.5** (Texas-Rot-Kanal) detektiert wurden.

Attachments

Tabel S1- Simulated CW EPR spectra details of selected compounds at 9.4 GHz frequency (Chapter 2).

Figure S1- Comparison between synthesized and commercial 4-amino TEMPO **2**-in water (Chapter 2).

Figure S2- Room temperature CW-EPR spectra of TEMPO derivatives (in water) used in this research; 4-NH_2-TEMPO **2**, HCO_2-TEMPO **5** and NC-TEMPO **6** (Chapter 2).

Figure S3- Experimental and simulated CW-EPR spectrum of DKP **15b** in acetonitrile solvent (Chapter 2).

Figure S4- RP-HPLC chromatogram of compound **7** (Chapter 3).

Figure S5- ^{1}H NMR (600 MHz, $CDCl_3$) spectrum of compound **7** (Chapter 3).

Figure S6- ^{13}C NMR (100 MHz, DMSO-d_6) spectrum of compound **7** (Chapter 3).

Figure S7- RP-HPLC chromatogram of compound **8** (Chapter 3).

Figure S8- ^{1}H NMR (600 MHz, $CDCl_3$) spectrum of compound **8** (Chapter 3).

Figure S9- ^{13}C NMR (100 MHz, DMSO-d_6) spectrum of compound **8** (Chapter 3).

Figure S10- RP-HPLC chromatogram spectrum of compound **9** (Chapter 3).

Figure S11- ^{1}H NMR (600 MHz, $CDCl_3$) spectrum of compound **9** (Chapter 3).

Figure S12- ^{13}C NMR (151 MHz, $CDCl_3$) spectrum of compound **9** (Chapter 3).

Figure S13- RP-HPLC chromatogram spectrum of compound **10** (Chapter 3).

Figure S14- ^{1}H NMR (600 MHz, $CDCl_3$) spectrum of compound **10** (Chapter 3).

Figure S15- ^{13}C NMR (151 MHz, $CDCl_3$) spectrum of compound **10** (Chapter 3).

Figure S16- RP-HPLC chromatogram spectrum of compound **11** (Chapter 3).

Figure S17- ^{1}H NMR (600 MHz, $CDCl_3$) spectrum of compound **11** (Chapter 3).

Figure S18- ^{13}C NMR (151 MHz, $CDCl_3$) spectrum of compound **11** (Chapter 3).

Figure S19- RP-HPLC chromatogram spectrum of compound **12** (Chapter 3).

Figure S20- ^{1}H NMR (600 MHz, $CDCl_3$) spectrum of compound **12** (Chapter 3).

Tabel S. 1 Simulated CW EPR spectra details of selected compounds at 9.4 GHz frequency* (Chapter 2).

Compound Nr. (as in text)	Line width (mT)	Hyperfine tensor A (MHz)	Correlation time (τc /s)
UGI **12b** (acetonitrile)	0.08,0.4	21.5,21.8,90.8	3e-11
DKP **15a** (acetonitrile)	0.08,0.5	20.5,20.8,90.8	3e-12
DKP **15a** (water)	0.2,0.04	28.0,24.0,91.5	9e-11
DKP **15b** (acetonitrile)	0.08,0.48	20.5,22.2,90.3	5e-12
Peptide **16** (water)	0.19,0.05	24.0,26.0,92.5	1.87e-10
Peptide **17** (water)	0.19,0.05	24.0,26.0,93.0	2.67e-10
Peptide **18** (methanol)	0.08,0.4	21.0,24.0,91.8	1.47e-10
Peptide **19** (water)	0.19,0.05	24.0,26.0,92.5	4.6e-11

*For all simulation the g tensor [2.008 2.006 2.0020] with an isotropic value of 2.005 is used. Line width is a combination of two Gaussian and Lorentzian line shapes.

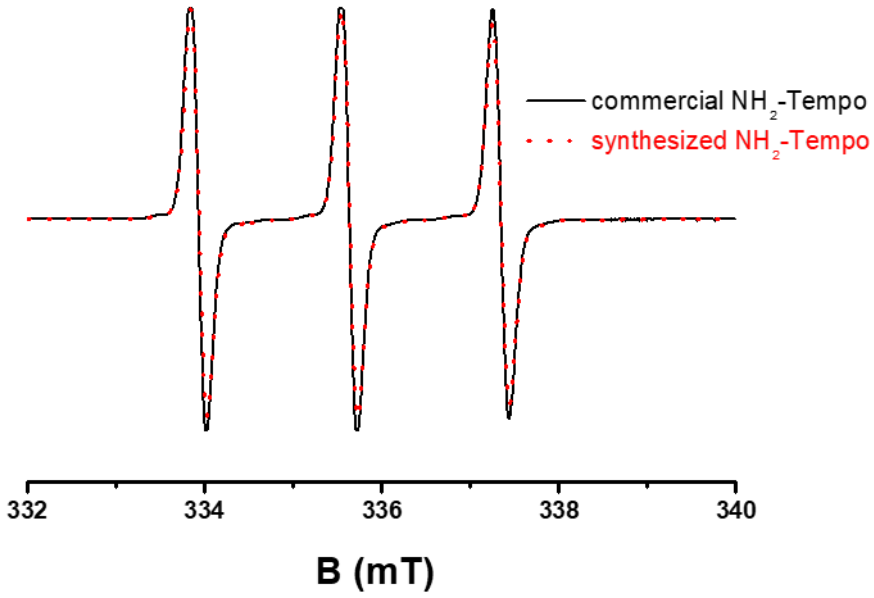

Figure S. 1 Comparison between synthesized and commercial 4-amino TEMPO **2**-in water (Chapter 2).

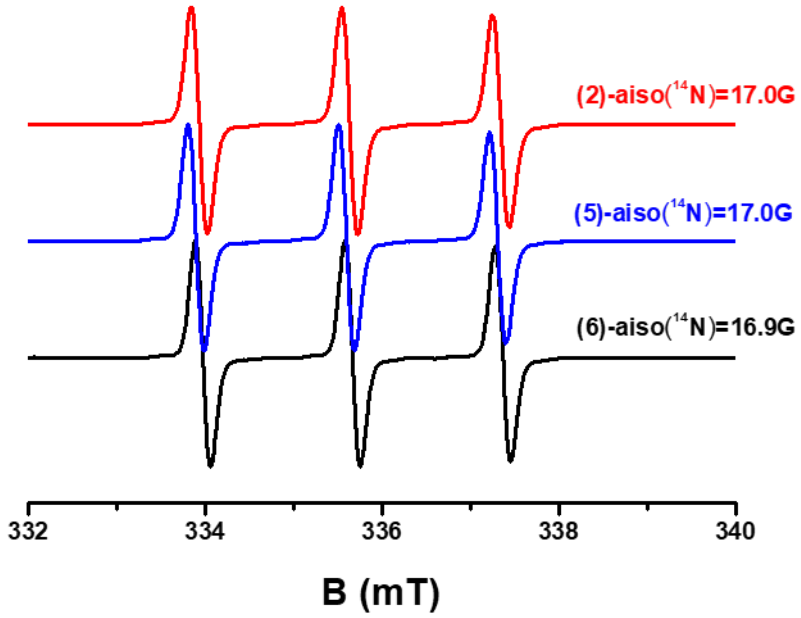

Figure S. 2 Room temperature CW-EPR spectra of TEMPO derivatives (in water) used in this research; 4-NH2-TEMPO **2**, HCO2-TEMPO **5** and NC-TEMPO **6** (Chapter 2).

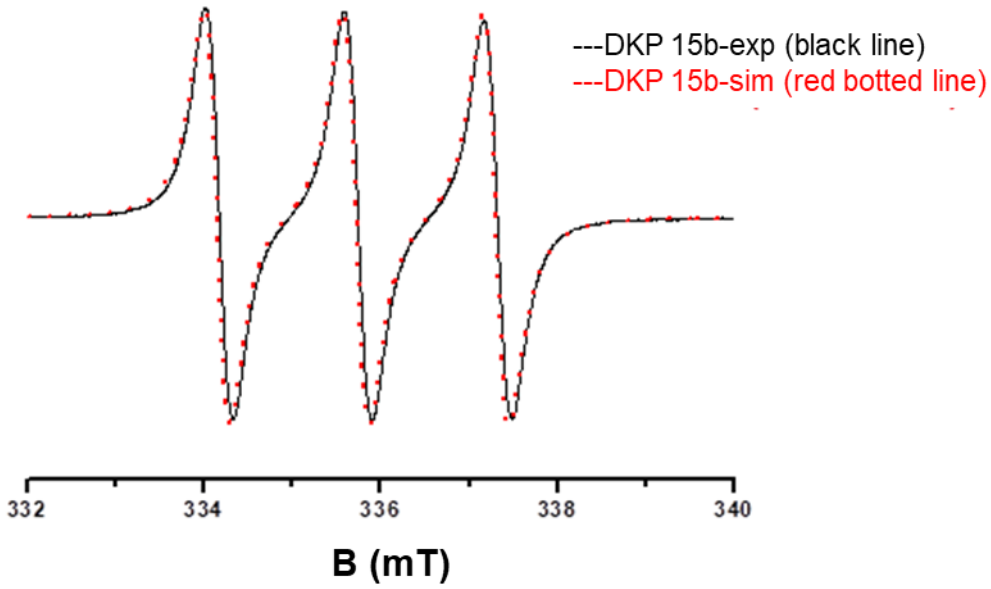

Figure S. 3 Experimental and simulated CW-EPR spectrum of DKP **15b** in acetonitrile solvent (Chapter 2).

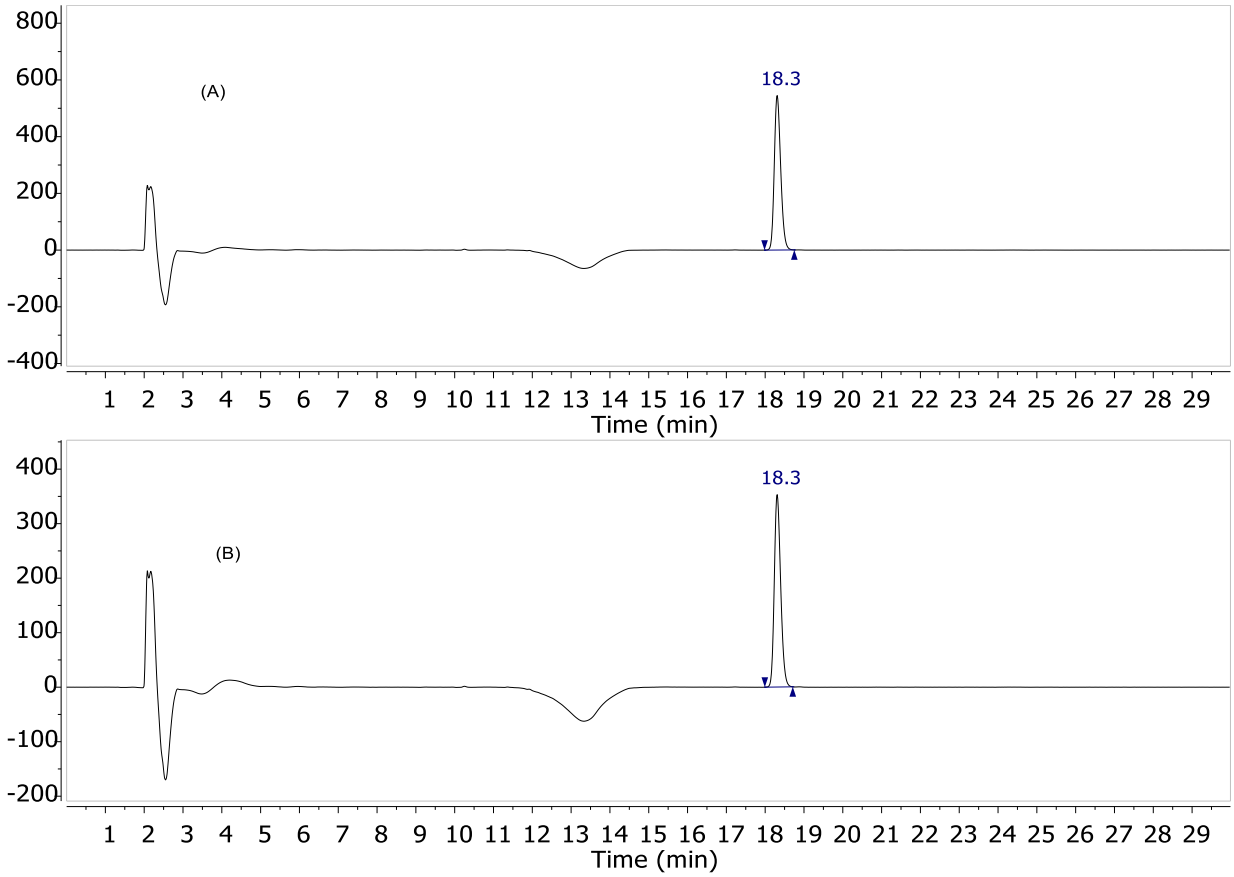

Figure S. 4 RP-HPLC chromatogram spectrum of compound **7** a) 210 nm, b) 215 nm (Chapter 3).

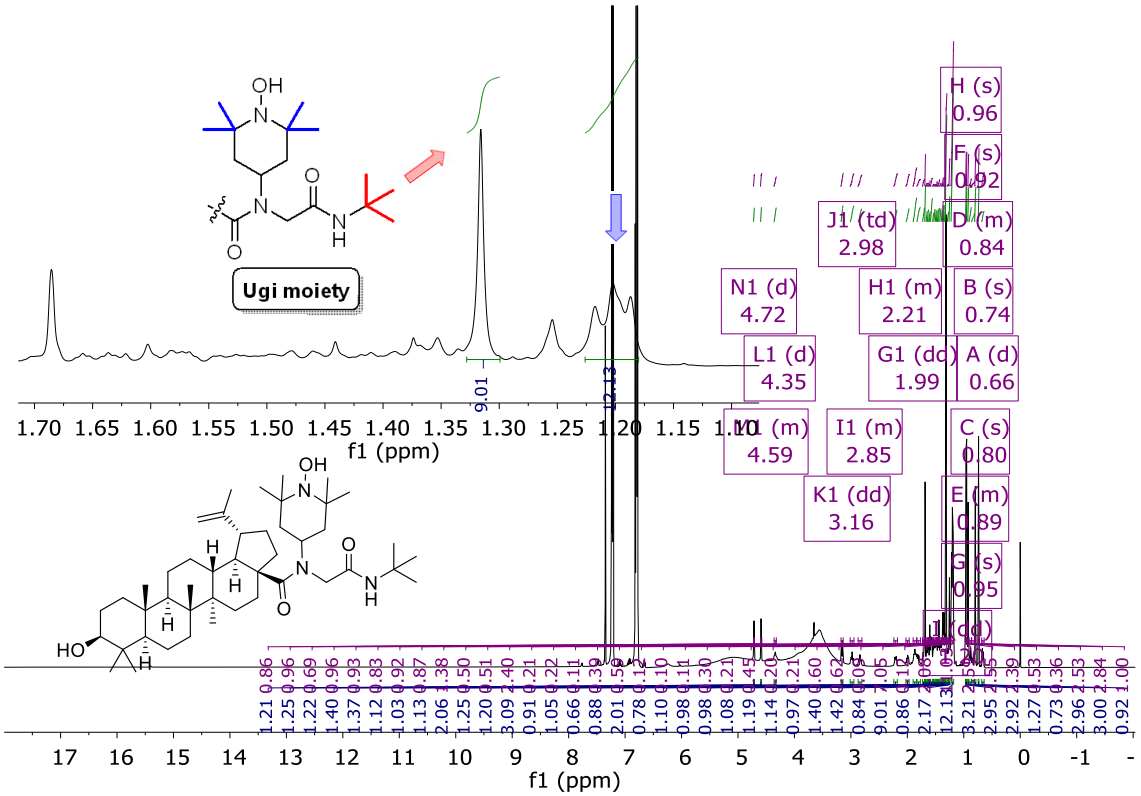

Figure S. 5 ^{1}H NMR (600 MHz, $CDCl_3$) spectrum of compound **7** (Chapter 3).

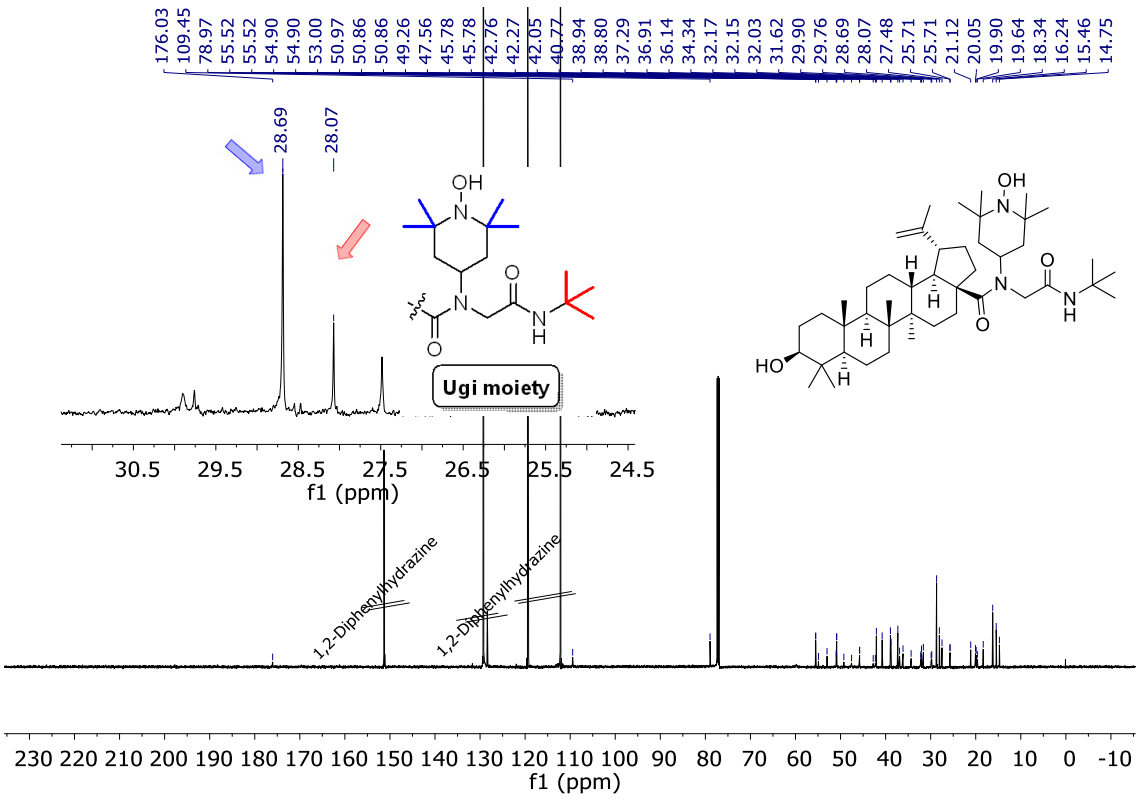

Figure S. 6 ^{13}C NMR (151 MHz, $CDCl_3$) spectrum of compound **7** (Chapter 3).

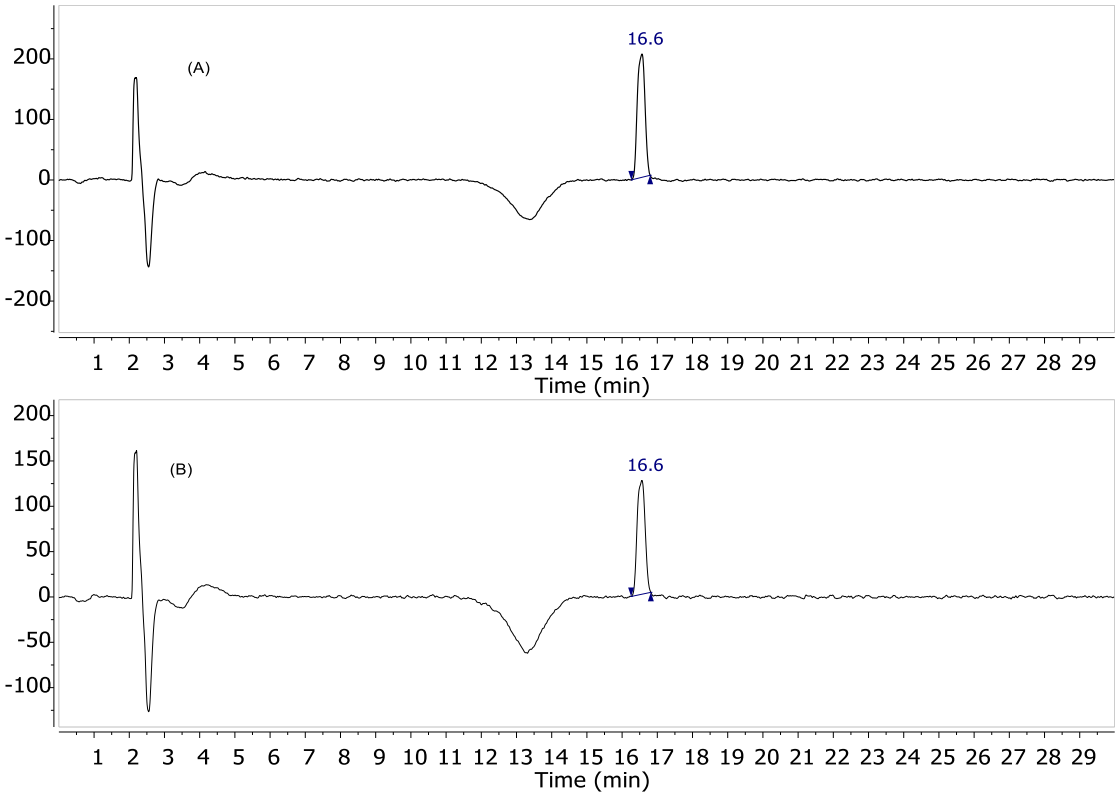

Figure S. 7 RP-HPLC chromatogram spectrum of compound **8** at a) 210 nm, b) 215 nm (Chapter 3).

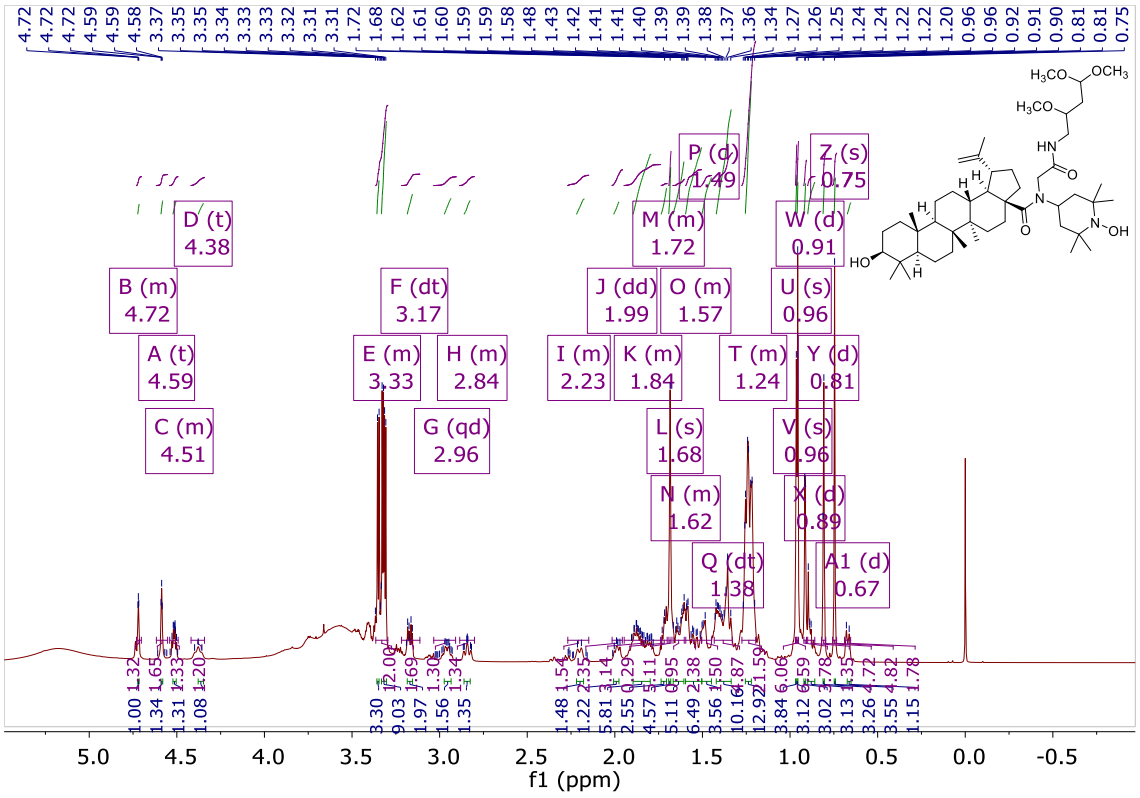

Figure S. 8 ^{1}H NMR (600 MHz, $CDCl_3$) spectrum of compound **8** (Chapter 3).

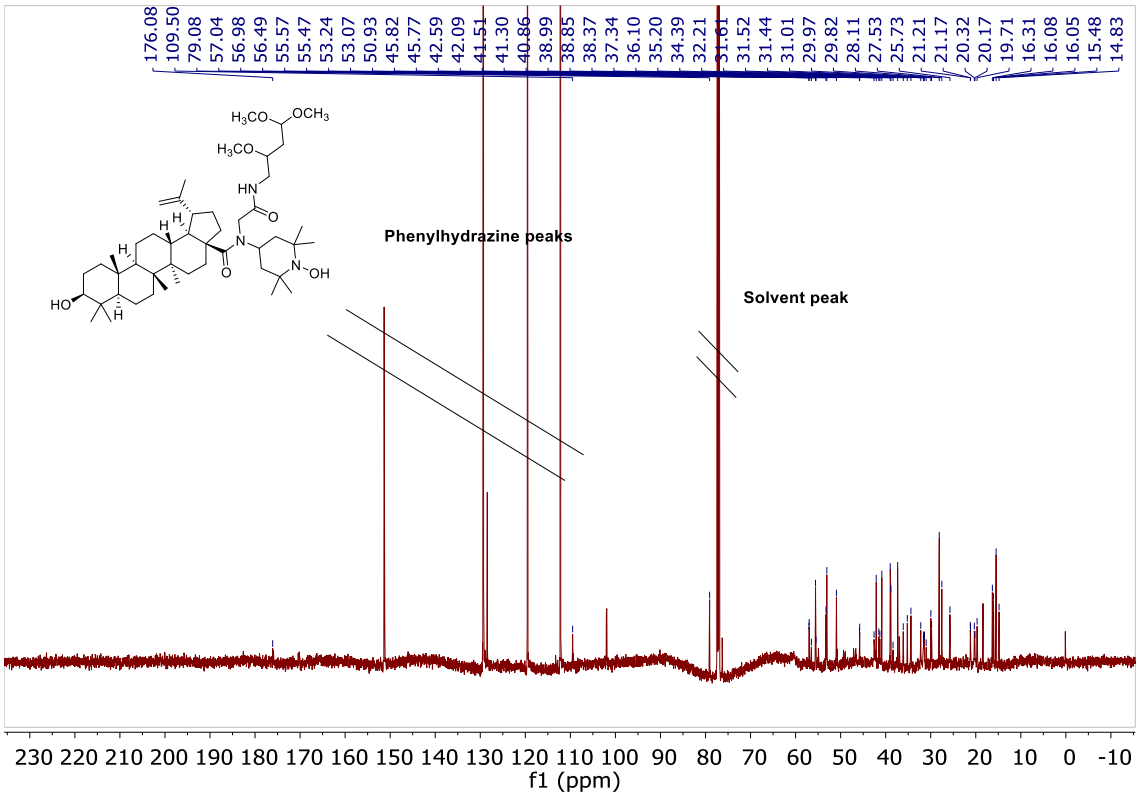

Figure S. 9 ^{13}C NMR (151 MHz, $CDCl_3$) spectrum of compound **8** (Chapter 3).

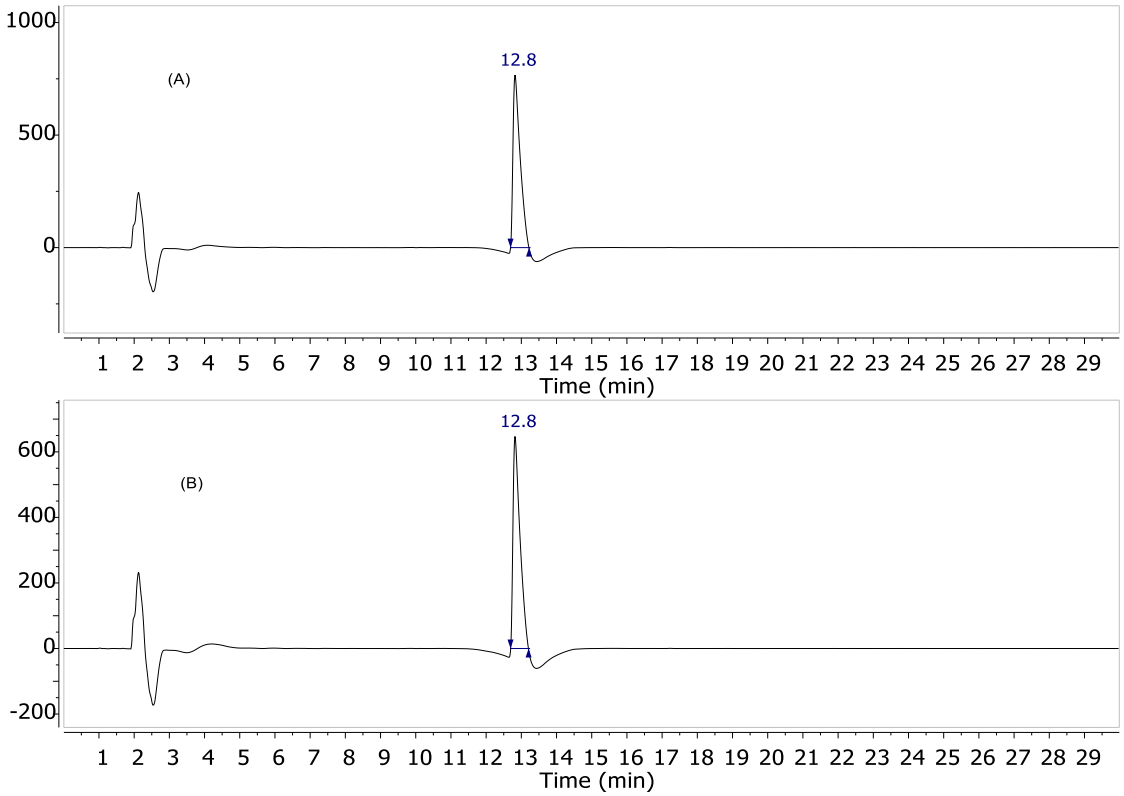

Figure S. 10 RP-HPLC chromatogram spectrum of compound **9** at 210 nm, 215 nm (Chapter 3).

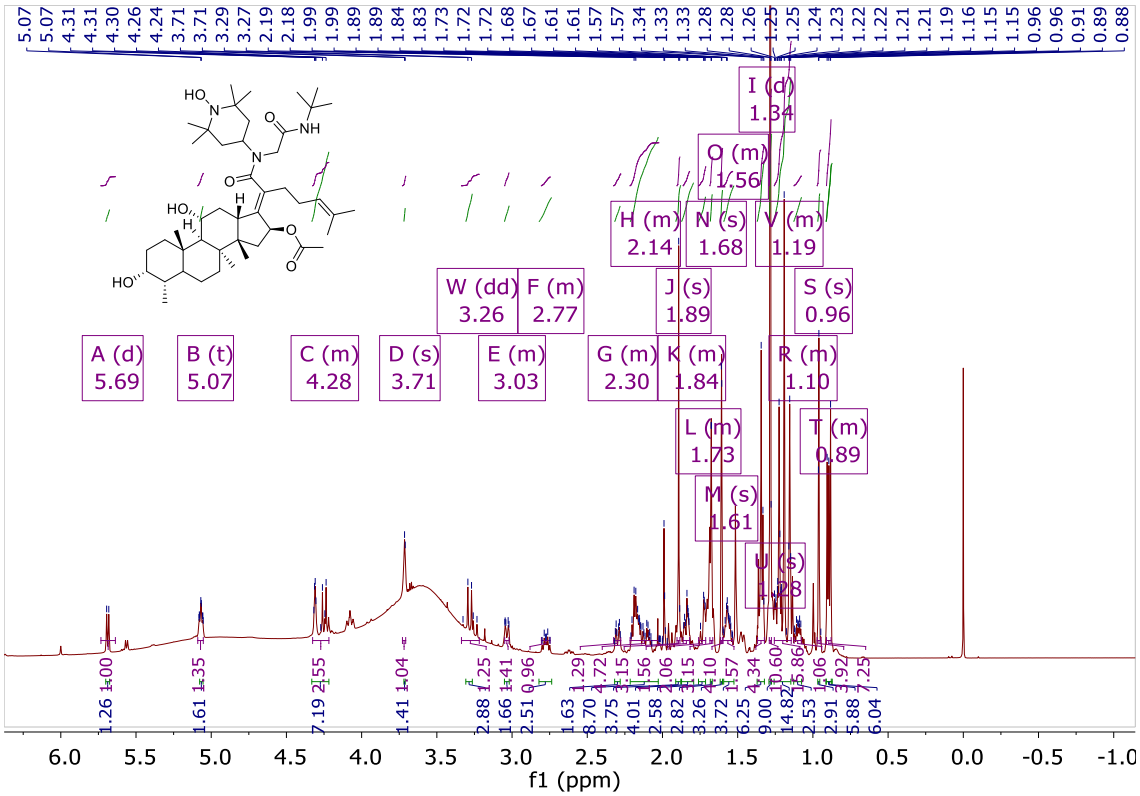

Figure S. 11 ^{1}H NMR (600 MHz, $CDCl_3$) spectrum of compound **9** (Chapter 3).

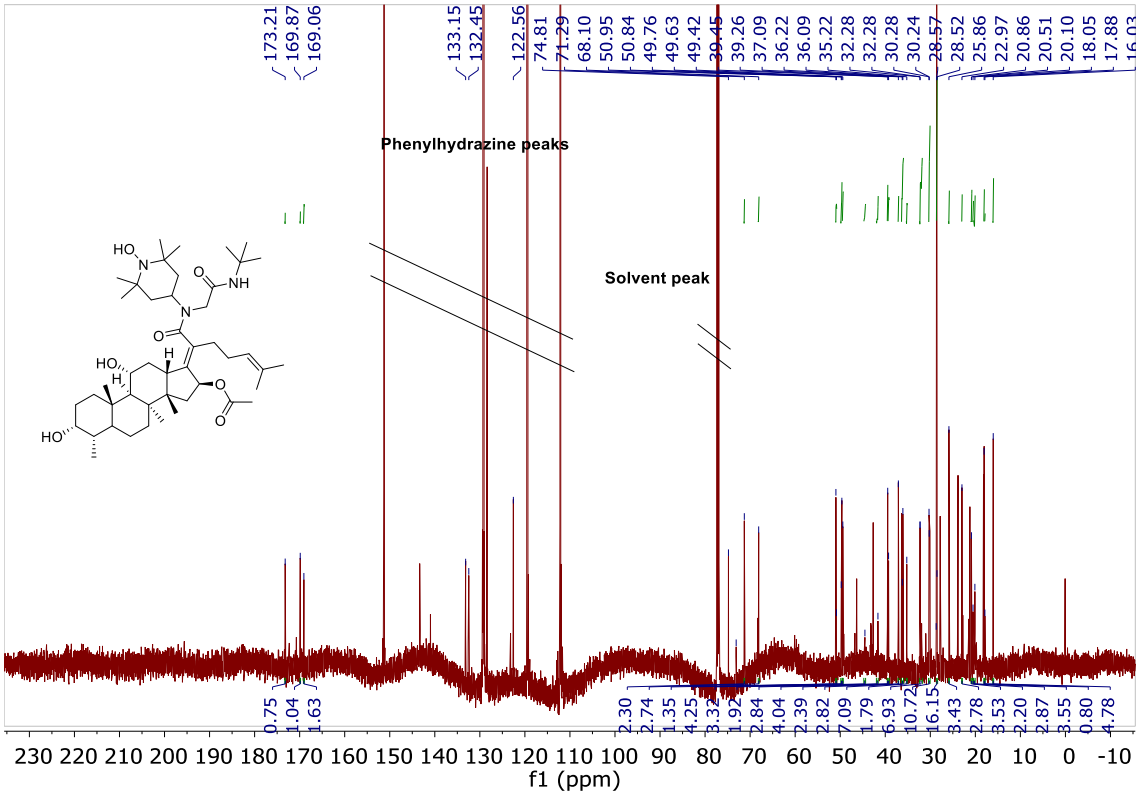

Figure S. 12 ^{13}C NMR (151 MHz, $CDCl_3$) spectrum of compound **9** (Chapter 3).

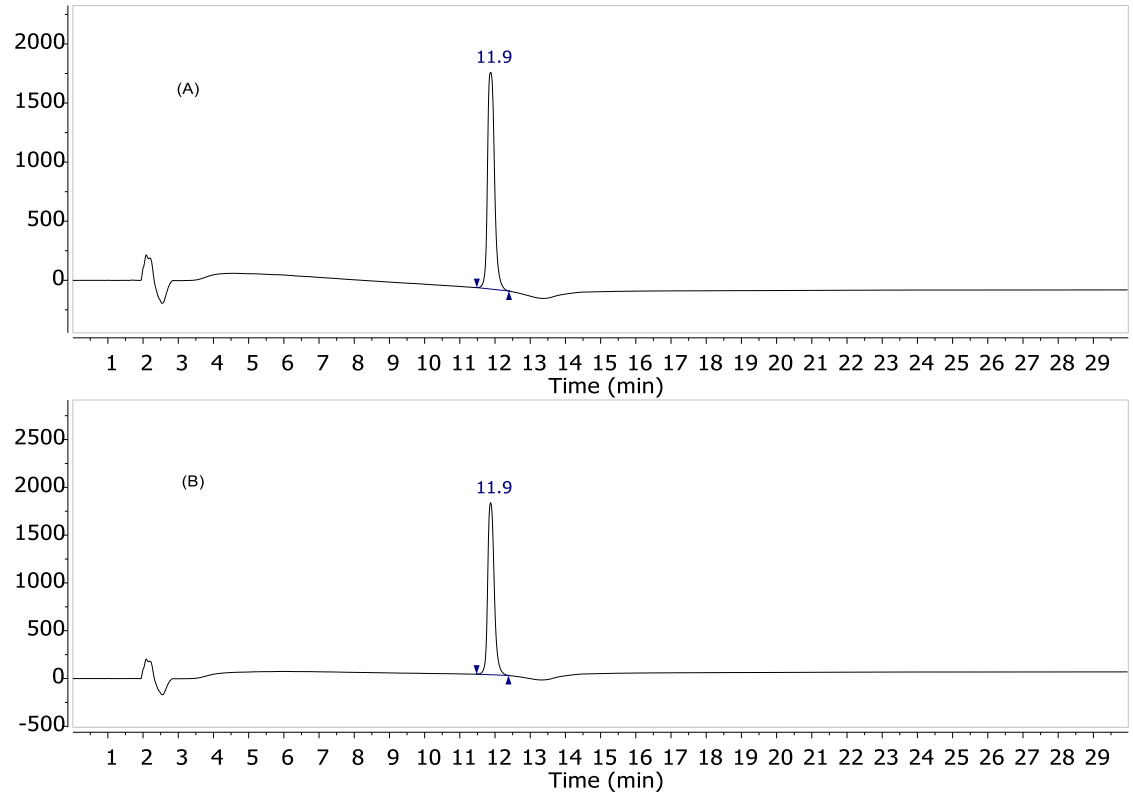

Figure S. 13 RP-HPLC chromatogram spectrum of compound **10** a) 210 nm, b) 215 nm (Chapter 3).

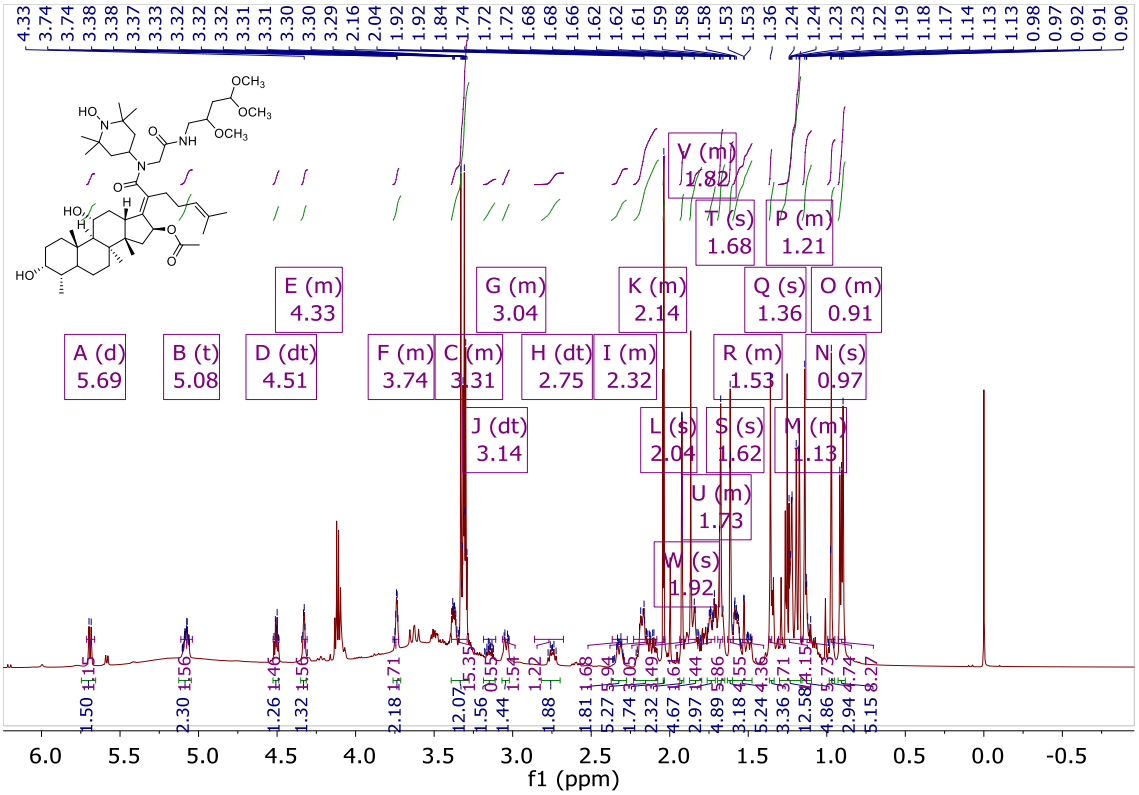

Figure S. 14 ^{1}H NMR (600 MHz, $CDCl_3$) spectrum of compound **10** (Chapter 3).

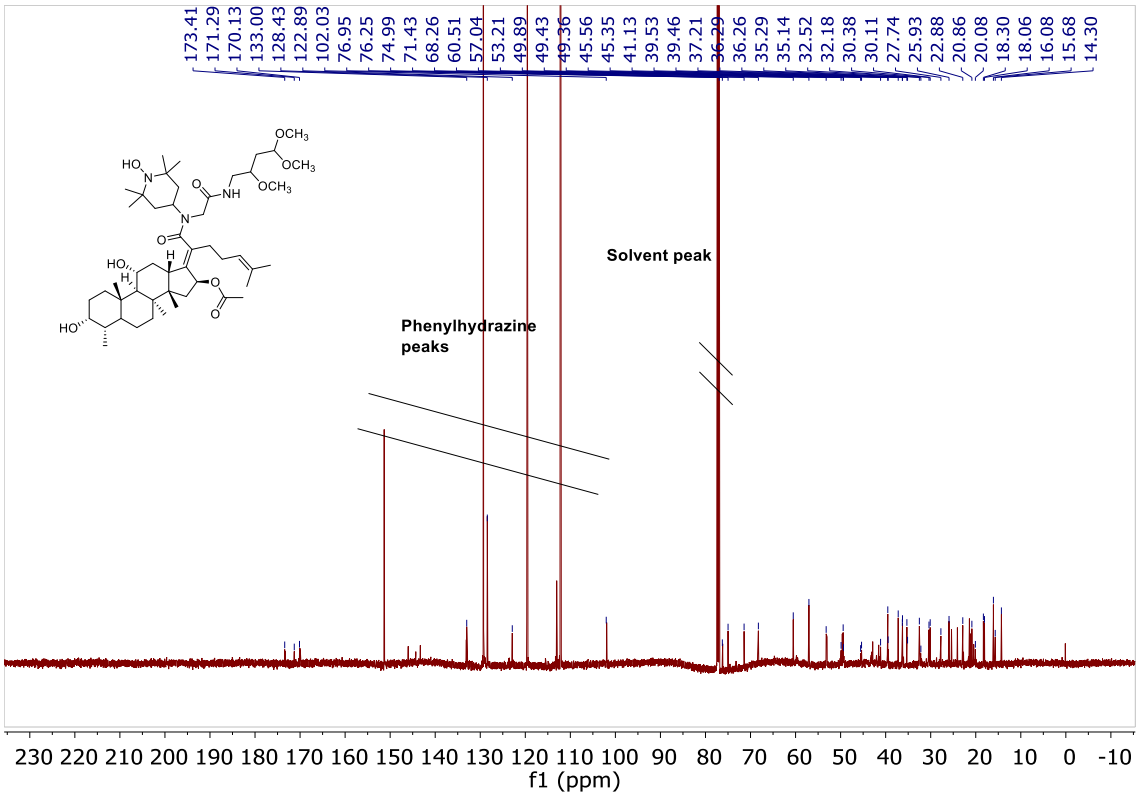

Figure S. 15 ^{13}C NMR (151 MHz, $CDCl_3$) spectrum of compound **10** (Chapter 3).

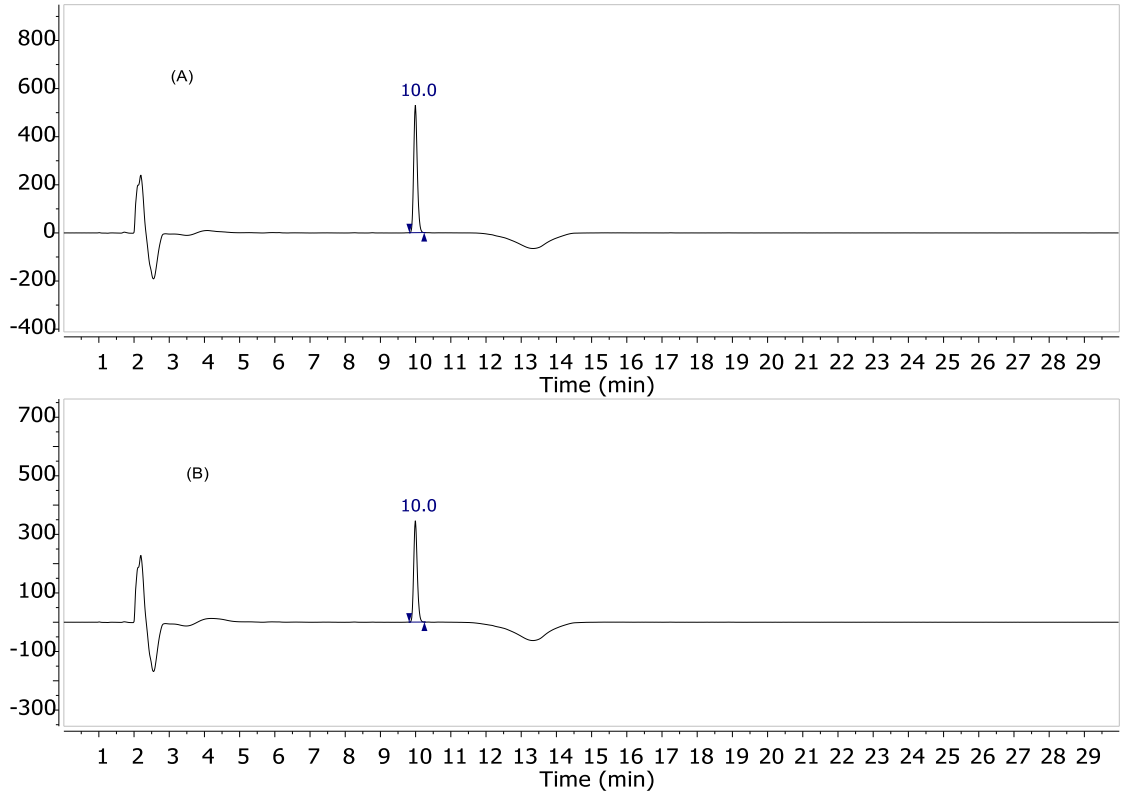

Figure S. 16 RP-HPLC chromatogram spectrum of compound **11** a) 210 nm, b) 215 nm (Chapter 3).

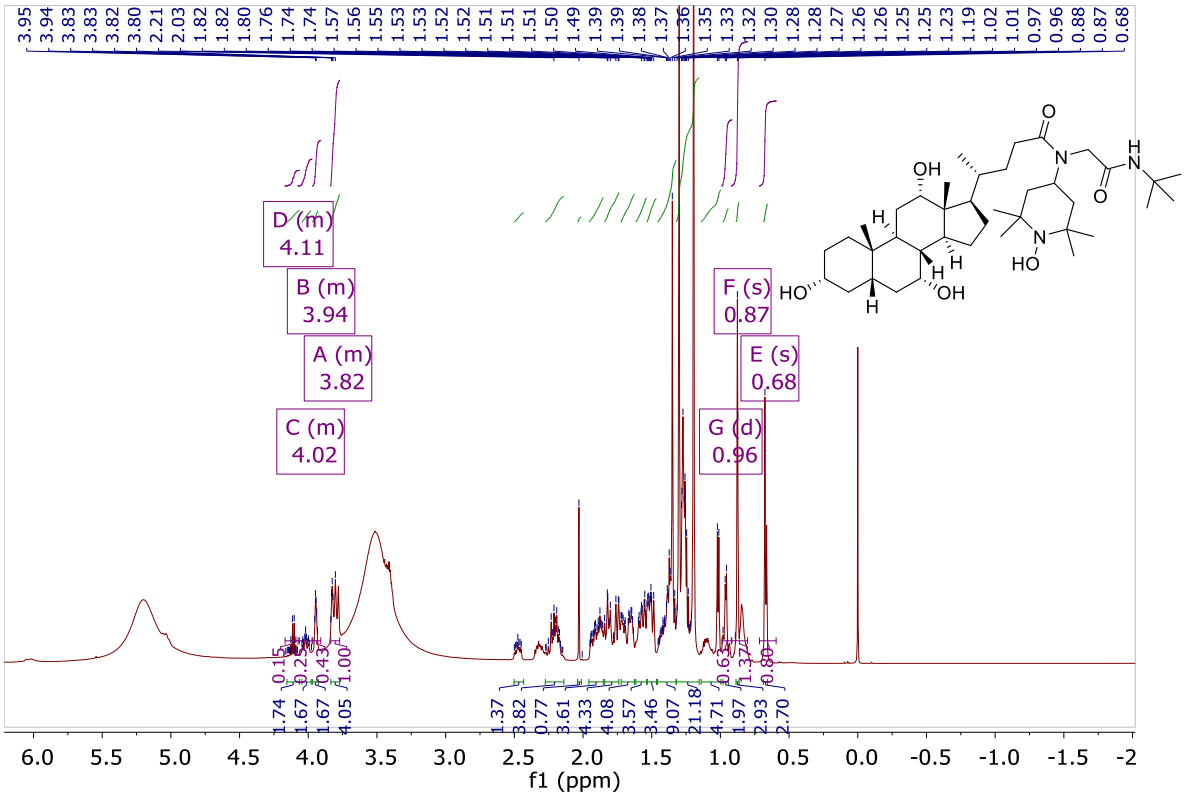

Figure S. 17 ^{1}H NMR (600 MHz, $CDCl_3$) spectrum of compound **11** (Chapter 3).

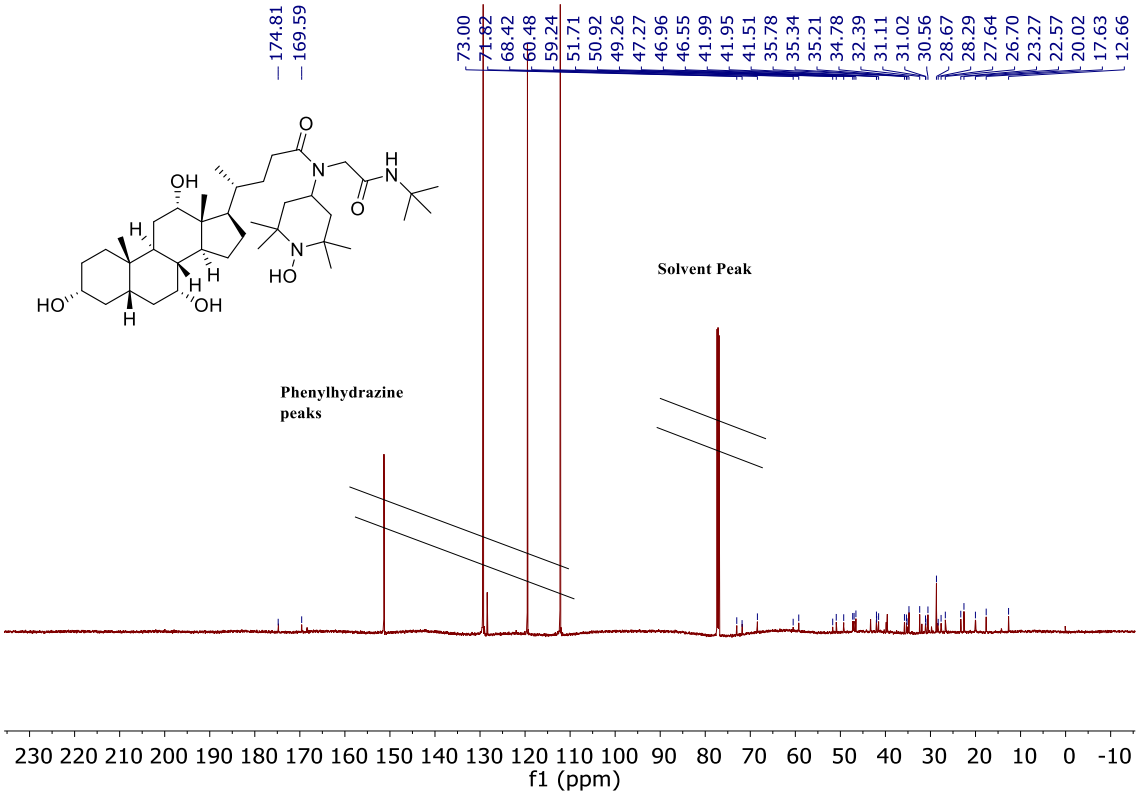

Figure S. 18 ^{13}C NMR (151 MHz, $CDCl_3$) spectrum of compound **11** (Chapter 3).

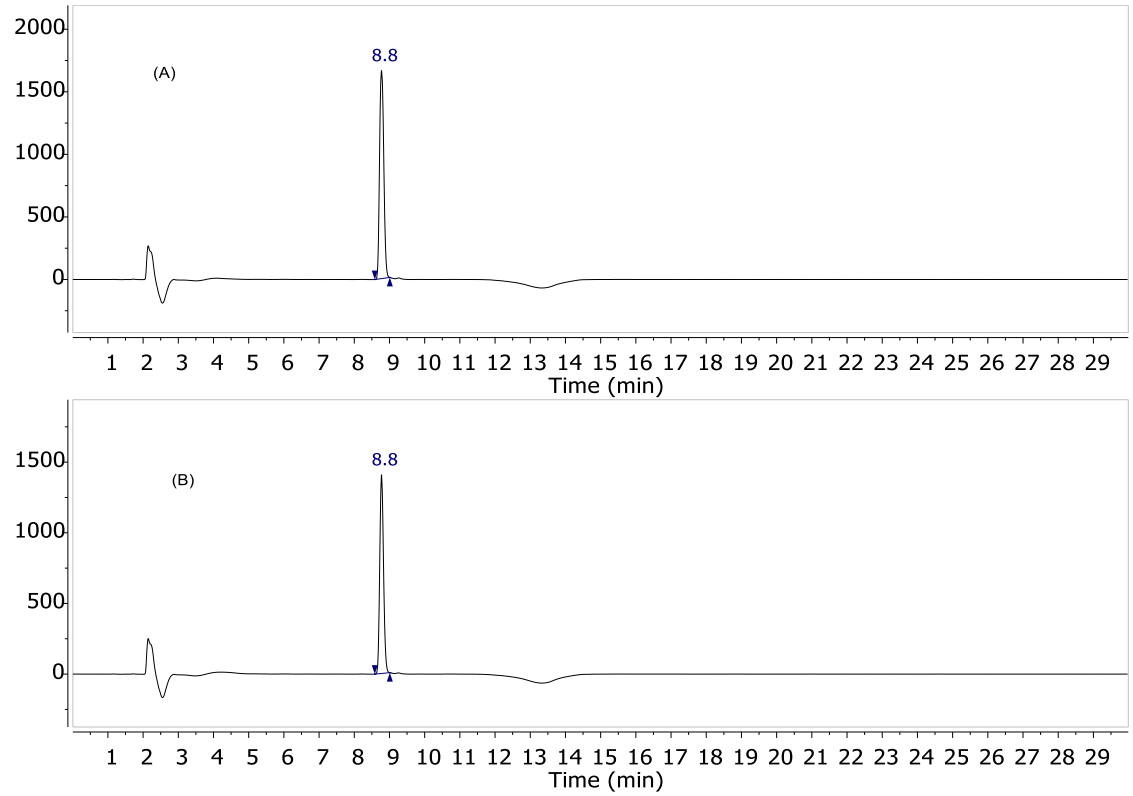

Figure S. 19 RP-HPLC chromatogram spectrum of compound **12** a) 210 nm, b) 215 nm (Chapter 3).

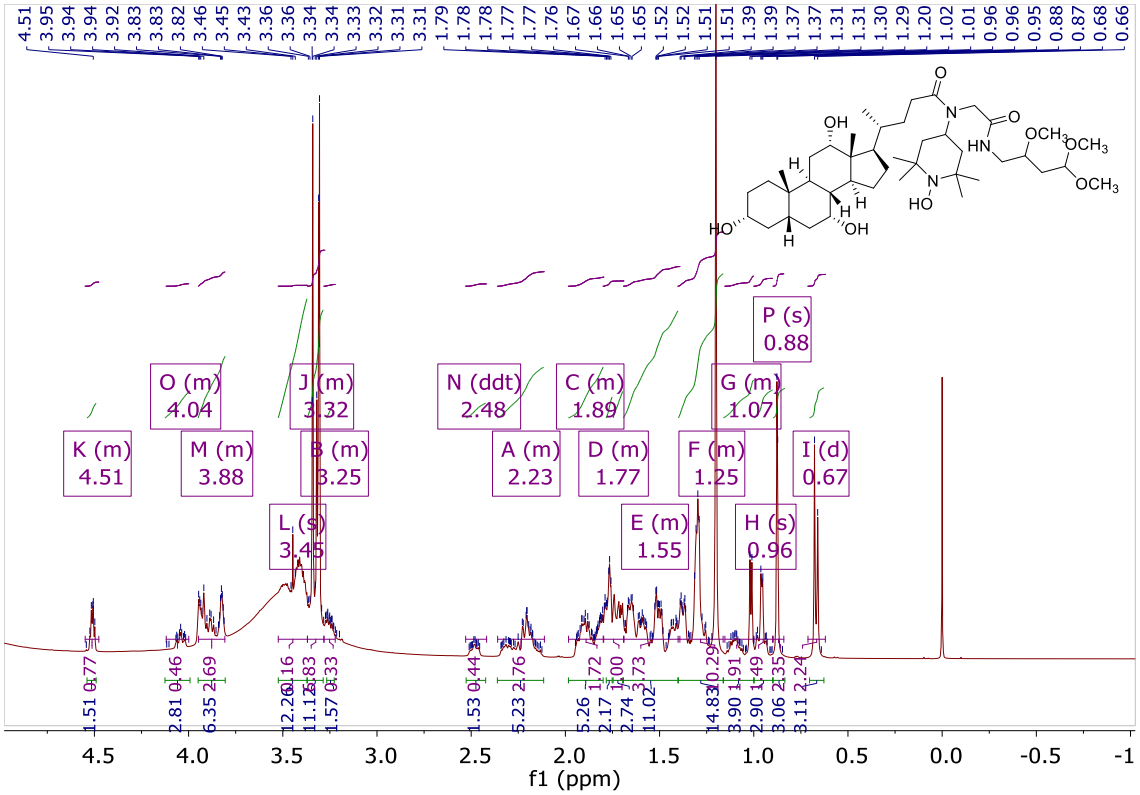

Figure S. 20 ^{1}H NMR (600 MHz, $CDCl_3$) spectrum of compound **12** (Chapter 3).

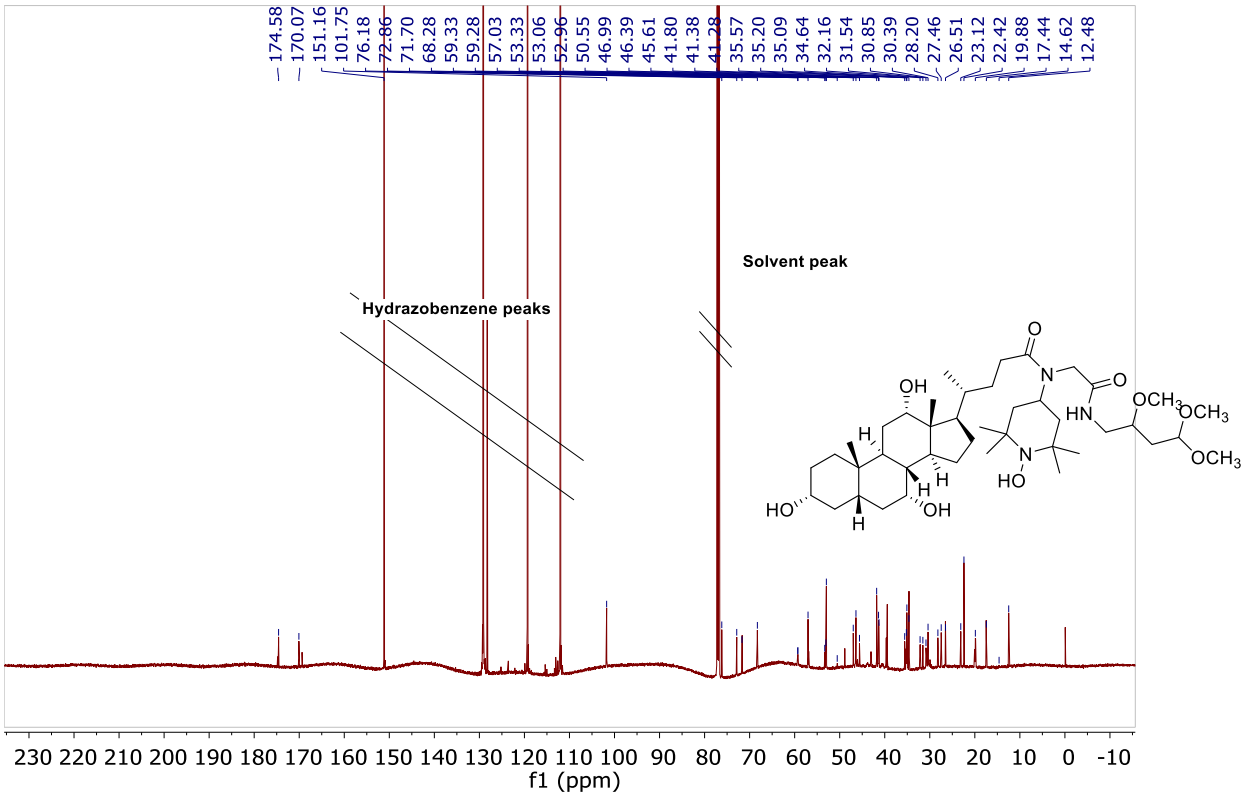

Figure S. 21 ^{13}C NMR (151 MHz, $CDCl_3$) spectrum of compound **12** (Chapter 3).

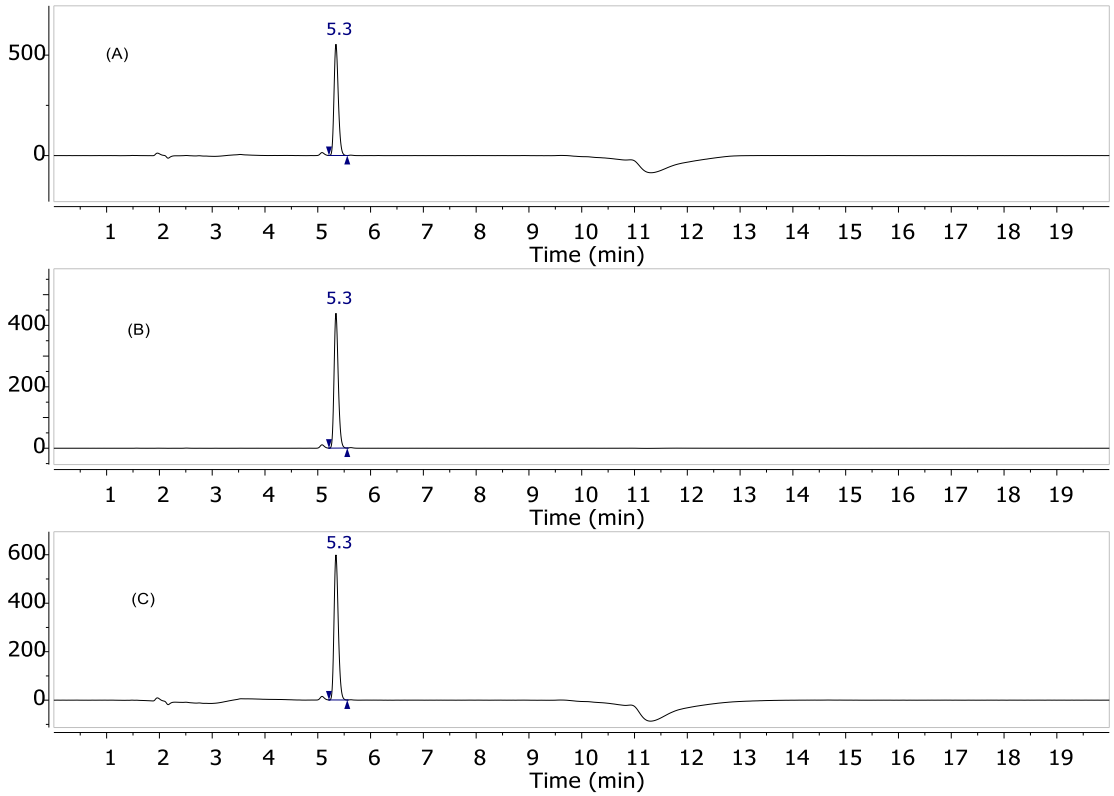

Figure S. 22 RP-HPLC chromatogram spectrum of compound **13** a) 210 nm, b) 215 nm, C) 254 nm (Chapter 3).

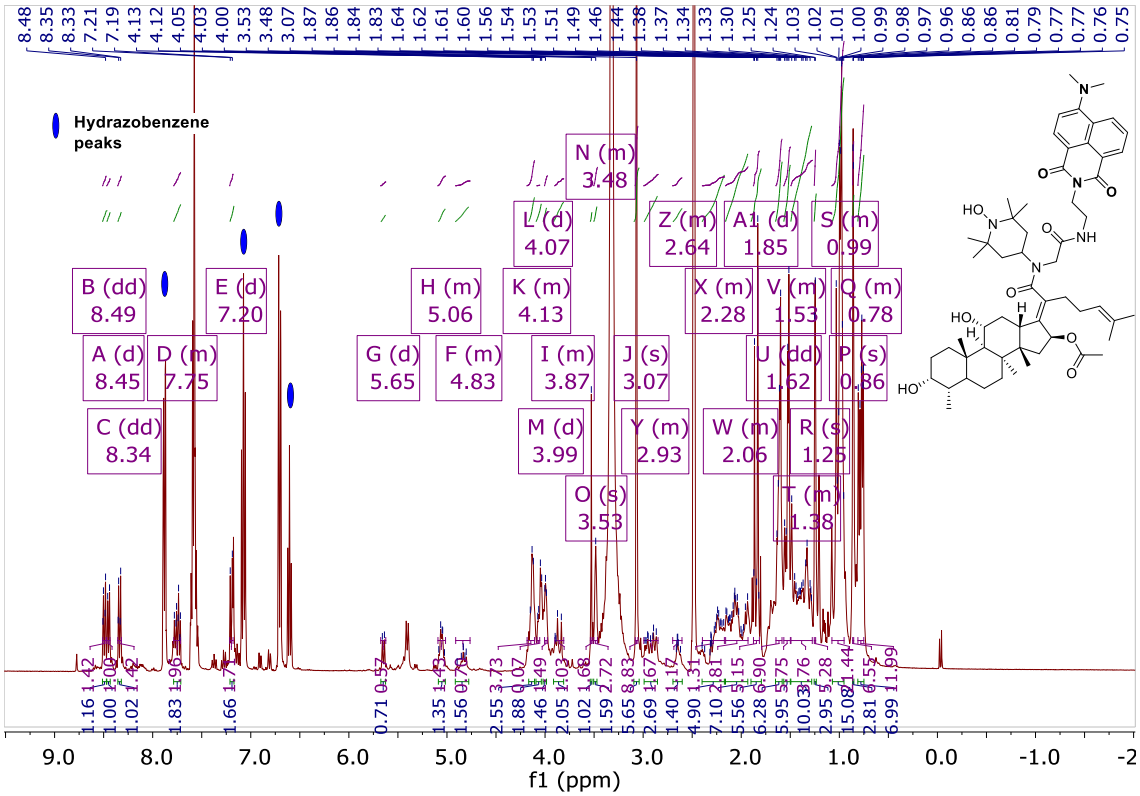

Figure S. 23 ^{1}H NMR (400 MHz, DMSO-d_6) spectrum of compound **13** (Chapter 3).

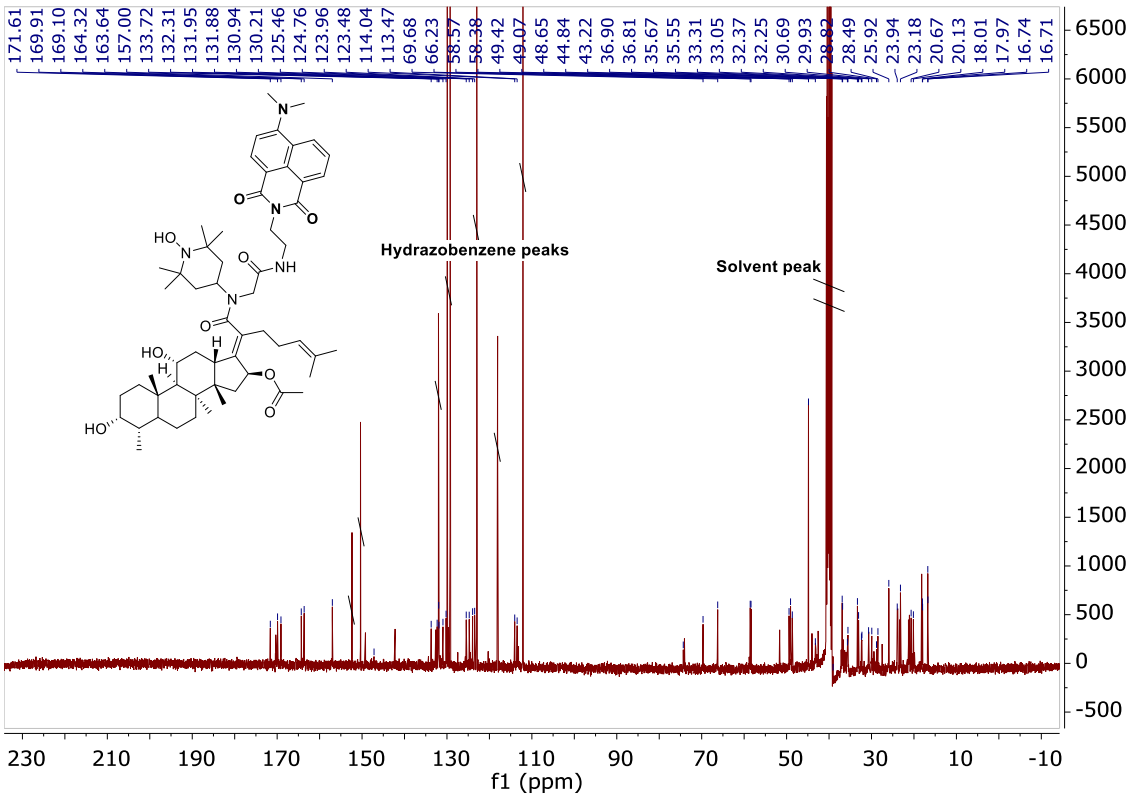

Figure S. 24 ^{13}C NMR (101 MHz, DMSO-d_6) spectrum of compound **13** (Chapter 3).

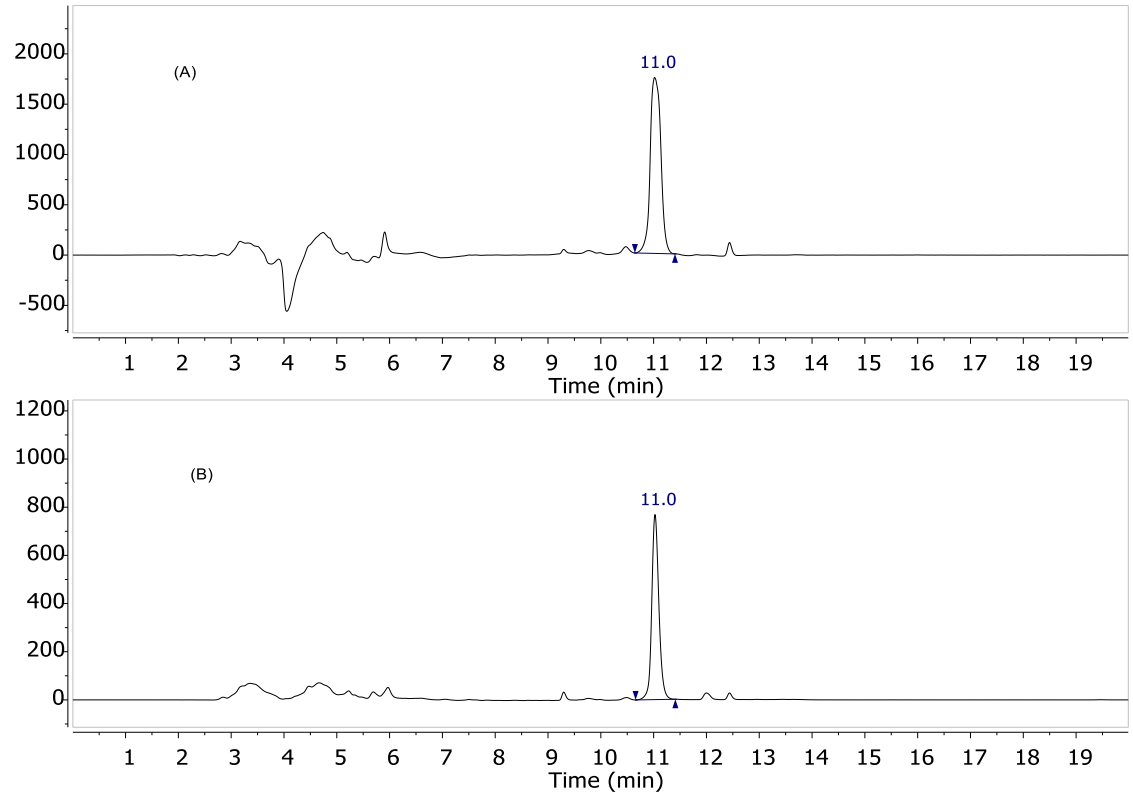

Figure S. 25 RP-HPLC chromatogram spectrum of compound **15** a) 210 nm, b) 215 nm (Chapter 3).

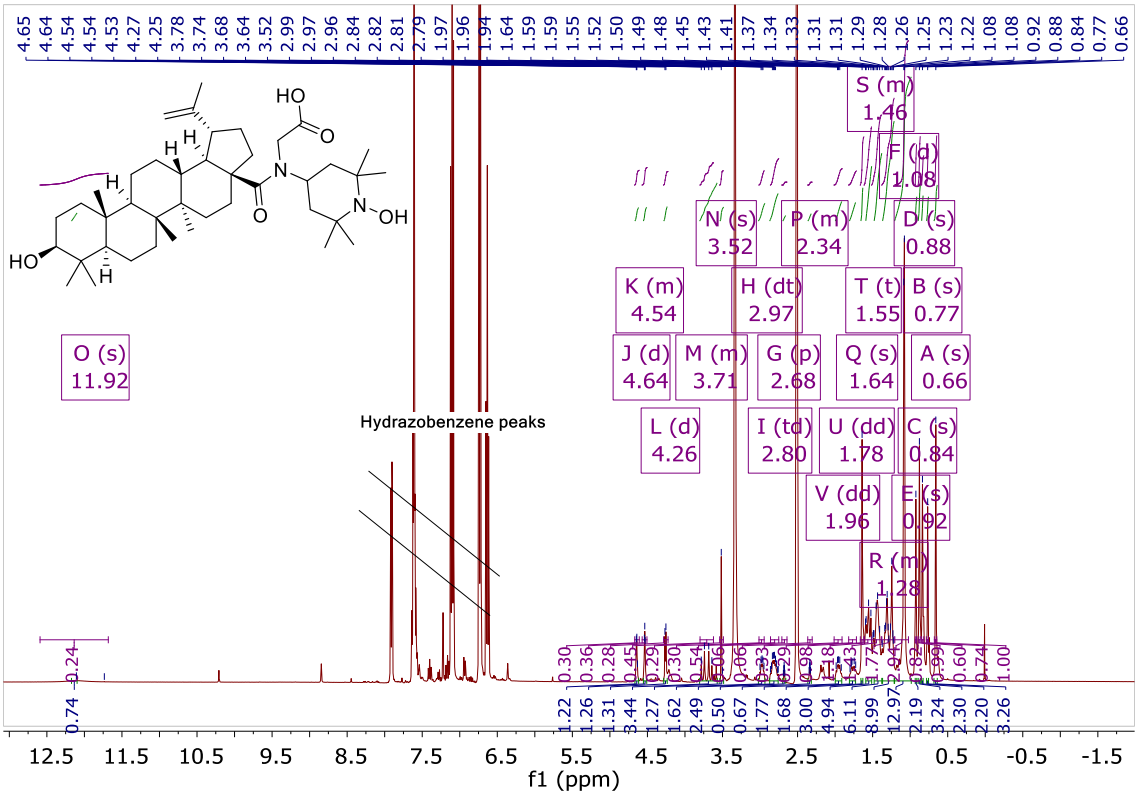

Figure S. 26 ^{1}H NMR (400 MHz, DMSO-d_6) spectrum of compound **15** (Chapter 3).

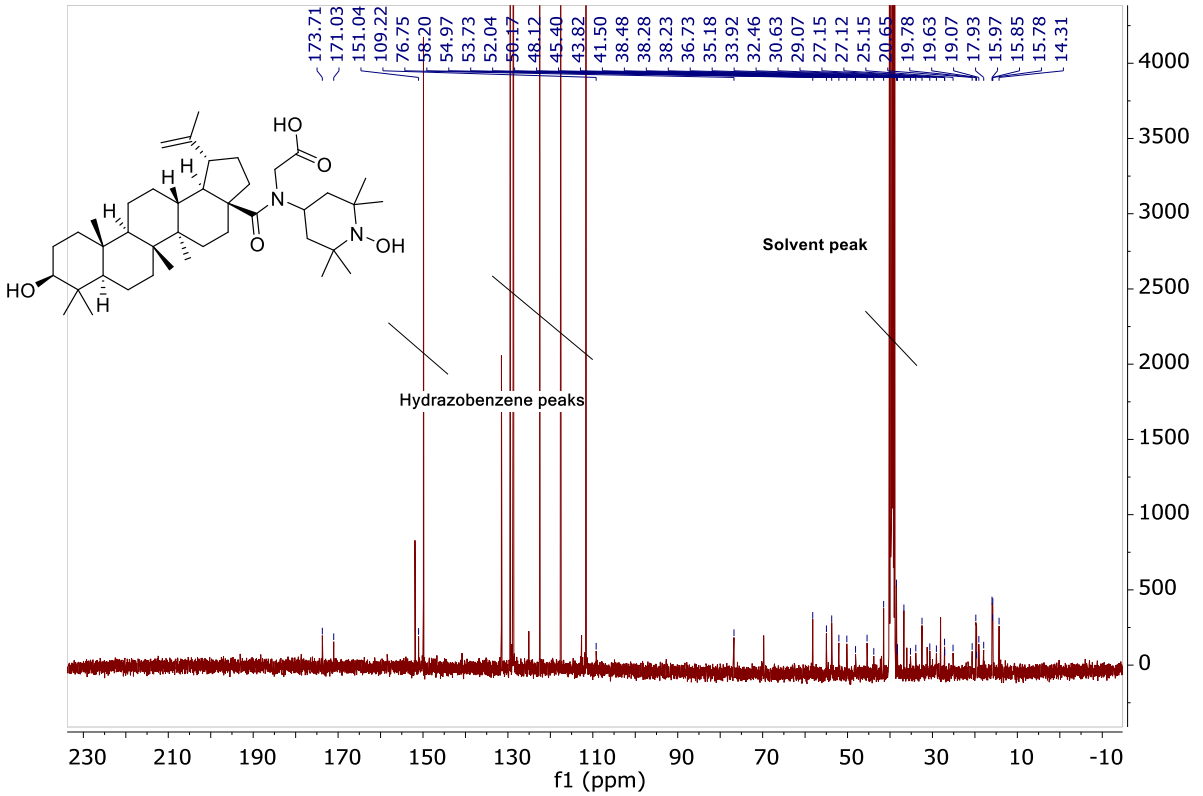

Figure S. 27 ^{13}C NMR (101 MHz, DMSO-d_6) spectrum of compound **15** (Chapter 3).

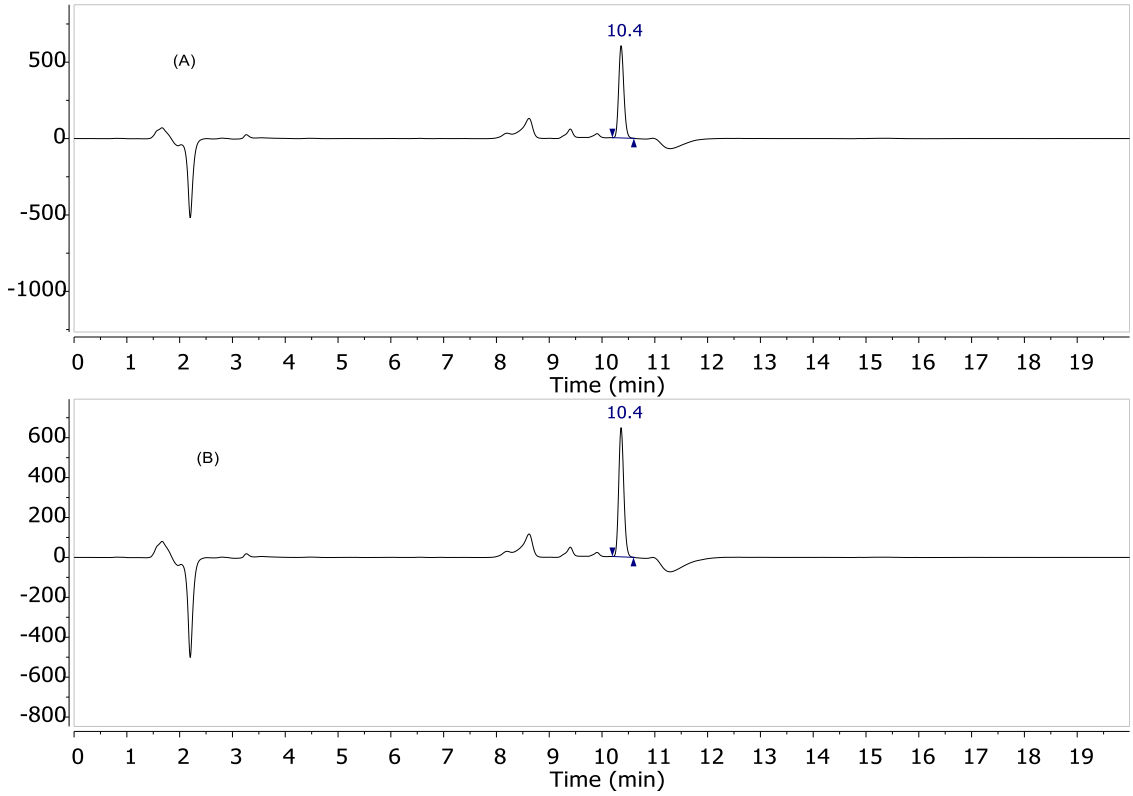

Figure S. 28 RP-HPLC chromatogram spectrum of compound **17** a) 210 nm, b) 215 nm (Chapter 3).

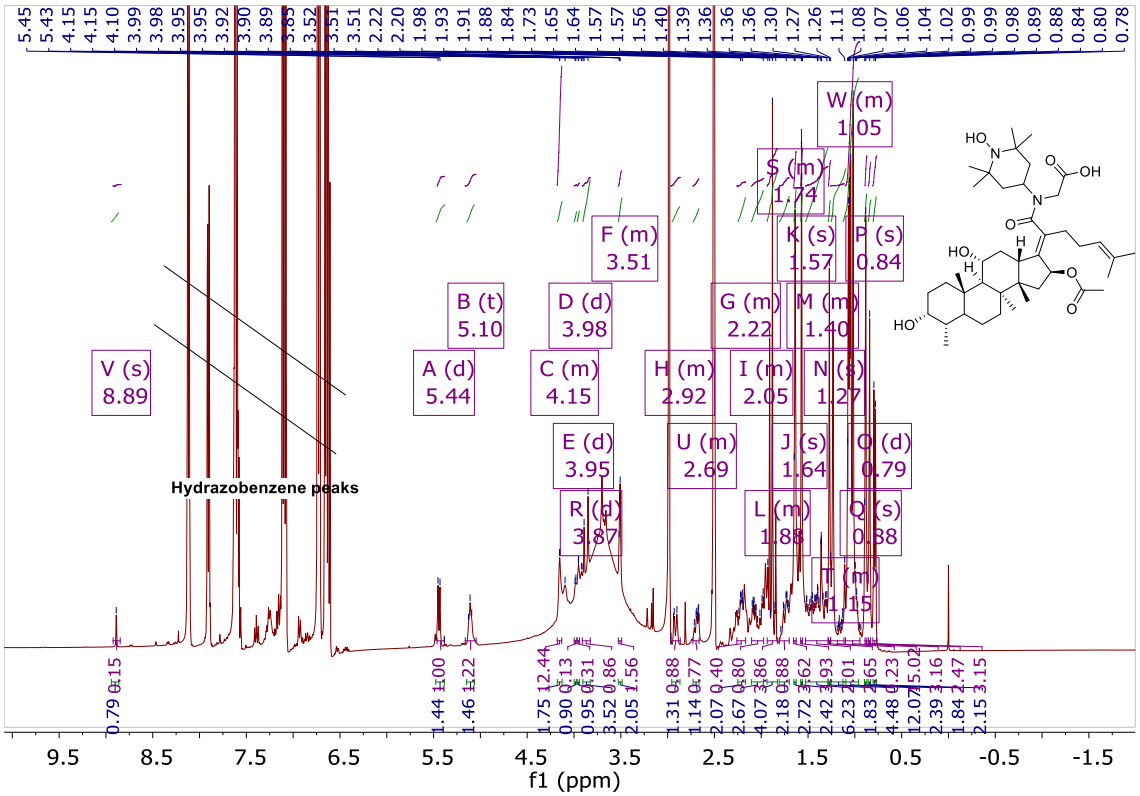

Figure S. 29 ^{1}H NMR (400 MHz, DMSO-d_6) spectrum of compound **17** (Chapter 3).

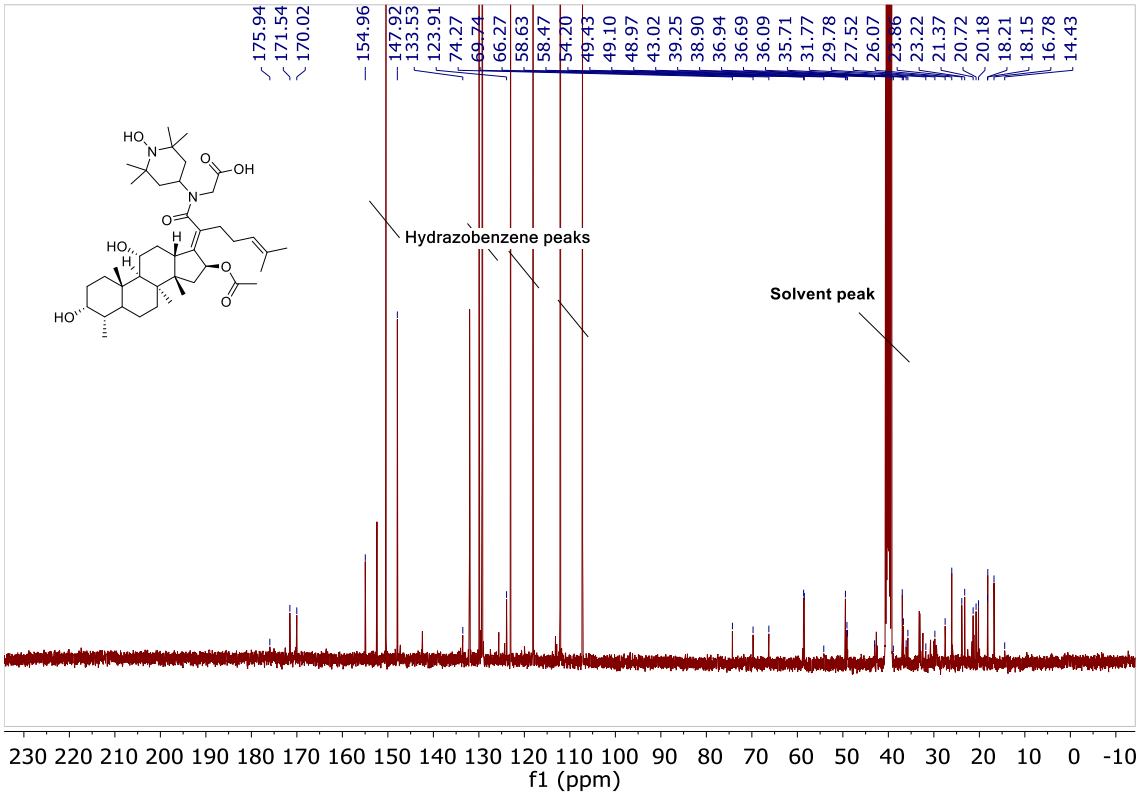

Figure S. 30 ^{13}C NMR (101 MHz, DMSO-d_6) spectrum of compound **17** (Chapter 3).

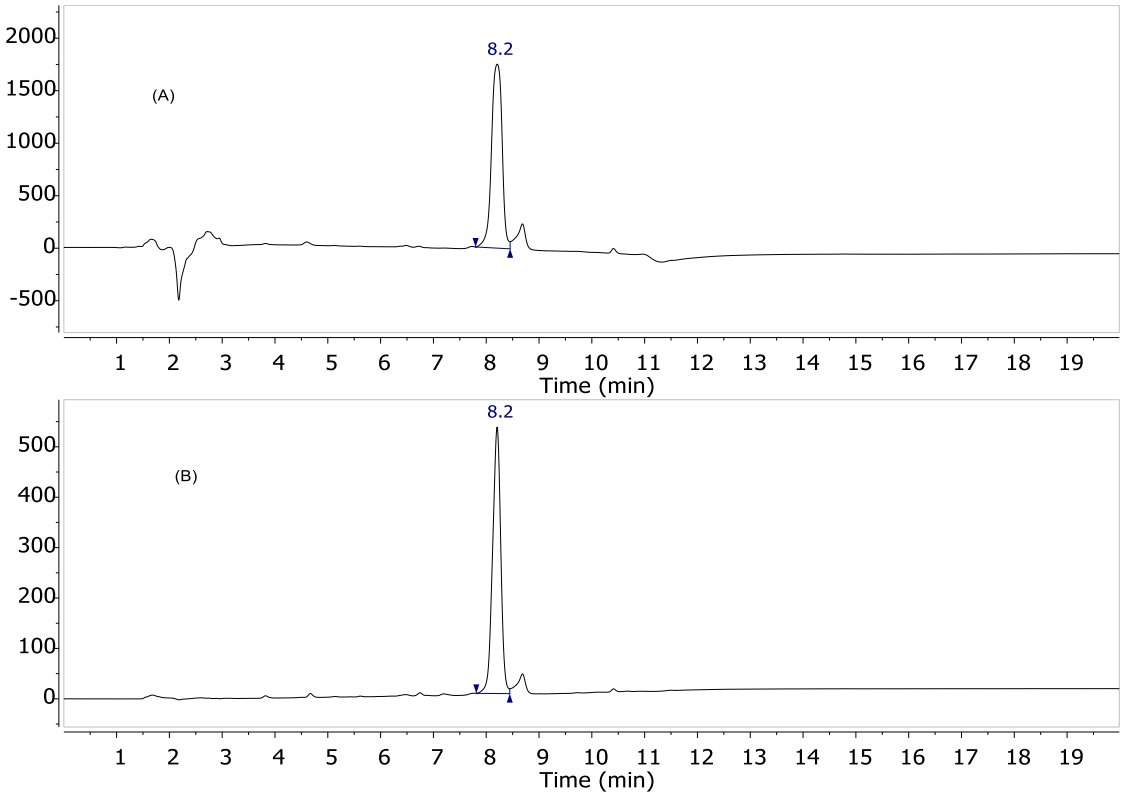

Figure S. 31 RP-HPLC chromatogram spectrum of compound **18** a) 210 nm, b) 215 nm (Chapter 3).

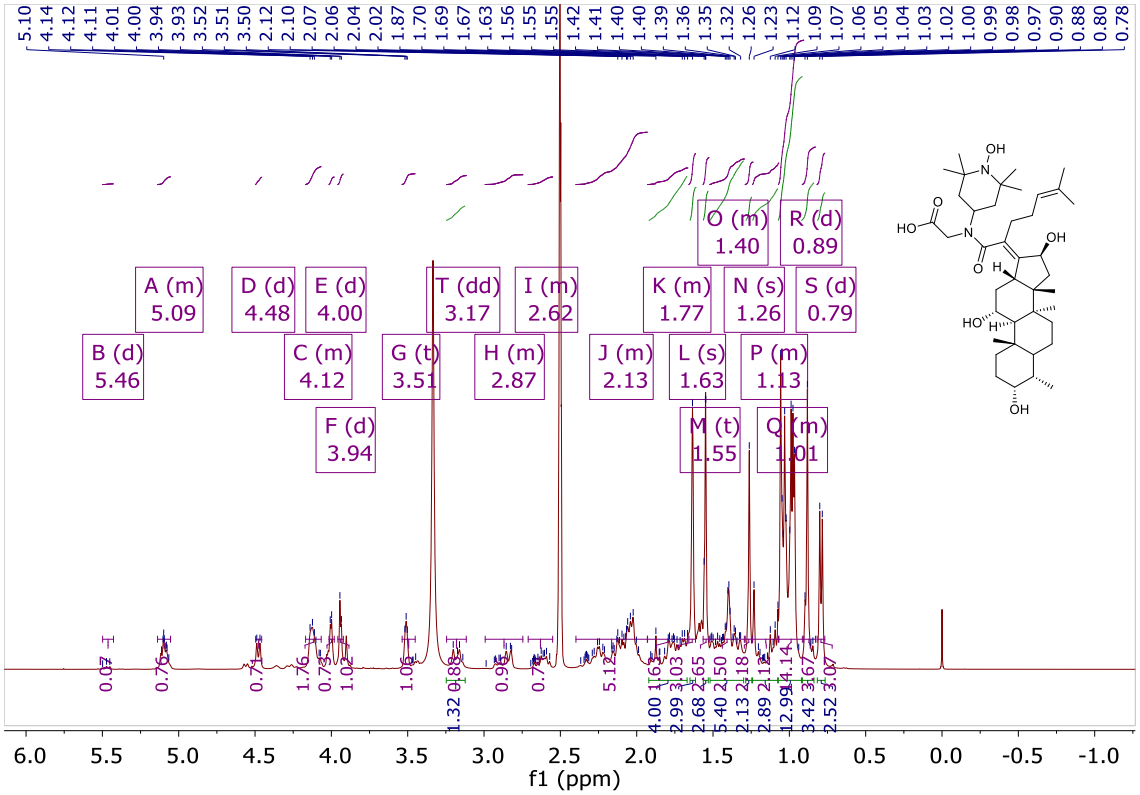

Figure S. 32 ^{1}H NMR (400 MHz, DMSO-d_6) spectrum of compound **18** (Chapter 3).

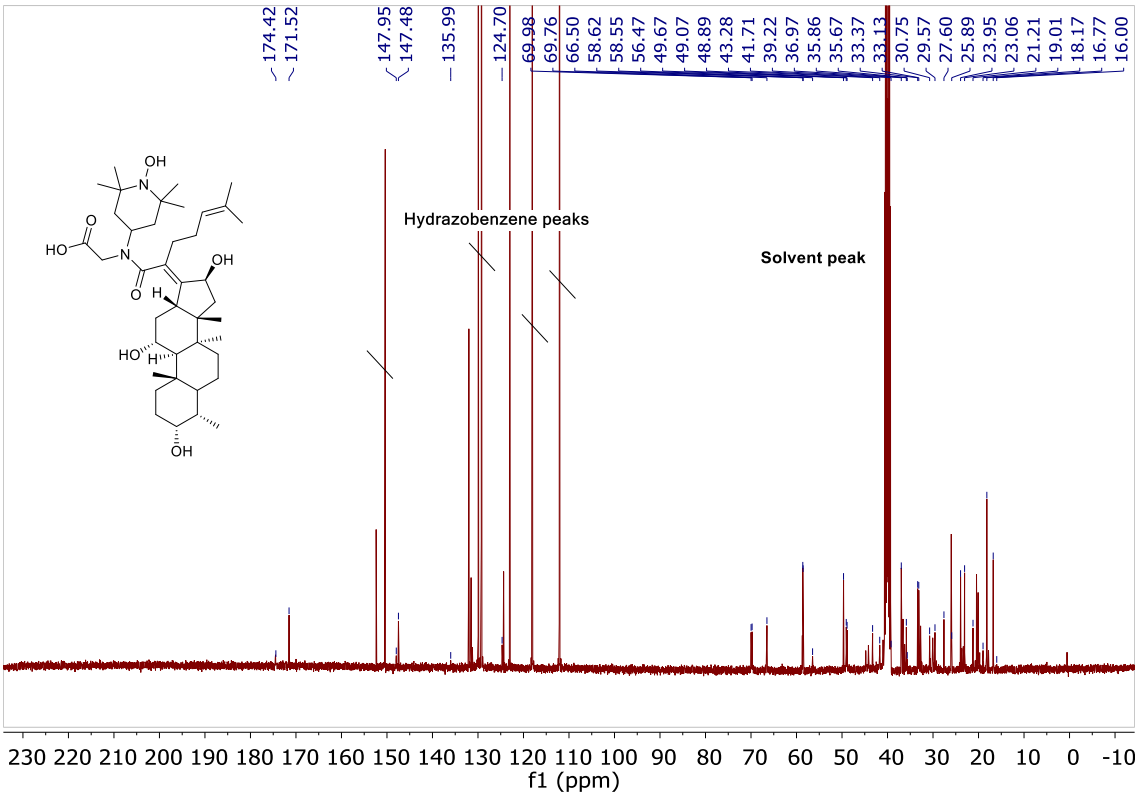

Figure S. 33 ^{13}C NMR (101 MHz, DMSO-d_6) spectrum of compound **18** (Chapter 3).

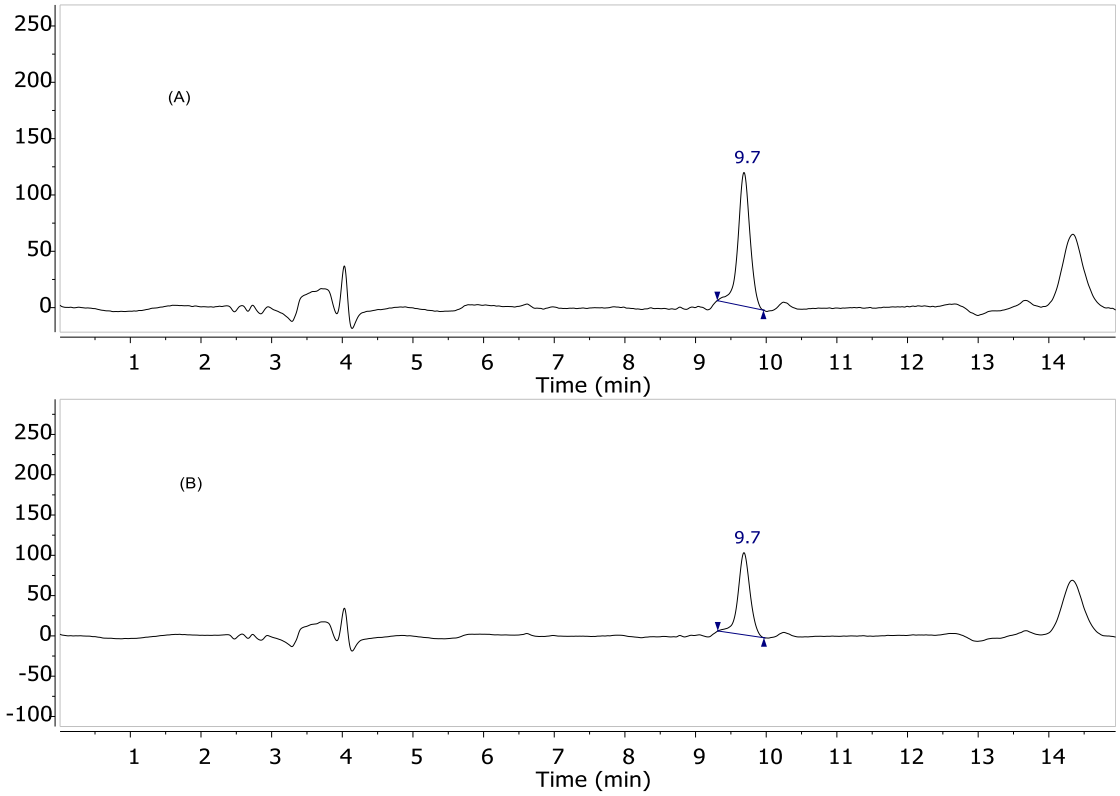

Figure S. 34 RP-HPLC chromatogram spectrum of compound **19** a) 210 nm, b) 215 nm (Chapter 3).

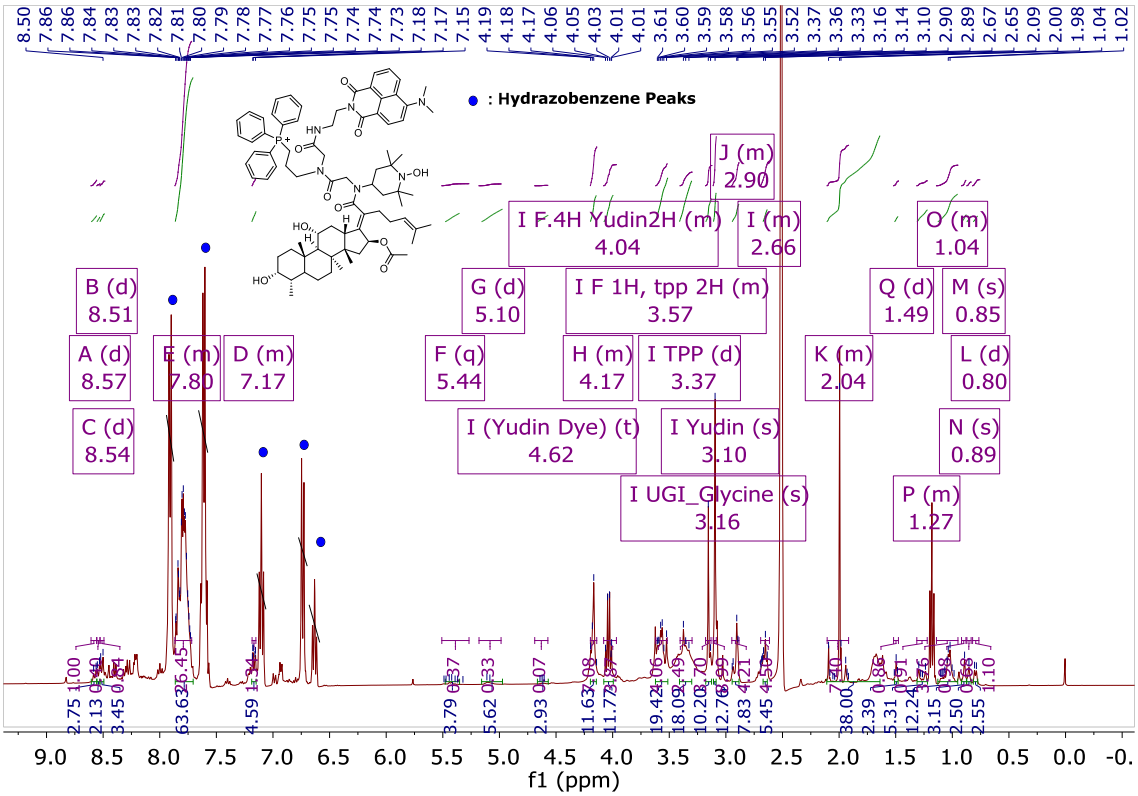

Figure S. 35 ^{1}H NMR (400 MHz, DMSO-d_6) spectrum of compound **19** (Chapter 3).

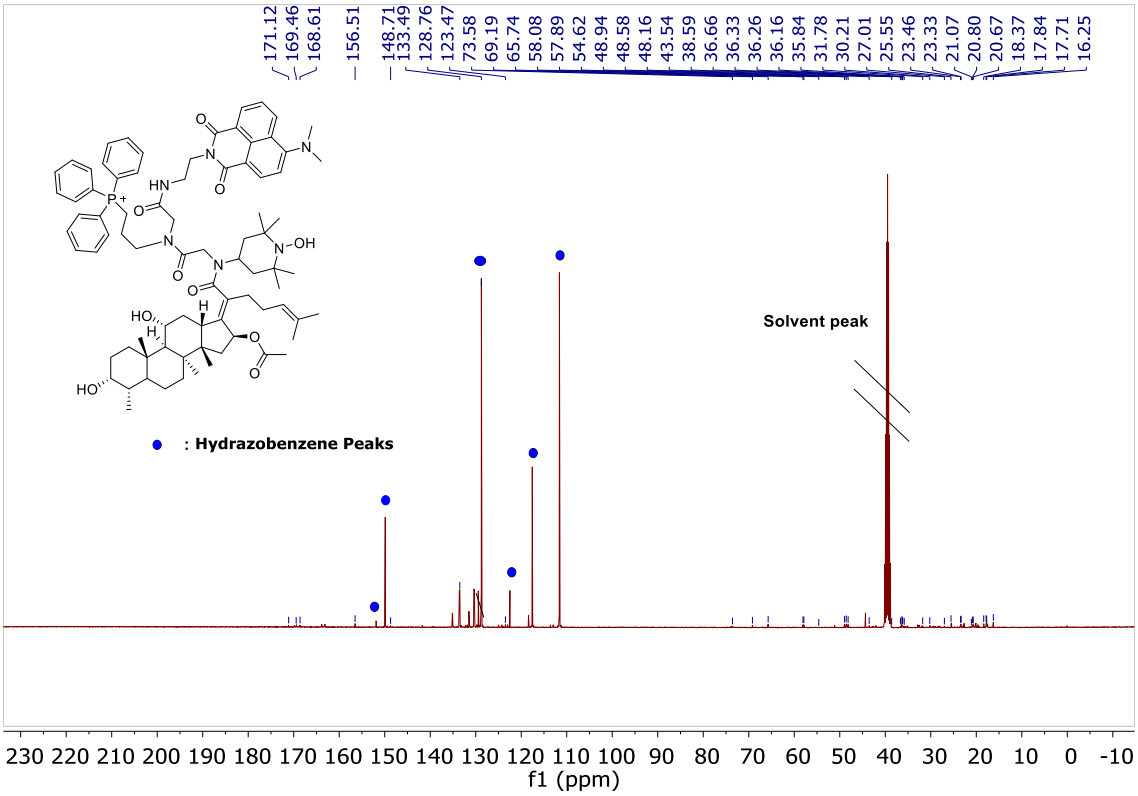

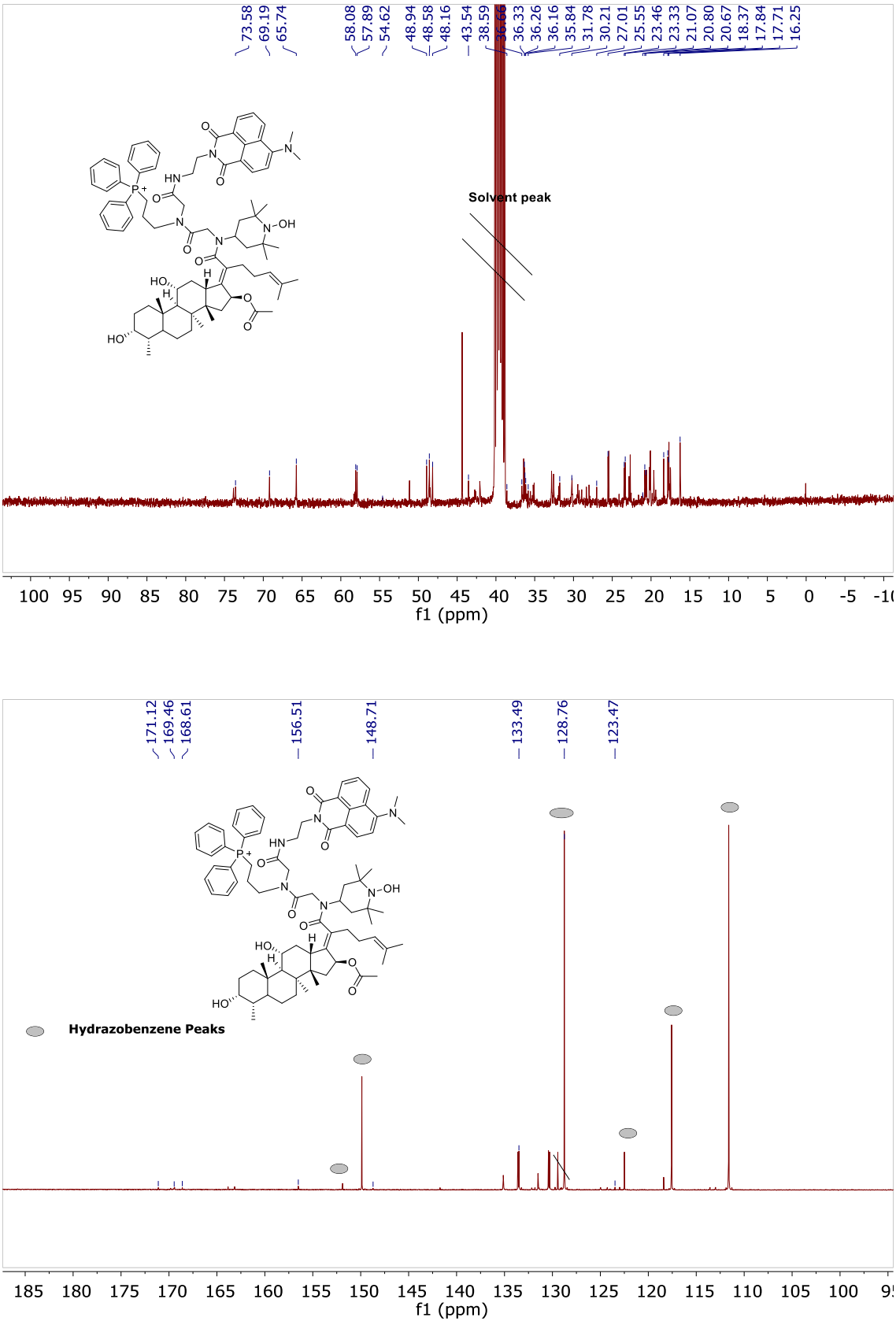

Figure S. 36 ^{13}C NMR (101 MHz, DMSO-d_6) spectrum of compound **19** (Chapter 3).

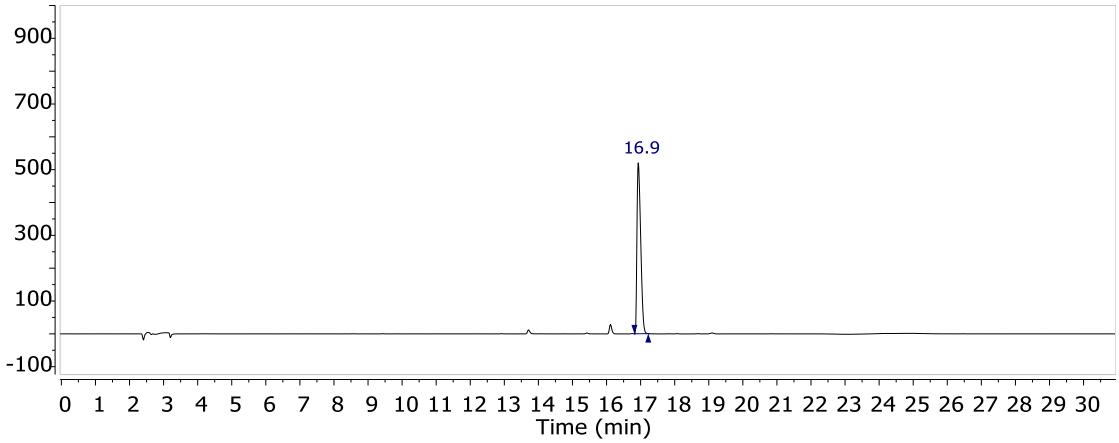

Figure S. 37 RP-HPLC chromatogram spectrum of probe **5** at 254 nm (Chapter 4).

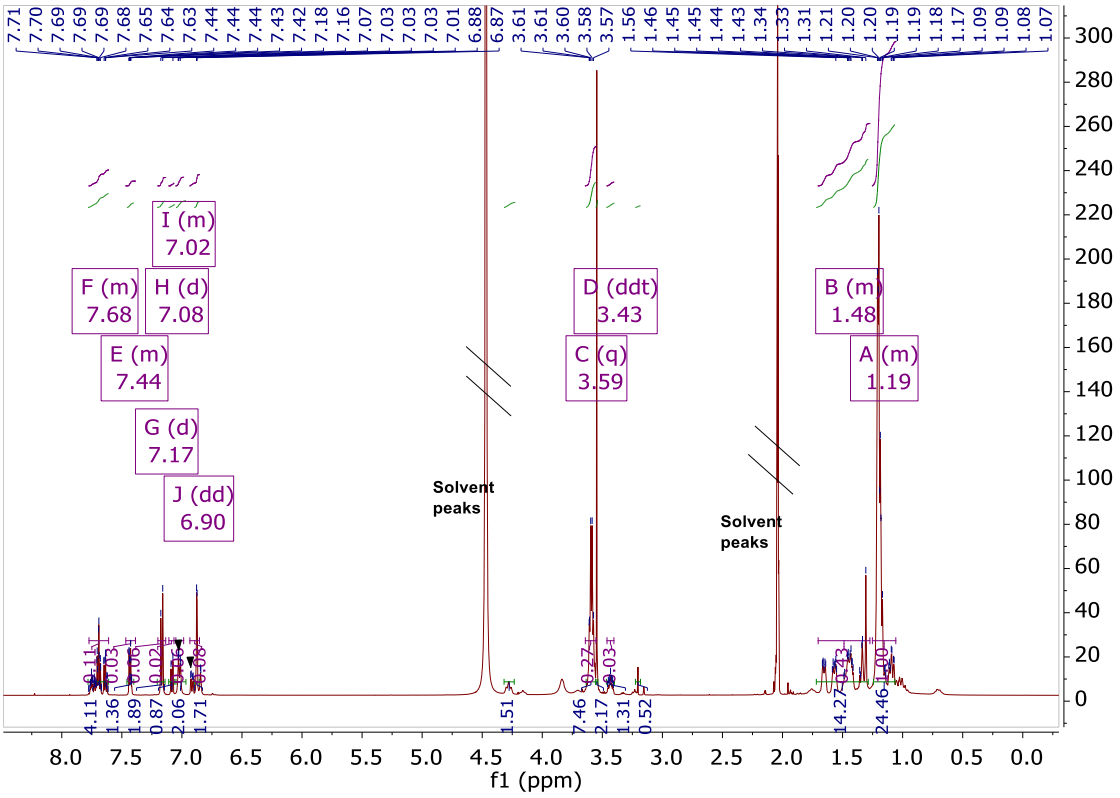

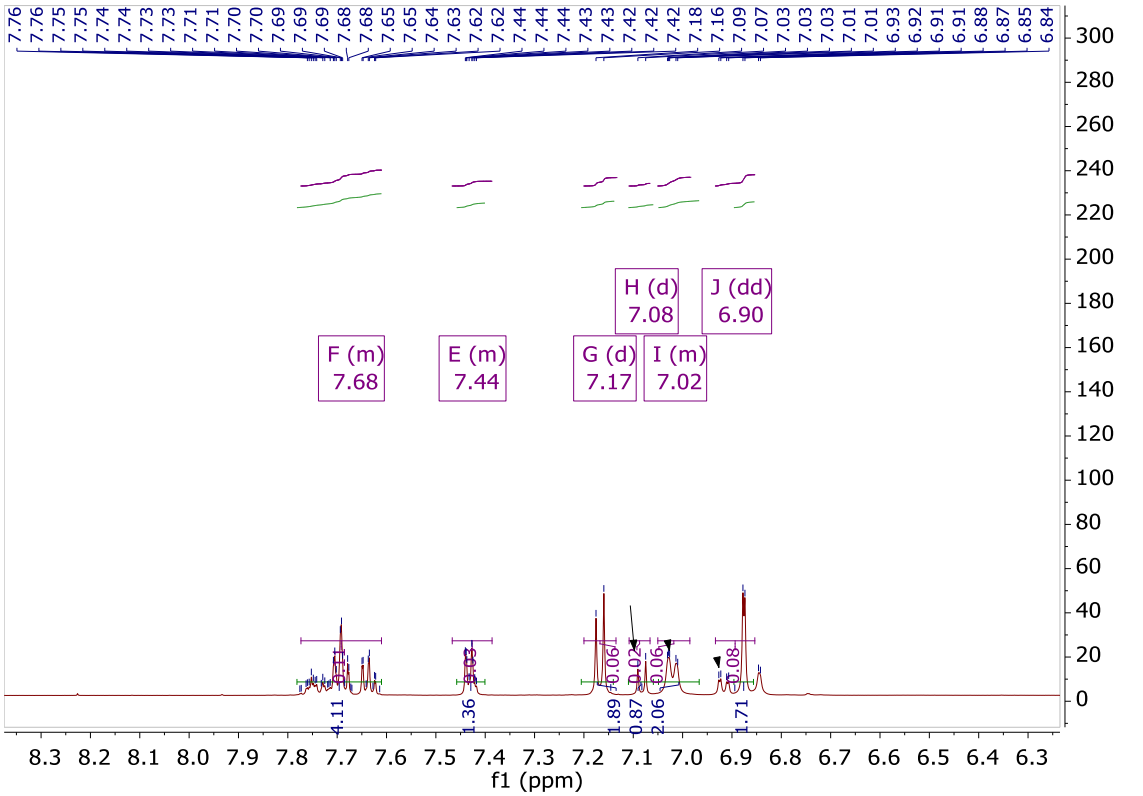

Figure S. 38 ^{1}H NMR (600 MHz, CD_3COCD_3) spectrum of probe **5** (Chapter 4).

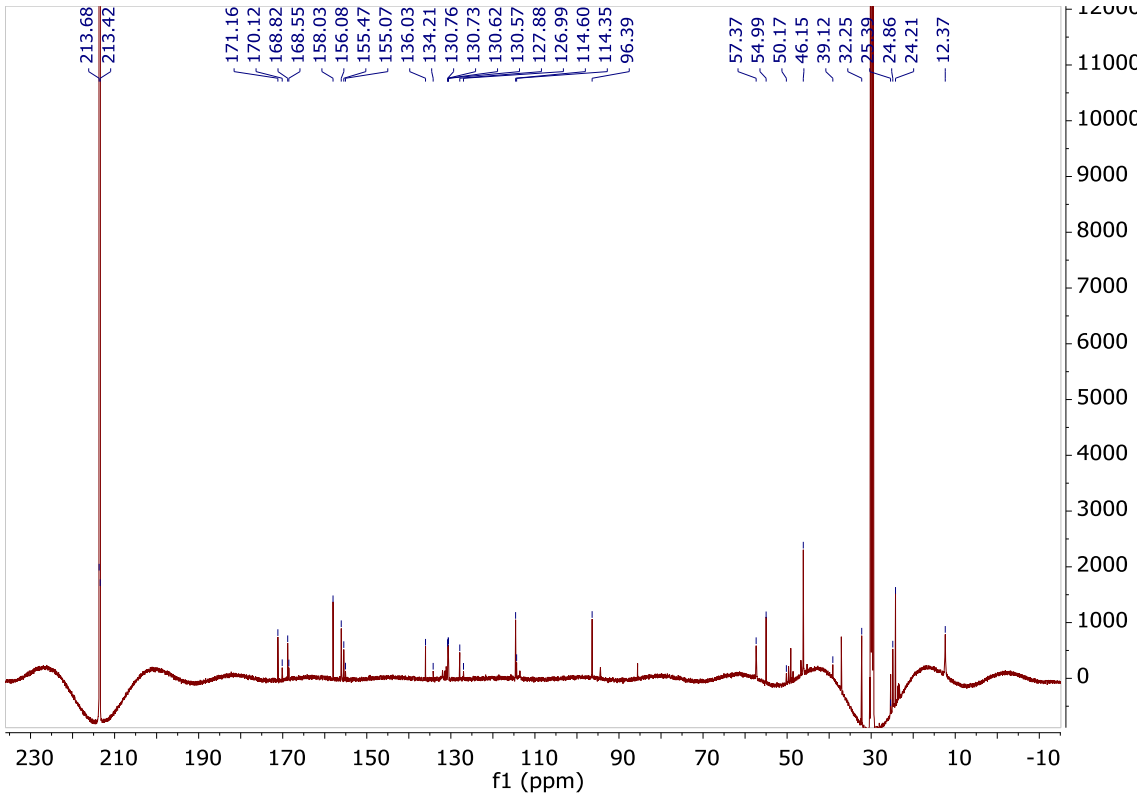

Figure S. 39 ^{13}C NMR (151 MHz, CD_3COCD_3) spectrum of probe **5** (Chapter 4).

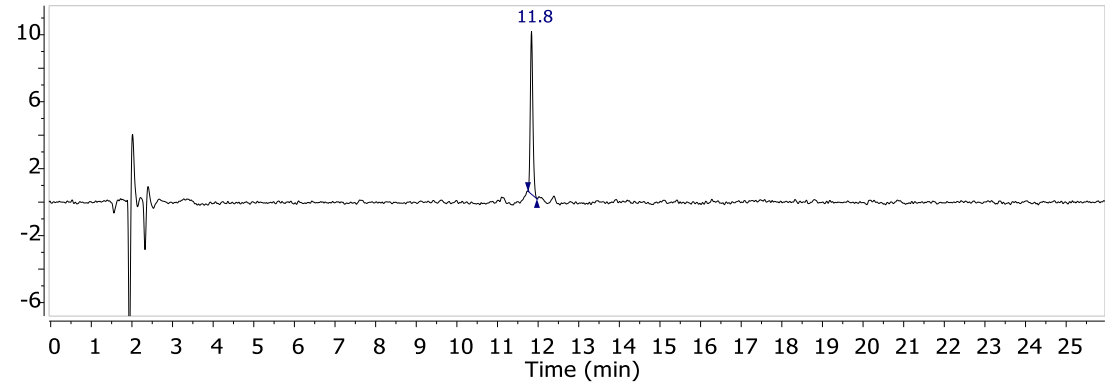

Figure S. 40 RP-HPLC chromatogram spectrum of probe **6** at 254 nm (Chapter 4).

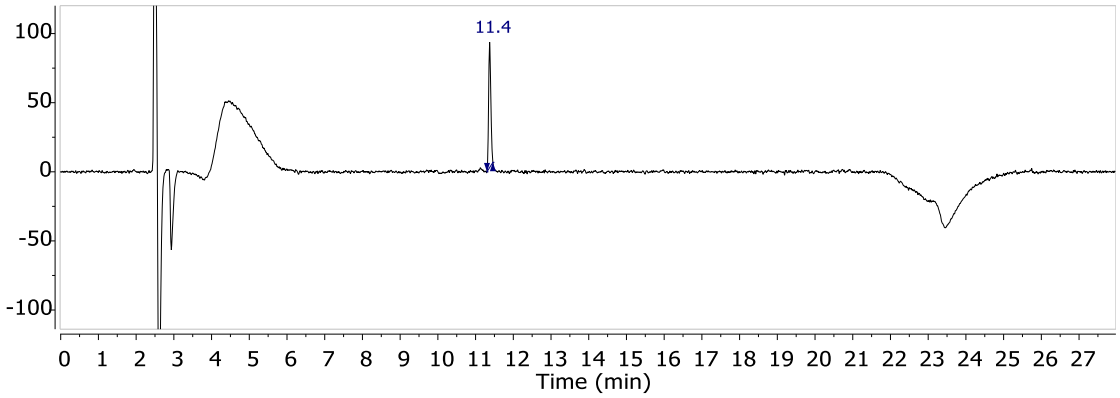

Figure S. 41 RP-HPLC chromatogram spectrum of probe **7** at 254 nm (Chapter 4).

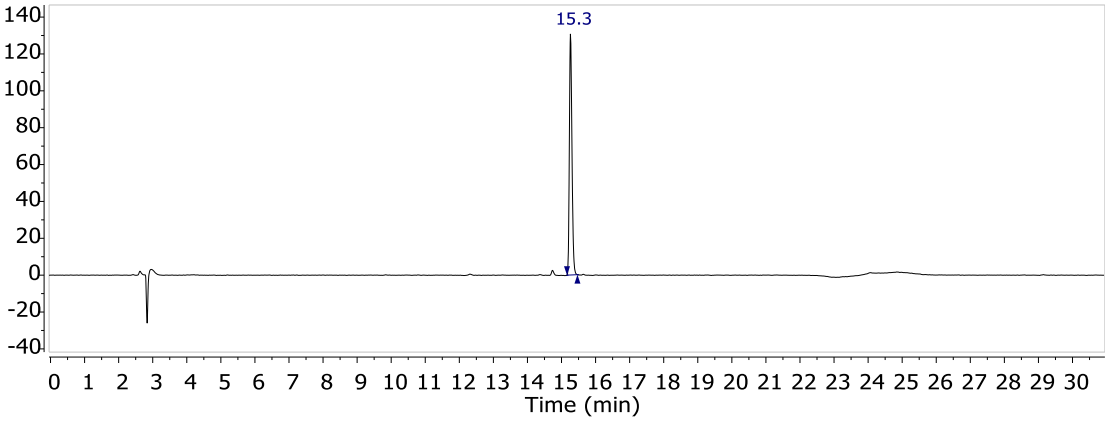

Figure S. 42 RP-HPLC chromatogram spectrum of probe **8** at 254 nm (Chapter 4).

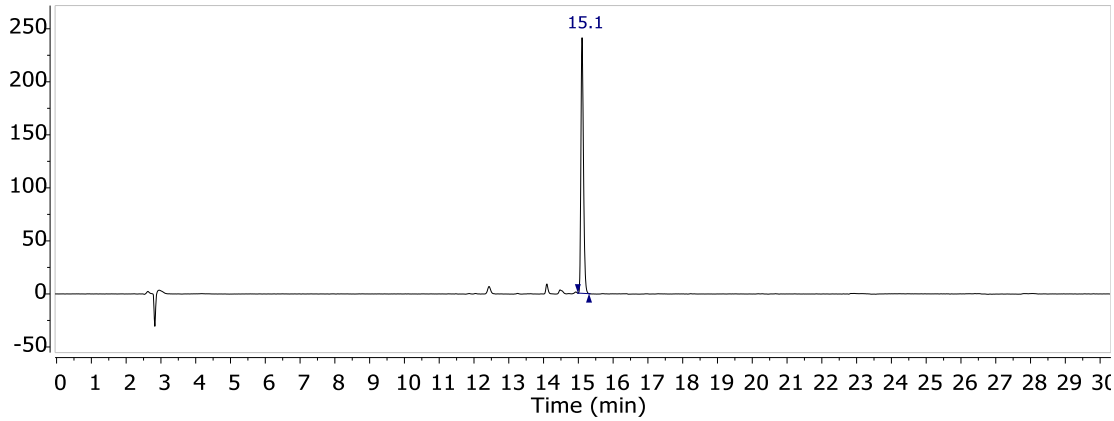

Figure S. 43 RP-HPLC chromatogram spectrum of probe **9** at 254 nm (Chapter 4).

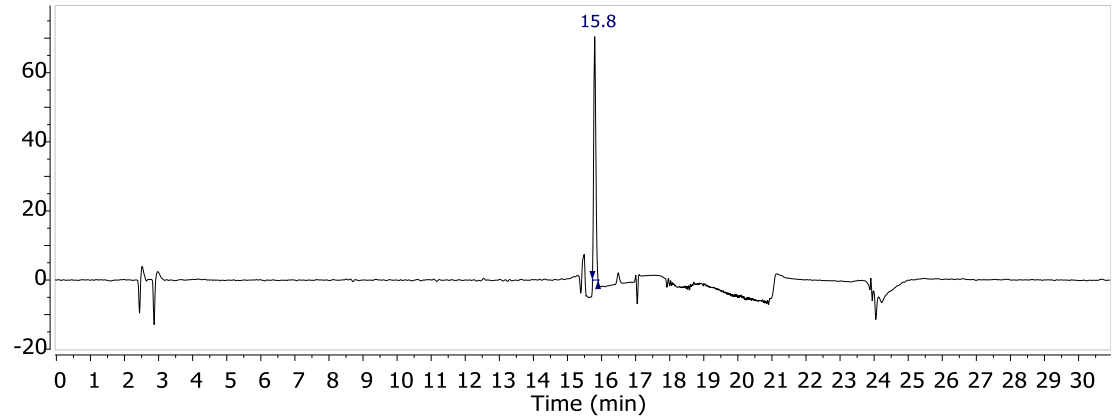

Figure S. 44 RP-HPLC chromatogram spectrum of probe **10** at 254 nm (Chapter 4).

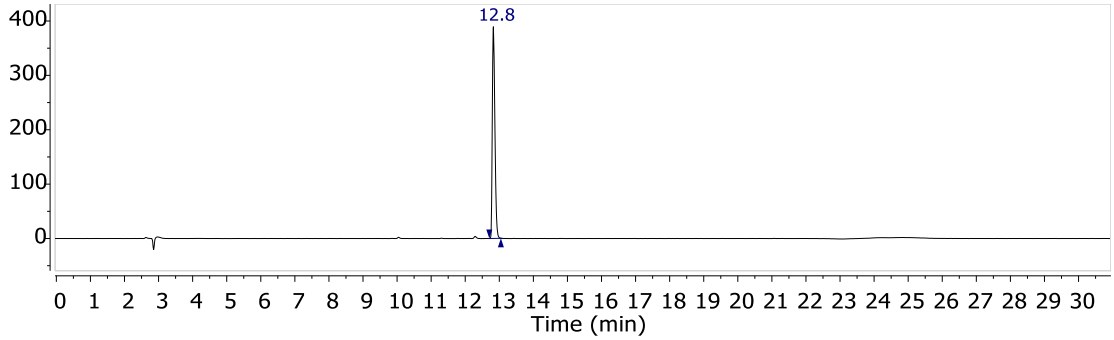

Figure S. 45 RP-HPLC chromatogram spectrum of probe **11** at 254 nm (Chapter 4).

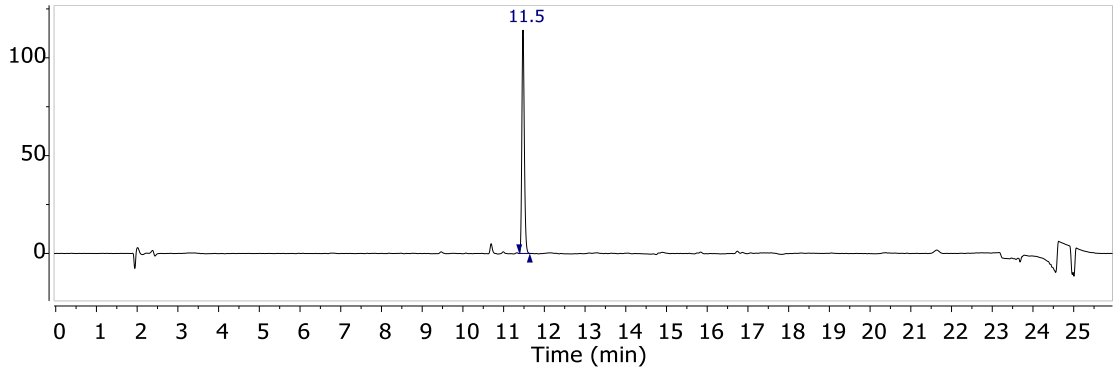

Figure S. 46 RP-HPLC chromatogram spectrum of probe **12** at 254 nm (Chapter 4).

M.Sc. Haider Na'mh Abdula Sultani

1. General Information

Name	Haider Na'mh Abdula Sultani
Date of Birth	August, 25th 1984
Place of Birth	Baghdad-Iraq
Nationality	Iraqi

2. Education

2015- 2020 Ph.D. Student at the Leibniz Institute of Plant Biochemistry – Department of Pharmacy, Halle (Saale), Germany.
Supervisors: Prof. Dr. Bernhard Westermann
Prof. Dr. Peter Imming

2013-2014 Researcher, Pharmacy department, Martin-Luther-Universität Halle-Wittenberg Halle (Saale), Germany.

2009 - 2012 M.Sc in Medicinal Chemistry.
Research topic: Inhibitory Effects of New Mercapto Xanthine Derivatives in Human mcf7 and k562 Cancer Cell Lines.
Isra University, Amman, Jordan.

2007 – 2012 Pharmacy Manager,
Amman- Jordan.

2003 - 2007 B.Sc. in Pharmacy
Al-Zaytoonah University, Amman, Jordan.

3. Languages

Arabic, English, German.

4. Publications

2019 Lam, Yen T.H.; Palfner, Götz; Lima, Celia; Porzel, Andrea; Brandt, Wolfgang; Frolov, Andrej; Haider N. Sultani et al. (**2019**): Nor-guanacastepene pigments from the Chilean mushroom Cortinarius pyromyxa. In Phytochemistry 165, p. 112048. DOI: 10.1016/j.phytochem.2019.05.021

Sakna, Sarah T.; Mocan, Andrei; Sultani, Haider N.; El-Fiky, Nabaweya M.; Wessjohann, Ludger A.; Farag, Mohamed A. (**2019**): Metabolites profiling of Ziziphus leaf taxa via UHPLC/PDA/ESI-MS in relation to their biological activities. In Food chemistry 293, pp. 233–246. DOI: 10.1016/j.foodchem.2019.04.097.

2019 Schmidt, Jürgen; Kuck, Dietmar; Franke, Katrin; Sultani, Haider; Laub, Annegret; Wessjohann, Ludger A. (**2019**): The unusual fragmentation of long-chain feruloyl esters under negative ion electrospray conditions. In Journal of mass spectrometry: JMS. DOI: 10.1002/jms.4357

2017 Farag, Mohamed A.; Ali, Sara E.; Hodaya, Rashad H.; El-Seedi, Hesham R.; Sultani, Haider N.; Laub, Annegret et al. (**2017**): Phytochemical Profiles and Antimicrobial Activities of Allium cepa Red cv. and A. sativum Subjected to Different Drying Methods: A Comparative MS-Based Metabolomics. In Molecules (Basel, Switzerland) 22 (5). DOI: 10.3390/molecules22050761

Sultani, Haider N.; Ghazal, Rasha A.; Hayallah, Alaa M.; Abdulrahman, Loay K.; Abu-Hammour, Khaled; AbuHammad, Shatha et al. (**2017**): Inhibitory Effects of New

Mercapto Xanthine Derivatives in Human mcf7 and k562 Cancer Cell Lines. In J. Heterocyclic Chem. 54 (1), pp. 450–456. DOI: 10.1002/jhet.2602

2016 Sultani, Haider N.; Haeri, Haleh H.; Hinderberger, Dariush; Westermann, Bernhard (**2016**): Spin-labelled diketopiperazines and peptide-peptoid chimera by Ugi-multi-component-reactions. In Organic & biomolecular chemistry 14 (48), pp. 11336–11341. DOI: 10.1039/C6OB02194H

6. Selected conference presentations

2019 Haider N. Sultani, Spin Labels for Detection and Treatment: Smart Fluorescent Probes and Modified Natural Products. 53th Ph.D. workshop "Naturstofftreffen" October 11, **2019**, Halle (Saale), Germany.

2018 Haider N. Sultani, Goran N. Kaluderovic, Bernhard Westermann, Smart ROS-Probes by double read-outs. 21th Lecture Conference, ORCHEM **2018**, September 10th to 12st, **2018**, Berlin, Germany.

Haider N. Sultani, Goran N. Kaluderovic,7th International Conference on Multicomponent Reactions and Related Chemistry, August 26th to 31st **2018**, Düsseldorf, Germany.

2017 Haider N. Sultani, Bernhard Westermann Spin-labelled diketopiperazines and peptide–peptoid chimera by Ugi-multi-component-reactions 8th Spin Conference on Nitroxides (Spin-2017), September 10th to 14st, **2017** in Padova, Italy.

2012 Sultani, Haider N, Hayallah, Alaa M, Inhibitory Effects of New Mercapto Xanthine Derivatives in Human mcf7 and k562 Cancer Cell Lines International Conference of Young Chemists (ICYC), April 8th to 10st, **2012**, Amman, Jordan.

Declaration

“I declare that I have completed this dissertation without unauthorized help of a second party and only with the assistance acknowledged therein. I have appropriately acknowledged and referenced all text passages that are derived literally from or based on the content of published or unpublished work of other authors.”

Erklärung

Hiermit erkläre ich an Eides Statt, dass ich die vorliegende Arbeit selbständig und nur unter Verwendung der angegebenen Literatur und Hilfsmittel angefertigt habe.

Haider Na’mh Abdula Sultani